JOURNAL OF THE
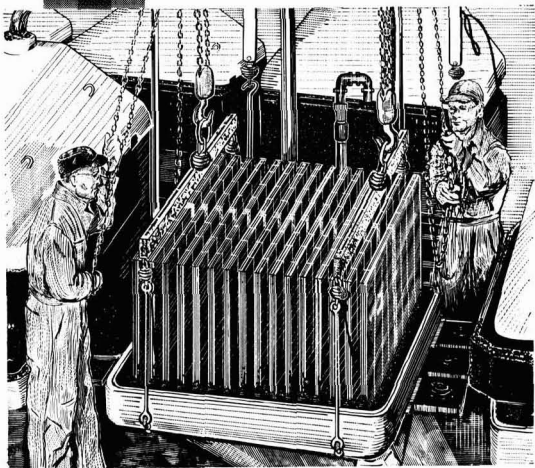
Electrochemical Society

GLC ANODES ARE CUSTOM MADE TO MEET VARYING ELECTROLYTIC CELL NEEDS

The custom made qualities of GLC Anodes give each cell operator performance characteristics best suited to his particular requirements.

These custom made qualities result from specialized anode production facilities, starting with the raw material mixing chambers and extending through extrusion, baking, graphitizing, oil impregnation and machining.

Equipment, designed exclusively for GLC, controls oil pickup to precise levels, and provides machining of superior accuracy. GLC Anodes are also distinguished for their uniformity of structure.

These factors combine to give GLC Anode customers improved cell operating economies that are a matter of record. May we review this record with you?

PRODUCTS
YOU CAN TRUST
ELECTRODE
GLC
DIVISION
®

GREAT LAKES CARBON CORPORATION

18 EAST 48TH STREET, NEW YORK 17, N. Y. OFFICES IN PRINCIPAL CITIES

Journal of the Electrochemical Society

CONTENTS

FUTURE MEETINGS OF
The Electrochemical Society

ॐ

Houston, Texas, October 9, 10, 11, 12, and 13, 1960
Headquarters at the Shamrock Hotel
Sessions will be scheduled on
Batteries, Corrosion, Electrodeposition,
Electrodeposition—Electrothermics & Metallurgy
Joint Symposium on Vapor Deposited Coatings,
Electronics (Semiconductors),
and Electrothermics and Metallurgy

★ ★ ★

Indianapolis, Ind., April 30, May 1, 2, 3, and 4, 1961
Headquarters at the Claypool Hotel

Sessions probably will be scheduled on
Electric Insulation, Electronics (including Luminescence and
Semiconductors), Electrothermics and Metallurgy,
Industrial Electrolytics, and Theoretical
Electrochemistry

★ ★ ★

Detroit, Mich., October 1, 2, 3, 4, and 5, 1961
Headquarters at the Statler Hotel

★ ★ ★

Los Angeles, Calif., May 6, 7, 8, 9, and 10, 1962
Hotel to be announced

★ ★ ★

Boston, Mass., September 16, 17, 18, 19, and 20, 1962
Headquarters at the Statler Hilton Hotel

Papers are now being solicited for the meeting to be held in Indianapolis, Ind., April 30-May 4, 1961. Triplicate copies of each abstract *(not exceeding 75 words in length)* are due at Society Headquarters, 1860 Broadway, New York 23, N. Y., *not later than January 2, 1961* in order to be included in the program. *Please indicate on abstract for which Division's symposium the paper is to be scheduled, and underline the name of the author who will present the paper.* Complete manuscripts should be sent in triplicate to the Managing Editor of the JOURNAL at 1860 Broadway, New York 23, N. Y.

Presentation of a paper at a technical meeting of the Society does not guarantee publication in the JOURNAL. However, all papers so presented become the property of The Electrochemical Society, and may not be published elsewhere, either in whole or in part, unless permission for release is requested of and granted by the Editor. Papers already published elsewhere, or submitted for publication elsewhere, are not acceptable for oral presentation except on invitation by a Divisional program Chairman.

ASSIGNMENT: HIT A TARGET 6000 MILES AWAY

Can you guide a 110-ton Air Force Titan missile far up into the sky, to bring its nuclear warhead down with pinpoint accuracy on a target one-fourth the way around the globe—a target you not only can't see but which continually moves with the spinning earth?

This was the problem in missile guidance the Air Force presented to Bell Telephone Laboratories and its manufacturing partner, Western Electric. The answer was the development of a command guidance system which steers the Titan with high accuracy.

Unlike self-contained systems which demand complex guidance equipment in the missile itself, Bell Laboratories Command Guidance

System keeps its master control equipment on the ground where it can be used over and over again. Thus a minimum of equipment is carried in the missile, and the ground station has full control of the missile during its guided flight. Techniques drawn from the communications art render the system immune to radio jamming.

Bell Laboratories scientists and engineers designed the transmission and switching systems for the world's most versatile telephone network, developed much of our nation's radar, and pioneered in missile systems. From their vast storehouse of knowledge and experience comes the guidance system for the Titan.
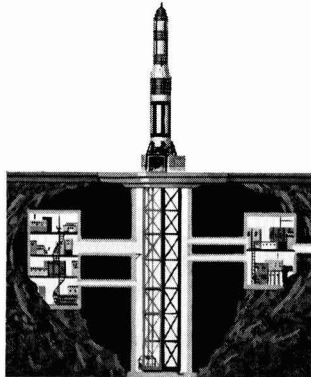
 BELL TELEPHONE LABORATORIES
WORLD CENTER OF COMMUNICATIONS RESEARCH AND DEVELOPMENT

Editorial

Profits and Policies

*C*ONGRESSIONAL Committee investigations do not always result in strong remedial legislation or court action against malefactors, but sometimes they receive attention which is very informative to the public. A case in point is the Kefauver subcommittee investigation of certain practices in the drug and pharmaceutical industry. No one has yet been accused of serious wrongdoing, but it has been suggested that new drugs are grossly overpriced, that profits are too high, that physicians are overwhelmed with promotional ballyhoo, that money is spent too freely in pushing questionable products at the expense of truly valuable research.

One countercharge is that Senator Kefauver, politically minded, will push the investigation to a publicity climax in July, at a convenient time before he will be a candidate in the August primary elections in Tennessee, then all will be forgotten.

One physician witness testified that he had received by mail more than 365 pounds of promotional literature and samples in a year, estimated that 24,000 tons of such material are distributed annually. The implication is that most of this is "junk mail" which should be discarded immediately. It has been suggested that the American Medical Association, or possibly a Government agency, should frequently prepare and distribute carefully written, authentic surveys of the properties and applications of new medicinal chemicals, minus the blatant Madison Avenue aspect which is so objectionable.

We all realize that successful drugs must support research on the many more unsuccessful ones. Drug houses spend money freely on research: we read that a single company spent $1,338,000 last year in grants for medical education and research (That is, outside its own laboratories. However, "medical education" does not necessarily mean scholarships for brilliant but impecunious medical students, and "research" may well mean merely clinical testing).

The drug companies are generous, too: Thomas A. Dooley, who does much to promote medical care and education in countries where witch doctors are still prevalent, states that his organization "Medico" receives annual gifts of supplies which would cost $150,000 at retail. Albert Schweitzer also can testify to the generosity of the supply houses. The pharmaceutical firms willingly finance conferences and symposia on the nature and use of new chemicals, even their rivals'—this is good publicity, and also aids in the quick interchange of information, which is greatly desired in the field. G. Malcolm Dyson, Director of Research of Chemical Abstracts Service, has stated: "Certain sections of industry want a more rapid survey of new material than can be obtained from the traditional abstracting procedures. This is particularly true in the medical/pharmaceutical field, where the life of a new drug is short."

A big factor in the background is the question of whether the industry shall be permitted to go its own way, or whether it shall come under closer Government control. We expect Government to see that we are not sold doubtful drugs with great claims but inadequate testing. We welcome thorough investigation, hope that any resulting legislation will be well considered and wise.

—CVK

Conn produces the "heart" of good tone quality by electrodeposition, with "Plus-4" Copper Anodes
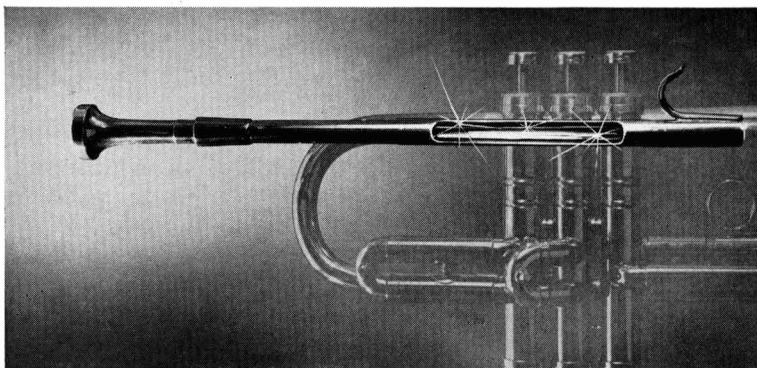
CONN ELECTRO-D TONE CHAMBER (mouthpipe) cut away to illustrate the "micro finish" interior surface. Chamber and mouthpiece receptacle are formed in one piece by electrodeposition; previously the two pieces were soldered together. (Patent pending.)

ELECTRO-D BELL, also formed by electrodeposition.

In a cornet or trumpet, good tone and easy playing depend largely on the inside shape and finish of the tone chamber (mouthpipe).

Aiming at perfection, C. G. Conn, Ltd., famous maker of band instruments, turned to forming these critical parts by electrodeposition of copper on stainless-steel mandrels. The deposited copper conforms perfectly to the precision mandrel—providing the exact taper and dimensions every time. It also gives the smooth mirrorlike inside surface that prevents acoustical losses. Even minor irregularities caused by forming sheet metal or tube can muffle, distort, or rattle the tone.

Using "Plus-4" Phosphorized Copper Anodes in its acid-copper electroplating tanks, Conn has found it gets the smooth, dense deposit it needs. The build-up of metal is fast and uniform, as "Plus-4" Anodes' extra "throwing power" is of particular value with the tubular shapes. There are few nodules, which minimizes finishing of the outside surface. And tank maintenance is simplified.

Conn also forms the bells used in cornets, trumpets, and trombones electrolytically. This gives still further control in the precision of the entire inside tone columns of its instruments—for increased resonance and live, powerful tone.

WRITE FOR INFORMATION on how you can obtain a test quantity of "Plus-4" Anodes to supply one tank. Address: The American Brass Company, Waterbury 20, Conn. In Canada: Anaconda American Brass Ltd., New Toronto, Toronto 14, Ontario.   59108

ANACONDA®

"PLUS-4"® ANODES Phosphorized Copper

Made by The American Brass Company

Oxygen Overpotential in Molten Carbonates

George J. Janz, Francisco Colom, and Fumihiko Saegusa

Department of Chemistry, Rensselaer Polytechnic Institute, Troy, New York

ABSTRACT

The overvoltage of the oxygen evolution reaction on Pt electrodes has been measured in a ternary mixture of molten Na_2CO_3-Li_2CO_3-K_2CO_3 with current densities up to 50 ma/cm² and temperatures up to 1000°C. Two well distinguished regions in the overvoltage-log current density relation are observed. At current densities less than 1 ma/cm² the marked dependence of the oxygen overpotential on the composition of the gas flow and on temperature are characteristic of a concentration-type overpotential most probably due to the build-up of oxide-ion in the melt. In the range of about 1-50 ma/cm², the oxygen overpotential seems activation controlled. From the temperature coefficient of the overpotential, a value for the energy of activation for oxygen evolution of 10.4 ± 1.1 kcal mole⁻¹ is obtained. The role of the platinum electrode as an oxygen ion electrode in the over-all process corresponding to the oxygen evolution reaction:

$$CO_3^{-2} \rightarrow CO_2 + O + 2\,\overline{e}$$

is discussed.

Studies of the oxygen overpotential in molten salts have been quite limited. Agar and Bowden (1) have investigated oxygen evolution on Ni and Pt electrodes in fused NaOH up to 340°C, whereas in molten nitrates a study of this process at temperatures up to 250°C has been reported by Karpatscheff and Patzug (2). Some measurements on the oxygen overpotential for sulfates, silicates, phosphates, and carbonates dissolved in fluorides, and for a Na,K/CO₃ mixture at 700°-900°C have been reported by Flood and Forland (3). The present communication describes the results of further measurements of the oxygen overpotential in molten carbonates. A ternary mixture, Li, Na, K/CO₃ (m. 403°C) was used to extend the temperature range for the studies over a much wider range. Platinum was selected for this study since results of emf measurements of oxygen ion activity in Na,K/CO₃ (4) and Na/SO₄,CO₃ (5) mixtures had confirmed that the CO₂-O₂, Pt electrode behaves as an oxygen-ion electrode in these melts.

Experimental

Chemicals.—Sodium, potassium, and lithium carbonates (Reagent Grade) were recrystallized, and dried at 500°C under CO₂ atmosphere. The purified carbonates were stored in a desiccator over P_2O_5 until required for use. In order to extend the measurements to the widest possible temperature range, the ternary mixture (6): 22.8% Li₂CO₃, 27.4% K₂CO₃, and 49.8% Na₂CO₃, m. 403°C was selected for the present investigation. The homogeneous melt of this composition was prepared preliminary to the measurements in a small auxiliary furnace using a CO₂ atmosphere and platinum crucible.

Apparatus.—The experimental assembly, illustrated schematically in Fig. 1, consisted of an electrically heated furnace, B, closed by a water-cooled brass top, A, supporting the ceramic tubes of the thermocouple well, gas delivery tube, and electrode leads, C, E, F, G, respectively, leading to a 20 ml capacity platinum crucible, D, which contained the melt and also served as the cathodic electrode. The latter was supported, as shown, on an alundum base. The anode was a platinum foil of 2 to 4 cm², and the reference electrode was a fine Pt wire placed nearby. A series of alundum disks above the crucible served as baffles to minimize heat losses. Two thermocouples, a Pt-Pt 10% Rh couple observed on a recording controller (L&N Speedomax H) and a chromel-alumel couple observed manually with a potentiometer were placed at the same level close to the cell in the furnace. The electrical circuit was the conventional arrangement for the direct measurement of electrode polarization. The d-c current source consisted of four 45-v batteries in series and
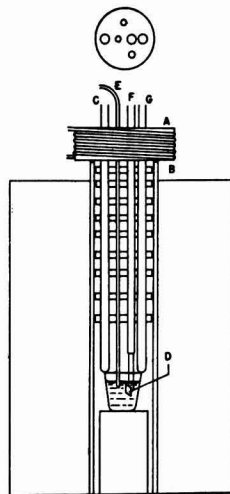
Fig. 1. Experimental assembly for oxygen overpotential measurements in molten carbonates.

Table I. Variation of oxygen overvoltage (η) on platinum with current density (I) in molten Li_2CO_3-Na_2CO_3-K_2CO_3 Mixtures

I, ma/cm²		25	20	15	10	5	3	1	0.5	0.2	0.1	0.05	0.01
mv	A (i)	T, 420°C;		gas flows: (cc/min)		CO_2, 1.5; O; 1.3							
$\eta(i\uparrow)$		420	391	368	333	286	257	226	206	195	177	173	84
$\eta(i\downarrow)$		429	396	368	332	279	245	198	173	154	169	173	—
	A (ii, a, b)	T, 420°C				CO_2, 50; O_2, 42.8							
$\eta \begin{matrix}(i\uparrow)\\(i\downarrow)\end{matrix}$ a		487	458	430	399	339	304	250	224	190	176	162	—
		540	472	472	458	400	358	301	256	212	190	169	143
$\eta \begin{matrix}(i\uparrow)\\(i\downarrow)\end{matrix}$ b		580	540	475	459	415	368	293	260	230	208	190	—
		550	547	534	502	469	440	370	334	285	271	249	155
	B (i)	T, 480°C				CO_2, 4.4; O_2, 3.7							
$\eta(i\uparrow)$		504	484	437	397	327	282	204	168	129	101	83	48
$\eta(i\downarrow)$		445	430	419	382	315	273	197	163	134	108	84	—
	B (ii)	T, 480°C				CO_2, 50; O_2, 42.8							
$\eta(i\uparrow)$		573	540	433	374	321	256	191	162	132	100	70	12
	B (iii)	T, 480°C				O_2, 42.8 alone							
$\eta(i\uparrow)$		—	468	436	394	323	273	189	155	131	119	105	65
	C (i)	T, 515°C				CO_2, 4.4; O_2, 3.7							
$\eta(i\downarrow)$		407	395	376	337	284	238	168	131	105	86	72	45
$\eta(i\uparrow)$		495	473	434	384	308	252	181	144	109	88	72	—
	C (ii)	T, 515°C				CO_2, 50; O_2, 42.8							
$\eta(i\downarrow)$		540	545	497	482	307	254	180	148	115	98	84	49
$\eta(i\uparrow)$		509	462	385	336	287	244	183	156	123	108	88	
	C (iii)	T, 515°C				O_2, 42.8 alone							
$\eta(i\downarrow)$		479	454	408	354	280	221	139	99	69	55	38	10
	C (iv)	T, 515°C				CO_2, 50; O_2, 42.8							
$\eta(i\downarrow)$		484	454	415	348	266	221	160	137	114	98	86	63
$\eta(i\uparrow)$		405	377	354	323	252	210	156	130	107	114	100	—
	D (i)	T, 600°C				CO_2, 4.4; O_2, 3.7							
$\eta(i\downarrow)$		378	348	319	281	240	210	167	150	130	102	72	18
$\eta(i\uparrow)$		346	318	296	262	231	209	193	178	122	93	58	—
	D (ii)	T, 600°C				CO_2, 43; O_2, 37							
$\eta(i\downarrow)$		348	324	298	271	231	201	155	134	111	94	74	32
$\eta(i\uparrow)$		358	335	312	282	238	212	175	152	116	92	69	—
	D (iii)	T, 600°C				CO_2, 50; O_2, 42.8							
$\eta(i\downarrow)$		325	302	274	240	194	167	123	103	81	68	53	22
$\eta(i\uparrow)$		326	310	289	262	219	196	155	125	91	70	53	
	D (iv)	T, 600°C				O_2, 42.8 alone							
$\eta(i\downarrow)$		354	318	288	247	183	148	90	62	30	15	4	—4

Table I (Cont'd)

mv	D (v)	T, 600°C				CO₂, 50; O₂, 42.8							
$\eta(i\downarrow)$		350	329	304	270	213	177	130	108	87	71	52	35
$\eta(i\uparrow)$		361	342	307	276	225	187	136	112	85	65	56	
	E (i)	T, 700°C				CO₂, 43; O₂, 37							
$\eta(i\downarrow)$		304	285	267	235	201	153	107	82	57	41	30	20
$\eta(i\uparrow)$		339	315	289	269	218	173	113	83	54	39	29	
	E (ii, a, b)	T, 700°C				CO₂, 50; O₂, 42.8							
$\eta\ (i\downarrow)$	a	284	262	240	208	163	142	98	73	49	32	22	11
$(i\uparrow)$	a	279	259	238	214	184	158	101	74	45	30	21	—
$\eta\ (i\downarrow)$	b	290	266	240	210	170	143	100	79	52	35	28	18
$(i\uparrow)$	b	294	270	247	218	181	152	96	70	47	33	26	—
	E (iii)	T, 700°C				O₂, 42.8 alone							
$\eta(i\downarrow)$		313	286	259	234	182	142	71	38	8	—8	—12	—16
	F (i, a, b)	T, 800°C				CO₂, 50; O₂, 42.8							
$\eta\ (i\downarrow)$	a	257	233	206	173	137	113	65	42	30	21	13	10
$(i\uparrow)$	a	300	275	233	206	157	120	63	39	23	16	11	
$\eta\ (i\downarrow)$	b	333	316	283	220	159	120	68	48	34	28	25	22
$(i\uparrow)$	b	352	308	260	220	152	113	63	45	32	27	25	
	F (ii)	T, 800°C				O₂, 42.8 alone							
$\eta(i\downarrow)$		315	294	259	220	152	101	25	16	—6	—9	—10	—10
	G (i)	T, 900°C				CO₂, 16; O₂, 13.6							
$\eta\ (i\downarrow)$		246	232	206	164	103	69	33	22	18	15	14	14
$(i\uparrow)$		—	224	178	146	87	56	—	—	—	16	14	—
	G (ii, a, b, c)	T, 900°C				CO₂, 50; O₂, 42.8							
$\eta\ (i\downarrow)$	a	233	224	206	162	101	70	35	26	21	19	17	15
$(i\uparrow)$	a	245	222	196	151	92	63	33	25	18	17	16	—
$\eta\ (i\downarrow)$	b	230	212	188	154	98	69	30	19	13	11	9	9
$(i\uparrow)$	b	230	215	187	149	97	64	29	18	13	13	11	9
$\eta\ (i\downarrow)$	c	278	248	218	173	115	76	35	27	18	15	13	13
$(i\uparrow)$	c	256	241	216	170	107	74	33	25	18	15	13	—
	G (iii)	T, 900°C				O₂, 42.8 alone							
$\eta(i\downarrow)$		286	252	180	134	52	26	7	3	1	0	0	—
	H (i)	T, 1000°C				CO₂, 50; O₂, 42.8							
$\eta\ (i\downarrow)$		217	200	176	121	68	39	8	0	—4	—9.7	—7	—8
$(i\uparrow)$		255	220	170	120	64	35	7	—1	—5	—7	—7	—
	H (ii)	T, 1000°C				No gas flow							
$\eta\ (i\downarrow)$		264	243	230	202	156	120	64	41	25	19	14	11
$(i\uparrow)$		265	250	235	222	156	125	55	34	18	15	13	—

a cascade of variable resistors through which the current was drawn.

The gases, CO_2 and O_2, were bubbled through the melt when measurements were in progress using a gold tube extension on the alundum gas inlet, E. The gases were passed through drying trains con-taining successively silica gel, P_2O_5, and silica gel, monitored on flowmeters, and mixed before entering the melt.

Measurements.—Exploratory measurements with relatively high current densities, 200 ma/cm² showed platinum present in the melts after the ex-

periments (due to attack of the crucible). Small coherent gray particles, presumably platinum, were noted after dissolution of the melt in water after the measurement and the crucible showed attack. Using current densities of 50 ma/cm² and less, no insolubles were noted in the above test after an experiment, and no visible corrosion of the crucible was noticeable. While these observations qualitatively showed that corrosion did not occur to a great extent in the duration of the experiments, the possible formation of surface oxides electrochemically on the platinum anode is not ruled out. To condition the anode, and thus obtain higher reproducibility in measurements, the first measurements in each experiment were made at relatively high temperatures (700°-900°C). Current densities were restricted to an upper limit of 50 ma/cm² in all measurements in view of the above observations relative to corrosion effects.

The results of the measurements for the range 420°-1000°C in the ternary carbonate mixture are summarized in Table I. The resistive potential drop for an electrode separation of 0.1 cm may be estimated as 6 mv maximum at c.d. of 20 ma/cm² from the specific conductivity of molten carbonates at 800°-900°C. The correction may be neglected since the value is less than the limits of accuracy of the measurements. The composition and rate of the gas bubbling through the melt, and the overpotential measurements for the run-up ($i\uparrow$) and run-down ($i\downarrow$) are given, with several checks to illustrate the reproducibility of the results at various current densities. The procedure in general was to apply a high c.d. to the anode initially and subsequently decrease the polarization current gradually to a low value. After the first run-down, the current was increased to its initial value for a check run. Overpotential measurements were made immediately after each current change; a minimum of approximately 10 min was required in each case for the potential to reach constancy. At the temperature limits, 420° and 1000°C, only a few measurements were made.

Results

Analyses of the data summarized in Table I gave a series of curves, of which three are illustrated in Fig. 2 to show the relation between the overpotential, η, and logarithm of current density, log i, in molten carbonates for oxygen evolution. The curves in Fig. 2 were selected to illustrate the results at the three temperatures, 480°, 600°, and 900°C, with the same gas mixture and flow rate in each case. Inspection shows that these curves exhibit two well distinguished regions in each case. At low c.d. (<1 ma/cm²) the overpotential changes with increasing temperatures until the η — log i relation is very nearly parallel to the abscissas (Fig. 2) at the higher temperatures (near 1000°C). In the c.d. range of 1-50 ma/cm² the slope of the η — log i relation is very nearly constant at any one temperature, and shows a smaller temperature dependence in contrast to the preceding region. Temperature coefficients of the overpotential at constant current density $(\partial \eta / \partial T)_i$ from these data are summarized
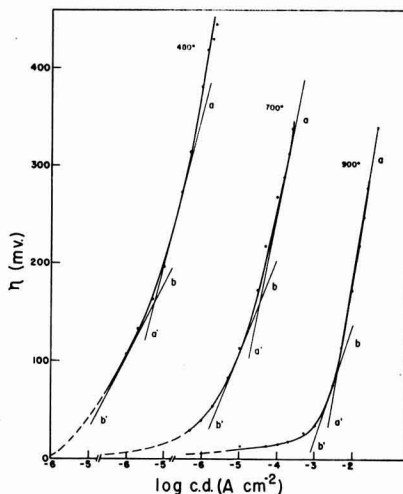
Fig. 2. Oxygen overpotential-current density relations in molten carbonates as a function of temperature. Data are for: A, 480°C; B, 600°C; C, 900°C; and a gas flow in each case of: CO_2, 50 cc/min; O_2, 42.8 cc/min. The lines a-a' and b-b' are theoretical.

in Table II. Inspection of the results shows that for the two temperature ranges, $(\partial \eta / \partial T)_i$ is much less at lower c.d. than at higher c.d., the difference being approximately an order of magnitude.

Since molten carbonates are not chemically inert to O_2 and CO_2, the variations in the rates of flow for the gas mixture bubbling through the melt cannot be interpreted simply as a stirring effect on overpotential. The dependence of η on the gas composition could be checked readily by variation of the CO_2/O_2 ratio in the feed gas. The results at 515°C are illustrated in Fig. 3. It is readily noted that the overpotential is markedly less when the concentration of O_2 in the gas mixture is increased at low c.d. (<1 ma/cm²) whereas it is essentially independent of this variable at higher c.d. (>1 ma/cm²).

At constant overpotential, the temperature dependence of current density may be expressed by:

$$\left(\frac{\partial \ln i}{\partial T} \right)_\eta = \Delta H / RT^2 \qquad [1]$$

The results analyzed accordingly for values of η equal to 0, 200, and 300 mv, where the data for the former were gained by extrapolation, are illustrated in Fig. 4. The slopes of the lines were calculated by the least-squares method. The values for ΔH thus found were 10.4 ±1.1 kcal/mole for $\eta = 0$, and 9.1 ±1.1 kcal/mole for $\eta = 200$ and 300, respectively. The variation in ΔH is less than the probable error and may be taken as constant, i.e., 9-10 kcal/mole in molten carbonates.

Table II. Temperature coefficient of oxygen overpotential in molten carbonates

Temperature range	420°-600°C		600°-1000°C	
c.d. (ma/cm²)	0.05	20	0.05	20
$(\partial \eta / \partial T)_i \times 10^3$ (v/°C)	−0.5	−1.05	−0.06	−0.25
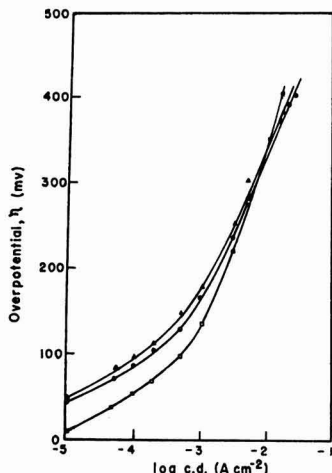
Fig. 3. Oxygen overpotential-current density relation in molten carbonates as a function of gas composition. Composition and flow rates of gas; upper curve, CO_2, 50 cc/min; O_2, 42 cc/min; middle curve, CO_2, 4.4 cc/min; O_2, 3.7 cc/min; lower curve, O_2 only, 42.8 cc/min (measurements at 515°C).

Whereas the melts were white after the experiments in the present investigation, some attack on the Pt with the formation of platinum oxide on the electrode seems not improbable. The data from related experiments having Pt in contact with molten carbonates (6-8) confirm some chemical attack in these basic melts, most probably an oxidation of Pt with simultaneous reduction of the alkali metal oxide species from the thermal dissociation of the molten carbonates.

Discussion

Reference has already been made to the emf studies of the $Pt(O_2)$ electrode in molten Na, K/CO_3 (4) and Na/CO_3, SO_4 (5) mixtures in which measurements confirmed that this electrode really behaves as an oxygen (oxide ion) electrode in such basic melts. In the present investigation the reproducibility of the measurements in the $\eta - i$ cycles, and the reproducible zero overpotential at zero c.d. in each experiment are most readily understood in the function of the $Pt(O_2)$ electrode as an oxygen-ion electrode in carbonate melts.

Relative to this point, the thermal dissociation of the alkali metal carbonates to the corresponding oxide and CO_2 is well established; the most recent investigation in this field being that of Motzfeld (6) for Na_2CO_3 up to 1050°C using the Knudsen effusion technique. While no such measurements have been reported for the ternary carbonate melt, there is little doubt that the carbonates in the mixture dissociate into the oxide ion and CO_2. In the present study it seems most likely that the activity of the oxide ion is given by the expression:

$$a_{0^{-2}} = K \frac{a_{CO_3^{-2}}}{p_{CO_2}} \qquad [2]$$

in accord with the dissociation equilibrium for the carbonates:

$$CO_3^{-2} \leftrightarrows CO_2 + O^{-2} \qquad [3]$$
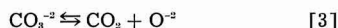
for which both the rate of dissociation and the equilibrium will be functions of the temperature in the conventional manner.

Some information on the nature of the electrode processes contributing to the over-all reaction:

$$CO_3^{-2} \rightarrow CO_2 + O + 2\,\bar{e} \qquad [4]$$
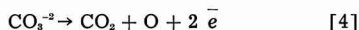
at the anode can be gained from the dependence of the overpotential on current density and temperature.

In general the overpotential is expressed in terms of the logarithm of current density by the following equations:

$$\eta_c = \frac{RT}{n\mathbf{F}} \ln \left(1 - \frac{i}{i_o}\right) \qquad [5]$$

and

$$\eta_a = a - \frac{RT}{n\alpha\mathbf{F}} \ln i \qquad [6]$$

where η_c and η_a are the overpotentials for concentration and activation controlled electrode processes, respectively, and where the latter equation is the well-known Tafel equation. Both types may arise in the present system for, if the carbonate dissociates to form the oxide ion, both (a) the transfer of the oxide ion from the bulk of the solution to the layer of the melt in contact with the anode by migration or diffusion, and (b) the discharge of the oxide ion directly to form atomic oxygen

$$O^{-2} \rightarrow O + 2\bar{e} \qquad [7]$$

or, in view of the probable formation of oxides on the anode surface

$$O^{-2} + M \rightarrow M-O + 2\bar{e} \qquad [8]$$
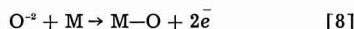
followed by processes such as

$$M-O + M-O \rightarrow M + O_2 \qquad [9]$$
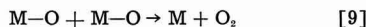
leading to oxygen evolution, undoubtedly are steps in the over-all process.

In the case of activation control [i.e., (b) above] with $\alpha = 0.5$, the slope of the $\eta - \log i$ equation is
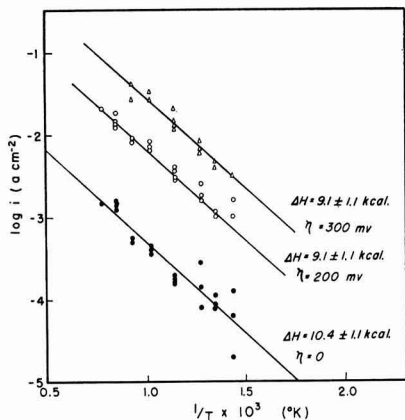
Fig. 4. Temperature dependence of the current density at constant oxygen overpotential in molten carbonates.

$\Delta H = 9.1 \pm 1.1 \ kcal.$
$\eta = 300 \ mv$
$\Delta H = 9.1 \pm 1.1 \ kcal.$
$\eta = 200 \ mv$
$\Delta H = 10.4 \pm 1.1 \ kcal.$
$\eta = 0$

equal to $2.303\ RT/F$ for a two electron transfer in the electrode process (i.e., $n = 2$). For concentration polarization with $n = 2$ in this system, a slope of $2.303\ RT/2F$ is to be predicted. The theoretical slopes for activation and concentration type overpotential, a-a' and b-b', respectively, are shown in Fig. 2.

The temperature coefficient of η at constant current density, from the preceding equations, is given by

$$\left(\frac{\partial \eta_c}{\partial T}\right)_i = \frac{\eta_c}{T} - \frac{RT}{F}\left(\frac{i}{i-i_o}\right)\left(\frac{\partial \ln i_o}{\partial T}\right) \quad [10]$$

and

$$\left(\frac{\partial \eta_a}{\partial T}\right)_i = -\frac{E}{RT^2} \left/ \left(\frac{\partial \ln i}{\partial \eta}\right)_r = -\frac{E}{\alpha FT} \quad [11]\right.$$

Using the value of 9-10 kcal/mole found in the present investigation as the activation energy for anodic oxygen evolution, $(\partial \eta_a/\partial T)_i$ is predicted as approximately equal to -1.0×10^{-3} v/°C in the range 500°-600°C, and -0.6×10^{-3} v in the neighborhood of 1000°C. On the other hand, it has been found for a number of cases that $(\partial \eta_c/\partial T)_i$ is generally less than $(\partial \eta_a/\partial T)_i$ by approximately one order of magnitude. Comparison with the experimental results (Table II) shows that the temperature dependence of η found is consistent with the above concepts in the first approximation.

Some additional support for the above interpretation of the $\eta - \log i$ relations is seen in the effect of the composition of the gas flow on η. The change in the composition of the gas ($CO_2 + O_2$), i.e., the change in p_{O_2}, is related to the oxygen ion activity (refer Eq. [2]). The decrease in η (see Fig. 3) in the region of low c.d. when oxygen only is bubbled through the melt is thus as predicted for concentration rather than activation overpotential in this range. As indicated earlier the present experiments do not lend themselves to check the effect of stirring (by changes in the gas flow rate) since the melt is not chemically inert to the gas used for this purpose. A decreasing importance of the region of concentration polarization at low c.d. would be predicted with increasing temperatures, i.e., enhanced thermal decomposition of the carbonates and thus increased oxide ion activity at more elevated temperatures, in light of the above. This effect is clearly illustrated by the present results (e.g., see Fig. 2).

In summary, the preceding considerations show that the experimental results are more readily understood in accord with the carbonate dissociation-oxide ion scheme rather than through the direct electrochemical oxidation of the carbonate ion, and that the overpotential is in large part the concentration type in the region of low c.d. ($<1\ ma/cm^2$) and the activation type at higher c.d. ($1-50\ ma/cm^2$).

A point that frequently arises in the field of high-temperature chemistry is the need for an estimate or "forecast" of the behavior of systems at higher temperatures, largely owing to the lack of the necessary data for the high-temperature systems. A comparison of the results of the present study with the values found for oxygen evolution on Pt in aqueous electrolytes is thus instructive. In molten carbonates, the value of ΔH, the activation energy for the over-all process in the region of higher current densities from the present results is in the range 9-10 kcal mole^{-1}. In $0.1N$ NaOH, $0.1N$ HNO$_3$, and $0.2N$ H$_2$SO$_4$, the values for the parameter are (9) 13.8 ± 0.6, 18, and 22.1 kcal mole^{-1}, respectively.

Acknowledgments

Any discussion of this paper will appear in a Discussion Section to be published in the June 1961 JOURNAL.

REFERENCES

1. N. N. Agar and F. P. Bowden, *Proc. Roy. Soc.*, **A169**, 206 (1939).
2. S. Karpatscheff and S. Patzug, *Z. physik. Chem.*, **173**, 383 (1935).
3. H. Flood and T. Forland, *Discussions Faraday Soc.*, **1**, 302 (1947).
4. E. Baur and R. Brunner, *Z. Elektrochem.*, **41**, 794 (1935).
5. H. Flood, T. Forland, and K. Motzfeld, *Acta Chem. Scandinav.*, **6**, 252 (1952).
6. K. Motzfeld, *J. Phys. Chem.*, **59**, 139 (1955).
7. D. L. Douglas, Private communication.
8. G. J. Janz and M. R. Lorenz, Unpublished work.
9. J. O'M. Bockris, "Modern Aspects of Electrochemistry," p. 266, Academic Press, Inc., New York (1954.)

Study of the Recuperation
Reaction in the Leclanche Dry Cell

M. P. Korver, R. S. Johnson,[1] and N. C. Cahoon[2]

Research Laboratory, Union Carbide Consumer Products Company,
Division of Union Carbide Corporation, Cleveland, Ohio

ABSTRACT

The cathodic reaction in the Leclanché dry cell has been described previously as consisting of two steps. The first of these steps is the electrochemical reduction Mn^{IV} to Mn^{II}. The second step is the chemical reaction of Mn^{II} produced in the first step with unreacted Mn^{IV} to form an insoluble Mn^{III} compound. Two chemical reactions can occur producing MnOOH and $ZnO \cdot Mn_2O_3$, manganite and hetaerolite, respectively. The latter reactions, termed recuperation reactions, have been subjected to analysis and rate studies to determine the effects of factors such as pH, concentration, and temperature. These reactions are found to be slow enough to limit dry cell operation under certain conditions. The more active depolarizers, such as electrolytic MnO_2, show more rapid recuperation reaction than the natural MnO_2 ore. The basic concepts of heterogeneous chemical kinetics have been applied to this problem, and a simple mathematical equation was found which was applicable to all the data. These findings, correlated with previous results, support the cathodic reaction mechanism theory previously presented.

Progress in dry cell technology for many years was based largely on empirical efforts since only meager fundamental data were available. The reaction,

$$Zn + 2NH_4Cl + 2MnO_2 = ZnCl_2 \cdot 2NH_3 + Mn_2O_3 + H_2O \quad [1]$$

was accepted as representative of the operation of a battery. Early experimental work in this laboratory (1) by French and MacKenzie resolved the cathodic portion of reaction [1] into two separate reactions. The first of these is the electrochemical reduction of Mn^{IV} to Mn^{II}, reaction [2]; the second is the chemical removal of Mn^{II} by further reaction with unused Mn^{IV} to form the Mn^{III} reduction product. From more recent findings (2), it appears that the chemical reactions at the cathode can be represented by two distinct types of chemical processes. Reactions [3] and [4], the "recuperation reactions," involve removal of the Mn^{++} produced by the primary reaction. These can be shown as follows:

$$MnO_2 + 4H^+ + 2e = Mn^{++} + 2H_2O \quad [2]$$

$$MnO_2 + Mn^{++} + 2(OH)^- = 2MnOOH \quad [3]$$

$$MnO_2 + Mn^{++} + 4(OH)^- + Zn^{++} = ZnO \cdot Mn_2O_3 + 2H_2O \quad [4]$$
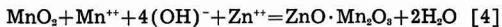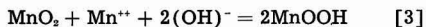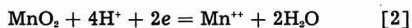
Reaction [2] found an important application in the utilization test (3), a rapid means of evaluating manganese dioxide depolarizers on the laboratory bench. However, certain samples of depolarizers did not perform as well in experimental cells as results of the utilization test had indicated. It was obvious that some other factor limited the service of these particular depolarizers. An important example was

synthetic pyrolusite prepared by the thermal decomposition of manganese nitrate (4). This material gave efficient depolarization in the utilization test, but its effectiveness in experimental cells was substandard. It seemed probable that the rates of the recuperation reactions might be critical for the group of samples. This paper presents the results obtained from a study of several depolarizer samples.

Experimental

To study the reactions between MnO_2 and Mn^{++}, a solution containing manganous chloride is reacted with solid manganese dioxide. The progress of the reaction is followed by observing the decrease in Mn^{++} concentration.

In first attempts to establish a satisfactory method of studying the rate of the recuperation reaction, it was found that an increase in temperature increased the rate of the reaction to such an extent that accurate temperature control in a thermostat became necessary. For example, one depolarizer sample studied at pH 7 was completely reduced to MnOOH at 35°C in about 8% of the time required at 21°C. This finding is in accord with the well-known observation that the electrical output of a dry cell on a standard flashlight test, such as 4 ohm HIF, is increased a considerable amount by an increase in temperature, such as given above, when other factors do not interfere with cell operation. Thus, cell performance at practical temperatures can well be limited by the recuperation reaction rate. Similarly, other factors, such as depolarizer type, electrolyte pH, etc., were found to be as important as the temperature in influencing the reaction rate. From this work, both technique and apparatus were finally selected for precise control of the variables.

In conducting an experiment, approximately one mole of MnO_2 along with one-half liter of 2M NH_4Cl solution is introduced into the reaction vessel, a six-necked, three-liter flask. This mixture is stirred, and high-purity nitrogen is bubbled in for at least an hour. A second flask (serving as a reservoir) in the water bath contains a liter of solution 2M in NH_4Cl and 1.5M in $MnCl_2$. This also has nitrogen bubbled through it to purge the solution of dissolved atmospheric oxygen. The contents of the reservoir flask are allowed to equilibrate with the bath held constant within 0.5° and the pH is adjusted with concentrated NH_4OH to the proper value. The liter of solution is then pumped from the reservoir into the reaction flask by using a small pressure of nitrogen. A calomel half-cell and a glass electrode are suspended in the reaction mixture. These electrodes are connected to a L&N Speedomax recorder-controller which in turn controls an automatic pump. Since in the recuperation reactions hydroxyl ions are consumed, the pump injects a standardized quantity of NH_4OH into the reaction mixture when the pH falls below a predetermined value. By this method, the solution pH is automatically maintained within 0.3 of a pH unit.

During the course of the reaction, small samples of slurry are extracted and immediately centrifuged. The supernatant liquid is then put through a sintered glass filter. A 5 ml portion is retained for analysis. The quantity of Mn^{++} is determined by the method of Lingane and Karplus (5). From these values of concentration and the total volume of solution, the uptake of Mn^{++} can be obtained.

Discussion

It is well known that Mn^{++} reacts with manganese dioxide (6). It is also recognized by others that this reaction is important in the functioning of the dry cell (7). However, physicochemically the reaction has not been too well characterized and there appears to have been no work done on the kinetics of the reaction. Cowley and Walkley (8) have reported some work on this reaction in connection with the cause of the potential drift of manganese dioxide electrodes.

A study (9) has been conducted on the isotopic exchange in the MnO_2-Mn^{II} system. Although it is not definitely stated by Pullman and Haissinsky, the work in this laboratory suggests that they used acid solutions. They concluded that the exchange reactions occur much faster with precipitated oxides than with those prepared by the ignition of $Mn(NO_3)_2$. The latter were of the pyrolusite type.

The recuperation reactions are of a heterogeneous type in which a solid reacts with a solution to form an insoluble product on the surface of the original solid phase. As with all heterogeneous reactions, the problem of diffusion—or mass transfer—of the reactants to the reacting surface—or interface—imposes an additional limitation to the over-all reaction rate. Under certain circumstances, this diffusion may become rate controlling. As the reaction progresses at the solid surface, the surface area of the MnO_2 is diminished progressively. The new solid phase formed on the surface of the original solid can

further significantly retard the diffusion of the reactants toward the reaction zone.

Interpretation of Results

Let Z define the total moles of divalent manganese consumed at any time t (in minutes) per mole of MnO_2 initially present. The moles of MnO_2 present at time $t = 0$ are readily calculated from the weight of the starting material and its "free MnO_2"[3] content, which is obtained by the usual methods of ore analysis. From Eq. [3] and [4], it is obvious that $Z = 1$ when the reaction is completed, provided the process is stoichiometric.

Representative data for electrolytic MnO_2 are shown in Fig. 1. Here Z is plotted as a function of time t (in minutes). During this experiment, the temperature was maintained at $43.95°$ $\pm 0.05°C$ and solution pH held at 5.40 ± 0.15. The experimental data may be represented quite well by the relation:

$$\frac{t}{Z} = \frac{t}{b} + \frac{1}{k} \quad [5]$$

where b and k are constants selected by the conventional method of least squares.

By taking the limit as t approaches zero, it is seen that Z also approaches zero. At the other limit, as t becomes infinitely large, Z approaches b. Thus, b represents the maximum value of Z. If the reaction was stoichiometric and it went to completion, then b would be unity.

By differentiating once and with the proper substitutions, one obtains

$$\frac{dZ}{dt} = k \left(1 - \frac{Z}{b} \right)^2 \quad [6]$$

Clearly, this is the rate expression for the process under conditions of constant temperature and pH, and with a given starting material. The constant k is the specific rate constant and dZ/dt is the instantaneous rate in terms of moles uptake of Mn^{++} per

[3] Free MnO_2 is the amount of MnO_2 in the depolarizer which is available to react electrochemically.
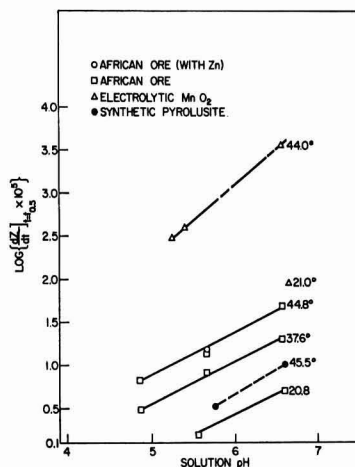

Fig. 1. Relationship of recuperation rate with time for electrolytic MnO_2.

Table I. Reaction rate constants and half-life values for several types of MnO_2

Type of oxide	Temp, °C	Solution pH	b	k	$Log\left\{\left[\dfrac{dZ}{dt}\right]_{t=t_{0.5}} \times 10^5\right\}$
African ore	44.80	6.56	0.755	0.00220	1.679
African ore	37.55	6.56	0.760	0.000926	1.310
African ore	20.90	6.60	0.510	0.000225	0.708
African ore	44.74	5.65	0.702	0.000556	1.140
African ore	37.55	5.65	0.625	0.000333	0.920
African ore	20.65	5.55	0.588	0.0000625	0.188
African ore	44.70	4.85	0.552	0.000272	0.826
African ore	37.55	4.85	0.395	0.000122	0.491
Electrolytic MnO_2	43.95	6.55	1.272	0.142	3.553
Electrolytic MnO_2	43.95	5.40	1.056	0.01613	2.605
Electrolytic MnO_2	43.95	5.25	1.007	0.01163	2.471
Electrolytic MnO_2	20.93	6.65	0.940	0.00741	2.268
Synthetic pyrolusite	45.32	6.60	0.996	0.000426	1.026
Synthetic pyrolusite	45.31	5.75	0.158	0.000133	0.522
Activated MnO_2	38.09	6.60	1.362	0.0263	3.410
Activated MnO_2	20.75	6.55	1.056	0.00400	2.294
Activated MnO_2	37.60	5.73	1.013	0.00833	2.342
Activated MnO_2	20.94	5.68	0.833	0.00120	1.398
Activated MnO_2	45.20	4.90	0.732	0.00152	1.522
Activated MnO_2	38.09	4.86	0.761	0.000435	1.082

mole of MnO_2 initially present per minute. When the reaction is half completed, that is, at the half-life ($t = t_{0.5}$), the instantaneous rate is one-fourth of k. For reasons pointed out later, the half-life rate $\dfrac{dZ}{dt}\Big]_{t\,=\,t_{0.5}}$ is a useful quantity in this study.

In Fig. 1, the t/Z values obtained in this experiment are plotted as a function of t. It is seen that, except for the initial readings, the data conform to a straight line well within the range of the experimental error. From Eq. [6], one sees that for any given finite time there is a finite, single value for the rate. At time zero, the rate is numerically equal to k and as time increases the rate becomes slower. As the time becomes infinitely large, the reaction approaches completion and the reaction rate tends toward zero. Thus, it is seen that Eq. [5] and [6] not only fit the experimental data but also possess the necessary qualities of a rate expression.

Equation [6] shows that the rate is proportional to the square of the fraction of unreacted MnO_2 that is present. The reaction might be considered to be second order with respect to this unreacted portion; however, the order of reaction is of little significance in a system as complex as that of MnO_2.

A number of manganese dioxide samples from different sources has been studied. These have been tested in the temperature range of 21°-45°C and within the solution pH interval of about 4.8-6.6. The values of temperature and pH are those which appear to be comparable to the ones found in actual dry cell testing. Further work showed that Eq. [5] served as the best mathematical representation of the data from experiments using all types of manganese dioxides studied. Thus, the equation has a general application to this kinetics problem.

Reaction rate as a function of temperature.—In Fig. 2, the logarithm of the rate at the half-life is plotted as a function of pH. The lines are isotherms. Starting materials were electrolytic MnO_2, synthetic pyrolusite, and African ore. Values of k, b, and the reaction rates at the half-life for electrolytic MnO_2,

African ore, activated MnO_2 (10), and synthetic pyrolusite appear in Table I. For a given oxide, the vertical distance between the lines gives the change in the logarithm of the rate at the half-life with the change in temperature. Using the well-known Arrhenius equation, $k = se^{-\Delta H_a/RT}$, and the change in the rate with temperature variation, one can evaluate ΔH_a, the apparent energy of activation.

For three of the oxides studied, the values in kilocalories are:

Electrolytic MnO_2	26. ± ? kcal/mole
African ore	17. ± 4 kcal/mole
Activated ore	22. ± 4 kcal/mole

Although only one set of values was available for calculation of the apparent energy of activation of electrolytic MnO_2, the value is presented so that a general order of magnitude for the calculation is available for comparative purposes. The average value of about 20 kcal for the apparent energy of
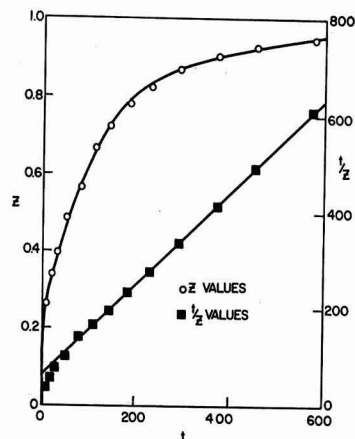

Fig. 2. Logarithm of the reaction rate as a function of temperature and solution pH.

activation confirms that the fundamental reaction involved is not under diffusion control (11).

It is likely that the lower the energy of activation, the more rapid is the reaction. On this basis, African ore, for which the lowest value is presented, should be the most active depolarizer. However, actual test and battery performance show African ore to possess the lowest recuperation reaction rate of this group of depolarizers. Therefore, we must conclude that the value of s in the Arrhenius equation, concerned with such factors as depolarizer surface area, crystal type and structure, particle size, etc., is important in influencing the recuperation reaction rates.

Reaction rate as a function of solution pH.—If one assumes a linear relationship and the fact that pH involves the logarithm of the hydrogen ion activity, one can show that

$$\frac{dZ}{dt}\bigg]_{t\,=\,t_{0.5}} = K(OH^-)^m \qquad [7]$$

where K is a constant, m is the slope of the straight lines in Fig. 2 and (OH^-) is the hydroxyl ion concentration. Theoretically, the above would be correct for only one temperature and at constant mean ion activity coefficient. However, with the narrow temperature and pH ranges, Eq. [7] is no doubt a close approximation. The slopes of the lines for African ore are 0.49 ± 0.01.

If the hydroxyl ion concentration in the bulk of the solution were the important factor, then from the chemical reaction, Eq. [3], one could suggest that the rate should be proportional to the square of the hydroxyl ion concentration. The data show that this is not the case. What is important is the concentration of the hydroxyl ions in the immediate vicinity—no doubt sorbed on the surface—of the MnO_2 particles. The concentration on the surface is, of course, influenced by the concentration in the bulk of the solution. This phenomenon of preferential ion adsorption is well recognized.

Reaction rate as a function of stirring speed.— With the particular experimental setup, it was found that changing the stirring speed from 480 to 390 rpm had no appreciable effect on the reaction rate. These values represent the useful range with the present apparatus. At stirring speeds below 390 rpm, the solid phase tends to form a mass in the bottom of the reaction vessel and hence is removed from the reaction system. With the plastic stirrer and the all-glass reaction vessel, it seemed unwise to increase the stirring speed much above 480 rpm. With this limited range of stirring speeds, however, it is doubtful whether the boundary regions of the particle would be changed and the diffusion varied to any extent.

Reaction rate as a function of oxide type.—A comparison of the reaction rates for the different oxides and the logarithm of the rate of recuperation reaction at the half-life (under conditions of 21°C and a solution pH of 6.5) are shown in Table II. As would be expected, a correlation exists between reaction rate and the general order of dry cell performance. In spite of the fact that there is a cor-

Table II. Reaction rate of representative MnO_2 samples at the half-life

Type of MnO_2	$Log\left\{\dfrac{dZ}{dt}\bigg]_{t\,=\,t_{0.5}} \times 10^3\right\}$
Activated ore	2.38
African ore	0.660
Synthetic pyrolusite	0.013
Electrolytic MnO_2	2.13

relation, the true relationship between "rate" and "service" is no doubt complicated. On this account, it is considered unwise to attempt to predict the battery quality of manganese dioxide from recuperation rate measurements alone.

Reaction Mechanism

A plausible mechanism for this topochemical process has been proposed. In the absence of zinc, the chemical reaction is described by Eq. [3]. Before the reaction can occur, the reducing agent (Mn^{++}) and hydroxyl ions must first be adsorbed on the surface. After adsorption, the reduction of the MnO_2 occurs. At the site of reaction, a layer of Mn^{+++} oxide is formed. The x-ray diffraction pattern shows that this product is isostructural with the mineral manganite, $MnOOH$. Half of the mass of the material is formed by the reduction of the MnO_2 and the other half is produced by oxidation of the adsorbed Mn^{++}. A microscopic examination of the particles taking part in the reaction shows that the particles have actually increased in size. All four samples studied had approximately the same particle surface area of 0.20–0.50 m^2/g, even though the screen analysis showed differences in the per cent through the 200 mesh screen. Particle surface area is the term given to the total external area of all of the particles in a 1-gram sample and is calculated from settling rate curves.

At first, the MnO_2 particles are adjacent to the solution phase and the reaction goes fairly rapidly. Once the reaction has been initiated, the MnO_2 is separated from the adsorbed reactants by a layer, or film, of $MnOOH$. This layer offers a resistance to the reaction and the rate is slowed down. It has been shown that the rate is proportional to the second power of the fraction of remaining, unreacted MnO_2.

The reduction of the MnO_2 could be accomplished by the migration of hydrogen ions and electrons across the manganite barrier, going from the outermost surface toward the unreacted MnO_2. This process of an ion migration in manganese oxides has been recognized previously (12). These adsorbed divalent manganese ions lose an electron. They are thus oxidized to the trivalent state and are immediately precipitated as $MnOOH$. Under most conditions, the trivalent manganese ion is unstable.

The various oxides obey the same rate equation and they have the same characteristics, such as apparent energy of activation, of the same order of magnitude. It is thus concluded that all of these manganese dioxides react through the same mechanism. The slowest rate was that displayed by syn-

thetic pyrolusite. This can be attributed to the fact that pyrolusite has a lower oxidation potential than a more reactive form, such as electrolytic MnO_2. This so-called recuperation reaction is an oxidation-reduction process. The MnO_2 is the oxidizing agent and the divalent manganese is the reducing agent.

When zinc is present in solution as dissolved zinc chloride, the resultant reaction product is hetaerolite ($ZnO \cdot Mn_2O_3$) rather than manganite. It is probable that the zinc occurs in the solid phase by virtue of a coprecipitation process along with the Mn^{++} that becomes oxidized and precipitated. When the reaction product is hetaerolite, the reaction rate is about the same as in the absence of zinc. An example of this is shown in Fig. 2. It is highly possible that the hydrogen ions and electrons migrate more rapidly through a hetaerolite layer than through a barrier of manganite. It is conceivable that this by-product layer on the surface of the manganese dioxide particle could constitute a barrier to prevent the completion of the recuperation reaction. If this were true, it should result in a change in the slope of the observed reaction rate. At this time, we have seen no evidence for such interference.

REFERENCES

1. H. F. French and A. A. MacKenzie, Unpublished work.
2. N. C. Cahoon, R. S. Johnson, and M. P. Korver, *This Journal*, **105**, 296 (1958).
3. N. C. Cahoon, *ibid.*, **99**, 343 (1952).
4. M. L. Kaplan, U. S. Pat. 1,287,041 (1917).
5. J. J. Lingane and R. Karplus, *Anal. Chem.*, **18**, 191 (1946).
6. W. Feitknecht and W. Marti, *Helv. Chim. Acta*, **28**, 129 (1945); O. T. Christensen, *Z. Anorg. Chem.*, **27**, 321 (1901).
7. H. F. McMurdie, P. N. Craig, and G. W. Vinal, *Trans. Electrochem. Soc.*, **90**, 509 (1946).
8. J. M. Cowley and A. Walkley, *Nature*, **161**, 173 (1948).
9. B. Pullman and M. Haissinsky, *J. Phys. Radium*, **8**, 36 (1947).
10. C. F. Burgess, U. S. Pat. 1,305, 250, June 3, 1919.
11. S. Glasstone, K. J. Laidler, and H. Eyring, "The Theory of Rate Processes" McGraw-Hill Book Co., Inc., New York and London (1941).
12. H. Strung, *Naturwiss.*, **78**, 89 (1943).

The Nitric-Hydrofluoric Acid Pickling of Zircaloy-2

M. A. DeCrescente,[1] P. F. Santoro, A. S. Powell, and R. H. Gale

Materials Development Laboratory, Nuclear Division, Combustion Engineering, Inc., Windsor, Connecticut

ABSTRACT

The dissolution of Zircaloy-2 has been studied in the temperature range 15.6°-37.8°C in unagitated and agitated hydrofluoric-nitric acid solutions. The dissolution rate was found to increase with HF concentration and agitation. The energy of activation for the Zircaloy-2 pickling process compares very well with the value for the unalloyed zirconium pickling process, 3.3 kcal/mole. The energy of activation does not depend on agitation.

Smith and Hill (1) studied the rate of dissolution of unalloyed zirconium in hydrofluoric-nitric acid mixtures using Zr^{95} as a radioactive tracer. They reported an energy of activation of 3.3 kcal/mole for the process. The pickling of Zircaloy-2 (1.45 w/o Sn, 0.133 w/o Fe, 0.044 w/o Ni, 0.08 w/o Cr) was studied by Friedl, et al. (2) in order to determine the safe limits of pickling bath operation. A value of 5.0 kcal/mole for the energy of activation was calculated from a temperature-dissolution rate study. Friedl postulated that (a) the differences in agitation used in the two studies may account for the observed differences in the temperature dependency of the dissolution rate, or (b) a real difference in the energy of activation existed. In the study carried out by Hill and Smith, the pickling rate of zirconium increased with stirring rate up to a point beyond which the rate remained constant. Their experiments were carried out on the "flat" part of the pickling rate-stirring rate curve. The pickling investigation by Friedl on Zircaloy-2 was carried out at a constant stirring rate, 100 rpm, presumably on the sloping part of the pickling rate-stirring rate curve.

stirring rate curve. Both investigators agree that un-ionized hydrofluoric acid is the active etchant.

The work of Smith and Hill has established that the dissolution of zirconium is HF diffusion controlled and not adsorption or reaction controlled. The high energy of activation obtained by Friedl, if real and independent of agitation, would indicate that the alloying elements have provided a diffusion barrier less permeable to the HF. The work reported here was initiated (a) to resolve the effect of alloying constituents in the pickling of Zircaloy-2 and (b) to explain the variable results encountered in production pickling. The effect of hydrofluoric acid concentration, temperature, and agitation on the pickling of Zircaloy-2 in HF-HNO$_3$ mixture would be determined for this purpose.

Experimental

Vapor blasted reactor grade Zircaloy-2 specimens were degreased with ethyl alcohol, washed with a synthetic detergent, rinsed with demineralized water, and stored in a vacuum desiccator. The pickling was carried out in a 1-liter polyethylene beaker immersed in a constant temperature water bath

[1] Present address: CANEL, Middletown, Connecticut.

Table I. Pickling rates of Zircaloy-2 in unagitated solutions

Run[*]	°C	$\frac{1}{T°K} \times 10^3$	Vol % HF	Molarity[HF]	Pickling rate, mils/min	Pickling rate/[HF], mils/min
1	15.6	3.46	2.5	0.69	0.280	0.404
2	15.6	3.46	3.0	0.83	0.325	0.398
3	15.6	3.46	3.5	0.97	0.400	0.408
4	15.6	3.46	4.0	1.11	0.451	0.405
5	21.1	3.40	2.5	0.69	0.304	0.447
6	21.1	3.40	3.0	0.83	0.364	0.446
7	21.1	3.40	3.5	0.97	0.451	0.452
8	21.1	3.40	4.0	1.11	0.493	0.450
9	26.7	3.34	2.5	0.69	0.307	0.491
10	26.7	3.34	3.0	0.83	0.367	0.494
11	26.7	3.34	3.5	0.97	0.469	0.496
12	26.7	3.34	4.0	1.11	0.544	0.495
13	32.2	3.28	2.5	0.69	0.349	0.534
14	32.2	3.28	3.0	0.83	0.445	0.543
15	32.2	3.28	3.5	0.97	0.532	0.542
16	32.2	3.28	4.0	1.11	0.574	0.541
17	37.8	3.22	2.5	0.69	0.400	0.577
18	37.8	3.22	3.0	0.83	0.490	0.590
19	37.8	3.22	3.5	0.97	0.514	0.583
20	37.8	3.22	4.0	1.11	0.643	0.585

[*] Area = 0.0975 dm².

($\pm 0.1°C$). A preliminary study showed that the pickling rate was independent of area and vapor blast pretreatment (3). The temperature of the pickling solution was measured with a paraffin-coated thermometer. All specimens were pickled for 2 min in 700 ml of fresh solution prepared from C.P. reagents and deionized water just prior to use, rinsed 4 min, dried and stored in a vacuum desiccator until weight changes were determined.

Initially, the pickling was carried out in unagitated solutions (runs 1-20). In order to minimize local concentration and temperature effects, subsequent tests were carried out in solution, agitated by means of a polyethylene stirrer (Runs 27-32). Dissolution rates were measured over the hydrofluoric acid (Baker and Adamson reagent grade, 40 w/o) concentration range, 2.5 to 4.0 v/o. Forty v/o nitric acid (Baker Analyzed reagent grade, 70 w/o) was used in each case. These concentrations represent the composition of standard zirconium production pickling solution (2).

Results

Dissolution of Zircaloy-2 in unagitated solution.— Pickling rates were determined by measuring the change in weight of a Zircaloy-2 specimen after 2-min exposures to pickling solutions freshly prepared for each determination. Table I contains the pickling rates of Zircaloy-2 in unagitated HF-HNO₃ solutions.

The observed rates plotted against HF concentrations (40 v/o HNO₃) at 15.6°, 21.1°, 26.7°, 32.2°, and 37.8°C gave straight lines through the data.

Effect of agitation on pickling.—The dissolution of Zircaloy-2 in 3.5% HF-40% HNO₃ was studied at 21.7°C (71°F) at a series of stirring rates. A plot of these data appears in Fig. 1. The increase in pickling rate with stirring is characteristic of a diffusion-controlled mechanism.

A series of experiments were carried out in 3.5% HF-40% HNO₃ at a stirring rate of 500 rpm in order

to determine if local temperature and concentration effects have any influence on the temperature dependence of the pickling rate.

The influence of agitation on the observed pickling rates can be explained as follows:

As the dissolution reaction proceeds, the concentration of reactants immediately surrounding the specimen in an unstirred solution may decrease below the bulk concentration, especially if the rate of diffusion of reactants to the specimen's surface is low. An apparent decrease in pickling rate results. Mixing serves to remove any concentration gradients which may be found. Also the temperature of the solution at the metal surface may increase above the bulk temperature if the heat of reaction is not effectively dissipated. An apparent increase in the pickling rate results. Although the two effects, diffusion and temperature, counterbalance each other it can be seen by comparison of the pickling rates in unagitated solution (Table I) to the rates in agitated solution that the temperature effect is the more important of the two. Mixing facilitates dis-
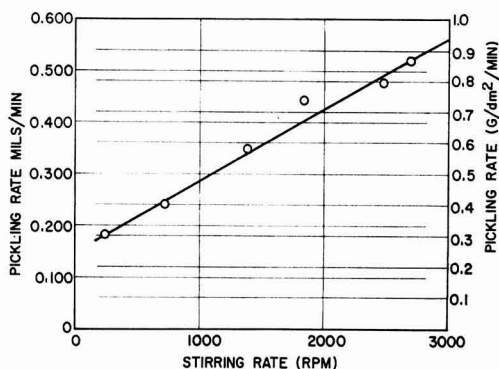
Fig. 1. Effect of agitation on pickling rate at 21.7°C
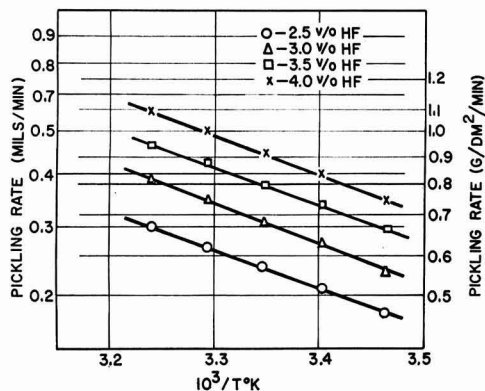
Fig. 2. Log of pickling rate vs. 1/T°K at 2.5, 3.0, 3.5, and 4.0 v/o HF, unagitated. Θ = 2.5 v/o HF; $\triangle$ = 3.0 v/o HF; $\square$ = 3.5 v/o HF; X = 4.0 v/o HF.
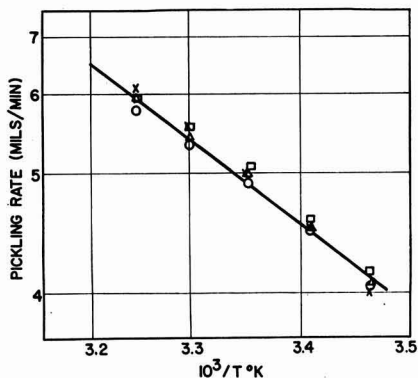
Fig. 3. Pickling rate per mole of HF, [pickling rate]/[HF] vs. 1/T°K, unagitated.

sipation of the heat of reaction and provides a uniform temperature throughout the bath.

Kinetic treatment.—A plot of pickling rate (mils/min) at 2.5, 3.0, 3.5, and 4.0% (unagitated solution) vs. reciprocal absolute temperature yielded straight lines (Fig. 2). Very close agreement of the slopes was observed and a value of 3.3 kcal/mole for the energy of activation of the pickling process resulted.

v/o HF	2.5	3.0	3.5	4.0
E_{act} (kcal/mole)	3.2	3.4	3.2	3.4

Under conditions of high acidity (HNO₃), all of the fluoride present exists as undissociated HF. The rate data obtained, therefore, were recalculated on the basis of HF concentrations, i.e., rate/[HF], and log rate/[HF] plotted against 1/T°K (Fig. 3). The four lines in Fig. 2 are resolved into one straight line. This behavior indicates that the rate of pickling of Zircaloy-2 is dependent only on the concentration of undissociated HF at constant tempera-
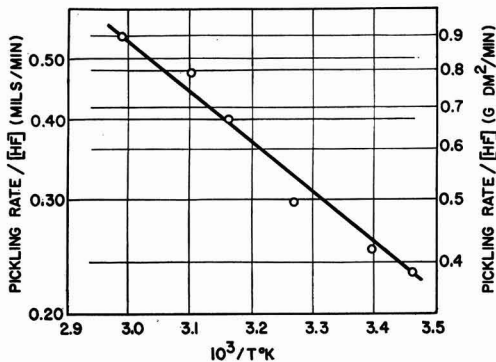
Fig. 4. Pickling rate vs. 1/T°K agitated

tures. Nitric acid does not directly take part in the pickling reaction but its presence insures complete association of HF.

When an Arrhenius plot was prepared from the pickling data obtained using agitated baths (500 rpm), an energy of activation of 3.6 kcal/mole resulted (Fig. 4). The agreement between the activation energies in the agitated and unagitated solutions is well within experimental error. It is evident from this agreement that the heat of reaction and the thermal properties, e.g., heat capacity, of the solution remain constant within experimental error in the temperature range studied.

The experimental energy of activation for the Zircaloy-2 pickling process, 3.2-3.6 kcal/mole, agrees quite favorably with the results of Smith and Hill (3.3 kcal/mole) obtained with pure Hf-free zirconium. A diffusion process identical to the one described for unalloyed zirconium must be postulated as the rate-controlling step.

It is apparent therefore that alloying zirconium with Sn, Fe, Cr, Ni does not alter the zirconium pickling mechanism. The permeability of the diffusion layer to HF is not affected by alloying. Neither can the high energy of activation observed by Friedl be attributed to the effect of stirring. It is interesting to note that the Zircaloy-2 used by Friedl had been rejected for pressurized water-reactor application because of stringer-like corrosion. The discrepancy in the energy of activation observed by Friedl *et al.* may be related to the stringer corrosion susceptibility of the material.

REFERENCES

1. T. Smith and G. R. Hill, *This Journal*, **105**, 117 (1958).
2. E. B. Friedl, W. E. Berry, P. D. Miller, and F. W. Fink, BMI-1270, June 1958.
3. A. S. Powell and M. A. DeCrescente, Unpublished results.

Hydrogen Pickup in Various Zirconium Alloys during Corrosion Exposure in High-Temperature Water and Steam

Stanley Kass

Bettis Atomic Power Laboratory, Westinghouse Electric Corporation, Pittsburgh, Pennsylvania

ABSTRACT

The hydrogen pickup during corrosion in high-temperature water and steam of various binary and ternary alloys of zirconium with iron and tin has been studied. The total hydrogen content of specimens exposed to 400°C steam was found to be greater than that of specimens exposed to 360°C water. Furthermore, the per cent of theoretical hydrogen absorbed in the various alloys was markedly affected by the binary or ternary alloy addition. The per cent theoretical hydrogen absorbed by binary zirconium-iron alloys increased as the iron content was increased from 0.3 to 1.5 weight per cent (w/o) and the value for zirconium-tin alloys increased slightly as tin was increased from 0.5 to 0.9 w/o. The hydrogen pickup behavior of ternary zirconium-tin-iron alloys reflected the behavior of zirconium-iron binary alloys.

Several facts relating to the hydrogen pickup of zirconium alloys during corrosion in high-temperature water are known. Goldman and Thomas observed the amount of hydrogen pickup by zirconium exposed to degassed water is proportional to the amount of corrosion, and when corrosion testing is carried out in hydrogenated water, more hydrogen is picked up than when the corrosion medium is degassed water (1). The latter is believed to occur because more hydrogen is available for reaction in the hydrogenated water than is available only from the stoichiometric amount produced during the corrosion processes. Goldman and Thomas also noted that higher corrosion rates and higher hydrogen pickup rates occur in Zircaloy-2 as the initial hydrogen content of the metal is increased. Recently, workers at Battelle Memorial Institute, Columbus, Ohio, confirmed the observation that the amount of hydrogen pickup is proportional to the amount of corrosion (2). Previously reported experiments by Thomas and Kass showed that pre-oxidation of Zircaloy-2 in dry oxygen at 400°C has no effect on the 400°C steam corrosion kinetics (3). The interchangeability of the corrosion data obtained in both dry oxygen and steam indicates that the corrosion of Zircaloy-2 in 400°C steam is not associated with corrosion product hydrogen. On the other hand, it was observed that crystal bar zirconium exhibits spalling (breakaway) in high-temperature steam but not in dry oxygen, suggesting that hydrogen is in some way related to "breakaway" in the corrosion of zirconium.

Recent studies have determined the hydrogen pickup in Zircaloy-2 during corrosion for extended periods in high-temperature water and steam (4). These studies show there is a definite increase in the hydrogen content of Zircaloy-2 during corrosion testing and this hydrogen increase is independent of the initial hydrogen content, up to about 1000 ppm, after which the rate of hydrogen uptake rises sharply with increasing initial hydrogen content.

The studies described below were undertaken to determine hydrogen pickup in various binary and ternary alloys of zirconium with iron and tin during corrosion exposure in 360°C (680°F) water and 400°C (750°F) steam.

Experimental Procedures

Materials.—Fifteen-pound ingots were double arc-melted from high-purity tin, iron, and reactor-grade sponge zirconium[1] at the Bureau of Mines, Albany, Oregon. The ingots were forged and rolled at 788°C (1450°F) to 0.190-in. strip and then cold rolled with intermittent vacuum anneals at 788°C to 0.017-in. strip.

Experimental techniques.—Foils 1.5 x 4 x 0.017 in. were bright etched in an aqueous solution containing 39% HNO_3 and 3.5% HF at 100°F for sufficient time to remove 0.001 in. per surface. After washing and soaking in tap water for 6 to 8 hr to remove all residual etchant, the foils were rinsed in alcohol and air dried. Four foils from each ingot were degassed at 800°C for 48 to 72 hr in vacuum (less than 10^{-6} mm Hg). After degassing, the 1.5 x 4 x 0.015-in. foils were sheared into 0.5 x 0.5 x 0.015-in. specimens and submitted to corrosion tests in 360°C water at saturation pressure and in 400°C steam at 100 atm using methods and precautions outlined previously (5, 6). Weight gain measurements were made periodically. A minimum of two specimens per alloy were removed periodically from the corrosion test and were analyzed for hydrogen using the hot vacuum extraction method.

Experimental Results and Discussion

Tables I and II show the corrosion weight gains and total hydrogen contents of the various alloys after each of the exposure periods. (The contribution of the hydrogen uptake to the weight gain has been regarded as negligible; thus the weight gain

[1] Arc-melted reactor grade zirconium contains approximately 300 ppm iron, 20 ppm chromium, 20 ppm nickel, <10 ppm tin, <40 ppm nitrogen.

Table I. 360°C water test results

Alloy		Days of test						
		28	56	84	112	140	169	197
Zr	Weight gain, mg/dm²	10	23	64	121	165	210	277
	Hydrogen content, ppm	16	25	151	264	416	735	970
	% Theoretical H₂	19	21	23	31	50	40	47
Zr + 0.29% Fe	Weight gain, mg/dm²	15	25	24	42	42	52	76
	Hydrogen content, ppm	70	79	89	191	227	264	322
	% Theoretical H₂	32	26	34	50	55	53	49
Zr + 0.51% Sn	Weight gain, mg/dm²	10	19	24	36	61	80	158
	Hydrogen content, ppm	14	13	16	28	194	247	368
	% Theoretical H₂	8	5	5	7	20	21	21
Zr + 0.88% Sn	Weight gain, mg/dm²	9	21	81	139	188	234	298
	Hydrogen content, ppm	17	19	177	505	537		738
	% Theoretical H₂	30	9	21	28	22		26
Zr + 0.93% Sn 0.25% Fe	Weight gain, mg/dm²	11	21	18	28	38	47	55
	Hydrogen content, ppm	50	69	67	98	139	161	203
	% Theoretical H₃	32	25	46	34	39	39	38
Zr + 1.54% Fe	Weight gain, mg/dm²	20	37	36	61	68	74	87
	Hydrogen content, ppm	233	173	310	393	502	509	833
	% Theoretical H₂	80	54	88	69	72	71	101
Zr + 0.50% Sn 1.54% Fe	Weight gain, mg/dm²	21	42	42	58	70	78	91
	Hydrogen content, ppm	249	266	341	544	570	583	740
	% Theoretical H₂	96	65	74	84	79	63	74

value is considered being due solely to oxide film formation.) The tables contain an additional entry, per cent theoretical hydrogen which is defined as the ratio of hydrogen pickup in the sample to the stoichiometric amount of hydrogen produced by the corrosion reaction, $Zr + 2H_2O = ZrO_2 + 4H$.

Corrosion behavior.—Maximum corrosion resistance in 360°C water was shown only by the alloys which contain iron as binary or ternary additions. The unalloyed zirconium samples gained weight throughout the test and exhibited adherent oxide

films. The addition of 0.5% tin to zirconium resulted in lower weight gains, but the 0.88% tin alloy yielded weight gains higher than unalloyed zirconium. The two iron binary alloys demonstrated an improvement in corrosion resistance. Furthermore, iron additions greatly improved the corrosion properties of zirconium-tin alloys.

The steam data further verified the noncorrosion resistant nature of unalloyed zirconium and zirconium-tin alloys. The addition of 0.5% tin delayed spalling from 42 to 56 days, but the 0.88% tin alloy

Table II. 400°C steam test results

Alloy		Days of test							
		14	28	42	56	70	84	98	112
Zr	Weight gain, mg/dm²	58	80	Spalled					
	Hydrogen content, ppm	186	630						
	% Theoretical H₂	46	87						
Zr + 0.29% Fe	Weight gain, mg/dm²	19	25	34	43	67	72	67	71
	Hydrogen content, ppm	92	133	125	128	209	181	194	
	% Theoretical H₂	54	51	38	29	28	22	28	
Zr + 0.51% Sn	Weight gain, mg/dm²	43	125	129	Spalled				
	Hydrogen content, ppm	184	547	747					
	% Theoretical H₂	36	45	38					
Zr + 0.88% Sn	Weight gain, mg/dm²	346	Spalled						
	Hydrogen content, ppm	760							
	% Theoretical H₂	24							
Zr + 0.93% Zn 0.25% Fe	Weight gain, mg/dm²	18	29	44	53	82	83	84	86
	Hydrogen content, ppm	85	151	151	178	204	205	205	
	% Theoretical H₂	47	43	32	34	25	25	26	
Zr + 1.54% Fe	Weight gain, mg/dm²	33	43	58	79	Spalled			
	Hydrogen content, ppm	258	354	402	418				
	% Theoretical H₂	82	79	80	57				
Zr + 0.50% Sn 1.54% Fe	Weight gain, mg/dm²	32	40	63	78	114	Spalled		
	Hydrogen content, ppm	320	433	460	504	758			
	% Theoretical H₄	82	92	70	56	50			

spalled between 14 and 28 days exposure. Small additions of iron were again observed to produce corrosion resistant material; however, the 1.5% iron alloy failed by spalling after 56 days of exposure. Beneficial effects on the properties of zirconium-tin alloys were also observed to occur with iron additions. The 0.25% iron alloy, with or without tin, exhibited the best corrosion resistance.

Hydrogen contents.—The total hydrogen contents of the various alloys are noted to increase with increasing corrosion exposure, and higher hydrogen uptakes are obtained at 400°C than at 360°C. (It should be noted that all specimens were initially degassed to approximately 2 ppm hydrogen.) In water, the unalloyed zirconium is seen to pick up the largest amount of hydrogen while the 0.93% tin-0.25% iron alloy exhibited the lowest total hydrogen content. In steam, very high hydrogen uptakes are noted. The addition of 0.5% tin produced essentially no change in the hydrogen pickup of unalloyed zirconium, but the 0.88% tin alloy showed a higher hydrogen uptake. Small additions of iron to zirconium or zirconium-tin alloys produced markedly lower total hydrogen contents. It is also noted that the hydrogen uptake of zirconium-iron alloys increases with increasing iron content.

Relationship between corrosion and hydrogen uptake.—Examination of the hydrogen pickup of the zirconium alloys during aqueous corrosion shows that there is an initial period in which the rate of hydrogen pickup decreases with time, followed by a period in which a new rate operates. This behavior is consistent with the corrosion reaction of zirconium and its alloys (hence, with the rate at which the hydrogen is produced) which is characterized by the relationship $W = kt^n$. It does not necessarily follow, however, that the hydrogen should be picked up at an identical rate because the hydrogen pickup process depends on many other variables including nature of the original film, alloy content and distribution, concentration gradient of hydrogen from the metal oxide interface to the center, rate of hydrogen diffusion at testing temperature.

If the 360°C weight change and hydrogen content data are plotted as functions of time on logarithmic scales, reasonably straight lines with the following slopes are obtained:

Alloy	Weight gain slope	Hydrogen slope
Unalloyed Zr	1.76	2.10
0.51% Sn	0.85 then 2.32	0.22 then 3.92
0.88% Sn	1.63	1.89
0.29% Fe	0.40 then 1.32	0.20 then 0.88
1.54% Fe	0.77	1.19
0.93% Sn + 0.25% Fe	0.45 then 0.55	0.35 then 1.34
0.50% Sn + 1.54% Fe	0.78	0.84

The corrosion slopes represent the exponent "n" in the equation relating weight gain and time. Thus, only the iron bearing alloys are seen to be corrosion resistant in 360°C water. High hydrogen slopes are associated with high corrosion slopes, indicating a relationship between corrosion and hydrogen pickup. If the hydrogen uptake behavior follows an exponential rate law, then equations of the form $H =$

Kt^{n^1}, where n^1 is the hydrogen slope, are to be expected. Remarkable similarity between the values of n and n^1 for each of the alloys is observed.

If it is assumed that the diffusion of hydrogen is a controlling step in hydrogen buildup, then parabolic relationship between hydrogen content and time is to be expected. A slope of 0.5, which indicates parabolic behavior, does not appear in these instances.

When the hydrogen data of the corrosion resistant alloys (those containing iron) are reviewed, it is apparent that the increase during the initial exposure period is great, then the hydrogen increase becomes smaller. The fact that hydrogen pickup decreases after the first exposure period requires an explanation. One possible mechanism is that the oxide film acts, in some way, as a barrier to the diffusion of hydrogen ions, protons, hydroxyl ions, to the metal-oxide interface. This suggests that the hydrogen pickup of samples oxidized in a nonhydrogenating medium subsequently transferred to a hydrogen producing medium should not show large increases in hydrogen content.

Factors influencing the behavior of ternary alloys.—The following analysis and comparisons were made in an attempt to observe whether the behavior in water and steam with respect to hydrogen pickup of the ternary alloys is directly influenced by the behavior of the component binary alloys. A more convenient way of examining the hydrogen absorption phenomenon during aqueous corrosion exposure is to express the amount of hydrogen picked up by the specimens as a function of the amount of hydrogen liberated by the specimens during corrosion. In this manner differences in the corrosion resistance of the alloys under study can be normalized.

Figures 1 and 2 summarize the behavior of the per cent theoretical hydrogen of the zirconium-tin and zirconium-iron binary alloys in 360°C water. The curve pertaining to the tin alloys initially shows a minimal value at approximately 0.5% tin. After prolonged exposure (greater than 112 days), no differences are observed between the 0.5 and 0.9% alloy. Different behavior is noted for the effect of iron. The per cent theoretical hydrogen increases with increasing iron concentration. It is thus apparent that iron contributes to the pickup of hydro-
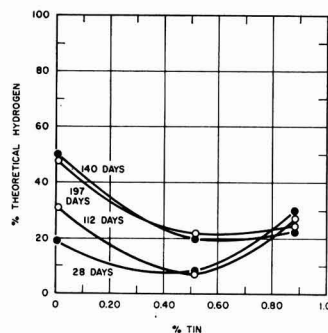
Fig. 1. Hydrogen pickup of zirconium-tin alloys in 360°C water.
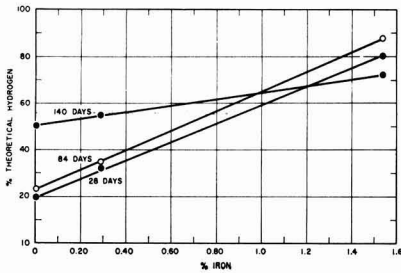
Fig. 2. Hydrogen pickup of zirconium-iron alloys in 360°C water.
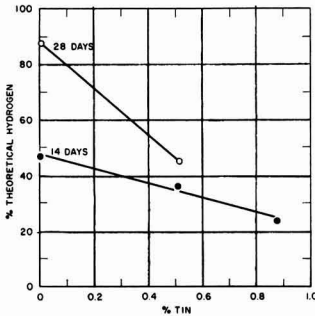
Fig. 3. Hydrogen pickup of zirconium-tin alloys in 400°C steam.
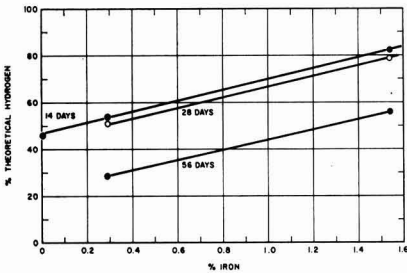
Fig. 4. Hydrogen pickup of zirconium-iron alloys in 400°C steam.

gen during water corrosion while the influence of tin is slight.

Figures 3 and 4 show the same alloys after exposure to 400°C steam. Although the data are very limited because of the low corrosion resistance of binary tin alloys, the per cent theoretical hydrogen is indicated to decrease with increasing tin content. The iron containing alloys show an increase in per cent theoretical hydrogen as the iron content is increased from 0.29 to 1.5 w/o. The higher iron concentration reproducibility exhibited higher per cent theoretical hydrogen after all test periods than the low iron alloy.

The manner in which the per cent of theoretical hydrogen varies with time for simultaneous tin and iron additions in 360°C water is shown in Fig. 5. It
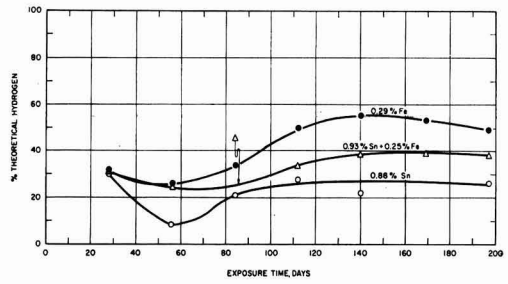
Fig. 5. Hydrogen pickup of zirconium—1% tin—0.25% iron alloy in 360°C water.
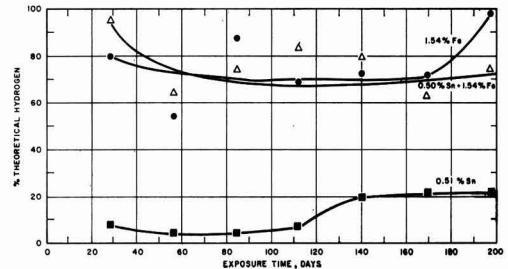
Fig. 6. Hydrogen pickup of zirconium—0.5% tin—1.5% iron alloy in 360°C water.

is observed that the ternary alloy shows per cent theoretical hydrogen between the values obtained for the tin and iron binary alloys. The tin binary alloy exhibits the lower value while the iron binary alloy exhibits a higher value.

Figure 6 shows similar summary plot of the alloys representing the 0.5% tin-1.5% iron alloy in 360°C water. Here it is noted that the ternary alloy clearly reflects the behavior of the binary iron alloy with respect to the pickup of hydrogen during corrosion exposure.

Acknowledgment

REFERENCES

1. K. M. Goldman and D. E. Thomas, USAEC Report, WAPD-MM-184, 1953.
2. C. M. Schwartz and D. A. Vaugh, USAEC Report, BMI-1120, Aug. 1, 1956.
3. D. E. Thomas and S. Kass, *This Journal*, **104**, 261 (1957).
4. K. M. Goldman, S. Kass, W. W. Kirk, and D. E. Thomas, Unpublished Work, Bettis Laboratory.
5. B. Lustman and F. Kerze, "Metallurgy of Zirconium", Chap. 6, McGraw-Hill Book Co., New York (1955).
6. S. Kass, *Corrosion*, **106**, 2, (1960).

A New Explanation of Gas Evolution in Electrically Stressed Oil-Impregnated Paper Insulation

Z. Krasucki, H. F. Church, and C. G. Garton

British Electrical and Allied Industries Research Association, Leatherhead, Surrey, England

ABSTRACT

In void-free oil-impregnated paper, gas evolution starts at a critical stress which is markedly dependent on the degree of dryness of the paper. The gas first formed arises from decomposition of water in the cellulose, the nature of the impregnant having little effect. Subsequent more rapid gassing resulting from decomposition of the oil is a secondary process depending on ionization within gas bubbles previously formed. Study of the fundamental primary process suggests that water absorbed by the cellulose is ionized by electron bombardment in regions of high stress and is then decomposed electrochemically.

Although alternative materials are available, paper impregnated with an insulating liquid is still widely used as the insulation for high voltage cables and inductive windings or as the dielectric for capacitors where reliability under moderate temperature conditions and low cost are of importance.

If gas pockets within the stressed insulation are avoided, life under a-c stress is usually long. It is known however that in oil-impregnated paper, electrical discharges occur above a certain critical value of applied stress, E_i, even if the paper is so well impregnated that no voids are present initially. If the voltage be maintained at the discharge inception level, the discharges increase rapidly in magnitude, sometimes to several times the initial value within the first minute, and life may be very limited. E_i is directly dependent on the hydrostatic pressure on the oil, but when different makes of oil-impregnated paper capacitors were compared at the same internal pressure (normal atmospheric) mean values of E_i covering a range of 5:1 were observed. The cause of these large differences was not known. The effects of such factors as the density and type (rag or kraft) of paper, and the viscosity and iodine number of the oil, on discharge inception stress are relatively very small (1).

When observations on electrically stressed oil-impregnated paper are made under the microscope, the onset of discharges coincides with the sudden appearance of a gas bubble in the oil. A systematic study has been made to determine which part of an oil-paper dielectric gives rise to gas formation in the absence of initial gas bubbles, and to elucidate the mechanism of the process.

When electrical discharges take place within a gas bubble already present, they generate further gas through decomposition of the oil, and the bubble increases in size. This paper, however, is not concerned with the rate of gas production in oil once gaseous ionization has started; the latter phenomenon has been investigated extensively, is known to be dependent on the nature of the oil and the presence of additives, and gassing tests have been developed to assist in the selection of oils where they are required to withstand discharges.

The novel feature of the present work is the attempt to investigate the primary process of the formation of the first gas bubble.

The conditions under which gas could be evolved when oil alone was stressed were first investigated; afterwards a number of solid dielectrics, including capacitor paper, cellophane, polyethylene, polystyrene, polyethylene terephthalate, glass, and mica, were studied immersed in oil or other liquids.

Tests in Oil Alone

When oil is filtered completely free from particles and fibers and is not supersaturated with dissolved gas, gassing cannot normally be induced to take place by the application of electric stress using immersed metal electrodes without breakdown occurring simultaneously. The following exceptions to this are known.

(i) Gas evolution under stress has been reported at very low pressures even from degassed oil (2), but the origin of the initial gas phase is not known.

(ii) With one electrode in the form of an extremely sharp needle (radius 1 μ or less) and several millimeters spacing between the electrodes, localized intrinsic breakdown of the oil at the needle point, with gas evolution, is possible without general breakdown ensuing. With normal transformer and capacitor oils under these conditions, the gas bubbles produced move away from the point at such high velocity that they are difficult to observe. If, however, an extremely viscous liquid is used so that the products of the localized breakdown (carbon and gas bubbles) remain where they are formed, breakdown channels may gradually grow from the point and lead eventually to general breakdown. Tree-like conducting channels formed in this way in hexachlordiphenyl are illustrated in Fig. 1.

These exceptional methods of initiation of gassing are not believed to occur in normal oil-impregnated paper dielectrics, e.g., in capacitors and cables. First, these systems normally operate at near atmospheric
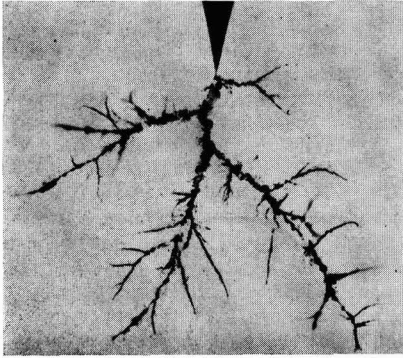
Fig. 1. Breakdown channels in hexachlordiphenyl

Fig. 3. Evolution of gas at the point of contact between a needle electrode and solid dielectric (cellophane).

or higher pressure. Second, the applied stress is usually insufficiently high for local intrinsic break-down to take place except perhaps in the case of dielectrics containing abnormal conducting inclusions or other localized faults which would lead to failure on proof test. Gassing by the mechanism discussed later in this paper and consequent failure by the action of discharges usually occur at much lower electric stresses than those required for intrinsic failure. The observations reported here do however suggest how manufacturers can raise discharge inception stress of liquid-impregnated paper insulation and increase working stress.

Effects of Stress on Liquid-Solid Mixed Dielectrics

When moist cellulosic fibers bridge the gap between electrodes in oil, they give rise to gas formation at relatively low electric stress. Gas bubbles are formed only when the fibers form a continuous bridge between the electrodes, and evolution is then observed at points of contact between the fibers and the electrodes. Evolution of gas has also been observed at points where fibers touch one another in the electrode gap provided bridging occurred.

In an effort to understand the cause of this, various solid-liquid mixed dielectrics were studied, using thin sheet solid material and simple electrode forms.

In the first experiments the sheet dielectric material to be tested was attached to the plane electrode of the test cell shown in Fig. 2. The other electrode was a needle of about 40 μ radius at the tip which could be moved relative to the plane electrode. The electrode gap could be observed with a microscope through optically flat windows. The cell was designed so that vacuum impregnation of the system with dielectric liquids could be effected, and tests if required could be carried out at reduced pressure. The following observations were made at atmospheric pressure:

(i) With the cell filled with filtered mineral oil no gassing was observed below the breakdown voltage so long as a gap existed between the needle and the solid dielectric attached to the plane electrode, whatever the nature of the solid.

(ii) With the solid insulation in the form of un-dried cellulose (cellophane or paper in equilibrium with ordinary room atmosphere) and the needle touching the solid, small gas bubbles were evolved continuously at the point of contact above a critical applied stress. Figure 3 shows gas evolution at the point of contact between the needle electrode and sheet cellophane immersed in mineral oil. The gas bubbles moved rapidly away from the needle and, in degassed oil, dissolved in a few minutes. The phenomenon was observed with both a-c and d-c applied stress but not necessarily at the same magnitude of stress. The onset of gassing coincided with "discharge inception" when the system was connected to a discharge detector.

(iii) The critical gassing stress increased with the state of dryness of the cellulose. With cellulose (paper or cellophane) which had been in equilibrium with air almost saturated with water vapor, gassing commenced at a stress of 6-7 v (peak) per micron. For cellulose exposed to ordinary room air (relative humidity say 65%), the critical stress was considerably higher (about 70 v/μ for two thicknesses of 10 μ capacitor paper) and this rose several times with further drying until with very dry paper or cellophane no gassing was observed below the breakdown stress (280 v/μ for two thicknesses of

SCREW ADJUSTMENT FOR ELECTRODE GAP

"O" RING

BRASS STOPPER

GLASS TAP

NEEDLE ELECTRODE (STEEL)

PLANE ELECTRODE (STAINLESS STEEL 12·5 mm DIA.)

FLAT GLASS WINDOWS 16 mm DIA.

BRASS STOPPER "O" RING.

23 cms

17 cms

Fig. 2. Test cell

Fig. 4. Dependence of minimum voltage for gas evolution (V_g) on dryness of oil-immersed cellophane.

10 μ paper). The rather lower critical stresses observed in actual capacitors with moisture free paper dielectric are presumably due to the occurrence of sites with an enhanced local stress from conducting particles or thin places in the much larger area involved.

The effect of progressive oven drying on the voltage V_g at which gas evolution commenced at the needle electrode for cellophane of 75 μ thickness, previously exposed to atmospheric humidity, is shown in Fig. 4.

(iv) With solid dielectrics of relatively low water absorption, e.g., polyethylene, polystyrene, polyethylene terephthalate, polytetrafluoroethylene, mica, and glass, no gassing was observed up to stresses approaching breakdown [in most cases 400-600 v (peak) per micron] even after long exposure to high humidity. Stresses which could be applied to these materials without gassing or breakdown occurring after exposure to almost 100% R.H. for periods of ½-1 hr are shown in Table I, which also includes gassing stresses for cellulosic materials which had

been exposed to the damp atmosphere before immersion in the oil.

(v) Other materials of high water absorption, e.g., cellulose triacetate and gelatine, behaved like cellophane and paper, i.e., when damp gassing occurred at low stress, but the gassing stress increased with drying. Results for cellulose triacetate and gelatine in the damp condition are included in Table I.

(vi) Evolution of gas under electric stress from incompletely dried cellulose occurred when a silicone fluid, carbon tetrachloride, pentachlordiphenyl, or carbon disulfide was substituted for mineral oil, the minimum gassing st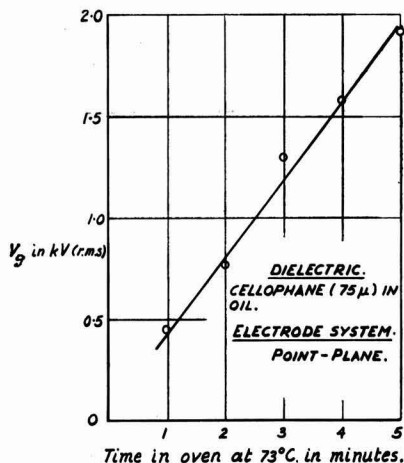ress being substantially unaffected by the change of immersion medium. Carbon disulfide is especially interesting in that it is not expected to yield gaseous decomposition products. The gas bubbles must therefore arise from the solid or its contained moisture.

Since the voltage at which gas is evolved from oil-impregnated cellulose increases with increasing dryness of the cellulose, it should be possible to increase the discharge inception voltage of an oil-impregnated paper capacitor by special attention to the drying of the dielectric. Measurements were therefore made of resistivity and discharge inception voltage on samples of rag paper (40 μ thickness) dried to different degrees. Vacuum dried paper was allowed to regain moisture to the required degree and immediately immersed in oil and assembled into a small capacitor with aluminum electrodes under the oil. The electrodes were flat foils 6 μ thick, pressed on to the dielectric the area of which was 4 cm². A-C discharge inception voltages were measured with a detector sensitive to 0.5 p coulomb. The results are shown in Fig. 5 where discharge inception stress E_i is plotted as a function of resistivity of the impregnated paper. E_i increased with increasing resistivity by a factor of 4 between paper in equilibrium with room atmosphere and "dry." The resistivities shown in Fig. 5 are considerably lower than corresponding resistivities for ordinary rolled paper capacitors. This is due to the tight clamping employed in the present tests which gave a more intimate contact with the paper.

Table I. Evolution of gas from solid dielectrics which had been exposed to damp atmosphere

Substance	Thickness, μ	Behavior under electric stress	Gassing stress, v (peak)/μ
Polyethylene	45	No evolution of gas bubbles at voltages up to the breakdown voltage 3.4 kv (peak)	>76
Polystyrene	12	No evolution of gas bubbles at voltages up to 7 kv (peak)	>580
Polyethylene terephthalate	12	No evolution of gas bubbles at voltages up to 4.7 kv (peak)	>390
Polytetrafluoroethylene	17	No evolution of gas bubbles at voltages up to 7 kv (peak)	>410
Mica	10	No evolution of gas bubbles at voltages up to the breakdown voltage 5.4 kv (peak)	>540
Glass	150	No evolution of gas bubbles at voltages up to the breakdown voltage 10 kv (peak)	>67
Capacitor paper	10	Evolution of gas bubbles at about 70 v (peak)	7
Cellophane	75	Evolution of gas bubbles at 420 v (peak)	6
Cellulose triacetate	30	Evolution of gas bubbles at about 570 v (peak) (BDV = 2.46 kv (peak))	19
Gelatine	33	Evolution of gas bubbles at 280 v (peak)	7
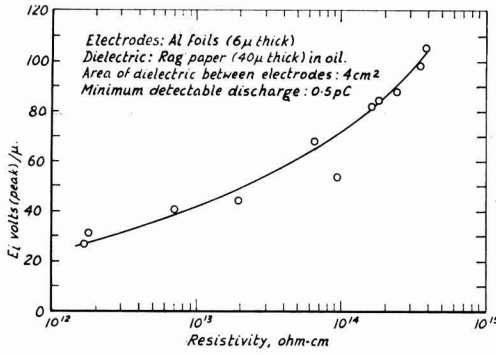
Fig. 5. Variation of discharge inception stress (E_i) with resistivity of oil immersed paper.
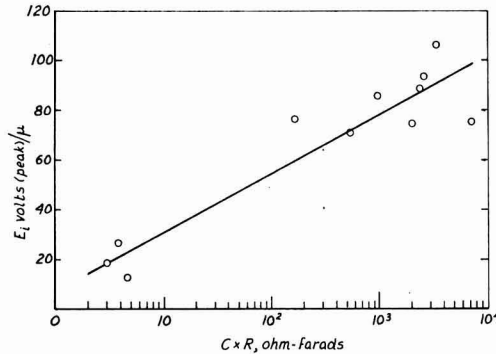
Fig. 6. Dependence of discharge inception stress (E_i) of kraft paper capacitors ($C = 0.02\mu$ F) on C × R.

In addition to the above tests on clamped plate capacitors, some normally wound 0.02 μF kraft paper units (4 paper layers x 10 μ) were impregnated in the laboratory with capacitor oil. The insulation resistance was varied by vacuum drying the units to different degrees before impregnation. Only a few tests have been made so far, but the results shown in Fig. 6 indicate that the more thorough the drying process the greater is the E_i value of the capacitor. Although precise measurements of moisture content of the paper dielectric of these capacitors were not made, these results and others suggest that E_i increases from 15 to more than 100 v (peak) per μ as moisture content decreases from a few per cent to to less than 0.1%.

Discussion of Results

The observations reported here strongly suggest that the gas initially generated in electrically stressed paper impregnated with a dielectric liquid is derived from water contained in the cellulose. Provided gas bubbles are not present initially, the threshold value of stress for gassing at normal pressures is low only with impregnated materials containing an appreciable amount of absorbed moisture, and is increased by drying. The gas observed is not water in the vapor phase formed, say, through local heating at points of contact between the electrodes or conducting inclusions and the cellulose; bubbles

of steam produced in this way would condense in a small fraction of a second, contrary to the observed life of the bubbles of several minutes.

Water in liquid form can be electrolyzed readily into its constituent gases at a frequency of 50 cps at suitable current density. Experiments, in which the gas evolved from moist electrically stressed paper under an insulating liquid was collected, also showed that an explosive mixture of hydrogen and oxygen was formed from the water with both d-c and a-c (50~) voltages, although under mineral oil some of the oxygen may be absorbed immediately by oxidation of the oil. The average leakage current density through an oil-impregnated paper capacitor, however, is insufficient to account for the observed rate of gas evolution at the discharge inception stress on the basis of electrolysis of the water (3), unless some mechanism exists to cause a great increase in current in a few very small areas where abnormal stresses are present. Such a local enhancement of conductivity cannot be explained by moisture movement toward high stress regions; theoretical considerations based on energy of sorption of water in cellulose rule this out as a major effect even at stresses of the same order of magnitude as the intrinsic strength of cellulose. Experimental results have confirmed this.

Tests performed on paper in various states of dryness show however that its conductivity increases very greatly as the breakdown stress is approached especially when it is moist. Figure 7 shows the effect of varying the d-c measuring voltage on the resistivity of 28 cm^2 areas of kraft capacitor paper 20 μ thick (2 x 10 μ layers) after conditioning in various atmospheres. The observed great increase in conductivity of cellulose containing moisture at high stresses may be a consequence of electron emission from the electrodes, the electron bombardment of
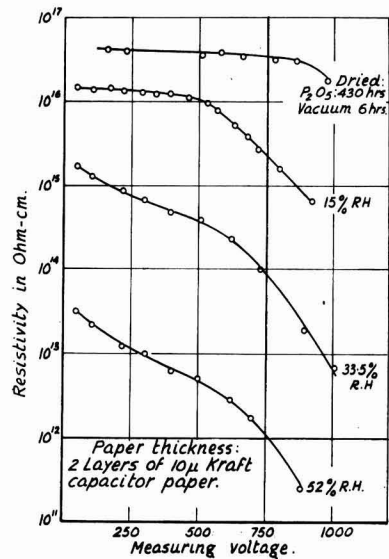
Fig. 7. Effect of measuring voltage on resistivity of paper in various states of dryness.

the cellulose causing dissociation of the bound water molecules. Although the maximum applied stress in Fig. 7 is only 0.5 mv/cm, locally it may be several times higher due to stress concentration at the edges or at any microscopic irregularities on the electrodes, and because of variations of thickness of the paper and the presence of conducting inclusions. Stresses of more than 1 mv/cm would certainly be sufficient for electron emission.

It is possible therefore that gas evolution in a capacitor commences at local points of stress concentration, say near the site of a conducting inclusion in the paper or at electrode edges, where the resultant high degree of dissociation of the water would lead to rapid electrolysis.

Such a mechanism would explain why discharge inception stress in oil-impregnated paper capacitors is not greatly affected by time of application of d-c stress or frequency of a-c stress and is little dependent on temperature which has a very considerable effect on leakage current at working stress. In a well sealed capacitor, temperature may have an indirect effect on discharge inception stress by causing a change of pressure, but at constant pressure the effect of temperature is small. It is clear therefore that a simple electrochemical mechanism based on

average currents at working stress is inadequate, but that an explanation involving electron emission at high stress is in agreement with experimental observations.

The practical value of this work is that it demonstrates the importance of very thorough drying of oil-impregnated paper insulation if the highest possible working stress is required.

Acknowledgment

REFERENCES

1. P. Cucka, Electrical Research Association Technical Report Ref. L/T356, 1957.
2. H. Basseches and M. W. Barnes, *Ind. Eng. Chem.*, **50**, 959 (1958).
3. H. F. Church and C. G. Garton, *Proc. I.E.E.*, **100**, IIA, 111 (1953).

ZnS:Cu, Cl and (Zn, Cd)S:Cu, Cl Electroluminescent Phosphors

A. Wachtel

Research Department, Westinghouse Electric Corporation, Bloomfield, New Jersey

ABSTRACT

Procedures for the preparation of ZnS: Cu,Cl and (Zn,Cd)S: Cu,Cl EL[1] phosphors are based on firing in an atmosphere containing elementary S. Cl-incorporation is controlled by firing in capped silica tubes or in open boats in a current of $N_2 + S_2Cl_2$. Dependence of brightness on activator concentration is established on the basis of presumably constant excess Cu as Cu_2S. The use of Pb was found to be disadvantageous. Introduction of Cd causes formation of the hexagonal phase and a (Cu,Cd)S compound and simultaneous decrease of electroluminescence brightness as well as dependence of electroluminescence emission color on Cd concentration. A two-step firing procedure is given by means of which this effect may be partially avoided.

This paper deals with efforts to improve the brightness and maintenance of blue and green emitting EL phosphors, as well as attempts to prepare phosphors emitting at longer wave lengths by means of partial substitution of Zn by Cd. While a considerable amount of data on the preparation of ZnS:Cu, Cl EL phosphors has appeared in the literature (1), the experimental procedures used in the present study are based on those developed by Lehmann (2). These may be summarized as follows:

1. The highest EL output is obtained for compositions prepared with only ZnS, Cu, and Cl and preferably excluding other cations such as Pb.

2. A considerable improvement of the phosphor is obtained by firing in an atmosphere containing elementary S. It is believed that this improvement

---

[1] Electroluminescence or electroluminescent is hereafter abbreviated EL.

is due to reduction of the number of S-vacancies and consequently deep traps which otherwise tend to form.

The second point necessarily implies that the addition, or presence after firing, of ZnO is detrimental. This is contrary to data first obtained by Destriau (3) and then by a number of workers in the field [a review as well as original data have been published by Wendel (4)]. An explanation may be offered in terms of a model for the EL excitation mechanism as proposed by Lehmann (5) according to which electrically conducting inclusions in ZnS crystallites similar to the Cu-rich surface layers proposed by Zalm, Diemer, and Klasens (6) and by Zalm (7) provide sufficient local intensification of the applied field. Accordingly, either ZnO or Cu_2S may play such a role. Lehmann, has shown experimentally that Cu_2S is preferable.

Experimental Techniques

Unfired mixes were prepared by slurrying pure ZnS (RCA No. 33Z19) with aqueous solutions of $Cu(C_2H_3O_2)_2 \cdot H_2O$ and NH_4Cl, followed by drying, addition of S and remixing. Firing was usually done in 10 g quantity of material filled into transparent silica tubes, 75 mm long, 15 mm ID, and 17 mm OD, closed at one end and capped with similar tubes 18 mm ID and 20 mm OD. Several such tubes could be arranged in a larger silica tube near its closed end and protected with an atmosphere of purified N_2 in the usual manner. All fired phosphors were washed in NaCN solution followed by H_2O and alcohol, and were then dried and screened.

EL-brightness readings were performed with a Spectra Brightness Spot Meter,[2] using a demountable cell filled with 40% (by volume) suspensions of phosphor in castor oil. Since small geometrical deviations of the cell assembled at different times could not always be avoided, the effective field strength across the phosphor layer was standardized by operating the cell at a voltage such that a standard phosphor (also included) had a predetermined brightness.

ZnS:Cu, Cl Phosphors

Mechanism of Cl incorporation.—The amount of Cl incorporated at a given concentration of Cu was estimated in a relative but sensitive manner by visual comparison of the blue-green hue of emission of the fired phosphor. Preliminary investigations indicated that the Cl content decreases with increasing batch size and increases slightly with firing time and the volume of the firing container used, so long as this volume is small enough to permit the phosphor mix to be surrounded by a saturated atmosphere of its own thermal decomposition products. For larger sample sizes fired, an empirical relationship

$$\% Cl = x(0.97 + 0.003 \text{ g ZnS})$$

was found to result in equal emission color, where x is the amount of Cl added to a 10-g sample.

The observations suggested that, during the initial stages of firing, thermal decomposition releases substantially all of the added Cl to the atmosphere. As the firing proceeds this Cl is subsequently absorbed at a slower rate. The sulfur added appears to decrease strongly the Cl incorporation inasmuch as it causes a shift in emission to shorter wavelengths (8), i.e., in favor of the blue emission band. This may be compensated for by higher Cl additions such as presently described.

The EL brightness was found to reach a broad maximum for firing temperatures in the neighborhood of 950°C. Singly fired phosphors were usually characterized by nonhomogeneous Cl content, i.e., a mixture of more bluish and more greenish emitting portions. Grinding and refiring with no additions other than S always resulted in homogeneous, brighter, and more reproducible phosphors. During the refiring, about 30% of the incorporated Cl is lost, which must be compensated for in the initial unfired composition, since after firing the rate of Cl

incorporation is strongly reduced. Firing times of 1.5 hr were found to result in equilibrium conditions.

Activator concentration.—An EL ZnS:Cu, Cl phosphor is known to require the presence of a high concentration of activator sites (9, 10) whose formation is, for present purposes, assumed to be a function of coactivator (Cl) incorporated, so long as the molar concentration of Cu appreciably exceeds that of Cl. The performance of an EL phosphor depends, however, not only on the amount of incorporated (at least partially charge-compensated) Cu, but also on the conducting phase of Cu_2S whose formation depends on, and is a function of, the presence of excess Cu during the firing process.[3] Conditions for keeping this constant and at a near-optimum value were empirically determined for 10-g quantities fired to obey the relationship

$$\text{mole \% Cu} = 0.55 + 0.45 \text{ mole \% Cl}$$

Under present conditions, the sintering of the phosphor appears to be determined entirely by the amount of excess Cu_2S formed, so that a rapid, although approximate and only relative, estimate of excess Cu concentration could be made in this manner.

Phosphors prepared with Cl additions up to 30 mole % and corresponding additions of Cu showed approximately equal sintering. Figure 1 shows the EL brightness obtained at two frequencies over a portion of this range of compositions. The fact that an EL output appreciably higher than zero is noted for no Cl addition may be explained by a small Cl content of the raw materials, and the brightness found at this point was noted to be quite variable, depending on the particular lot of ZnS used. The similarity of the curves to the dependence of brightness on Al addition as noted by Froelich (11) is quite evident. It is also interesting to note that compositions resulting in maximum EL brightness are such that about 25% of the added Cu is retained after NaCN washing, which is the same figure reported by Froelich (12) for ZnS:Cu, Mn phosphors fired at 1100°C in H_2S. The practical aspects of these results are presented in more detail in a recent

[3] NaCN-washed EL phosphors show an increase in green/blue ratio of emission and lose most of the EL when refired at the original firing temperature (950°C).
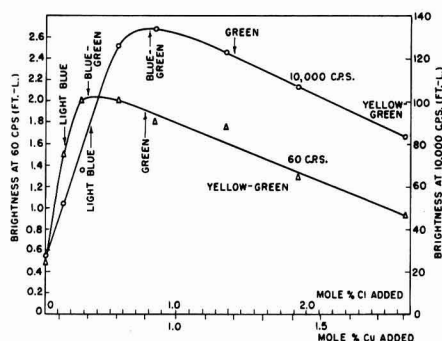

Fig. 1. Brightness of ZnS:Cu, Cl phosphors fired with 5 wt % S at 950°C, 2 x 90 min, as a function of activator addition. The Cl additions specifically refer to 10-g quantities fired in silica tubes of 13.5 ml volume.

[2] Photo Research Corp., Hollywood, Cal.

Table I. Typical activator additions and retained concentrations (in mole %) for 10-g batches of ZnS, fired at 950°C—2 x 90 min

	Light blue	60 cps green	10,000 cps green
Cu added	0.62	0.71	0.89
Cu retained after NaCN washing	0.033	0.105	0.50
Cl added	0.14	0.34	0.75
Cl retained	0.095	0.16	0.32

patent (13). Table I shows typical values of Cu and Cl found by chemical analysis of NaCN-washed phosphors designed for light blue emission, as well as maximum brightness at 60 and at 10,000 cps excitation, respectively.

Effect of Pb.—Because of the frequent use of Pb (15) in the preparation of EL phosphors, its effect was also investigated. Table II shows the results obtained, where the first three samples (except for S) represent a composition obtained by averaging a number of representative formulations described in the patent literature. Samples 4, 5, and 6 differ only in the use of extra NH_4Cl, so as to compensate for the effect of Pb which consists of volatilizing excess Cl as $PbCl_2$.

In samples 7, 8, and 9, an attempt was made to duplicate present compositions, except that Pb was also used which, in turn, required higher Cl additions so as to maintain a blue/green hue of emission color similar to that presently representing optimum activation incorporation. Sample 10 is a normal control phosphor prepared without Pb.

It can be seen that in all cases the use of Pb resulted in a strong reduction of EL as compared to the control. Since the use of 5 mole % Cl alone would result in a nearly 100% coactivated and almost non-EL phosphor, any advantages of the use of Pb, as observed by others, is probably restricted to cases where raw materials with high Cl content were employed.

Effect of ZnO.—Figure 2 shows the effect of increasing additions of ZnO to compositions designed either for 60 cps or for 10,000 cps excitation. The initial slight increase in brightness lies within the reproducibility of phosphor preparation and measurements.

The presence of ZnO results in an effect similar to an increase in Cl addition. Most of the S added
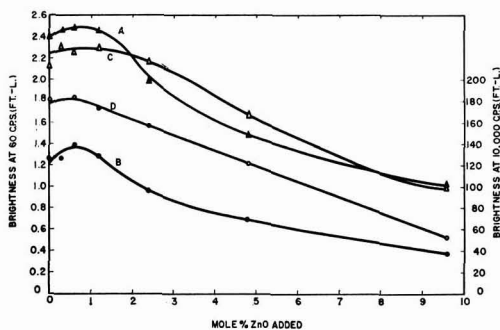
Fig. 2. Brightness of ZnS:Cu, Cl phosphors with activator additions designed for 60 cps and for 10,000 cps excitation, respectively, as a function of ZnO added before firing. A, 60 cps phosphor excited at 60 cps; B, 60 cps phosphor excited at 10,000 cps; C, 10,000 cps phosphor excited at 60 cps; D, 10,000 cps phosphor excited at 10,000 cps.

evaporates before reaction with ZnO can occur; the remainder, however, may react with ZnO and can no longer decrease incorporation of Cl. Moreover, Kröger and Dikhoff (14) have shown that oxygen itself causes preferential association with Cu and has a definite solubilizing effect. Since the decreased brightness observed may therefore be interpreted as merely a departure from optimum final activator and Cu_2S concentrations, a number of phosphors were prepared with about a tenth of the usual additions of Cl so as to match the green/blue ratio of emission of normal phosphors. The best results obtained were, however, only about one-third of the output normally obtained at 60 cps, while at 10,000 cps the EL was comparatively negligible. Similarly poor results were obtained by firing phosphors without free S, even in the absence of ZnO.

Effect of alkali chlorides.—The incorporation of Cl, although subject to the parameters described above, appeared to be independent of its form of addition, so long as no extraneous cation is included. On the other hand, the addition of Cl in the form of alkali chlorides as originally reported by Beutler and Prener (16) results in a shift in emission color to the blue.[4] With increasing atomic weight of the cation, the shift becomes more pronounced. The

[4] On the basis of enough Cl to result in green emission color if introduced as NH_4Cl, $ZnCl_2$, or HCl. Otherwise, there is, of course, no color shift.

Table II. EL response obtained with various compositions containing Pb

Sample No.	Composition in mole % before firing						Fluorescence emission color	EL brightness	
	ZnO	1/3 { Pb(OH)₂ / 2PbCO₃	PbCl₂	Cu (C₂H₃O₂)₂·H₂O	NH₄Cl	S		60 cps	10,000 cps
1*	7.2	0.28	—	0.085	—	—	Green-blue	0.15	2.0
2	7.2	0.28	—	0.085	—	15	Blue	0.05	2.5
3	7.2	0.28	—	0.085	—	15	Blue-green	0.10	3.4
4	7.2	0.28	—	0.085	0.84	15	Blue	0.30	5.6
5	7.2	0.28	—	0.085	5.5	—	Green-blue	0.20	5.8
6	7.2	0.28	—	0.085	5.5	15	Green-blue	0.30	6.4
7	—	—	0.28	0.77	5.0	—	Yellow-green	0.60	20.0
8	—	—	0.28	0.77	5.0	15	Green	0.20	25.0
9	Sample No. 8 refired with 15 mole %S only						Green	0.80	45.0
10	—	—	—	0.77	0.75	15	Blue-green	3.0	180.0

* Fired in open boat in current of N_2. All other samples are fired in capped tubes.

Table III. Effective Cl retention in mole % estimated by emission color of ZnS fired with 0.75 mole % Cu and 2.75 mole % Cl added as alkali chlorides

HCl	LiCl	NaCl	KCl	RbCl	CsCl
1.25*	0.32	0.12	0.10	0.07	0.055

* On the basis that about 45% of the added Cl is incorporated. Actually, this would require at least 1.25 mole % Cu addition.

mechanism whereby this occurs has not been ascertained but seems to resemble the Cl-gettering action of K_2CO_3 as described by Ranby (17) and could be interpreted either as decreasing incorporation of the chloride due to decreasing solubility of the K-salt in the ZnS lattice, or decreasing association of chloride with Cu activation sites (18, 19) due to increasing association of the Cl with the alkali metal ions. The effect is, of course, noticeable only at Cu concentrations well above those normally employed in photoluminescent phosphors. Table III shows the results of adding 2.75 mole % Cl as alkali chlorides to ZnS with 0.75 mole % Cu, where the effective Cl concentration of the fired phosphors was estimated on the basis of emission color. With the exception of the values for Rb and Cs which are very uncertain due to the difficulty of comparing deep hues, the points may be plotted as a straight line of log Cl vs. log atomic weight of the cation.

The EL output of the blue-emitting phosphors (such as those fired with KCl) does not differ significantly from normal blue-emitting ZnS:Cu, Cl prepared without KCl but with a sufficiently low addition of NH₄Cl. The output of the greener-emitting phosphors fired with NaCl and LiCl is, however, considerably poorer. It may be noted that the emission color of the phosphor fired with LiCl matches that of a normal EL phosphor fired with 0.75 mole

% NH₄Cl (optimum for 10,000 cps excitation) while the EL brightness is only about 60% of such a control sample.

It was interesting to observe that high concentrations of KCl also inhibit the effective incorporation of additional Cl added in an "available" form (i.e., as NH₄Cl, ZnCl₂, etc.) to the extent that for each mole per cent KCl present, about 0.5-0.75 mole % NH₄Cl is required to shift the emission color from blue to green. Here again, however, green-emitting phosphors prepared in this manner are characterized by very poor output.

The effect of KCl on maintenance of output during operation is particularly pronounced. Table IV shows the result of measurements in PVCA (polyvinyl chloride acetate copolymer) dielectric taken at 4000 cps on phosphors fired with variable additions of KCl and NH₄Cl. The last two rows represent normal control phosphors. It can be seen that the maintenance of the blue-emitting control phosphor is quite poor, but can be improved by a factor of 5 by the use of KCl. Inasmuch as the maintenance of ZnS:Cu, Cl phosphors increases with activator concentration (20), it seems not too far fetched to visualize that the very high Cl additions made in the present manner somehow become available with respect to their influence on maintenance, although without corresponding formation of green-emitting centers.

Use of S_2Cl_2.—The firing technique as described earlier in this paper was developed mainly because the composition of the atmosphere surrounding the phosphor during firing is a function of the composition of the unfired mix, so that the Cl incorporation could be controlled in a simple manner. Incorporation of Cl from a continuous supply such as HCl, introduced from the outside, would presumably continue until all of the Cu has been transformed into

Table IV. Properties of KCl-fluxed ZnS:Cu, Cl phosphors fired with 0.2 mole % Cu, as a function of additional Cl added as NH₄Cl.
Brightness measurements at 400 cps in castor oil; maintenance measurements at 4,000 cps in PVCA dielectric

KCl, mole %	NH₄Cl, mole %	Particle size, μ	Brightness, ft-L	Emission Color	Spectra meter ratios*			% Maintenance after 20 hr	Brightness x maintenance
					r	g	b		
10	0	2-6	3.95	Blue	0.025	0.257	0.718	11.7	0.46
10	1	2-10	3.6	Green-blue	0.030	0.335	0.635	35.0	1.26
10	2	2-10	3.9	Green-blue	0.043	0.390	0.567	—	—
10	5	3-12	3.25	Blue-green	0.053	0.497	0.450	—	—
10	10	3-20	2.3	Green	0.060	0.570	0.370	84.0	1.93
20	0	2-10	2.35	Blue	0.020	0.200	0.780	27.6	0.93
20	2	2-10	4.65	Light blue	0.033	0.307	0.660	42.5	1.98
20	4	2-10	3.3	Green-blue	0.040	0.333	0.627	—	—
20	10	3-15	2.5	Blue-green	0.052	0.402	0.546	—	—
20	20	6-25	2.85	Green	0.058	0.507	0.435	80.3	2.3
30	0	2-3	3.2	Blue	0.023	0.181	0.796	46.0	1.47
30	3	1-3	3.95	Light blue	0.035	0.275	0.690	58.8	2.32
30	6	2-6	1.95	Green-blue	0.040	0.290	0.670	—	—
30	15	3-20	1.9	Green-blue	0.042	0.350	0.608	—	—
30	30	6-40	4.1	Blue-green	0.047	0.393	0.560	66.6	2.74
50	0	2-4	2.3	Blue	0.017	0.193	0.790	35.8	0.83
50	5	1-2	3.65	Green-blue	0.034	0.322	0.644	55.6	2.03
50	10	1-4	1.7	Green-blue	0.035	0.345	0.620	—	—
50	20	3-50	3.45	Blue-green	0.030	0.333	0.637	—	—
50	50	8-50	3.55	Blue-green	0.033	0.365	0.602	80.0	2.83
0	0.35	5-15	20.0	Green	0.070	0.630	0.300	37.0	7.4
0	0.08	3-10	4.7	Light blue	0.025	0.260	0.715	8.7	0.41

* Ratios of the response at the Spectra Meter settings "red", "ft-L" (green), and "blue," respectively, divided by the sum.

green-emitting Cu-Cl centers. followed by eventual conversion of the ZnS into $ZnCl_2$. In order to limit this reaction, mixtures of HCl + H_2S are generally employed, and investigations of a quantitative nature pertaining to such reactions have been published by Kröger, Hellingman, and Smit (9) and by Kröger and Smit (21).

As mentioned before, the role of S in similarly limiting the incorporation of Cl has been verified experimentally, although only in a qualitative manner. However, unlike H_2S, the S constitutes an oxidizing environment during firing which is advantageous for the formation of good EL phosphors. In order to carry this one step further, the addition of Cl in elementary form was considered. The most convenient manner of accomplishing this was in the form of S_2Cl_2 added to the N_2 by aeration in a gas scrubbing bottle. For this purpose, no S or halide was added to the unfired mix, which was placed in an open boat near the closed end of the firing tube. It turned out that the equimolecular addition of S and Cl effected in this manner resulted in Cl incorporation to the extent normally obtained for phosphors designed for high-frequency excitation. The phosphors were characterized by a lighter (less yellow-green) body color after NaCN washing, and a stronger dependence of brightness on applied voltage. Details pertaining to the preparation of this type of phosphor have also been described (22).

(Zn, Cd)S:Cu, Cl Phosphors

The same firing technique, using capped silica tubes as described, was used throughout this phase of the investigation. The CdS raw material was RCA33C291. The Cu and Cl additions were generally maintained at those suitable for high-frequency excitation, so as to favor the long wavelength emission band.

Figure 3 shows the results of substituting an increasing molar percentage of CdS for ZnS. A small
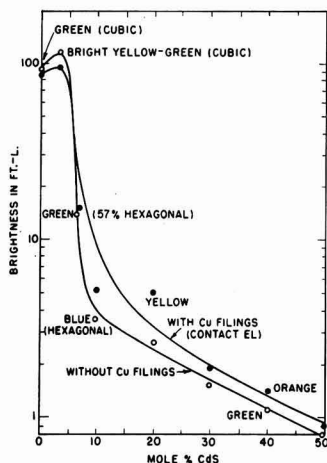
Fig. 3. Effect of Cd concentration on EL and contact-EL of (Zn, Cd)S:Cu, Cl phosphors. Measurements taken at 1000 v, 8,000 cps in 200 μ castor oil cell with 25 μ Mylar protection.

addition (3.3%) results in the expected shift in emission color to yellow-green and somewhat improved brightness. Increasing additions of Cd, however, rapidly decrease the output of the phosphors. While this may be caused partly by the introduction of deep traps associated with Cd as proposed by Zalm (7), three additional phenomena were noted, particularly in the region of rapid decreasing EL:

1. Formation of hexagonal phase. The first two points in Fig. 3 represent samples which are 100% cubic, the third sample is 57% hexagonal, and the rest are 100% hexagonal. It should be mentioned that Zalm (7) also considered the cubic phase of ZnS to be more suitable from the standpoint of EL, while Jaffe (23) noted a corresponding decrease of EL on introduction of Mg into ZnS, occurring simultaneously with formation of hexagonal material.

2. A shift in EL excited emission color back to shorter wave lengths. The emission color of (0.9Zn, 0.1Cd)S was greenish blue, although its photoluminescence was green-yellow as expected for this composition. No explanation of this phenomenon can be given at present.

3. Formation of a dark-colored separate phase, insoluble in NaCN solution. When prepared in pure form, this material is black and shows a hexagonal x-ray diffraction pattern very similar to that of CdS. Chemical analysis shows 18.5% Cu. Its exact identity has not as yet been established, although it appears to be some type of (Cd, Cu)S.

The decreasing EL output caused by the introduction of Cd into ZnS:Cu, Cl phosphors appears to occur simultaneously with the formation of hexagonal material and is associated with the formation of the (Cd,Cu)S phase. Phosphorescence observed in such phosphors strongly indicates that the mechanism in which high activator concentrations normally quench phosphorescence in ZnS:Cu, Cl phosphors is disturbed. Since, on the other hand, the characteristic ultraviolet-excited fluorescence is not so strongly influenced, the following mechanism may be proposed. The Cu_2S inclusions tend to be associated primarily with the cubic modification of the base material. Introduction of more than a few per cent of Cd causes formation of a hexagonal phase which allows the excess Cu to combine with CdS to form a separate compound which is not capable of fulfilling the same role of field intensification as Cu_2S. At the same time, depletion of this excess Cu disturbs the Cu-equilibrium of the system during firing and lowers the activator concentration of the phosphor to the point whereby persistent phosphorescence may be observed. Removal of the Cu_2S effectively destroys the EL-excitation mechanism.

The hypothesis was tested by mixing the phosphors with Cu-filings and subjecting them to contact-EL (24). Because of this comparatively inefficient manner of EL excitation, as well as the lower activator concentration of the (Zn, Cd)S:Cu, Cl phosphors, the increase in brightness obtained was small. On the other hand, the normal shift in EL-excited emission color was now observed. This

Fig. 4. Brightness at 600 v, 10,000 cps excitation of (9Zn:1Cd)S:Cu, Cl prepared from ZnS:Cu, Cl phosphor + CdS as a function of firing temperature. Firing times, 1 hr.

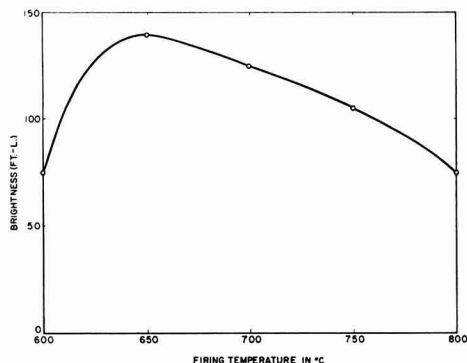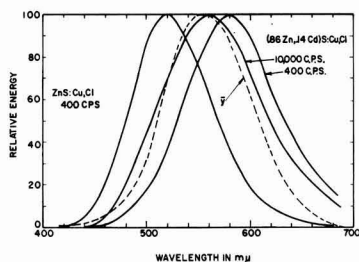Fig. 5. Spectral distribution of (0.86 Zn, 0.14 Cd)S:Cu, Cl in comparison with that of green-emitting ZnS:Cu, Cl and sensitivity of human eye.

means that, at high Cd concentration, the slightly brighter orange contact EL represented a considerably higher emittance than the slightly less bright green, normally excited EL. It should also be mentioned that cubic or hexagonal photoluminescent ZnS:Cu(0.01%), Cl performed about equally well when subjected to contact EL.

Among several methods tried to overcome this interference, only one was at least partially successful: A normally prepared, but not NaCN-washed, green-emitting ZnS:Cu, Cl EL phosphor is mixed with unfired CdS and S and refired at a lower temperature. Figure 4 shows the effect of refiring temperature on 0.9 ZnS:Cu, Cl + 0.1 CdS which can be seen to be quite critical. At the present stage of development, the procedure is, however, not very reproducible and apparently subject to the particle size and technique of mixing of the two components to be refired. At best, 14 mole % CdS have been incorporated into ZnS:Cu,Cl without formation of the separate (Cd, Cu)S phase and formation of hexagonal structure. Figure 5 shows the emission spectra obtained at two frequencies of excitation of a (0.86Zn, 0.14Cd)S:Cu,Cl phosphor prepared in this manner. Although the spectral distribution at 10,000 cps resembles the eye-sensitivity distribution more closely, the brightness obtained was only about one-third that of the green-emitting ZnS:Cu,Cl phosphor prior to refiring with CdS. However, it should be mentioned that even refiring at 650°C of ZnS:Cu, Cl without CdS addition resulted in decreased

brightness, generally to the extent of about 25%. The method is therefore a compromise designed to effect maximum incorporation of CdS with a minimum of chemical interference. Etching of such phosphors in HCl revealed that they are not homogeneous, inasmuch as the emission color continuously shifted to shorter wave lengths with increasing time of etching. This type of phosphor may therefore represent an optically filtered system of little practical importance.

Summary

Procedures for the preparation of lead-free ZnS:Cu,Cl and (Zn, Cd)S:Cu,Cl have been presented, based on firing of the raw materials in an oxidizing atmosphere containing sulfur vapor. The dependence of EL output on activator concentration is meaningful only for phosphors fired with additions of Cu such as to result in presumably similar concentrations of excess Cu_2S and consequently similarly efficient excitation processes. Control of incorporated Cl may be effected by firing in capped silica tubes or by firing in N_2 + S_2Cl_2. Alkali chlorides decrease the incorporation of Cl, more so with increasing atomic weight of the cation. Experiments with KCl have resulted in blue-emitting phosphors with greatly improved maintenance.

Substitution of Zn by Cd decreases the emittance as well as the dependence of EL-excited emission color on Cd concentration which is normally observed with ultraviolet excitation. This effect occurs simultaneously with formation of hexagonal (Zn, Cd)S and a (Cd,Cu)S compound which is insoluble in NaCN solution. A two-step firing procedure may be employed by means of which this interference is partially avoided through formation of a non-homogeneous optically filtered system. The brightness of such phosphors, however, is low.

Acknowledgments

REFERENCES

1. See H. F. Ivey, Bibliography on Electroluminescence and related Topics, I.R.E. Trans. Electron Devices, ED-6, 203 (1959).
2. W. Lehmann, Canadian Pat. 579,685, July 14, 1959.
3. G. Destriau, Phil. Mag., 38; 700, 774, 800, 885 (1947).
4. G. Wendel, Z. Phys. Chem., 206, 169 (1956).
5. W. Lehmann, This Journal, 104, 45 (1957).
6. P. Zalm, G. Diener, and H. A. Klasens, Philips Research Repts., 9, 81 (1954).
7. P. Zalm, ibid., 11, 353 (1956).
8. S. Rothchild, U.S. Pat. 2,541,384, Feb. 13, 1951.
9. F. A. Kroger, J. E. Hellingman, and N. W. Smit, Physica, 15, 990 (1949).
10. R. Bowers and N. T. Melamed, Phys. Rev., 99, 1781 (1955).

11. H. C. Froelich, *This Journal*, **100**, 496 (1953).
12. H. C. Froelich, U. S. Pat. 2,743,239, April 24, 1956.
13. A. Wachtel, U. S. Pat. 2,874,128, Feb. 17, 1959.
14. F. A. Kröger and J. A. M. Dikhoff, *This Journal*, **99**, 144 (1952).
15. H. H. Homer, R. W. Rulon, and K. H. Butler, *ibid.*, **100**, 566 (1953).
16. C. C. Bentler and J. S. Prener, U. S. Pat. 2,755,255, July 17, 1956.
17. P. W. Ranby, U. S. Pat. 2,866,116, Dec. 23, 1958.
18. J. S. Prener and F. E. Williams, *Phys. Rev.*, **101**, 1427 (1956).
19. J. S. Prener and F. E. Williams, *This Journal*, **103**, 342 (1956).
20. W. A. Thornton, in press.
21. F. A. Kröger and N. W. Smit, *Physica*, **16**, 317 (1950).
22. A. Wachtel, Canadian Pat. 579,687, July 14, 1959.
23. P. M. Jaffe, in press.
24. W. Lehmann, *This Journal*, **104**, 45 (1957).

Gold-Activated (Zn,Cd)S Phosphors

M. Avinor[1]

Philips Research Laboratories, N.V. Philips' Gloeilampenfabrieken, Eindhoven, Netherlands

ABSTRACT

Gold is shown to produce three emission bands in CdS at 640, 800 and 1150 mμ. The long wave band appears only when a coactivator is used while the short wave bands are observed with activation by gold alone. The 1150 mμ band in CdS is shown to correspond to the 530 mμ gold band in ZnS.

The greenish fluorescence of gold-activated zinc sulfide is well known (1-3), but the properties of the luminescent centers have been investigated only limitedly. It was generally assumed in earlier work that they differed considerably in character from the centers of copper and silver in zinc sulfide. This was attributed to the theoretical possibility of gold being incorporated in the trivalent as well as the monovalent state. By using trivalent metals as coactivators instead of halogens, Kröger and Dikhoff (4) showed that the gold band was composed of two bands at 470 and 530 mμ, and that the latter became predominant by coactivation.

There is some likelihood of confusing the short wave band of gold at 470 mμ with the self-activated band of zinc sulfide at 460 mμ. However, the short wave band seems to be really due to gold because the two gold bands remain distinct even when the activator concentration is increased to 1 mole % (5). At such high activator concentration the self-activated band is usually completely suppressed. The two gold bands were assumed (4) to correspond to the "blue" and "green" bands of copper, although the order of the coactivated bands of silver (435 mμ), copper (516 mμ) and gold (530 mμ) does not correspond to their order in the periodic system.

Recently a further attempt was made by Henderson, Ranby, and Halstead (6) to find a correlation between the luminescent properties of Cu, Ag, and Au in ZnS and in (Zn,Cd)S phosphors. These authors did not control the atmosphere in which they fired their phosphors and they used chlorine coactivation through the addition of fluxes. No systematic correlation between the bands of the various activators could be found, although the authors claimed to have demonstrated three emission bands for copper and gold and two bands for silver.

The short wave silver band in ZnS was shown by Van Gool (7) to be situated at 388 mμ, by starting from CdS and tracing the shift of the emission bands

in a series of mixed (Zn, Cd)S crystals up to ZnS. The short and the long wave bands are rather well resolved in CdS. In the present work we investigated the emission bands of gold by starting from CdS and following the bands as more and more of the cadmium was replaced by zinc.

Experimental

The aluminum coactivator was added to the pure base material as a solution of the ammonium alum, and the gold was added as a solution of the chloride. The powders were dried at 120°C overnight and then fired in small quartz test tubes at 950°C for 2 hr in a stream of pure hydrogen sulfide. After withdrawal from the furnace the tubes were allowed to cool, again in a stream of hydrogen sulfide. The products were ground and refired in hydrogen sulfide at 1100°C for 1 hr. An activator concentration of 2.10^{-4} atom per mole was used, which is about the optimum concentration for these sulfide phosphors. No fluxes were used.

The present experiments were limited to activation by gold alone or gold balanced by an equal molar concentration of a trivalent coactivator. Phosphors with activator to coactivator ratio different from unity were not investigated. It is known, however, that in the case of copper and silver additional emission bands may appear (4, 7).

The emission was measured by a recording spectrophotometer with photomultiplier or lead sulfide detector, and the usual corrections were applied for obtaining equal energy spectra. Excitation was by the ultraviolet, blue, and green lines of a high-pressure mercury lamp for phosphors containing a high proportion of CdS. Filters were used to remove progressively the longer wave lines as the emission bands shifted towards the ultraviolet. For 20 mole % or less of CdS the 313 mμ line of mercury was used, unless otherwise indicated. In this way the excitation was mostly fundamental for the various compositions and allowed detection of both the impurity and the edge emission.
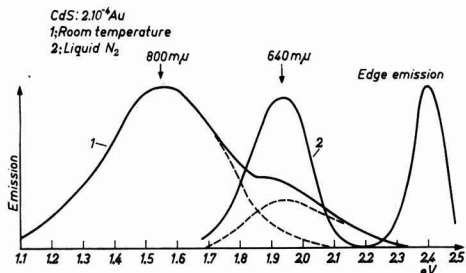
Fig. 1. Emission spectrum of gold-activated CdS at room and liquid nitrogen temperature.
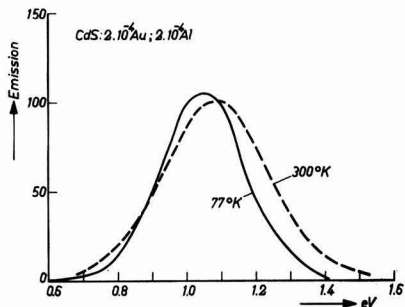
Fig. 2. Emission spectrum of CdS activated by equal amounts of Au and Al at room and liquid nitrogen temperature.

Fig. 3. Emission spectra of (Zn,Cd)S phosphors activated by gold and aluminum at room temperature.

Fig. 4. Shift of emission peak of coactivated (Zn,Cd)S phosphors activated by Au, Cu, and Ag. Room temperature.

Fig. 5. Absorption spectrum of gold-activated CdS. Room temperature.

Results

We find that whereas copper (8) and silver (7) are known to give two emission bands each in CdS, gold produces three distinct bands. Two bands are found at 640 mμ and 800 mμ when gold alone is used as an activator (Fig. 1). The third band appears as the only band at 1150 mμ when the gold activator is balanced by a trivalent coactivator such as aluminum (Fig. 2). The same emission band is also found when indium is used instead of aluminum. On cooling to liquid nitrogen temperature it shows only a slight shift toward longer wave lengths (Fig. 2), and no other emission bands appear. When zinc is substituted for cadmium in the host lattice this band is displaced in a regular manner toward shorter wave lengths (Fig. 3, 4) and appears at 530 mμ in zinc sulfide. Thus the 1150 mμ coactivated gold emission in CdS corresponds very well to the emission bands of coactivated silver and copper at 730 and 1020 mμ, respectively (Fig. 4).

The optical absorption of the coactivated gold centers in CdS extends beyond the fundamental absorption edge (Fig. 5) and gives the powder a reddish brown body color. In this respect, too, the coactivated gold centers resemble closely the coactivated centers of copper and silver.

Omission of the coactivator shows important differences between gold and the other activators. The short wave emissions of copper and silver appear in CdS when the activator concentration exceeds the coactivator concentration. With no coactivator at all gray products are obtained on firing in

an atmosphere of hydrogen sulfide, indicating that much of the activator remains unincorporated as the free sulfide. Gold alone as an activator, however, is well incorporated in CdS with only a small change in the absorption spectrum (Fig. 5). Two emission bands have been found in this case (Fig. 1) at 640 and 800 mμ. The small amount of chlorine introduced with the gold (which was added as gold chloride) is probably driven out by the current of hydrogen sulfide on firing, and its effect as a coactivator is not felt. This is supported by the observation that the two bands are both different from the coactivated band, that these bands do not appear in a coactivated phosphor, and also by the slight effect on the
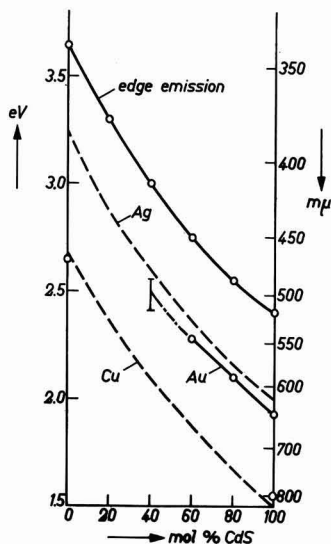
Fig. 6. Shift of emission peak of the short wave bands of (Zn,Cd)S phosphors activated by Au, Cu, and Ag. Liquid nitrogen temperature.

Fig. 7. Emission spectra of gold-activated (Zn,Cd)S phosphors at liquid nitrogen temperature. Fundamental excitation was used for each composition. Intensities were normalized with respect to the "edge emission."

absorption spectrum. The coactivated band appears, together with other bands, when high chloride concentrations are used, as in the experiments of Henderson, et al. (6).

The 640 mμ band predominates at low temperatures in CdS activated by gold alone, but in contrast to coactivated phosphors the edge emission is not suppressed (Fig. 1) so that the visible emission looks yellow. Indeed, it is remarkable that for high zinc content and fundamental excitation the edge emission surpasses in intensity the activator emission (Fig. 7).

On introducing zinc into the lattice the 640 mμ band is displaced towards shorter wave lengths, but its intensity falls quickly so that the band cannot be traced into the zinc-rich region (Fig. 7). Further interference arises from the strong edge emission and from the coactivated band which comes up even without addition of coactivator as the zinc content is increased. However, if normal displacement of the band with zinc content is assumed (Fig. 6), this band should appear at about 400 mμ in zinc sulfide. No such emission has been reported to date.

The 800 mμ band which appears at room temperature in CdS activated by gold alone (Fig. 1) is rather wide and of weak intensity. Its intensity is about 10% of the intensity of the 640 mμ band at low temperatures. The displacement of this band with zinc content also could not be followed because of interference from other bands as the zinc content was increased. If we assume normal displacement with zinc content, we see (Fig. 6) that this band should correspond to the 470 mμ gold band in ZnS.

It is interesting to note that in gold-activated ZnS with higher gold concentration the coactivated band at 530 mμ appears even when no coactivator is added. In Fig. 8 is given the emission of ZnS(Au) for long wave u.v. excitation so that interference from the
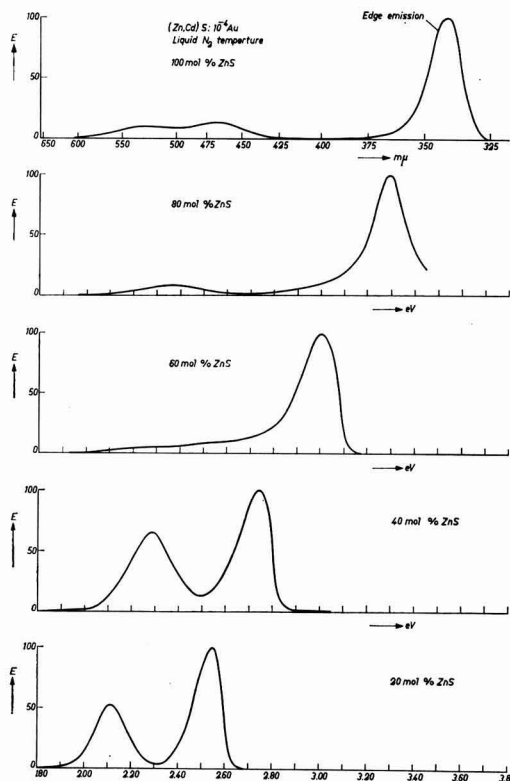
edge emission is eliminated. We see that both the coactivated band at 530 mμ and the short wave band at 470 mμ appear in comparable intensities. The emission can be well accounted for by assuming
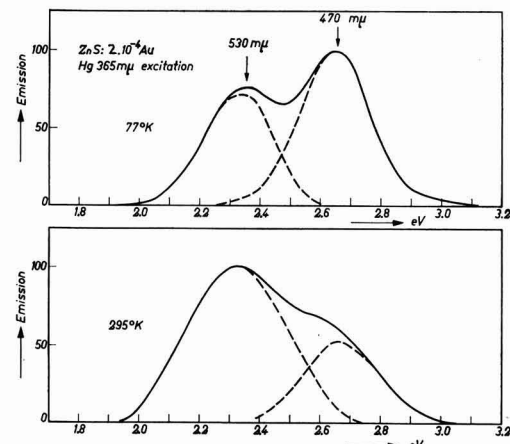
Fig. 8. Emission spectrum of gold-activated ZnS at room and liquid nitrogen temperatures. Resolution into sub-bands was done assuming that these change only in intensity, and not in position, with temperature.

these two bands to change only their relative intensities and not their position with temperature.

Discussion

The emissions of coactivated gold phosphors were found to correspond closely to coactivated copper and silver emissions over the whole range from CdS to ZnS, and it may be concluded that in this case gold is incorporated in the same state as the other activators. In view of the work of Henderson, et al. (6) it is interesting to note that chlorine, and presumably also other halogens, do not fully coactivate gold in (Zn,Cd)S phosphors. Such a marked difference between the halogens and the trivalent metals has not been observed for activation by copper and silver.

On the other hand, the short wave emission bands of gold show notable differences from the short wave bands of copper and silver. The nature of these centers is still unknown.

REFERENCES

1. C. J. Milner, Trans. Faraday Soc., 4, 101 (1938).
2. S. T. Henderson, Proc. Roy. Soc., A173, 323 (1939).
3. H. W. Leverenz, "An Introduction to the Luminescence of Solids," John Wiley & Sons, Inc., p. 211, New York (1950).
4. F. A. Kröger and J. Dikhoff, Physica, 16, 297 (1950).
5. W. van Gool, Private communication.
6. S. T. Henderson, P. W. Ranby, and M. B. Halstead, This Journal, 106, 27 (1959).
7. W. van Gool, Philips Res. Repts., 13, 157 (1958).
8. E. Grillot and P. Guintini, Comp. Rend. Paris, 239, 418 (1954).

Electrolytic Reduction of Nitro- and Dinitronaphthalenes

R. N. Boyd and A. A. Reidlinger

Department of Chemistry, Washington Square College, New York University, New York, New York

ABSTRACT

The polarographic reduction of mono- and dinitronaphthalenes was studied in buffered solutions at four different pH values. The relative wave heights of the multiple waves could be reasonably interpreted in terms of certain electron changes, and these were also checked by coulometric measurements on electrolyses run at controlled potentials. The first stage in reduction appeared to be a four-electron change. At pH 2.1 reduction often proceeded to completion, but there was polarographic evidence of intermediate stages for the homonuclear dinitro compounds. At pH 11, 1,4-dinitronaphthalene shows a two-electron change which may be due to a quinoid intermediate, as may a ten-electron change at pH 9.4 for the same compound.

The polarographic behavior of numerous dinitro derivatives of benzene has been investigated by Pearson (1), Bergman and James (2), and others, but very little has been done (3-5) with nitro compounds in the naphthalene series. Therefore, all ten possible dinitronaphthalenes were prepared, and the polarographic reduction of 5 x 10^{-4}M solutions of the nitro compounds in 80% ethanol was studied in four buffered solutions.

Electrolytic reductions at constant potentials of 2 − 5 x 10^{-4}M solutions of the nitro compounds in 80% ethanol were carried out at pH 2.1 using a stirred mercury cathode. The amount of current passed in each reduction was measured by a silver coulometer, and these coulometric values were compared with the relative wave heights of the polarographic curves in order to determine the particular reduction processes associated with each wave.

Experimental

Nitro compounds.—The nitro- and dinitronaphthalenes were prepared by previously published procedures, and the melting points of the products agreed with the literature values.

In particular, 2,3-dinitronaphthalene was prepared by the method of Chudozilov (6), m.p. 170-170.5° (Lit.: 170.5-171°), since the procedure given by Hodgson and Turner (7) led to a product which, although claimed to be the 2,3-isomer, melted at 159° and was found in the present work and by Ward (8) to be 1,7-dinitronaphthalene (mixed m.p. of alleged 2,3-isomer and authentic 1,7-isomer gave no depression).

Polarographic and coulometric procedure.—The polarographic and constant-potential coulometric studies were carried out with the same equipment, in the same manner and in the same buffers, as described for the work with the nitrotetralins (9), except that 2,6-dinitronaphthalene was run at a concentration of 1.0 x 10^{-4}M because of its extremely low solubility in 80% ethanol.

Polarographic data are given in Table I and constant-potential coulometric data in Table II.

Discussion

In Table II there is a comparison of the n values estimated from the relative wave heights of the polarographic curves and those obtained by coulo-

Table I. Polarographic reduction of the nitro- and dinitronaphthalenes[a]

	2.1		6.4		9.4		11.0	
	$E_{1/2}$	i_d/C	$E_{1/2}$	i_d/C	$E_{1/2}$	i_d/C	$E_{1/2}$	i_d/C
1-Nitro	−0.30	11.0	−0.51	10.4	−0.73	10.8	−0.83	10.3
	−0.65	15.8	?	?				
2-Nitro	−0.30	10.3	−0.49	11.1	−0.70	11.0	−0.82	10.9
	−0.72	15.7	?	?				
1, 2-Dinitro	−0.12	10.4	−0.30	10.1	−0.42	10.1	−0.44	?
	−0.38	30.1	−0.62	29.8	−1.06	31.4	−0.83	?
							−1.09	?
1, 3-Dinitro	−0.16	10.4	−0.33	10.2	−0.52	10.7	−0.62	9.8
	−0.27	21.1	−0.50	20.2	−0.76	21.2	−0.86	20.6
	−0.93	30.7	−1.45	?				
1, 4-Dinitro	−0.06	9.3	−0.29	9.7	−0.36	9.5	−0.39	5.6
	−0.36	29.1	−0.62	28.6	−0.93	25.5	−1.49	28.4
					−1.32	29.0		
1, 5-Dinitro	−0.22	22.9	−0.37	10.6	−0.57	10.3	−0.63	10.4
	−0.78	29.6	−0.50	19.7	−0.74	20.4	−0.84	20.2
			−1.48	26.9				
1, 6-Dinitro	−0.22	23.6	−0.38	10.1	−0.58	10.2	−0.64	10.5
	−0.82	31.1	−0.51	20.7	−0.74	21.2	−0.85	21.6
			−1.43	26.7				
1, 7-Dinitro	−0.22	24.1	−0.35	9.3	−0.50	10.5	−0.58	10.7
	−0.86	29.9	−0.51	19.7	−0.76	20.3	−0.85	21.4
			−1.36	26.5				
1, 8-Dinitro	−0.26	24.7	−0.48	19.8	−0.64	20.2	−0.72	20.7
	−0.69	29.9	−1.23	28.1	?	?	?	?
2, 3-Dinitro	−0.20	21.7	−0.34	9.9	−0.51	10.1	−0.60	10.4
	−0.67	28.3	−0.45	19.0	−0.68	18.9	−0.77	19.9
			−1.39	24.0				
2, 6-Dinitro	−0.14	5.2	−0.34	5.5	−0.49	5.6	−0.55	5.5
	−0.28	12.5	−0.55	10.9	−0.78	11.2	?	?
	−0.90	16.7	−1.36	14.6				
2, 7-Dinitro	−0.23	21.2	−0.37	10.3	−0.55	10.4	−0.63	10.6
	−0.81	29.3	−0.52	20.2	−0.73	19.7	−0.82	21.4
			?	?				

[a] The values of $E_{1/2}$ are in volts vs. S.C.E., and those of i_d/C are in $\mu a/mmole/l$. A question mark indicates that the wave is too indefinite to assign values with any degree of certainty. The pH values listed are the apparent values for the ethanolic solutions used in the electrolyses. The values of i_d/C are the sums of the individual wave heights.

metric analyses. It is evident that there is fairly good agreement between the two sets; and there is excellent agreement between them in the cases where the polarographic waves are well defined. It appears likely that for these compounds the electrolytic processes are the same at a stirred mercury cathode as at a dropping mercury electrode.

As has been found with derivatives of benzene (1, 2) and tetralin (9), the first of the multiple waves obtained from the polarographic reductions of nitro derivatives of naphthalene is usually one corresponding to a four-electron change, the transformation of a nitro group to a hydroxylamino group. This is especially true when the reductions are carried out at the higher pH's.

Kasagi (3) reported a single wave for "mononitronaphthalene" (presumably the 1-isomer) at about −0.9 v. Apparently the electrolytic medium he used, benzene-ethyl alcohol-lithium chloride, was alkaline (comparable to pH 11 in the present work). Thus his report of two waves of equal height for "dinitronaphthalene" (probably the 1,5-isomer) at potentials below −1.0 v agrees with the present re-

sults for 1,5-dinitronaphthalene at pH 11 or even at pH 9.4, and the two waves (as well as that for the mononitro compound) represent four-electron changes.

The constancy of wave height reported by Bezuglyi and Ogdanets (5) for "mononitronaphthalene" over a pH range of 2 to 12, and the variation of $E_{1/2}$ with pH for 1- and 2-nitronaphthalene reported by Imoto (4), also agree with the present findings.

Figure 1 shows two polarographic curves; curve A is a polarogram (uncorrected for residual current) that was obtained from a solution of 1,2-dinitronaphthalene at apparent pH 2.1; curve B is a polarogram (uncorrected for residual current) that was obtained from the same solution after an electrolysis in which a quantity of electricity equivalent to 3.9 electrons per molecule of dinitro compound had been passed through the cell. It can be seen that curve B is approximately two-thirds the height of curve A, and that it has the same half-wave potential as the second wave in A. The conclusion that can be drawn from these facts are the

Table II. Constant potential reduction of the nitro- and dinitronaphthalenes[a]

Compound	E_r	n (coulom.)	n (polarog.) [b]
1-Nitro	−0.35	3.97	4
	−0.80	5.83	6
2-Nitro	−0.35	4.00	4
	raised to −0.95	5.93	6
1, 2-Dinitro	−0.20	3.90	4
	−0.70	11.75	12
1, 3-Dinitro	−0.17	4.31	4
	raised to −0.40	8.28	8
	−0.90	12.48	12
1, 4-Dinitro	−0.13	4.07	4
	−0.65	11.93	12
1, 5-Dinitro	−0.50	7.59	(9)
	−0.85	11.64	12
1, 6-Dinitro	−0.40	8.65	(9)
	−0.90	11.91	12
1, 7-Dinitro	−0.35	10.00	(10)
	raised to −0.92	11.91	12
1, 8-Dinitro[c]	−0.50	8.85	10
	−0.85	11.58	12
2, 3-Dinitro	−0.40	8.15	(9)
	−0.90	12.15	12
2,6-Dinitro	−0.17	4.19	4
	−0.85	12.03	12
2, 7-Dinitro	−0.37	8.09	8
	−0.95	11.55	12

[a] E_r is the potential of the cathode (vs. S.C.E.) at which the reduction was carried out; n is the number of electrons involved in the reduction. The apparent pH was 2.1.
[b] Estimated to nearest integral number of electrons from wave heights of the polarographic curves.
[c] At pH 6.4 and −0.80 v, n was 8.17. When E_r was raised to −1.30 v, n was 12.47.

following: (a) the first wave of curve A corresponds to a four-electron change; (b) the second wave, which is twice the height of the first, undoubtedly represents an eight-electron change; (c) the intermediate reduction product, most likely an hydroxylamine, was stable enough in the acidic solution to yield a satisfactory polarogram.

The chemical (and electrolytic) reduction of nitro compounds in acid solution leads to the formation of amines, and it is highly probable that those polarographic reductions of dinitro compounds which require twelve electrons lead in acid to complete reduction with the formation of diamines. As the pH increases, reduction becomes more difficult and the polarographic curves show that eight- and ten-electron changes are commonly found. At pH 11 the curves are too diffuse in some cases to permit interpretation. At this pH the rate of condensation of intermediate products can be appreciable, and the diffuseness is probably due to secondary processes involving these condensation products.

It can be seen from Table I that, as the pH increases, the separation between the component waves for the dinitro compounds also generally increases. Pearson (1) found this to be true for dinitrobenzenes and dinitrotoluenes [as the present
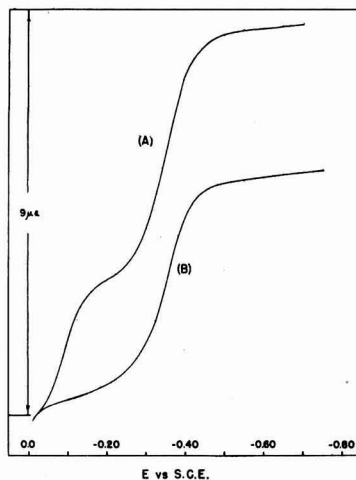
Fig. 1. Polarograms of 1,2-dinitronaphthalene at pH 2.1. A, Original nitro compound; B, after reduction equal to 3.9 electrons per molecule.

authors did for the tetralin series (9)] and it is attributed to a decrease in salt formation as the medium becomes more alkaline. For if $-NR_2$ or $-NHOH$ is an electron-releasing group but $-NR_3^+$ (and presumably $-NH_2OH^+$, too) is electron-attracting, one should expect that the nitro group in an N-arylhydroxylamine would accept electrons (be reduced) less readily than a nitro group in an N-arylhydroxylammonium salt.

The difference in the relative ease of reduction between 1-nitronaphthalene and 2-nitronaphthalene is smaller than that found for the corresponding 5- and 6-nitrotetralins (9). An examination of molecular models showed that if there were any interference between the 1-nitro group and the hydrogen atom of the 8-position, it was much less than the interference at corresponding positions in 5-nitrotetralin (9). Hence it is reasonable that 1- and 2-nitronaphthalene resemble each other more closely than do 5- and 6-nitrotetralin [or o- and m-nitrotoluene (1)].

The polarograms obtained in the present work for 1,3-dinitronaphthalene bear a striking similarity to the curves obtained previously for compounds of similar "meta" structure, namely m-dinitrobenzene (1, 2), 2,4-dinitrotoluene (1) and 5,7-dinitrotetralin (9). In general, present results for the homonuclear dinitronaphthalenes (except for the 2,3-isomer which as a β,β-isomer is unique in structure) agree with the findings for ortho-, meta-, and para-dinitro groups in the benzene (1, 2) and tetralin series (9).

Where two nitro groups are "ortho" or "para" with respect to each other in the homonuclear dinitronaphthalenes, the greater separation of the component waves can be attributed to a lessening of the positivity (and hence reducibility) of the nitro group in the initially formed nitrohydroxylamine. For example, resonance should play a greater part in the stabilization of the 1,2- and 1,4-deriva-

tives (I and II, respectively) than it does in the case of the 1,3- or 2,3-derivative (III).

I

II

III
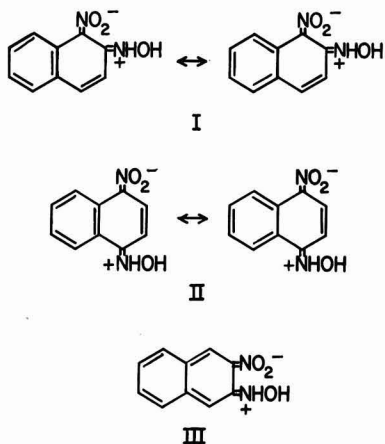
No important extra structures can reasonably be drawn for the 1,3-isomer; in the instance of 2,3-dinitronaphthalene only one quinoid structure (III) can be drawn, and it can make only a small contribution to the resonance energy. This may account for the anomalous behavior of the 2,3-isomer, which was not unexpected. The decrease in the positivity of the nitro group in the nitrohydroxylamine derived from 2,3-dinitronaphthalene certainly would not be so great as that in the 1,2- and 1,4-isomers, and hence the separation of the component polarographic waves should be less marked.

At pH 6.4, and in alkaline solutions, all the heteronuclear dinitronaphthalenes except the 1,8-isomer are reduced in much the same manner. The first wave corresponds to a four-electron change, and the second wave to an eight-electron change.

From Table I it can be seen that the separation of the component waves is distinctly greater in the curves obtained from 1,7-dinitronaphthalene than in the curves obtained from 1,5-, 1,6-, and 2,7-dinitronaphthalene, and is greatest of all in the curve for 2,6-dinitronaphthalene. Of the heteronuclear nitrohydroxylamines, quinoid structures can be drawn only for the 1,5-, 2,6-, and 1,7-isomers (IV, V, and VI, respectively).

IV

V

VI
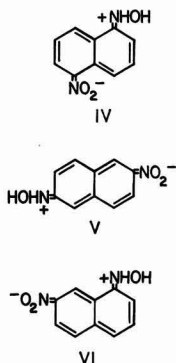
The quinoid structure for the 2,6-isomer (V) is undoubtedly the most important of these (2,6-naphthoquinone, for example, is the only known heteronuclear naphthoquinone); and, therefore, the reducibility of the remaining nitro group should be most affected. It is notable that 2,6-dinitronaphthalene also shows a four-electron wave in acid solution (as well as at pH 6.4 and in alkaline media). The occurrence of a four-electron step in acid solution indicates an unusual stability for the hydroxylamine stage (V), since reduction in acid generally leads to a diamine (or some other highly reduced product).

The separation of waves for the 1,7-isomer is less (only one p-benzoquinoid ring, VI) than for the 2,6-isomer, and it is in accord with conjecture that the separation for the 1,5-isomer (no p-benzoquinoid ring, IV) is not appreciably greater than for the 1,6- and 2,7-isomers, for which one can write no quinoid structures at all.

1,8-Dinitronaphthalene is the only dinitronaphthalene that does not show an initial four-electron wave in any of the buffered solutions studied. It has been reported (10) that 2,2'-dinitrobiphenyl also does not give a four-electron wave at any of the pH values studied; instead, its first wave at pH 6.4 corresponds to an eight-electron change. Large-scale reduction (11) at a controlled potential and at pH 6.4 showed benzo(c)cinnoline (VII) to be the major reduction product obtained from 2,2'-dinitrobiphenyl.
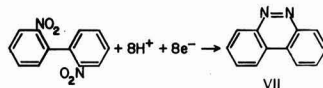
It is possible that the polarographic reduction product from 1,8-dinitronaphthalene at pH 6.4 (and at higher pH values) is correspondingly 1,8-naphthopyrazole (VIII).
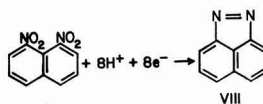
At pH 2.1 the probable ten-electron reduction could be interpreted as the formation of the dihydro derivative of the pyrazole (corresponding to the formation of a hydrazo compound). Under acidic conditions, where a low coulometric value was obtained for 1,8-dinitronaphthalene, the electrolyzed solution became deep purple in color. When the electrolysis was carried out at pH 6.4 the final solution was orange-yellow in color; yet it, too, turned to purple on standing in contact with air. It has been shown (10) that the dihydro derivative of benzo(c)-cinnoline undergoes dismutation to give a mix-

ture of benzo(c)cinnoline and 2,2'-diaminobiphenyl. Perhaps the dihydro derivative of the pyrazole also is similarly unstable.

A nine-electron change, such as found for 1,5- and 1,6-dinitronaphthalene, may be the result of two concurrent electrode processes (1); it would be awkward to account for an odd-electron change in any other way.

The polarographic curve for 1,4-dinitronaphthalene at pH 11 displays an unusual wave that appears to be associated with a two-electron step. This curve is very similar to the one that Holleck and Exner (12) obtained from 1,4-dinitrobenzene in alkaline solution. Holleck and Exner studied the reduction of the three isomeric dinitrobenzenes at the dropping mercury electrode over a wider range of pH values than is found in the work of Pearson (1). They stated that 1,4-dinitrobenzene gave very peculiar multi-stage curves that were caused by two concurrent processes. They claimed that in alkaline solution a two-electron change produced a stable quinone-like intermediate (IX) which was then reduced to N-(4-aminophenyl)hydroxylamine.
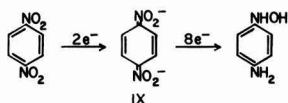
It would be expected that the double bonds between the nitrogen atoms and the ring would be similar in stereochemical requirements to carbon-to-carbon double bonds, and therefore all the atoms must be in the plane of the ring. It is indeed interesting that 1,4-dinitronaphthalene and 1,4-dinitrobenzene can satisfy the steric demands and do exhibit a two-electron change at pH 11; whereas 5,8-dinitrotetralin, in which neither nitro group can ever be coplanar with the aromatic ring (9), gives a first wave at pH 11 which corresponds to a typical four-electron change, and there is no evidence of a two-electron step.

If one accepts the proposal of a quinoid intermediate for a two-electron step, one might reasonably extend the general idea and suggest that polarographic waves which appear to represent ten-electron reductions can be interpreted by means of quinoid structures, too, rather than as N-(amino-aryl)hydroxylamines (12). This would mean that the reduction product would be a quinone diimine. It is therefore possibly more than merely coincidence that at pH 9.4 the only compounds that show waves indicating ten-electron changes, 1,4-dinitronaphthalene, 5,6-dinitrotetralin (9), and 6,7-dinitrotetralin

(9), are those for which diimines appear to be quite reasonable (X, XI, and XII, respectively).
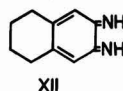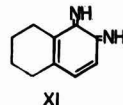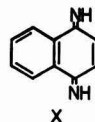
However, it should be pointed out that the potential of −1.32 v (Table I) for reduction of the alleged 1,4-diimine to a 1,4-diamine does seem high for an analog of 1,4-naphthoquinone.

REFERENCES

1. J. Pearson, *Trans. Faraday Soc.*, **44**, 683 (1948).
2. I. Bergman and J. C. James, *ibid.*, **50**, 60 (1954).
3. M. Kasagi, *Kogyo Kagaku Zasshi*, **54**, 745 (1951); *C. A.*, **47**, 7950 (1953).
4. E. Imoto, R. Motoyama, and H. Kakiuchi, *Bull. Naniwa Univ.*, **A3**, 203 (1955); *C. A.*, **49**, 15557 (1955).
5. V. D. Bezuglyi and N. D. Ogdanets, *Trudy Komissii Anal. Khim., Akad. Nauk S.S.S.R., Inst. Geokhim i Anal. Khim.*, **7**, 149 (1956); *C. A.*, **50**, 15345 (1956).
6. L. K. Chudozilov, *Coll. Czech. Chem. Comm.*, **1**, 302 (1929).
7. H. H. Hodgson and H. S. Turner, *J. Chem. Soc.*, **1943**, 635.
8. E. R. Ward, T. M. Coulson, and J. G. Hawkins, *ibid.*, **1954**, 4541.
9. R. N. Boyd, A. A. Reidlinger, and M. J. Sher, *This Journal*, **107**, 302 (1960).
10. S. D. Ross, G. J. Kahan, and W. A. Leach, *J. Am. Chem. Soc.*, **74**, 4126 (1952).
11. M. J. Sher, Ph.D. Dissertation, New York University, 1955.
12. L. Holleck and H. J. Exner, *Z. Elektrochem.*, **56**, 677 (1952).

Polarography of Some Aromatic Nitro and Carbonyl Compounds

Julia T. Gary and R. A. Day, Jr.

Department of Chemistry, Emory University, Atlanta, Georgia

ABSTRACT

The polarographic reduction of the nitro and carbonyl groups in 2-nitro-fluorenone, 2,7-dinitrofluorenone, and 2,5-dinitrofluorenone has been studied in buffered solutions over a pH range of about 1-13. To aid in interpreting the electrode reactions, additional polarographic studies were made with several compounds containing only the nitro or carbonyl group. These compounds were fluorenone, 4-nitrobiphenyl, 4,4'-dinitrobiphenyl, 2.4'-dinitrobiphenyl, 2,5-dinitrofluorene, and 2-aminofluorenone, and the polarography was carried out under the same solution conditions. The number of electrons involved in the reduction steps of several of these compounds was measured using the controlled cathode potential technique. It was found that the characteristic double waves of the carbonyl group in fluorenone are merged into a single two-electron wave in the dinitrofluorenones. This effect is apparently a general one, caused by the decrease in stability of the intermediate free radical brought about by the hydroxylamine groups in the aromatic nucleus.

The polarographic reduction of relatively few compounds containing both nitro and carbonyl groups has been reported in the literature. The nitrobenzaldehydes have been most thoroughly studied (1-4), and it has been possible to assign the various waves to the different steps in the reduction of the nitro and carbonyl groups.

We were particularly interested in the effect that an amino (or hydroxylamino) group has on the carbonyl waves in compounds where both groups are attached to a single aromatic nucleus. An aromatic nitro group is normally reduced at a lower potential than a carbonyl group; hence, when the carbonyl group is undergoing reduction the other substituent in the aromatic nucleus is the amino or hydroxylamino, not the nitro group. It has been observed that, whereas an aromatic aldehyde is normally reduced in two well-separated one-electron steps in sodium hydroxide solutions, the waves are apparently merged into a single two-electron step in meta-nitrobenzaldehyde (2). In the case of ortho and para-nitrobenzaldehydes the waves remain separate (2).

The ketone fluorenone is well known for its tendency to reduce in two well-separated one-electron steps in both acid, neutral, and basic media. It was therefore, of interest to study the behavior of the carbonyl group in fluorenone in cases where a nitro group was substituted in the 2 or 7 position of the fluorene nucleus. As the work progressed some dinitrofluorenones were studied and to aid in the interpretation of their behavior of the following compounds is described herein: fluorenone, 2-nitrofluorenone, 2,7-dinitrofluorenone, 2,5-dinitrofluorenone, 2-aminofluorenone, 4-nitrobiphenyl, 4,4'-dinitrobiphenyl, 2,4'-dinitrobiphenyl, and 2,5-dinitrofluorene.

Experimental

Polarographic data were obtained with a L&N Electrochemograph Type E. Half-wave potentials were corrected for IR drop and for lag caused by galvanometer damping. The electrolysis cell, experimental procedure, and buffer solutions were the same as described previously (5). However, because of the low solubility of several of the compounds in ethanol-water mixtures, a mixture of water and acetone was employed. The compound of interest was dissolved in acetone, and the cell solution was made by mixing equal volumes of this solution with the appropriate aqueous buffer. A single capillary of Corning marine barometer tubing was used. Its characteristics were: droptime 5.0 sec, $m = 1.34$ mg sec^{-1}, determined in a water-acetone mixture, buffered with citrate-phosphate (apparent pH 5.0) with an open circuit. The calculated value of $m^{2/3} t^{1/6}$ was 1.59 mg$^{2/3}$ sec$^{-1/2}$.

The coulometric measurements were carried out using a potentiostat of the Lingane-Jones type (6) and a hydrogen-oxygen coulometer. The cell, electrodes, and experimental procedures were essentially those recommended by Lingane (7).

Samples of 2-nitrofluorenone, 2-aminofluorenone, 2,5-dinitrofluorene, 2,5-dinitrofluorenone, and 2,7-dinitrofluorenone were kindly furnished us by the late Professor C. W. Bennett of Western Illinois State College (8). All other compounds studied were Eastman Kodak White Label chemicals. Reagent grade acetone was found to give no polarographic waves in the potential range normally employed.

Results

The half-wave potentials of the several compounds at different pH values are listed in Table I, along with measured and estimated values of the number of electrons consumed in the reduction process.[1] The behavior of the compounds will be discussed individually.

[1] A more complete list is available and may be obtained by writing to the authors.

Table I. Half-wave potentials of nitro and carbonyl compounds

Substance	pH (aq.)	Wave 1 $-E_{1/2}$	n	Wave 2 $-E_{1/2}$	n	Wave 3 $-E_{1/2}$	n
Fluorenone	1.5	0.61	[1][v]	0.86	[1]*		
	3.4	0.74	[1]	0.99	[1]		
	5.0	0.85	[1]	1.02	[1]		
	7.4	1.05	[2]				
	9.8	1.13	—	1.53	—		
	12.0	1.15	[1]	1.49	[1]		
2-Aminofluo-	1.3	0.62	[2]				
renone	3.7	0.77	[2]				
	5.0	0.86	[2]				
	7.0	1.02	[2]				
	9.6	1.13	[2]				
	12.0	1.18	[1]	1.45	[1]		
2-Nitrofluo-	1.4	0.20	4	0.68	2	0.98	2
renone	4.0	0.38	[4]	0.84	[2]		
	6.5	0.54	[4]	1.03	[2]		
	9.6	0.74	[4]	1.16	[2]		
	11.0	0.85	[4]	1.21	—		
4-Nitrobi-	1.4	0.20	[4]	0.74	[2]		
phenyl	3.8	0.38	[4]	0.87	[2]		
	6.8	0.63	[4]				
	9.2	0.76	[4]	1.06	—		
	11.2	0.79	—	1.00	—		
4, 4'-Dinitro-	1.4	0.15	8	0.78	2		
biphenyl	3.6	0.35	[8]	0.91	[2]		
	7.0	0.54	[4]				
		0.68	[4]				
	8.5	0.63	[4]	1.20	[2]		
		0.76	[4]				
	11.7	0.70	—	1.18	—		
2, 4'-Dinitro-	1.3	0.24	8	0.82	2		
biphenyl	3.0	0.33	[8]	0.87	[2]		
	4.0	0.40	[4]				
		0.62	[4]				
	7.9	0.67	[4]				
		0.82	[4]				
	11.7	0.65	—	1.09	—		
2, 5-Dinitro-	1.4	0.20	?				
fluorene	4.1	0.39	[8]				
	8.5	0.71	[8]				
	10.9	0.72	—	1.07	—		
	11.6	0.72	—	1.10	—		
2, 5-Dinitro-	1.5	0.20	8	0.61	2	1.01	2
fluorenone	4.0	0.36	[8]	0.88	[2]		
	6.3	0.42	4	1.04	2		
		0.56	4				
	8.5	0.55	[4]	1.15	[2]		
		0.71	[4]				
	10.2	0.73	—	1.16	[2]		
	11.5	0.72	—	1.16	[2]		
2, 7-Dinitro-	1.4	0.25	8	0.68	4	1.00	2
fluorenone	4.3	0.36	[8]	0.89	[4]		
	6.6	0.42	4	1.07	2		
		0.56	4				
	7.7	0.49	—	1.12	[2]		
		0.65	—				
	10.4	0.73	—	1.20	[2]	1.72	—
	11.3	0.74	—	1.20	[2]	1.75	—

Values of n given in brackets were estimated from the diffusion currents. Values not in brackets were measured coulometrically and rounded off to the nearest whole number.

Fluorenone gives two well-defined one-electron waves in both acid and basic media. In the pH range of about 7-9 the waves are merged. In ethanol-water solutions of low alcohol content these waves are usually separate over the entire pH range; however,

they are merged in the pH range of 6-8 in solutions which contain a high percentage of alcohol (9) and it is not surprising to find them merged here in a medium which is fairly high in acetone concentration. The 2-amino derivative is reduced in a single 2-electron step throughout the acid range; separation into two waves was not observed until the pH was raised to about 11. At pH 12 the waves were well separated into two one-electron steps. This behavior is in accord with that previously observed for meta-nitrobenzaldehyde (2) except at the highest pH studied.

In the case of 2-nitrofluorenone it is apparent that wave 1 corresponds to the reduction of the nitro group to hydroxylamine, this being a 4-electron step. Wave 2 is obviously due to reduction of the carbonyl, and here too the wave is a 2-electron step. There was no evidence of separation of the carbonyl wave into two steps at any pH although the wave-height did decrease appreciably at high pH values. A third wave was observed at pH 1.4, and the coulometric n-value corresponded to a 2-electron step. This probably corresponds to reduction of the hydroxylamino group to the amine. The wave was not observed at higher pH values.

The behavior of 4-nitrobiphenyl was similar to that of nitrobenzene (10, 11) in the low pH region, two waves of four and two electrons, respectively, being formed. The second wave was not observed in neutral media but did reappear in solutions of pH greater than 8.6. This behavior is not observed with nitrobenzene and may result from the fact that the unsubstituted benzene ring can supply electrons to the substituted ring, thereby facilitating the release of the hydroxyl group and the formation of a reducible quinoid structure (12). A macroelectrolysis was carried out in 0.1M HCl at a potential of −0.50 v. The reduction product was isolated and recrystallized. The melting point (152°-154°C) indicated that the product was 4-hydroxylaminobiphenyl. The product gave a characteristic red color with concentrated sulfuric acid.

At low pH values the compound 4,4'-dinitrobiphenyl gave reduction waves of eight and two electrons, respectively. This contrasts to the behavior shown by p-dinitrobenzene (10) in giving two waves of four and eight electrons. Apparently both nitro groups in the diphenyl compound are reduced to hydroxylamine simultaneously, whereas the two groups in the benzene ring are reduced in separate steps. In the pH range of about 7-10, however, the 8-electron wave of dinitrobiphenyl does split into two 4-electron steps. It is probable that each 4-electron wave corresponds to reduction of a single nitro group to the hydroxylamine, rather than to reduction of the two groups simultaneously to the nitroso stage. At low pH the hydroxylamine can add a proton, and the resulting positively charged group makes easier the reduction of the second nitro group. At higher pH the free hydroxylamine can act as an electron-releasing group, thereby making the reduction of the second nitro group more difficult. This would account for the splitting of the 8-electron wave as the pH is increased. The 2-electron step mentioned above was not present in solution of

about pH 7, but did reappear about pH 8.5. Hence, from pH 8.5 to 10 there were three waves of 4, 4, and 2 electrons, respectively. About pH 10 the first two waves were merged again. Complete reduction of both nitro groups to amines (12 electrons) was not observed at any pH, whereas p-dinitrobenzene did show complete reduction up to pH 4.1 (10).

The behavior of 2,4'-dinitrobiphenyl was very similar to that of the 4,4'-isomer. The initial 8-electron wave split into two 4-electron steps at a lower pH (about 4) and the two did not merge again until about pH 11. This behavior more nearly corresponds to that of m-dinitrobenzene (10) which gives two initial 4-electron waves up to pH 9.2. Again, however, no more than 10 electrons were taken up by the biphenyl compound whereas Pearson found complete reduction of m-dinitrobenzene at low pH values (10).

The behavior of 2,5-dinitrofluorene was different from that of both the dinitrobenzenes and the dinitrobiphenyls. Only one wave, corresponding to an 8-electron reduction, was observed over the pH range of about 1-10. Apparently both nitro groups are reduced simultaneously even though they are in different rings, and rotation of the two rings with respect to one another is not possible. This remained the case even at higher pH values where the 8-electron wave of the dinitrobiphenyls split into two 4-electron steps. Two waves were observed around pH 11 and 12, but in such basic solutions side reactions of the reduction products complicate the picture and the mechanism is complex.

The behavior of the nitro groups of both dinitrofluorenones resembled that of the dinitrobiphenyls more than that of dinitrofluorene. At low pH there was an initial 8-electron wave which split above pH 4 into two 4-electron waves. The waves were merged again at high pH. With both compounds wave 2 is obviously produced by reduction of the carbonyl group. The half-wave potentials are very near the values of those of 2-aminofluorenone and those of the second wave of 2-nitrofluorenone. At all pH values the current corresponded to the uptake of two electrons, there being no indication of a separation into two one-electron steps, nor a significant decrease in current at high pH. Apparently the two hydroxylamino groups in the fluorene nucleus (meta

to the carbonyl) greatly decrease the stability of the intermediate free radical formed by addition of one electron to the carbonyl group. The free radical is then reduced at its formation potential and dimerization does not occur. This effect is the same as that previously observed with m-nitrobenzaldehyde.

Both dinitrofluorenones give a 2-electron wave around −1.00 v at pH 1.4. This corresponds to the reduction of one hydroxylamine group to the amine. Wave 2 of 2,7-dinitrofluorenone in solutions of low pH corresponded to an uptake of four electrons. This is probably caused by over-lapping of the waves corresponding to the reduction of the carbonyl group and one of the hydroxylamino groups. In other words at pH 1.4 the 2,7 compound took up 14 electrons, corresponding to complete reduction of both nitro groups to amines, and the carbonyl group to the secondary alcohol. At pH values greater than 4 the reduction of the nitro groups stopped at the hydroxylamine stage, as is normally found for aromatic nitro compounds.

REFERENCES

1. A. Korshunov and L. N. Sazanova, *Zhur. Fiz. Khim.*, **23**, 1299 (1949).
2. R. A. Day, Jr. and R. M. Powers, *J. Am. Chem. Soc.*, **76**, 3085 (1954).
3. E. Gergeley and T. Iredale, *J. Chem. Soc.*, **1953**, 3226.
4. R. Portillo and G. Varela, *Anales fis. y quim.*, **40**, 839 (1944); *Anales bromatol*, **2**, 147 (1950).
5. R. M. Powers and R. A. Day, Jr., *J. Am. Chem. Soc.*, **80**, 808 (1958).
6. J. J. Lingane and S. L. Jones, *Anal. Chem.*, **22**, 1169 (1950).
7. J. J. Lingane, "Electroanalytical Chemistry," p. 251, Interscience Publishers, Inc., New York (1953).
8. C. W. Bennett, W. G. Jewsbury, and J. P. Dupuis, *J. Am. Chem. Soc.*, **68**, 2489 (1946); C. W. Bennett and W. W. Muelder, *ibid.*, **75**, 6039 (1953).
9. R. A. Day, Jr., S. R. Milliken, and W. D. Shults, *J. Am. Chem. Soc.*, **74**, 2741 (1952).
10. J. Pearson, *Trans. Faraday Soc.*, **44**, 683 (1948).
11. J. E. Page, J. W. Smith, and J. G. Waller, *J. Phys. Colloid Chem.*, **53**, 545 (1949).
12. I. M. Kolthoff and J. J. Lingane, "Polarography," Vol. II, p. 748, Interscience Publishers, New York (1952).

Kinetics of the Oxidation of Pure Tungsten from 500° to 1300°C

E. A. Gulbransen and K. F. Andrew

Chemistry Department, Westinghouse Electric Corporation, Pittsburgh, Pennsylvania

ABSTRACT

Kinetic studies were made on the oxidation of tungsten from 500° to 1300°C for time periods up to 6 hr, and for oxygen pressures from 0.1 atm to 0.00132 atm. The rate data were fitted to the parabolic rate law. A number of deviations and transitions were observed. For all of the experiments the initial slopes of the parabolic rate law plots were smaller than the final values found for thick films. A transition in the rate of oxidation was observed for weight gains of 2500-4000 μg/cm^2 at temperatures of 650°-800°C. Photographs of the oxidized surface above 650°C show that oxidation occurs in a preferential manner at the edges. Pressure had a strong effect on the rate of oxidation for the experiments above 950°C. At 1200°C weight loss curves were observed for pressures as high as 0.1 atm. Above 1200°C the oxidation reaction is similar to the combustion of graphite. The rate of oxidation is limited by the volatility of WO$_3$, the diffusion of oxygen to the surface, and the diffusion of W$_3$O$_9$ away from the surface.

The behavior of tungsten and its surface oxides in oxidizing and neutral atmospheres and in vacuum at high temperature is an interesting scientific problem. This paper presents results of an extensive study of the following problems: (*a*) the effect of time and temperature on the rate of oxidation of tungsten from 500° to 1300°C, (*b*) the effect of pressure on the time course of oxidation at four temperatures, (*c*) physical structure and crystal structure of the oxide scale, and (*d*) mechanism of reaction.

The oxidation of tungsten below 500°C has been studied by Gulbransen and Wysong (1) and by Gorbounova and Arslambékov (2). Gulbransen and Wysong (1) found the oxidation to follow the parabolic rate law between 400° and 500°C. Deviations were found to occur at 550° and below 400°C. A heat of activation of 45,650 cal/mole was calculated from the parabolic rate law constant. Tungsten oxides were found to volatilize at temperatures as low as 800°C for thick oxide films. Thin oxide films were found to require a higher temperature for volatilization of WO$_3$. Gorbounova and Arslambékov (2) found that the heat of activation for the temperature range of 390°-487°C was dependent on the surface preparation. Oxidation experiments on electrolytically polished samples gave a heat of activation of 46,500 cal/mole from the parabolic rate law constant while studies on mechanically polished samples gave a heat of activation of 41,000 cal/mole.

Dunn (3) studied the oxidation of tungsten from 700° to 1000°C and found the parabolic rate law followed. The temperature variation of the parabolic rate law constant was found to follow an exponential law of the Arrhenius type. An inflection was noticed at 850°-900°C and was attributed to a phase change in the oxides.

Scheil (4) studied the oxidation rate at 500° and 700°C over long periods of time and found a linear rate law. This was interpreted as evidence for the presence of a nonprotective film.

An intermediate type of rate law was suggested by Nachtigall (5) and Kieffer and Kolbl (6).

Webb, Norton, and Wagner (7) studied the oxidation of tungsten between 700° and 1000°C. The oxidation reaction was found to follow the parabolic rate law initially but transformed to a linear rate law for thick films. Two oxide layers appeared to form. In the outer layer a porous powdery yellow tungstic oxide WO$_3$ was formed, while in the inner layer a thin film of adherent oxide of uncertain composition was formed. Two rate processes were combined to give the over-all rate law. These were the parabolic rate law for the inner oxide layer and the linear rate law for the outer layer.

Baur, Bridges, and Fassell (8) studied the oxidation of tungsten rod and sheet from 600° to 850°C as a function of oxygen pressures from 20 to 500 psia. A linear rate law was found. Oxygen pressure increased the rate of oxidation. An equilibrium adsorption process was proposed to occur prior to the rate determining step.

Arkharov and Kozmanov (9) studied the composition of the oxide scale on tungsten between 500°-1350°C and the mechanism of reaction. They concluded that diffusion of oxygen was the rate-controlling process.

Semmel (10) studied the oxidation of tungsten in flowing air from 982° to 1371°C. The oxidation of tungsten was found to change from a linear to a parabolic rate law as the temperature was increased. Oxide melting was proposed to account for the decrease in oxidation rate above 1150°C.

Experimental

Kinetic studies were made using the vacuum microbalance method (11). Small strips of 5 mil tungsten sheet or small lengths of 9 mil wire were

suspended from a sensitive quartz beam microbalance operating inside an all glass and ceramic vacuum system (12). A 1-in. I. D. gas tight mullite furnace tube was used to enclose the sample. This tube was sealed directly to the all-glass vacuum system. No metal, rubber, grease joints or stopcocks were used in the reaction system. Pressures of less than 10^{-8} mm Hg could be attained after 24 hr of pumping (12).

To minimize the reaction of tungsten with the residual gases present in the vacuum system on heating to temperature the sample and furnace tube were pumped for several hours at a pressure of 10^{-6} mm Hg or lower. Purified oxygen was added after the furnace was raised and thermal equilibrium established. The time course of the reaction was followed semicontinuously by reading the balance position relative to a fixed point.

The furnace temperature was maintained constant to $\pm 1.5°C$ by the use of a calibrated high sensitivity recorder controller and a calibrated Pt-Pt + 10% Rh thermocouple.

Two microbalances of different sensitivities were used. For rapid reactions a specially constructed low sensitivity microbalance was used having a sensitivity of 0.234×10^{-3} cm/μg. The high sensitivity balance had a sensitivity of about 0.9×10^{-3} cm/μg. Four sample sizes were used corresponding to surface areas of 2.69 cm², 1.34 cm², 0.61 cm², and 0.32 cm². The specimens weighed 0.3770 g, 0.1533 g, 0.07019 g, and 0.0315 g, respectively. The wire samples were 1 cm long, weighed 0.0078 g, and had surface areas of about 0.0743 cm².

Weight gains of 8 mg could be measured on specimens having a surface area of 0.32 cm² and weighing 0.0315 g. This weight gain was equivalent to 94% of the metal reacting with oxygen to form WO_3.

Specimens were prepared from Westinghouse high-purity 5 mil cold rolled tungsten sheet or 9 mil wire. The spectrographic analysis of the sheet was as follows: Al, 0.0001-0.001; Mn, not detected; Fe, 0.001-0.01; Si, 0.001-0.01; Mg, 0.0001-0.001; Mo, 0.001-0.01; Cu, < 0.001; Ag, 0.0001-0.001; Ni, 0.0001-0.001; and Ca, 0.0001-0.001.

Spectroscopic analyses of the tungsten wire were as follows: Al, 0.0004; Mn, < 0.0005; Fe, 0.0020; Si, 0.003; Mg, < 0.0005; Ni, < 0.0005; K, 0.0035; Mo, 0.0015; C, 0.005; O, 0.0024; N, 0.0005; H, 0.0007; Cd, 0.002.

Specimens were cut to shape by a small shearing machine with the specimen hot or cold. The hole for the supporting wire was drilled by a high velocity jet of Al_2O_3. A tungsten etch containing NaOH and $K_3Fe(CN)_6$ was used to remove the scale formed by heating during the shearing operation. Samples were next washed with distilled water.

The surface was polished with emery paper through 4/0 and finally cleaned with petroleum ether and absolute alcohol.

Each oxidation experiment was made with a new specimen. The experimental results were reproducible to 10% except for the temperature ranges where transition effects were observed.

Initially, cold sheared specimens were used. However, the oxidation curves were not reproducible
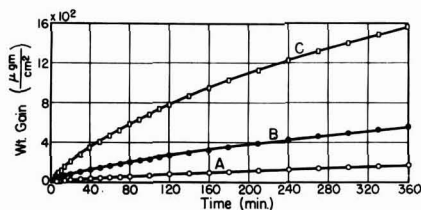
Fig. 1. Oxidation of tungsten, 500°-600°C, 0.1 atm. O_2, abraded, A—500°C, B—550°C, C—600°C.

due to excessive splitting of the metal during oxidation. This splitting effect opened up new areas of metal for reaction. Most of the results reported in this study were for hot sheared tungsten samples. Splitting also occurred for hot sheared samples but to a much lesser degree.

Results

Effect of temperature.—Abraded hot sheared tungsten strip specimens were oxidized over the temperature range of 500°-1150°C at a pressure of 0.1 atm of purified oxygen. For the 500°-650°C temperature range the time period was 6 hr. At 1150°C, a time period of 6 min was sufficient for nearly complete reaction of the tungsten sample. Figures 1 to 4 show weight gain versus time plots of the experimental measurements. Weight gain is given in micrograms per square centimeter and time in minutes. No correction was made for surface area changes during reaction.

To relate the weight gain in micrograms per square centimeter to oxide thickness in Angstroms a factor of 67.5 could be used. This factor was calculated from a density of 7.16 for the oxide WO_3 and a surface roughness ratio of unity. However, thickness calculations based on this factor were subjected to three limitations for heavily oxidized specimens. Reaction occurs more rapidly at the edges, cracking introduces porosity in the oxide layer, and surface area for reaction decreases. The factor 67.5 is significant only for the early stages of the oxidation reaction.

Figure 1 shows the weight gain curves for the 500°, 550°, and 600°C runs. The rate of oxidation decreases as the oxide thickens which indicates that the oxide scale was limiting the rate of oxidation. Calculations based on Fig. 1 show an average oxide film of about 100,000Å thick was formed on tungsten at 600°C in 6 hr. For the same oxidation conditions a 2120Å thick oxide film was formed on nickel and a 32,600Å thick oxide film was formed on zirconium.

Table I shows a summary of the oxide weight gains after 5, 10, 60, 180, 360 min of oxidation for the complete set of experiments. The color of the oxide at the surface and edges and the stability of the oxide scale to cracking and splitting were also tabulated.

Figure 2 shows oxidation curves for the 600°-750°C runs. S-shaped oxidation curves were observed in some of the experiments. Rapid changes in rate of oxidation occurred in the weight gain vs. time curves for weight gains of about 2,500 to 3,000 μg/cm². Small yellow crystals of oxide were formed on the 650°C oxidized surface while green oxide

Table I. Weight gain vs. time, tungsten oxidized at temperatures of 500°-1150°C, 7.6 cm of O_2 pressure, also color and adherence of oxide film

T, °C			($\mu g/cm^2$) Wt. gain at time, min			Color	Adherence of oxide	
	5	10	60	180	360		Surface	Edge
500	8.72	12.2	49	104	171	Blue black	Stable	Stable
500	19.5	31.0	91	180	283			
550	36.3	54.0	169	353	564	Blue black	Stable	Stable
600	67.4	119	473	1,020	1,560	Blue black with green edges	Stable	Stable
600†	93.5	143	523	1,080	1,620	Blue black	Stable	Split
600*	84.8	136	496	1,020	1,520	Blue black	Stable	Stable
612.5	90.0	149	569	1,270	1,710	Blue black	Stable	Stable
625	130	211	776	1,620	3,160	Black with yellow spots	Spalled	Split
625	140	263	1,340	2,880	4,660			
637.5	152	255	930	1,820	3,680	Black with yellow spots	Spalled	Split
650.0	228	330	1,130	2,930	8,020	Blue black with yellow covering	Spalled	Split
650.0	230	390	1,300	2,310	4,300	Blue black with yellow covering	Spalled	Stable
700	550	930	2,420	—	—	Black with green edges	Stable	Stable
750	1,050	1,600	3,380	—	—	Black with green edges	Stable	Stable
750	1,180	1,790	4,130	11,800	—	Black with green edges	Stable	Stable
750	1,340	1,740	3,740	—	—	Black with green edges	Stable	Split
775	1,470	2,000	4,980	—	—	Black with green edges	Stable	Split
800	1,590	2,140	8,780	—	—	Black with green edges	Stable	Split
800	1,730	2,310	9,300	—	—	Black with green edges	Stable	Split
825	1,830	2,760	—	—	—	Black with green edges	Stable	Split
850	2,980	4,940	16,100	—	—	Blue black, greenish yellowish edges	Stable	Split
900	2,510	4,060	17,600	—	—	Blue black, greenish yellowish edges	Stable	Split
950	3,620	5,940	—	—	—	Black with green edges	Stable	Split
950	3,950	6,140	—	—	—			
950	4,320	6,540	—	—	—			
1000	7,110	14,500	—	—	—	Black with greenish edges	Stable	Split
1050	13,800	21,900	—	—	—			
1100	16,000	25,000	—	—	—	Yellow-black	Stable	Split
1150	14,700	—	—	—	—			

† Heat treated at 1000°C overnight.
* H_2 reduced overnight at 600°C.

crystals formed on the edge of the samples oxidized at 700° and 750°C.

At 750°C a weight gain of 11,800 $\mu g/cm^2$ was found after 3 hr of reaction. Visual observations of the oxidized surface and the kinetic data show that tungsten has poor resistance to oxidation at 750°C. Rapid oxidation occurs in a preferential manner at the edges. Spalling occurred in some of the experi-

ments. If cracking or spalling occurs so that oxygen can react more rapidly with the metal, a rapid change will occur in the rate of oxidation. Due to stresses at the sample edges, cracking occurs first at the edges.
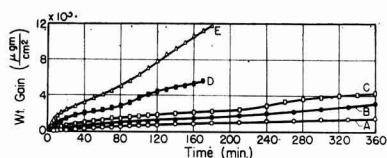
Fig. 2. Oxidation of tungsten, 600°-750°C, 0.1 atm. O_2, abraded, A—600°C, B—625°C, C—650°C, D—700°C, E—750°C.
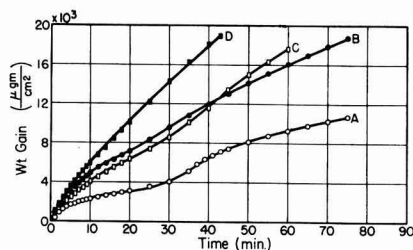
Fig. 3. Oxidation of tungsten, 800° to 950°C, 0.1 atm. abraded, A-800°C, B—850°C, C—900°C, D—950°C.

Figure 3 shows oxidation curves for the 800°-950°C oxidation runs. Again S-shaped curves were found at 800° and 850°C. A weight gain of 16,090 $\mu g/cm^2$ was observed at 850°C in 1 hr. Examination of the sample showed splitting had occurred at the edges. Calculations based on Fig. 1-3 shows that the increase in rate of oxidation with temperature becomes smaller above 800°C.

Figure 4 shows oxidation curves for the 950° to 1150° range of temperature. Reaction times of 6-45 min gave nearly complete reaction of the tungsten to form WO_3.

The 1100°C oxidation showed an initial reaction rate of 83.0 $\mu g/cm^2/sec$ and an average rate of 41.5 $\mu g/cm^2/sec$ for the 10-min run. Assuming a WO_3 scale is formed, the heat of formation of WO_3 contributes 0.34 $cal/cm^2/sec$ to the sample. Without radiation and convection losses this heat would raise the sample temperature 82°C/sec. Assuming black body conditions, radiation losses alone would limit the total temperature rise to 24°C. After the first minute of reaction the sample would assume a temperature rise of 12°C. However, convection currents in the gas would also transfer heat from the specimen and limit the temperature rise to less than 12°C.

If reaction occurs locally at the edges, local heating can occur which would lead to a higher temperature and a more rapid reaction at the edges. This factor combined with stress conditions at the edges leads to breakdown conditions for oxidation.

Figure 5 shows oxidation curves for the 1100° to 1200°C range of temperature using 9-mil wire speci-

mens. The 1100° and 1150°C runs show initial weight gains. After 2-5 min of oxidation the specimens start to lose weight at a nearly constant rate. The 1200°C curve shows a weight loss immediately after adding oxygen. As fast as oxide is formed evaporation occurs.
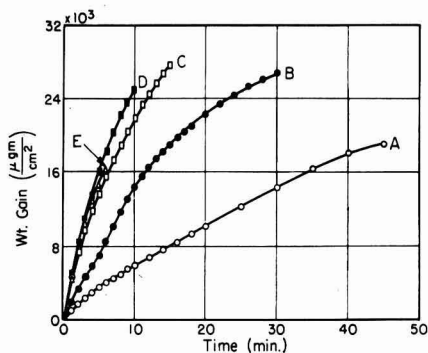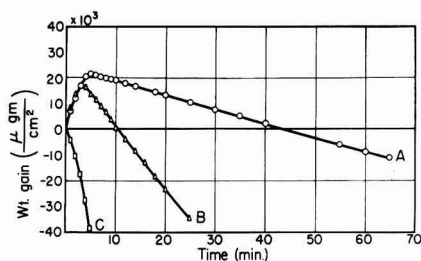
The 1100°C run showed an average reaction rate of 85.5 $\mu g/cm^2/sec$ for the first 4 min of reaction. This compares to a value of 83.0 $\mu g/cm^2/sec$ for the initial reaction rate of a strip specimen of tungsten. The wire specimens were oxidized over a fairly long time period to show the effect of evaporation on the oxidation process. At 1200°C the theoretical rate of evaporation of WO_3 was faster than the rate of oxidation. The net result is a weight loss curve.

Above 1200°C the rate of oxidation at 0.1 atm of oxygen pressure was too rapid to measure on our microbalance apparatus. Oxidation and evaporation of the 9-mil tungsten wire specimen was complete in 1 or 2 min of reaction time. To extend our results to 1300°C the oxidation reaction was studied at a pressure of 0.0013 atm. Figure 6 shows the results. Weight loss in $\mu g/cm^2$ was plotted against time in minutes. S-shaped weight loss vs. time curves were found.

Figures 5 and 6 suggest that for temperatures of 1200°C and higher evaporation of WO_3 occurred as fast as the oxide was formed. The form of the oxidation curve was governed by diffusion of oxygen to the surface and geometrical considerations of the decreasing surface available for reaction. As oxide volatilizes the surface area of metal decreased and a slower rate of reaction resulted.

Effect of pressure.—For many metals the effect of pressure on the kinetics of the oxidation reaction is less important than time and temperature. For tungsten which forms a volatile oxide oxygen pressure and the pressure of inert gases are very important.

Fig. 4. Oxidation of tungsten, 950°C to 1150°C, 0.1 atm. O_2, abraded A—950°C, B—1000°C, C—1050°C, D—1100°C, E—1150°C.
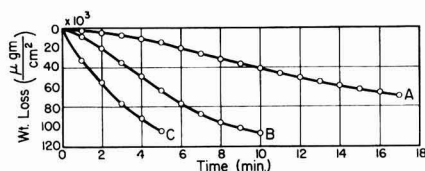
Fig. 6. Oxidation of tungsten, wire sample, 1200°-1300°C, 0.0013 atm. O_2, abraded, A—1200°C, B—1250°C, C—1300°C.

Fig. 5. Oxidation of tungsten, wire sample, 1100°-1200°C, 0.1 atm. O_2, abraded, A—1100°C, B—1150°C, C—1200°C.
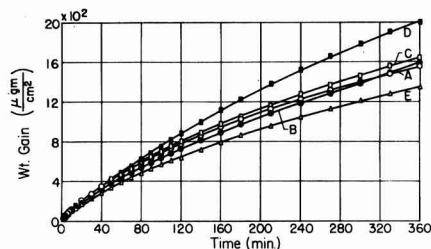
Fig. 7. Oxidation of tungsten at 600°C, effect of O_2 pressure, A—0.1 atm., B—0.068 atm., C—0.0355 atm., D—0.0132 atm., E—0.0079 atm.

Three temperatures were chosen for the studies on the pressure effect using strip specimens, 600°, 950°, and 1050°C. Additional experiments were made at 1000° and 1100°C. Figure 7 shows oxidation curves at 600°C for five pressures between 0.1 atm and 0.0079 atm. Each curve shows a slowly decreasing rate of reaction as the oxide thickens. Decreasing the oxygen pressure from 0.1 atm to 0.0132 atm slightly increased the rate of oxidation. The effect of pressure is small on the rate of oxidation. At 600°C the volatility of WO_3 was unimportant in the dry oxidation of pure tungsten. Figure 8 shows the effect of oxygen pressure on the rate of oxidation at 950°C together with the volatility curve of WO_3 (13, 14). Decreasing the oxygen pressure lowers the rate and extent of oxidation. The volatility of WO_3 and diffusion of WO_3 away from the surface has affected the time course of oxidation.

Figure 9 shows the effect of oxygen pressure on the time course of oxidation at 1050°C together with the volatility curve for WO_3 (14). At this temperature the oxygen pressure has a major effect on the time course of the reaction. For oxygen pressures of

Fig. 10. Oxidation of tungsten, wire sample, at 1200°C, effect of pressure, abraded, A—0.1 atm., B—0.047 atm., C—0.025 atm., D—0.012 atm., E—0.0066 atm., F—0.0033 atm., G—0.0013 atm.
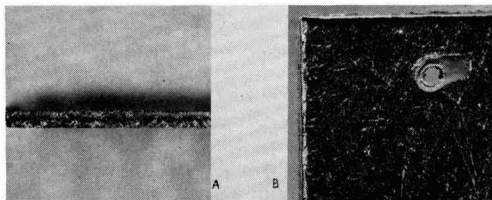
Fig. 11. Photograph Oxidized Tungsten Sample 750°C., 0.1 atm. of O_2, 2 Hours, Hot Sheared, 20x, A. Edge, B. Surface.

Fig. 8. Oxidation of tungsten, at 950°C, effect of pressure, A—0.1 atm., B—0.047 atm., C—0.0118 atm., D—0.00528 atm., E—0.0033 atm., F—0.00132 atm., G—volatility WO_3.
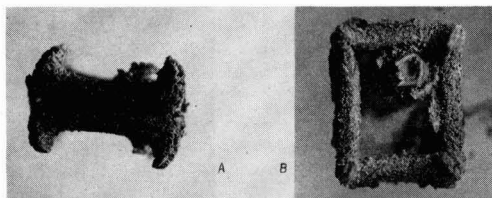
Fig. 12. Photograph Oxidized Tungsten Sample 950°C., 0.1 atm. O_2, 54 minutes, 20x, Hot Sheared, A. Edge, B. Surface.

0.0033 atm and lower, curves F and G, a weight loss is observed. This plot demonstrates the fact that two processes control the weight gain vs. time curves at 1050°C. The first process is the formation of the oxide scale and the second process is the volatility of WO_3 and its diffusion into the gas phase. The latter process is a function of the density of the oxygen atmosphere surrounding the specimen. Curve H shows the volatility curve of WO_3 in vacuum (14).

Table II summarizes the studies on the pressure effect at the temperatures of 600°-1100°C.

Figure 10 shows a study of the effect of oxygen pressure on the oxidation of wire specimens of tungsten at 1200°C for 7 pressures. Table III summarizes the data. Weight loss curves were obtained for all pressures at 1200°C. The maximum weight loss curve occurs at an oxygen pressure of 0.012 atm. The decrease in the rate of weight loss below 0.012 atm oxygen pressure is probably due to the lower rate of oxidation. Again S-shaped curves were obtained for the lower oxygen pressures. The S-shaped curve is due to the decrease in surface area.

Photographic studies.—To show the localized nature of the oxidation reaction at the edges a number of the oxidized samples were photographed at 20 X magnification. Figures 11-12 show photographs of both the edge and surface of the oxidized metal

Fig. 9. Oxidation of tungsten at 1050°C, effect of pressure, A—0.1 atm., B—0.0512 atm., C—0.0263 atm., D—0.0112 atm., E—0.0066 atm., F— 0.0033 atm., G—0.00131 atm., H—volatility WO_3.

Table II. Weight gain vs. time, tungsten oxidized at temperatures of 600°-1100°C, varying O₂ pressure, also color and adherence of oxide film

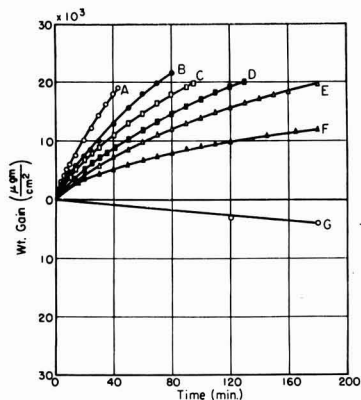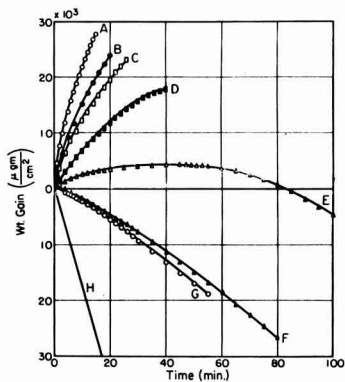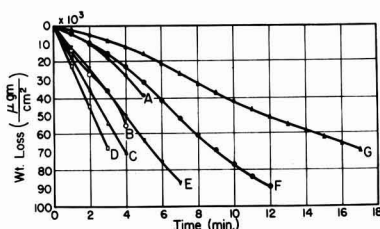| T, °C	O₂ pressure, cm Hg	(µg/cm²) Wt. gain at time, min					Color	Adherence of oxide Surface	Edge
		5	10	60	180	360			
600	7.6	67.4	119.0	473	1,030	1,560	Green edges Blue black	Stable	Stable
600	5.2	57.5	104	438	970	1,570	Black	Stable	Stable
600	2.7	71.0	119	480	1,060	1,640	Black	Stable	Spilt
600	1.0	74.8	125	492	1,380	2,000	Black	Stable	Spilt
600	0.50	67.4	109	393	860	1,350	Black	Stable	Stable
950	7.6	3,950	6,140	—	—	—			
950	3.6	2,970	4,660	18,800	—	—			Spilt
950	1.9	2,360	3,790	—	—	—			Spilt
950	0.9	2,300	3,980	14,800	—	—	Green edges Grey black	Stable	Spilt
950	0.4	1,550	2,850	11,900	—	—	Green edges Grey black	Stable	Spilt
950	0.25	1,070	2,100	9,700	19,600	—	Green edges Black	Stable	Spilt
950	0.10	1,370	2,230	6,600	11,900	44,700	Green edges Grey black	Stable	Spilt
1000	7.6	7,100	14,500	—	—	—	Green edges Black	Stable	Spilt
1000	0.90	4,000	6,930	22,500	—	—			Stable
1000	0.25	1,330	2,380	8,500	10,700	—			Stable
1050	10.0	14,100	—	—	—	—			Stable
1050	7.6	13,800	21,900	—	—	—			Stable
1050	5.3	10,100	15,800	23,100	—	—	Yellow edges Yellow grey Surface	Stable	Spilt
1050	3.9	9,200	15,000	—	—	—			Stable
1050	2.0	7,500	12,200	—	—	—			Stable
1050	0.86	3,820	6,850	—	—	—			Stable
1050	0.50	1,560	2,520	3,700	—	—			Stable
1050	0.25	−535	−1,820	18,800	—	—	Grey black	Stable	Stable
1050	0.10	−907	−2,180	—	—	—	Grey black	Stable	Stable
1100	7.6	16,000	25,000	—	—	—	Yellow black	Stable	Spilt
1100	3.9	11,600	19,100	—	—	—			
1100	0.25	−4,730	−10,700	—	—	—	Grey black	Stable	Stable

samples for experiments at 750°C and 950°C. Table IV shows a summary of the oxidation conditions, weight gains, and photographic observations on these samples. Initial breakdown of the oxide-metal interface occurs at the edges during oxidation for both hot and cold sheared samples. However, breakdown occurs on the cold sheared surfaces at an earlier stage of the reaction.

Rate law correlation.—Both the linear and parabolic rate laws have been used to explain the oxidation rate of metals. The linear rate states

$$W = At + C$$

A surface or interface reaction may control the rate of oxidation. In the above equation W is the weight

Table III. Weight gain vs. time, 9-mil tungsten wire, oxidized at 1200°C, varying O₂ pressure

O₂ pressure, Cm of Hg	µg/cm² Wt. gain at time, min		
	1	2	4
7.6	−4,000	−10,500	−27,500
3.57	−12,000	−27,000	−55,000
1.9	−17,000	−35,500	−70,500
0.91	−22,000	−44,500	—
0.502	−12,500	−23,000	−36,000
0.251	−4,000	−9,500	−22,500
0.099	−2,500	−5,000	−11,500

gain, t is the time, and A and C are constants. The parabolic rate law states

$$W^2 = At + C$$

Here the symbols have the same meaning as before. This equation has been derived from fundamental principles of diffusion (15, 16).

To test the application of the parabolic rate law and to show the existence of rapid changes in the rate of oxidation, plots were made of the square of the weight gain versus time over the temperature range. Because of the complex nature of the oxidation reaction of tungsten it is not expected that the parabolic rate law will hold over the complete time, temperature, and pressure conditions. Initial values of the constants probably represent diffusion controlled reactions. Changes from these conditions can be seen by the use of the parabolic rate law plots.

Figure 13 shows the parabolic rate law plot for the 500°C run. The plot shows a steady increase in the value of the rate law constant. An initial value of 4.18×10^{-13} $(g/cm^2)^2$ sec^{-1} was calculated for A. The value for the 5-6 hr time period was 1.75×10^{-12} $(g/cm^2)^2$ sec^{-1}. At temperatures as low as 500°C the protecting properties of the oxide decrease as the oxide thickens.

Similar plots for the oxidation runs at 550° and 600°C show curves like those of Fig. 13. At 625°C a

Table IV. Summary photographic studies oxidation of tungsten 600°-950°C

Temp, °C	Oxidation conditions Pressure, atm	Time	Type of Shearing	Weight gain $\mu g/cm^2$	Results
600	0.0343	6 hrs	Cold	2,850	Shows initial breakdown of oxide at edges
725	0.10	75 min	Cold	5,460	Reaction at edges with cracking
750	0.10	2 hrs	Hot	5,350	Reaction at edges and scratches on surface
850	0.10	75 min	Hot	18,700	Strong edge reaction with cracking
950	0.10	54 min	Hot	20,000	Strong edge reaction extending over surface

transition was noted from parabolic plots of the rate of oxidation data. Figure 14 shows the parabolic rate law plot of the 650°C run. A transition is found after 200 min of reaction or at an oxide thickness of 2400 $\mu g/cm^2$. After 300 min of reaction, Fig. 14 shows the parabolic rate law was again obeyed.

Transitions were found also for the oxidation runs at 650°, 700°, 750°, and 800°C. However, the weight gain for transition was larger. Table V shows the initial and final parabolic rate law constants.

Figure 15 shows a parabolic rate law plot of the 900°C oxidation run. The slope of the plot increased during the first 45 min of reaction to a nearly constant value. The initial value of A was 1.725 x 10^{-8} $(g/cm^2)^2$ sec^{-1} and the final value 1.45 x 10^{-7} $(g/cm^2)^2$ sec^{-1}. Similar parabolic rate law plots were found for the 950°, 1000°, 1050°, 1100°, and 1150°C runs.

This analysis suggests that the rate of oxidation of tungsten is not a simple function of the time of reaction. Adhesion of the oxide scale to the metal is very important. Localized cracking of the oxide scale may account for the rapid changes observed in the rate of oxidation.

Figure 16 shows a logarithmic plot of the parabolic rate law constants A vs. $1/T$. Three values from our earlier work (1) at 400°, 450°, and 500°C were included. In addition the data obtained by Dunn (3) and by Webb, Norton, and Wagner (7)

were included in the plots. Since the parabolic rate law constants were time dependent, both the initial and final values of the constants from our data were plotted.

Three straight lines were drawn to represent the data. The dashed line in Fig. 16 was drawn to present the initial values of the parabolic rate law constants and the earlier values of Gulbransen and Wysong (1). The slope of the dashed line gave a heat of activation of 44,500 cal/mole. This value was found also by Gulbransen and Wysong (1) to explain the oxidation of tungsten for temperature of 400° to 500°C. Gorbounova and Arslambékov (2)
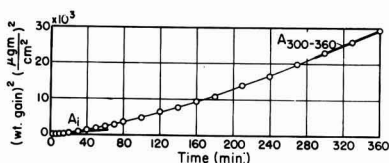
Fig. 13. Oxidation of W, parabolic plot, abraded through 4/0, 500°C, 0.1 atm. of O_2, $A_{Initial} = 4.18 \times 10^{-13}$, $A_{300-360} = 1.75 \times 10^{-12}$ $(g/cm^2)^2$ sec^{-1}.
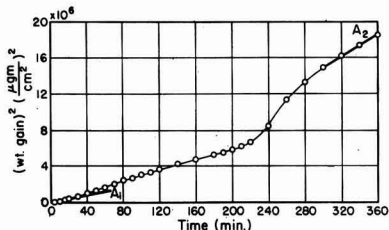
Fig. 14. Oxidation of W parabolic plot, abraded through 4/0, 650°C, 0.1 atm. of O_2, $A_{Initial} = 3.33 \times 10^{-10}$, $A_{300-360} = 1.03 \times 10^{-9}$ $(g/cm^2)^2$ sec^{-1}.
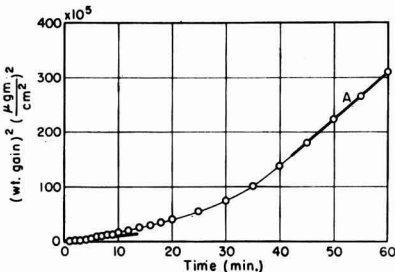
Fig. 15. Oxidation of W, parabolic plot, abraded through 4/0, 900°C, 0.1 atm. of O_2, $A_{45-60} = 1.45 \times 10^{-7}$ $(g/cm^2)^2$ sec^{-1}.

Table V. Parabolic rate law constants hot sheared tungsten, abraded, 500°-1150°C

Temp, °C	$A (g/cm^2)^2$ sec^{-1} initial value	$A (g/cm^2)^2$ sec^{-1} final value
500	1.59×10^{-12}	4.72×10^{-12}
550	5.56×10^{-12}	1.97×10^{-11}
600	3.34×10^{-11}	1.168×10^{-10}
600	3.34×10^{-11}	1.36×10^{-10}
625	1.39×10^{-10}	1.667×10^{-9}
650	2.78×10^{-10}	6.75×10^{-9}
700	8.33×10^{-10}	4.03×10^{-9}
750	3.17×10^{-9}	8.22×10^{-9}
750	5.00×10^{-9}	2.21×10^{-8}
750	3.67×10^{-9}	2.10×10^{-8}
775	5.56×10^{-9}	2.87×10^{-8}
800	8.05×10^{-9}	3.13×10^{-8}
800	6.67×10^{-9}	3.00×10^{-8}
850	3.22×10^{-8}	1.017×10^{-7}
900	1.725×10^{-8}	1.45×10^{-7}
950	4.13×10^{-8}	2.01×10^{-7}
1000	1.4×10^{-7}	3.33×10^{-7}
1050	4.7×10^{-7}	9.34×10^{-7}
1100		6.7×10^{-7}
		1.08×10^{-6}
1150		8.1×10^{-7}

Fig. 16. Log A vs $\dfrac{1}{T}$, $\triangle$ H_{AB} = 54,500 cals per mole, $\triangle$ H_{BC} = 32,500 cals per mole, $\triangle$ H_{AD} = 44,500 cals per mole.

obtained values of the heat of activation for the low-temperature range of 300°-487°C of 41,000-46,500 cal/mole.

44,500 calories per mole probably represents the heat of formation of defects and the heat of activation of diffusion of metal atoms for the early stage of oxidation when the oxide film is protecting the metal. The final values for the parabolic rate law constants could be fitted by two straight lines. The values below 750°C were fitted by a straight line which gave a heat of activation of 54,500 cal/mole. The high final values for A found between 600° and 700°C were due to the transition stage in the oxidation process. Above 750°C the parabolic rate law constants were fitted to a line having a heat of activation of 32,500 cal/mole. No interpretation can be given to the final values of the parabolic rate law constants.

The parabolic rate data of the several groups of investigators were in fair agreement with our data.

Effect of surface treatment and sample pretreatment.—Three sample pretreatments are compared: no pretreatment, reduced in H_2 at 600°C, and preheated to 1000°C in vacuum of less than 10^{-6} mm Hg. The results show that the as-received and abraded sample oxidized a little slower than abraded samples given a hydrogen or vacuum pretreatment. For practical purposes the rate of oxidation at 600°C is nearly independent of atmospheric pretreatments.

Two surface pretreatments are compared: electropolishing and abrasion. Electropolishing was carried out in a KOH solution. The results show that the electropolished sample reacted at a little slower rate than the abraded sample.

Crystal structure studies of oxide scales.—An extensive study was made of the crystal structure of the oxide scales formed after oxidizing tungsten from 600° to 1100°C. A Guinier-Hägg (17-21) type of focusing x-ray camera was used to bring out the presence of minor phases in the oxide scale. Monochromatic NiK_α radiation was used.

Monoclinic WO_3 was the principal oxide found in the scale for the complete temperature range. Studies on a sectioned oxide scale showed the outer layer to be WO_3 and the inner layer adjacent to the metal WO_3 and W_4O_{11}. The crystal structures of the oxygen compounds of tungsten have been reviewed by Hägg

and Magnéli (21). The x-ray diffraction method is not sensitive enough to show the oxide in contact with the metal.

Discussion of Mechanism of Oxidation

Experimental studies show that the time course of the oxidation curves depends strongly on the temperature, pressure, and the stress pattern of the metal at the edges. Eleven or more physical and chemical phenomena must be considered in developing a complete picture of the oxidation of tungsten. These are: (*a*) normal diffusion processes involving the formation of defects and the diffusion of metal or oxygen atoms through the oxide scale, (*b*) the adhesion of the oxide scale to the metal at the surface and at the specimen edges, (*c*) heat effects associated with the high rates of oxidation at the surface, (*d*) solid phase chemical reactions occurring in the oxide scale, (*e*) decrease in surface area as a result of scale formation, (*f*) diffusion of oxygen through the gas phase to the surface for reaction, (*h*) chemisorption of oxygen at the oxide or at the clean metal surface, (*i*) chemical reaction of oxygen at a clean metal surface, (*j*) desorption or evaporation of WO_3, (*k*) diffusion of WO_3 away from the surface into the gas phase, (*l*) decrease in surface area as a result of volatility of WO_3.

No one rate process can be used to explain the complex oxidation reaction of tungsten. At low temperatures the kinetics may be interpreted in terms of a simple diffusion process. However, at high temperature, the oxidation of tungsten closely resembles the combustion of graphite. It is useful to consider the reaction for three temperature ranges (*a*) 500°-600°C, (*b*) 650°-950°C and (*c*) 1000°-1300°C.

Mechanism of oxidation 500°-600°C.—For this temperature range and for lower temperatures the oxidation reaction is probably diffusion controlled. No evidence was found for local cracking at the specimen edges at 500°C after 6 hr of reaction. At 600°C some localized cracking was observed. A parabolic rate law plot of the 500°C data shows the rate law constant to increase with time. We conclude that the protective properties of the oxide scale are steadily becoming poorer. This may be a result of compositional changes in the oxide scale or to microscopic cracking of the oxide scale at the oxide-metal interface. These small cracks although not resulting in spalling give a short circuit for oxygen to reach the metal for reaction.

Composition changes are thermodynamically feasible and have been observed by Hickman and Gulbransen (22) in an earlier electron diffraction study. WO_3 is formed first and appears in the outer part of the scale. Solid phase reactions of tungsten with the higher oxide lead to the formation of WO_2 or other oxides of tungsten.

X-ray diffraction studies on the 600°C oxidized sample show no evidence for an oxide other than WO_3. This appears to conflict with the earlier studies of Hickman and Gulbransen (22). We interpret this discrepancy as due to the difficulties in sampling for our x-ray diffraction method and to the fact that Hickman and Gulbransen (22) worked at lower pressure and shorter oxidation times.

Pressure has only a minor influence on the time course of oxidation for this temperature range.

Mechanism of oxidation 650°-950°.—For this temperature range several new factors must be used to explain deviations from diffusion controlled oxidation. Residual stresses and strains in the metal at the edges give a highly localized oxidation reaction. Pressure also plays an active role at 950°C.

A rapid change is found in the oxidation curves at a scale thickness of 2000-4000 $\mu g/cm^2$. The change is one which leads to a more rapid oxidation. Localized edge type of oxidation develops and adhesion of the oxide scale becomes poor. Crystal structure studies show WO_3 to be the oxide formed.

We interpret the oxidation reaction in this temperature range as follows: A thin layer of oxide scale is formed according to the general laws of diffusion. After reaching a certain thickness the oxide cracks away from the metal at local areas. The cracked areas give access to oxygen and healing occurs until the critical thickness of oxide is again formed. This cracking process is a continuous one over the surface as a function of time. Since only the thin oxide film is formed under diffusion controlled conditions the major part of the oxide scale has little influence on the kinetics of the reaction.

Due to the intimate contact of oxygen with most of the oxide scale the highest oxygen containing oxide is formed, namely WO_3. This is observed in all of the x-ray diffraction studies. For thick oxide scales the only place where WO_2 could form would be in the thin oxide film at the metal-oxide interface.

Since oxygen pressure has a major influence on the time course of oxidation at 950°C the volatility of WO_3 in low oxygen atmospheres is beginning to influence the reaction.

Mechanism of oxidation 1000°-1300°C.—For this temperature range the mechanism of oxidation changes greatly with temperature and pressure. At 1000°C and 0.1 atm oxygen pressure an oxide scale is formed while at 1200°C and higher at 0.01 atm pressure no measurable oxide pickup is noted. However, a thin oxide scale may still be present on the metal. The oxide evaporates as fast as it is formed. We conclude the time course of oxidation is determined by the rate at which oxygen arrives at the surface, by diffusion of the volatilized oxide away from the surface, and by geometrical considerations of the sample surface area. At some temperature in this temperature range the theoretical rate of evaporation is greater than the rate of oxidation. This temperature depends on the oxygen pressure.

The mechanism of oxidation of tungsten at 1200°C and higher is similar to that observed in the combustion of carbon. Gulbransen (23) has derived rate equations for the combustion of artificial graphite under idealized conditions of low-temperature combustion at 425°-575°C and for small amounts of burning.

The combustion reaction of tungsten in oxygen is more difficult to study than the combustion of carbon since reaction variables are different. Oxide scales are formed on tungsten below 1200°C at 0.1 atm pressure. Therefore, studies must be made at temperatures above 1200°C where rapid reaction

occurs. Sample area considerations are important and the time period of reaction is very short. Our present methods are not sufficiently accurate for us to apply the absolute reaction rate theory (24) and to analyze the rate-limiting processes.

Other interpretations.—Semmel (10) suggests that the change in the oxidation curves above 1150°C is due to melting of the oxide. No evidence was presented except that the high-temperature runs showed the specimen to have rounded edges. Volatilization of WO_3 could also account for the rounding of the edges. We have seen no evidence for melting in our studies.

Arkharov and Kozmanov (9) interpret the change in the rate of oxidation above 1150°C as due to a structural transformation in the oxide. We suggest from our studies on the effect of pressure that volatility of the oxide is the major factor controlling the oxidation reaction in the temperature range of 1100°-1200°C.

Summary

1. Rate measurements were made on the oxidation of tungsten from 500° to 1300°C, for times up to 6 hr, and for oxygen pressures from 0.1 to 0.00132 atm.

2. The effect of surface preparation and sample pretreatment was also studied.

3. The kinetic data were fitted to the parabolic rate law. However, a number of deviations were observed. For all experiments the initial parabolic rate law constants were smaller than the final values found for thicker films. A transition was observed in the rate of oxidation for weight gains of 2500 to 4000 $\mu g/cm^2$ at temperatures of 650°-800°C.

4. The parabolic rate law data plotted on a logarithmic plot as a function of $1/T$ showed three straight lines. The initial values of the rate law constants were fitted to a line which gave a heat of activation of 44,500 cal/mole. The final values were fitted to another line which gave a heat of activation of 54,500 cal/mole. Above 800°C the final values could be fitted to a straight line which gave a heat of activation of 32,500 cal/mole.

5. Pressure had a strong effect on the rate of oxidation for the experiments at 950°, 1050°, and 1200°C. For these temperatures the volatility of WO_3 must be considered. At 1200°C weight loss curves were observed for pressures as high as 0.1 atm. At this temperature, diffusion of oxygen to the specimen limits the rate of oxidation.

6. Photographs of the oxidized specimens for temperatures of 600°-950°C show that the oxidation of tungsten occurs in a preferential manner at the edges. This causes localized heating and further reaction.

7. The poor protective properties of the oxide scale on tungsten is attributed to three factors: (*a*) the rapid oxidation reaction, (*b*) the poor adherence of the oxide to the metal, and (*c*) the volatility of the tungsten oxides.

Acknowledgment

REFERENCES

1. E. A. Gulbransen and W. S. Wysong, *Am. Inst. Mining Met. Engrs.*, **175**, 611 (1948).
2. K. M. Gorbounova and V. A. Arslambékov, *Proc. Acad. Sci. U.S.S.R., Phys. Chem. Section* (English Translation) **119**, 151 (1958).
3. J. S. Dunn, *J. Chem. Soc.*, **1929**, 1149.
4. E. Scheil, *Z. Metallkunde*, **29**, 209 (1937).
5. E. Nachtigall, *ibid.*, **43**, 23 (1952).
6. R. Kieffer and F. Kolbl, *Z. anorg. u. allgem. Chem.*, **262**, 229 (1950).
7. W. W. Webb, J. T. Norton, and C. Wagner, *This Journal*, **103**, 107 (1956).
8. J. B. Baur, D. W. Bridges, and W. M. Fassel, Jr., *ibid.*, **103**, 226 (1956).
9. V. I. Arkharov and Yu. D. Kozmanov, *Fiz. Metal. i Metalloved, Akad Nauk S.S.S.R. Ural Filial*, **2**, 361 (1956). Henry Brutcher Translation No. 4104.
10. J. W. Semmel, "High Temperature Materials," p. 510-519, John Wiley & Sons, Inc., New York (1959).
11. E. A. Gulbransen, "Advances in Catalysis," Vol. V, p. 119-175, Academic Press, Inc., New York (1953).
12. E. A. Gulbransen and K. F. Andrew, *Ind. Eng. Chem.*, **41**, 2762 (1949).
13. J. Berkowitz, W. A. Chupa, and M. G. Inghram, *J. Chem. Phys.*, **27**, 85 (1957).
14. P. E. Blackburn, M. Hoch, and H. Johnston, *J. Phys. Chem.*, **62**, 769 (1958).
15. C. Wagner, *Z. Physik. Chem.*, **21B**, 25 (1933).
16. C. Wagner, "Atom Movements," p. 153-73, American Society for Metals, Cleveland, Ohio, (1951).
17. A. Guinier, "X-Ray Crystallographic Technology," Hilger and Watts Ltd., London (1952).
18. A. Guinier, *Ann. Phys.*, **12**, 161 (1939).
19. R. M. M. D'Eye, A.E.R.E. Report, Harwell, Berks., England (1954).
20. R. Ruka nd K. F. Andrew, Westinghouse Research Report 6-40807-11-R3, May 1959.
21. G. Hägg and A. Magnéli, *Rev. Pure and Appl. Phys., Australia*, **4**, 235 (1954).
22. J. W. Hickman and E. A. Gulbransen, *Trans. Am. Inst. Mining Met. Engrs.*, **171**, 371 (1947).
23. E. A. Gulbransen, *Ind. and Eng. Chem.*, **44**, 1045 (1952).
24. K. J. Laidler, S. Glasstone, and H. Eyring, *J. Chem. Phys.*, **8**, 659 (1940).

Thermodynamic Properties of the Aluminum-Silver System

Thomas C. Wilder and John F. Elliott

Department of Metallurgy, Massachusetts Institute of Technology, Cambridge, Massachusetts

ABSTRACT

An electrode potential study of the liquid aluminum-silver system has been conducted with the cell

$$Al(1) \mid Al^{+++} \text{ (in KCl + NaCl)} \mid Al \text{ in } Ag(1)$$
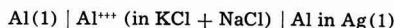
in the temperature range 700°-980°C. The activities of both components, $F_i{}^M$, $F_i{}^E$, F^E, and TS^E were determined for 700° and 900°C, and $H_i{}^M$ and H^M for the temperature range of 700°-980°C. The activity curves are found to be similar in shape to those estimated by Chou and Elliott, but they are more ideal in the vicinity of pure Al. Values for log γ_{Al} in the liquid systems Al-Fe, Al-Fe-C, and Al-Fe-Si-C at 1600°C have been redetermined using the distribution data of Chipman and Floridis, and Chipman and Langenberg.

The reversible concentration cell has proven in many cases to be a valuable and reliable method for determining the thermodynamic properties of an alloy system. When properly arranged and operated reversibly, this type of cell can be used to measure the potential between a pure metal, usually the selected reference state, and its alloy with another metal or metals. This paper reports the results of an experimental study of the liquid aluminum-silver system between 700° and 980°C with the cell:

$$Al(liq) \mid Al^{+++} \text{(in molten KCl)} + NaCl \mid$$

$$[Al \text{ in } Ag] (liq)$$
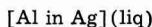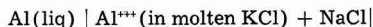
The driving force is the net transfer of aluminum from the pure state on the left to the alloy on the right. In this paper, the standard state for aluminum is the pure liquid metal. Several exceptions to this are noted as they arise.

The virtual cell reaction is

$$Al(\text{pure liquid}) \rightarrow [Al \text{ in } Ag] (\text{liquid}) \qquad (I)$$
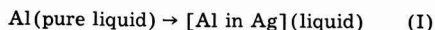
with three Faradays being transferred per gram atom of aluminum. The several thermodynamic relationships based on the reversible potential E of the cell are:

$$\overline{F}_{Al} - F°_{Al} = F^M_{Al} = -3FE \qquad [1]$$

$$\overline{S}_{Al} - S°_{Al} = S^M_{Al} = 3F \left(\frac{\partial E}{\partial T} \right)_{X_{Al}, P} \qquad [2]$$

Also from [1]

$$-3FE = RT \ln a_{Al} \qquad [3]$$

In these equations F is Faraday's constant, 23,063 cal/v eq. It is assumed that the valence of the aluminum ion in the electrolyte is 3. Experimental considerations justifying this assumption are discussed later.
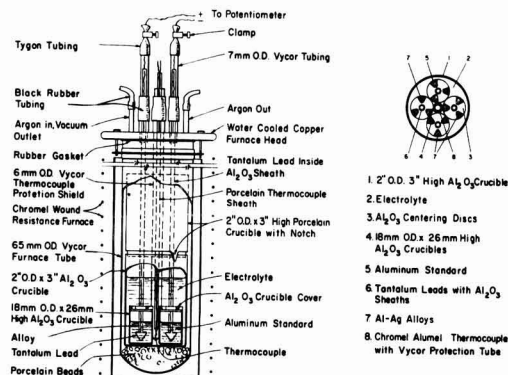
Fig. 1. Cell design. Left, 1A, cell apparatus (only 2 of 4 leads are shown; right, 1B, top view of cell.

The Experiments

Cell design.—Figures 1a and 1b show that each cell contained four electrodes, one of pure aluminum and the other three of aluminum-silver alloys. The metal electrodes were contained in doubly recrystallized pure alumina crucibles (Morganite). The large containing crucible and the sheathing for the tantalum lead wires were of 97% pure vitreous alumina. The small spiders which centered the leads in the electrode crucibles also were of high-purity alumina. The large upper porcelain crucible served as a thermal shield, and by means of holes in the bottom, it helped to guide and locate the cell leads. The chromel-alumel thermocouple was protected by a 6 mm Vycor tube. The lower end of this tube fitted into the central opening between the four electrode crucibles. The whole cell assembly was contained in a 65 mm Vycor tube that was fitted with a water-cooled brass top. Suitable fittings in the top permitted entry of leads, thermocouple sheath, and gas and vacuum connections so that the cell could be evacuated or pressurized as desired.

Cell preparation.—The initial step in making a cell was the preparation of the electrolyte. A sufficient quantity of an equimolar (azeotropic) mixture of KCl and NaCl (C.P.) was purified under vacuum produced by a mechanical pump. The mixture was slowly brought to fusion temperature and then held for 20 hr at 750°C. Several batches were purified by bubbling hydrogen chloride through the fused salt for approximately 10 hr which was followed by vacuum treatment. Cells containing electrolytes prepared in this manner produced potentials which were not as stable as with the straight vacuum treated electrolyte; hence, the simple vacuum treatment was used for all cells. Because of its high volatility, aluminum chloride was purified by subliming it at approximately 190°C under a vacuum of a few mm of Hg. The purified crystals were collected on a water-cooled Pyrex glass cold finger suspended 1 in. above the crude (C.P.) material.

The electrodes were prepared by weighing to the nearest 0.1 mg pieces of the appropriate pure met-

Table I. Lot analyses of pure metals

Metal	Impurity, wt %	
Aluminum*	Cu	0.002
	Fe	0.002
	Si	0.001
	Other	0.000
	(Al	99.995)
Silver**	Bi	<0.0001
	Cu	0.003
	Fe	<0.0001
	Pb	<0.0001
	(Ag	99.997)

* Gift of the Aluminum Company of America.
** Supplied by the American Smelting and Refining Company.

als. The three high-silver electrodes were prefused. All others were prepared by inserting bits of the pure metals in the electrode crucibles, and fusion occurred as the cell was brought to temperature. Analyses of the pure metals used are shown in Table I.

Tungsten, molybdenum, and tantalum wires were tried as leads initially. Only tantalum resisted attack by the aluminum alloys, and only slight attack was noted up to 900°C with exposure of 20 to 30 hr. Prolonged exposure at above 1000°C resulted in the wire splitting as a result of the formation of a solid brittle product. The temperature excursions used during the experiment were designed to avoid interference from this effect. The leads embrittled severely when exposed to the chloride vapors in the upper portion of the cell but not when in contact with the molten salt. Consequently, each lead was protected with an unbroken sheath of alumina from the electrode surface to the water-cooled head.

The clean cell crucible, alloys, electrode leads, etc., were completely assembled outside the large Vycor tube. With the thermal shield raised slightly above its normal position, the fused KCl-NaCl solution was transferred by a Vycor pipette from the purification tube to the cell. On solidification, the salt held the components of the cell securely in position so that the whole assembly could be handled as a single unit. This technique exposed the salt mixture to the air for a few seconds when it was liquid, and the upper surface after solidification was exposed for approximately ½ hr. In recognition that this was undesirable, a technique was devised for transferring the salt by syphon so it did not contact the air. This method greatly increased the difficulties of assembly and had no apparent effect on the performance of the cells, so it was abandoned in favor of the easier method.

After the salt had cooled sufficiently, pieces of purified AlCl₃ (about 5 g) were transferred quickly from a sealed container to the cell. Then the cell was placed in the large Vycor tube and the system was evacuated. This exposed the AlCl₃ to the air for no more than 30 sec. Subsequently, the cell tube was pressurized with purified argon and placed in the furnace. All cells were operated with an argon pressure of about 25 mm Hg above atmospheric pressure. Because of the very small pressure co-

efficient of the potential of this type cell, no corrections for the relatively small variations in atmospheric pressure were applied to the potentials read.

Operation of the cell.—A cell was run for approximately 30 hr. During this time potentials were steady and reproducible. A longer time at temperature was possible, but some of the electrolyte volatilized and condensed on the cooler portions of the system. Runs were discontinued before the level of the electrolyte was lowered sufficiently to interfere with the performance of the cell. The concentration of $AlCl_3$ did not change materially from the initial analysis, and repeated checks on the original and final weights of the electrodes showed virtually no change, within a few milligrams, in their weights from that charged. The electrolyte volatilized essentially without changing its concentration which indicated that the $AlCl_3$ had little effect on the azeotropic character of the base composition. At all times the electrolyte was colorless, transparent, and without sediment.

A cell was allowed to remain at 680°-700°C for 12 hr prior to the time measurements were taken. This permitted the cell to "stabilize" and fitted the work schedule. After this period, the potentials differed somewhat from the values obtained immediately after the new cell was brought to temperature. Several typical examples are shown in Table II. This stabilization procedure was followed because it resulted in the potentials being much less sensitive to the flow of small currents incident to taking measurements, and it has been found generally that the initial readings were not reproducible and apparently not reversible.

The temperature sequence followed in a run were usually approximated as follows: (a) 700°C, (b) 750°C, (c) 800°C, (d) 720°C, (e) 780°C, and (f) 850°C. On the high-silver side of the diagram, a similar pattern was followed with 9 or 10 readings being taken, and the final reading was at 983°C. Because of the volatilization problem, temperatures above 900°C were avoided if possible, but it appeared that satisfactory readings could be obtained at 1000°C. Slight attack of the leads and the thermocouple sheath and no attack of the alumina ware were observed in the high-temperature runs.

Sources of Error

Reversibility.—The major problems faced in the operation of a cell for establishing the thermodynamic relationships for a reaction such as Reaction I is that the cell function essentially in a reversible manner, and that the reaction occurring in the cell is actually the one ascribed to it. Several tests performed on the cells studied and a number of observations indicated that the cell used was reversible for the time and temperatures employed. The more significant of the observations were:

1. In seeking the null point at which the potentiometer potential balanced the potential of the cell, a small current from the potentiometer could be passed in either direction through the cell without disrupting the null point. In all cases the null point could be approached with assurance. The readings were not "soft" or vague.

2. Consistent readings were obtained for different cells which had alloy compositions that were the same. A potential reading at a given temperature could be reproduced again after the cell temperature had been raised or lowered. Also, there was no perceptible drift of the potentials with time.

3. The very slight attack on the ceramics and lead wires, the constancy of the $AlCl_3$ concentration in the electrolyte, the constancy of weight of the electrodes, and the absence of silver in the electrolyte indicated that side reactions or the replacement of aluminum by silver were of no consequence. Also, there was no sign of reaction with the other components of the electrolyte. Table III shows that the standard free energies of formation of the other components of the electrolyte were sufficiently low (negative) relative to that of $AlCl_3$ to avoid an exchange reaction.

4. Separate reference electrodes of pure aluminum agreed between themselves within an average of 0.1 mv. Potentials of duplicate alloy electrodes in different runs usually agreed within 0.15 mv at a given temperature. Duplicates were run on all but two of the alloys reported. (Rather than average readings, it was considered to be more suitable to use results from the one of a pair that showed the more stable readings.)

5. Results of a recent study (1) of the behavior of a number of metallic ions in the azeotropic composition of fuzed NaCl-KCl at 738°C indicated strongly that electrical conduction in the salt is essentially ionic. The presence of $AlCl_3$ in small concentrations and contact with liquid Al should not alter this. Writing the virtual Reaction I and Eq. [1] through [3], as shown, assumes that only trivalent aluminum is present in the electrolyte. An indication that the concentration of monovalent aluminum must be very low can be obtained from the data in Table III and the reaction

$$AlCl_3 + 2Al = 3AlCl \qquad (II)$$

Assuming that the activity coefficient of $AlCl_3$ and $AlCl$ are similar at low concentrations in the electro-

Table II. Effect of 12-hr "stabilization" on the potentials of new cells

Electrode No.	Temp, °C	X_{Al}	Potential in mv		Change, mv
			Initial	After 12 hr	
21-3	686	0.922	1.96	2.03	+0.07
21-4	686	0.571	11.54	12.33	+0.78
18-3	700	0.363	36.06	36.85	+0.79
22-2	696	0.174	105.0	103.9	−1.1
22-4	696	0.039	175.5	178.9	+3.4

Table III. Free energy of formation of chlorides at 800°C.

Reaction	$\Delta F°_f$, cal/g mole
$Na(1) + 1/2Cl_2(g) = NaCl(1)$	$-75,900^{(2)}$
$K(1) + 1/2Cl_2(g) = KCl(1)$	$-78,800^{(2)}$
$1/3Al(1) + 1/2Cl_2(g) = 1/3AlCl_3(g)$	$-42,400^{(2)}$
$Al(1) + 1/2Cl_2(g) = AlCl(g)$	$-32,380 \pm 3 \text{ kcal}^{(3)}$
$Ag(s) + 1/2Cl_2(g) = AgCl(1)$	$-18,500^{(2)}$
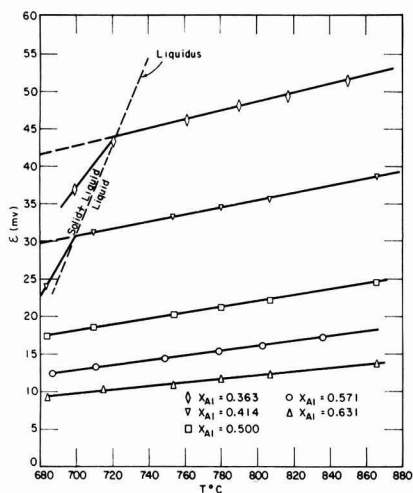
Fig. 2. Examples of emf vs. temperature plots for five liquid Ag-Al alloys.

Table IV. Potentials of experimental cells for liquid Al-Ag solutions

Electrode composition, X_{Al}	E, v		$\partial E/\partial T X_{Al} P$ v/°C × 10⁶
	700°C	900°C	
0.973	0.00080	0.00108	1.56
0.922	0.00207	0.00265	3.00
0.857	0.00352	0.00470	6.50
0.799	0.00472	0.00678	10.5
0.727	0.00665	0.0098	16.2
0.631	0.00961	0.0145	24.4
0.571	0.01276	0.0192	32.2
0.500	0.0180	0.0263	41.1
0.414	(0.0307) *	0.0404	48.2
0.363	(0.0428)	0.0539	56.3
0.308	(0.0623)	0.0730	53.1
0.245	(0.0919)	0.0998	40.5
0.174	(0.1260)	0.1348	43.6
0.093	(0.1635)	0.1764	65.4
0.039	(0.1851)	(0.2124) *	137

* Parentheses indicate that the liquid is metastable and potentials are extrapolated from results at higher temperatures.

lyte, and with N_{AlCl_3} equal to 0.01, N_{AlCl} is approximately 10^{-4}. This, with the clarity of the electrolyte and the constancy of the weight of the electrodes, was considered sufficient justification to conclude that Reaction II was of no significance in this work.

Other sources of error.—Temperatures were measured with chromel-alumel thermocouples made from a lot of wire that had been standardized against the melting points of Ag, Cu, Pb, Sn, and Al. No temperature gradients could be detected in the cell when the thermocouple was moved from the bottom of the crucible to the top of the electrolyte. Considering the uncertainty in the thermocouple calibration and uncertainties in the potentiometer circuit, it is estimated that the temperatures recorded were within ± 1°C of the true temperature.

A plot of E vs. °C yielded straight lines for all alloys at temperatures above the liquidus (Fig. 2). From these lines, potentials at several temperatures were obtained for subsequent calculations. Based on the scatter of experimental points about the line, it is estimated that a potential taken at 700° or 900°C (Table IV) for the subsequent calculations were within ±0.15 mv of the true value for cells in the composition range of 0.093 < X_{Al} < 0.857. The uncertainty is greater for the electrodes which were very high in silver because it was necessary to extrapolate the potentials from the liquid region down to the temperatures of which calculations were made.

Experimental Results

The potentials for the various alloy electrodes at 700° and 900°C and the temperature coefficients of the potentials are shown in Table IV. These results have been converted into alpha and beta functions (4) for correlation and to facilitate subsequent calculations. The defining equations are:

$$\alpha_{Al} = \frac{\ln \gamma_{Al}}{(1-X_{Al})^2} = \frac{-3F\,E/RT - \ln X_{Al}}{(1-X_{Al})^2} \quad [4]$$

and

$$\beta_{Al} = \frac{H_{Al}{}^M}{(1-X_{Al})^2} = \frac{-3F\left[E - T\left(\dfrac{\partial E}{\partial T}\right)_{P,X}\right]}{(1-X_{Al})^2} \quad [5]$$

Figure 3 shows the alpha function for aluminum at 700° and 900°C, and Fig. 4 shows the beta function which is applicable in the temperature range of 700°-950°C.

As X_{Al} approaches unity, the alpha and beta functions become very sensitive even to very small errors. In the limit, the functions must be finite and the extrapolation to this limit is based on the curve below $X_{Al} = 0.9$ rather than the points above this composition. At the other end of the composition
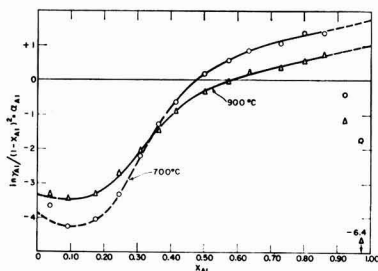
Fig. 3. Alpha function (α_{Al}) for liquid Al-Ag system. Dashed lines show extrapolation from higher temperatures.
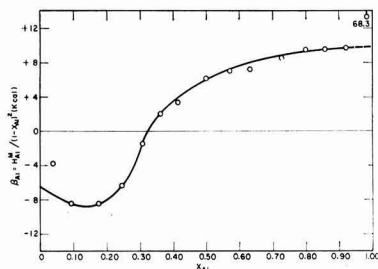
Fig. 4. Beta function (β_{Al}) for liquid Al-Ag alloys

Table V. Limiting activity coefficient of aluminum in liquid silver ($\gamma°_{Al}$)

Temp, °C	$-\log \gamma°_{Al}$	$\gamma°_{Al}$
950	1.36	0.044*
900	1.41	0.039*
800	1.52	0.030*
700	1.66	0.022*

* Liquid phase is metastable (mp pure Ag = 961°C).

scale, the point at $X_{Al} = 0.039$ has considerable uncertainty because the alloy was liquid only above 943°C. Thus it was necessary to extrapolate this point to the lower temperature by means of the value of dE/dT for this cell. This value had considerable uncertainty because the potential for the liquid phase could be measured only in the range of 943°-983°C. Figure 5 shows the alpha function at 950°C for which the limiting activity coefficient of aluminum in silver ($\gamma°_{Al}$) is 0.044. By the Gibbs-Helmholtz relationship and the limiting value of H^M_{Al} of -6460 cal/g atom the limiting value of the activity coefficient of aluminum can be obtained at various temperatures. The results given in Table V and the termini of the alpha function at pure silver in Fig. 4 are drawn accordingly.

Calculations

The alpha and beta functions for aluminum can be used to calculate the corresponding properties of silver by an application of the Gibbs-Duhem integration (4).

$$\ln \gamma_{Ag} = -\alpha_{Al} X_{Al} X_{Ag} + \int_{X_{Al}=0}^{X_{Al}} \alpha_{Al} dX_{Al} \qquad [6]$$

$$H^M_{Ag} = -\beta_{Al} X_{Al} X_{Ag} + \int_{X_{Al}=0}^{X_{Al}} \beta_{Al} dX_{Al} \qquad [7]$$

The molar excess mixing properties are

$$F^E = X_{Ag} RT \int_{X_{Al}=0}^{X_{Al}} \alpha_{Al} dX_{Al} \qquad [8]$$

$$H^M = X_{Ag} \int_{X_{Al}=0}^{X_{Al}} \beta_{Al} dX_{Al} \qquad [9]$$

The value of each integral on the right of Eq. [6] to [9] is obtained by determining the area under the appropriate curve in Fig. 3 or 4. From the results, the values of activities, activity coefficients and entropies can be found by usual thermodynamic formulas. The results of the calculations are included in Table VI.
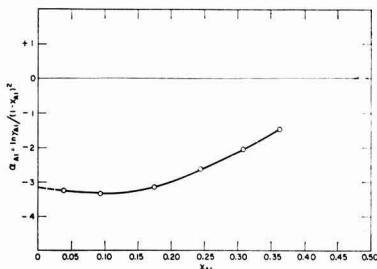
Fig. 5. Alpha function (α_{Al}) for silver-rich Ag-Al alloys at 950°C.

$$\left(\frac{\ln \gamma_{Al}}{(1X_{Al})^2} \right)_{X_{Al}=0} = \ln \gamma°_{Al} = -3.16$$
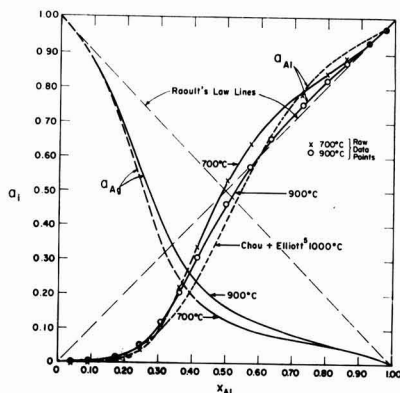
Fig. 6. Activity curves of Ag and Al in their binary system. a_{Ag} calculated by Gibbs-Duhem Equation.
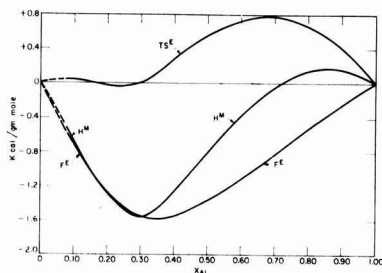
Fig. 7. Molar properties of mixing for Al-Ag system at 900°C.

Plots of the important functions are shown in Fig. 6 and 7.

Discussion of Results

The activity values obtained in this work are to be preferred over those calculated by Chou and Elliott (5) (Fig. 6), who obtained them by combining activities calculated from the phase diagram of the Pb-Ag system with data on the distribution of silver between liquid lead and liquid aluminum which was determined by Lorenz and Erbe (6). Hultgren and co-worker's (7) recalculation of Chou and Elliott's work using Kleppa's (8) calorimetrically determined heats of solution for the Pb-Ag system gives values of F^E for the Al-Ag system which are in reasonably good agreement with the present work. However, recent results by the present authors show a narrower solubility gap in the Ag-Al-Pb system than that reported by Lorenz and Erbe. These results will be reported in the near future, and a recalculation of the old Chou-Elliott results may be attempted in the light of the data now available. It is sufficient to say at this point that there is reasonable agreement between activities in the liquid phase obtained from the phase diagram calculations and those from the direct experimental results.

Activities in the Solid Phases

The results reported here have been used to estimate the activities in the solid phases in the Al-Ag system. This permits a comparison with the earlier

Table VI. Properties of the liquid aluminum-silver system
All values are computed from the curves in Fig. 3 and 4

Part A 700°C

X_{Al}	a_{Al}	a_{Ag}	γ_{Al}	γ_{Ag}	F^M_{Al} cal/g mole	F^M_{Ag} cal/g mole	F^E_{Al} cal/g mole	F^E_{Ag} cal/g mole	F^E cal/g mole
0.0*	0.00	1.000	0.0217	1.000	$-\infty$	0	-7410	0	0
0.05*	0.00118	0.946	0.0236	0.996	-13000	-110	-7240	-10	-370
0.10*	0.00320	0.873	0.0320	0.970	-11100	-260	-6660	-60	-720
0.20*	0.0168	0.651	0.0838	0.814	-7910	-830	-4800	-400	-1280
0.30*	0.0939	0.365	0.313	0.522	-4570	-1950	-2250	-1260	-1560
0.40*	0.304	0.197	0.759	0.328	-2300	-3140	-530	-2160	-1510
0.50	0.523	0.128	1.05	0.255	-1250	-3980	$+90$	-2640	-1280
0.60	0.674	0.094	1.12	0.235	-760	-4570	$+220$	-2800	-990
0.70	0.772	0.073	1.10	0.244	-500	-5060	$+190$	-2730	-690
0.80	0.843	0.056	1.05	0.280	-330	-5575	$+100$	-2460	-410
0.90	0.914	0.035	1.02	0.347	-175	-6480	$+30$	-2050	-180
0.95	0.954	0.020	1.00	0.399	-90	-7570	$+10$	-1780	-80
1.00	1.00	0.00	1.00	0.471	0	$-\infty$	0	-1460	0

Part B 900°C

X_{Al}	a_{Al}	a_{Ag}	γ_{Al}	γ_{Ag}	F^M_{Al} cal/g mole	F^M_{Ag} cal/g mole	F^E_{Al} cal/g mole	F^E_{Ag} cal/g mole	F^E cal/g mole	TS^E cal/g mole
0.0*	0.00	1.000	0.0390	1.000	$-\infty$	0	-7570	0	0	0
0.05*	0.00221	0.944	0.0443	0.994	-14200	-135	-7270	-15	-380	$+50$
0.10	0.00598	0.872	0.0578	0.969	-11900	-320	-6570	-75	-720	$+40$
0.20	0.0263	0.671	0.131	0.838	-8480	-930	-4730	-410	-1270	-20
0.30	0.1036	0.426	0.345	0.608	-5280	-1990	-2480	-1160	-1560	$+10$
0.40	0.275	0.254	0.687	0.424	-3010	-3190	-880	-2000	-1550	$+290$
0.50	0.460	0.168	0.921	0.336	-1810	-4150	-190	-2540	-1360	$+550$
0.60	0.607	0.120	1.01	0.300	-1160	-4940	$+30$	-2810	-1110	$+730$
0.70	0.722	0.087	1.03	0.290	-760	-5680	$+70$	-2880	-820	$+780$
0.80	0.819	0.060	1.02	0.298	-470	-6550	$+50$	-2820	-520	$+670$
0.90	0.907	0.033	1.01	0.326	-230	-7940	$+20$	-2620	-240	$+410$
0.95	0.952	0.018	1.00	0.350	-115	-9350	$+5$	-2450	-120	$+230$
1.00	1.00	0.00	1.00	0.384	0	$-\infty$	0	-2230	0	0

Part C 700°-900°C

X_{Al}	H^M_{Al} cal/g mole	H^M_{Ag} cal/g mole	H^M cal/g mole
0	-6460	0	0
0.05	-6900	$+20$	-330
0.10	-6900	$+10$	-680
0.20	-5100	-340	-1290
0.30	-1210	-1700	-1550
0.40	$+1210$	-2900	-1260
0.50	$+1480$	-3100	-810
0.60	$+1210$	-2760	-380
0.70	$+770$	-1940	-40
0.80	$+370$	-720	$+150$
0.90	$+100$	$+840$	$+170$
0.95	$+20$	$+1720$	$+100$
1.00	0	$+2670$	0

* For compositions below $X_{Al} = 0.42$ at 700°C and below $X_{Al} = 0.085$ at 900°C the liquid is metastable.

results of Hillert, Averbach, and Cohen's (9) measurements on solid alloys in this system.

A few potentials were obtained for alloys in the alpha phase (high Ag) as shown in Fig. 8. These potentials were extrapolated to 820°K (547°C) and corrected for the change of reference state of solid Al. The potentials obtained are in reasonable agreement with those of Hillert and co-workers.

In the composition range above $X_{Al} = 0.35$, the potentials of the liquid alloys were extrapolated to the liquidus temperatures to give the potentials at the corresponding solidus temperatures. When these potentials are then extrapolated to 820°K and corrected for the change in reference state, they result in an activity curve for aluminum having a very strong posi-

tive departure from ideality in the delta phase. Although the general character of the phase diagram and some uncertainty as to the position of the solidus line of the δ phase (9, 10) makes this calculation somewhat uncertain, there is a remarkably good agreement between the earlier results of Hillert, Averbach, and Cohen (9) (their Fig. 2) and those obtained here. It is to be noted that Wittig (11) recently has reported values of H^M for the ζ phase which are a little more exothermic than Hillert's values.

Activity Coefficients of Aluminum in Iron Alloys

The experimentally determined activities of aluminum in silver alloys and the enthalpies of solu-
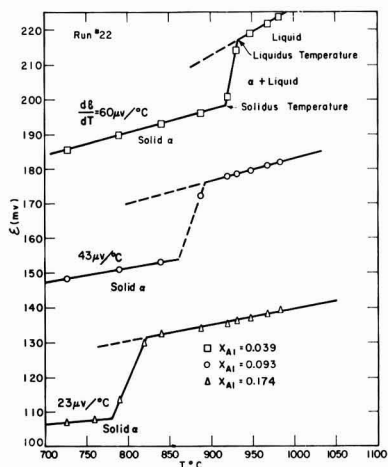
Fig. 8. Potentials for high melting Al-Ag alloys
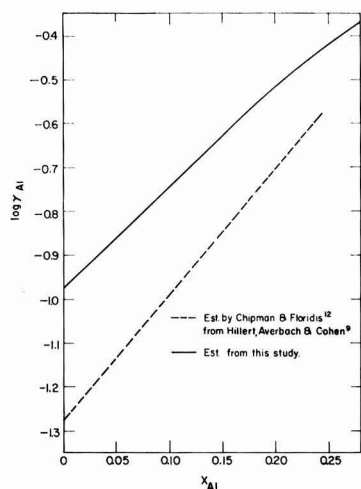
Fig. 9. Log γ_{Al} in liquid Al-Ag alloys at 1600°C. $\epsilon_{Al}^{(Al)}$ = 5.3

tion reported here differ somewhat from those reported by Hillert, Averbach, and Cohen (9) which Chipman and Floridis (12) used to determine the activity coefficients of aluminum in iron alloys from the distribution of aluminum between liquid silver and iron alloys. In addition, Chipman and Floridis assumed that log γ_{Al} in liquid Al-Ag alloys was inversely proportional to the absolute temperature.

By use of the experimental results reported here, the values for the activity coefficients of aluminum in the Fe-Al, Fe-Al-C, and Fe-Al-Si-C systems at 1600°C have been recalculated from the data reported by Chipman and Floridis (12) on the distribution of Al between layers of Fe and Ag. The results are shown in Fig. 9, 10, and 11 and in Table VII. It is to be noted that $\epsilon_{Al}^{i} = (\partial \ln \gamma_{Al})/\partial X_i$ for the infinitely dilute solution of i in Al-Fe alloys. The correction applied by Chipman and Langenberg

Table VII. Activity of aluminum in Al-Ag alloys at 1600°C

X_{Al}	Estimated by Chipman and Floridis (12) a_{Al}	Estimated from this work	
		a_{Al}	log γ_{Al}
0.00	0.00	0.00	−0.972
0.05	0.00363	0.0072	−0.854
0.10	0.0104	0.0184	−0.744
0.15	0.0215	0.035	−0.633
0.20	0.0400	0.061	−0.514

(13) for the silicon in the silver layer has been included in Fig. 11.

The recalculated results in Fig. 9, 10, and 11 can be used to redetermine the aluminum deoxidation constant for steelmaking by the same treatment
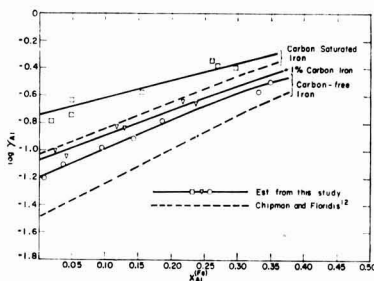
Fig. 10. Log γ_{Al} in Al-Fe alloys at 1600°C using Chipman and Floridis' distribution data (12). $\epsilon_{Al}^{(Al)}$ = +5.3 (carbon free.)
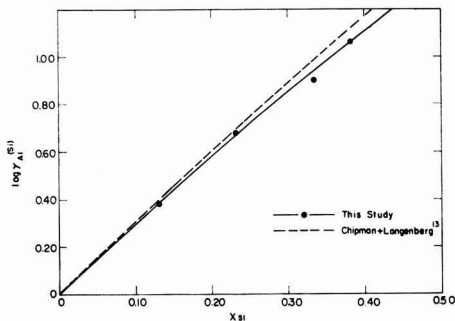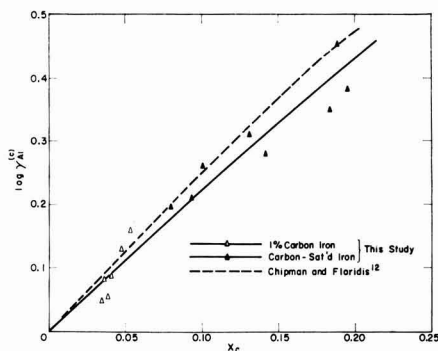
Fig. 11. Effect of carbon and silicon on log γ_{Al} in iron alloys at 1600°C using Chipman and Floridis' distribution data (12) $\epsilon_{Al}^{(C)} = +5.3$ $\epsilon_{Al}^{(Si)} = +7.0$

devised by Chipman and Langenberg (13). However, the results obtained differ very little from those of the earlier authors and consequently retreatment of the data here is not warranted. The essential reasons for the agreement in spite of different values of $\log \gamma_{Al}{}^{(Fe)}$ being used is that the calculation uses the infinitely dilute solution of Al in Fe as the reference state. This virtually cancels the effect of the change in values of $\log \gamma_{Al}$. Also, the uncertainties inherent in the calculation are probably greater than the change which would arise from the new calculation.

Conclusion

The thermodynamic properties of the liquid Al-Ag system have been determined by means of a high-temperature reversible concentration cell. The results may best be summarized by referring to Fig. 6 and 7 and to Table VI.

Values for $\log \gamma_{Al}$ in the liquid systems Al-Fe, Al-Fe-C, and Al-Fe-Si-C at 1600°C have been recalculated using the distribution data of Chipman and Floridis (12) and Chipman and Langenberg (13).

Acknowledgments

REFERENCES

1. D. L. Maricle, Ph.D. Thesis, Massachusetts Institute of Technology, September, 1959.
2. O. Kubaschewski and E. Ll. Evans, "Metallurgical Thermodynamics," 3rd. ed., p. 139, 336, Pergamon Press, Ltd., London (1958).
3. H. Villa, J. Soc. Chem. Ind., 69, S9 (1950).
4. C. Wagner, "Thermodynamics of Alloys," Addison-Wesley Press, Inc., North Reading, Mass. (1952).
5. Y. H. Chou and J. F. Elliott, (Unpublished, 1957).
6. R. Lorenz and F. Erbe, Z. anorg. u. allgem. Chem., 183, 311 (1929).
7. R. Hultgren and co-workers, "Compilation of Thermochemical Properties of Metals and Alloys," Published by the Metals Research Laboratory, The University of California, Berkeley, Calif.
8. O. J. Kleppa, J. Phys. Chem., 60, 446 (1956).
9. M. Hillert, B. L. Averbach, and M. Cohen, Acta Met., 4, 31 (1956).
10. M. Hansen and K. Anderko, "Constitution of Binary Alloys," McGraw-Hill Book Co., New York (1958).
11. F. E. Wittig, Paper 3H, Proceedings, The Symposium on the Physical Chemistry of Metallic Solutions and Intermetallic Compounds, Vol. I, (Symposium No. 9) National Physical Laboratory, H.M.S.O., London, 1959.
12. J. Chipman and T. P. Floridis, Acta Met., 3, 456 (1955).
13. J. Chipman and F. C. Langenberg, The Physical Chemistry of Steelmaking, (Proceedings of M.I.T. Conference on the Physical Chemistry of Iron and Steelmaking, 1956), Technology Press, M.I.T. (1958).

Gas Phase Charged and Electrolytically Charged Beta-Pd-H Alloys

James P. Hoare

Scientific Laboratory, Ford Motor Company, Dearborn, Michigan

ABSTRACT

Open-circuit potential vs. time curves were obtained on various palladium electrodes in hydrogen-stirred sulfuric acid solutions. Evidence is presented to show that the electrochemical properties of electrolytically charged β-Pd-H alloys are different from those of the gas charged alloys. Mechanisms for the charging processes involved are discussed.

Renewed interest in the mechanisms of the occlusion of hydrogen gas in palladium metal has prompted a re-evaluation of the earlier work with more modern techniques. It had been shown that β-Pd-H alloys formed by placing pure palladium metal in pure hydrogen gas under 1 atm are indefinitely stable (1) provided all oxidizing agents such as air or oxygen are excluded. Hoare, et al. (2) found that the gas charged β-Pd-H alloy had somewhat different electrochemical properties than the electrolytically charged β-Pd-H alloy; i.e., hydrogen is lost spontaneously from the electrolytically charged β-Pd-H alloy and its hydrogen overvoltage is lower. Flanagan and Lewis (3) made potential and relative resistance measurements on a thin (0.027 cm diameter) palladium wire in acid solutions. Although they were not able to reproduce the finding of Hoare and Schuldiner (4), they did confirm certain results reported by Ratchford and Castellan (5). However, recently (6) the results of Ratchford and Castellan have been shown to be compatible with those of Hoare and Schuldiner.

Contrary to what was found by Hoare and Schuldiner are the data reported by Flanagan and Lewis which show that, once the β-Pd-H alloy is formed electrolytically, hydrogen is not lost and the potential does not return to a positive value of 50 mv after the cathodic current is removed. This investigation is concerned with showing evidence for the existence of two kinds of β-Pd-H alloys and with a confirmation of the results reported by Flanagan and Lewis.

Experimental

In one series of experiments, potential measurements were taken on pure (99.5 + %) palladium cathodes made from 3 cm of 5-mil wire, 1 cm² plate of 2-mil foil, 1 cm² plate of 4-mil foil, 1 cm² plate of 4-mil foil whose surface was about 80% covered with polyethylene, and a bead melted from a strip of foil. In another series, both potential and relative resistance measurements were taken on a 15-mil palladium wire, 11 cm long and wound in the form of a toroid on a polyethylene ring. All experiments were carried out in 2N H₂SO₄ solution in a Teflon cell similar to that used before (7). The preparation of the triply distilled water, sulfuric acid solutions, palladium cathodes, and cell has been described elsewhere (4, 7). The hydrogen and helium gases were purified in standard multistage purification trains; the temperature of all experiments was 23° ±1°C. Relative resistance measurements were carried out as before (6). The hydrogen content of the Pd-H alloys was determined using ceric sulfate solutions (4). Electrical contacts to the cathodes were Pt wires imbedded in polyethylene to prevent any solumtion contact with the Pt or the weld area; the reference electrode is a Pt/H₂ electrode in the same solution.

Results and Discussion

Each palladium cathode was strongly anodized (about 0.1 to 0.5 amp/cm²) for about 30 min and then cathodized for about 2 hr at a current density of such a magnitude that the electrode was polarized to at least −100 mv against a Pt/H₂ electrode in the same solution. Finally, the circuit was opened and the potential vs. the Pt/H₂ electrode was recorded as a function of time. During this entire procedure, the sulfuric acid solution was stirred constantly by a steady flow of purified hydrogen. These results are presented in Fig. 1, zero time being taken at the moment when the cathodizing current is broken.

From Fig. 1, it is seen that the potential-time curves show a definite dependence on the ratio of the exposed area to the total volume of the cathode. As the value of this ratio decreases, the time required to reach a steady value of zero volt increases. Also, a point is reached at which the potential vs. Pt/H₂
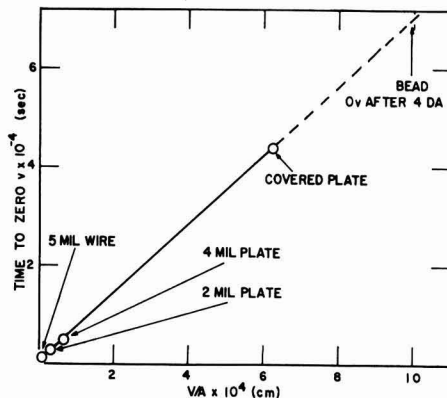
Fig. 2. Curves showing the length of time required for cathodized palladium electrodes to reach a steady value of zero volt vs. Pt/H₂ on open-circuit conditions as a function of the volume-to-surface ratio (V/A) of the electrode.

reverses sign and the curve passes through a maximum value. In fact, a cathode may be designed with a surface-to-volume ratio of such a value that the maximum value becomes a plateau at +50 mv. The palladium bead is such an example and this 50 mv potential was maintained for more than 30 hr before the drift to zero volt began. It was found that the exact shape of the curves was a function of the electrochemical history of the cathode, but the general form of the curves is that shown in Fig. 1. It is for this reason that all the cathodes, on which the curves in Fig. 1 were determined, were anodized and cathodized at approximately the same intensity and for the same duration with approximately the same hydrogen flow.

The volume-to-surface ratio (V/A) was determined (6); Fig. 2 shows that the time to reach zero volt after breaking the cathodizing circuit is a linear function of V/A. It is interesting to note that again (6) the bead falls to the left of this curve. Fallon (8) has also found that palladium beads after cathodization will return to the +50 mv value for a certain length of time.

In another series of experiments, the 15-mil palladium wire toroid was anodized and cathodized in the same manner as described above and the open-circuit potential after cathodization was recorded. The potential went to zero volt without going positive as shown in Fig. 3. However, if about 5-10% of the wire was covered with polyethylene near the weld area, the potential changed sign and, after passing through a maximum in a positive potential region, drifted back to a steady zero value. As long as the rapid flow of hydrogen was maintained, the potential would remain at zero volt indefinitely. Flanagan and Lewis (3) found that in certain cases the potential on their wires also went through a maximum value in a positive potential region.

After the wire had reached a steady value of zero volt, the hydrogen flow was reduced to a point where about one bubble passed through the solution per minute. When a potential reading was to be taken, the H₂ flow was returned to the original rate and the
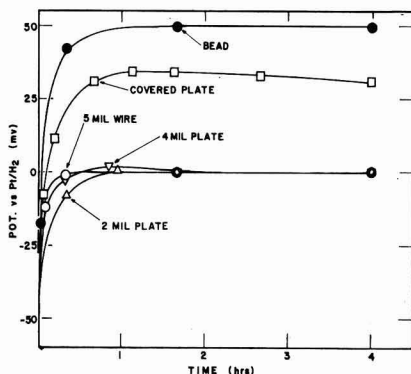

Fig. 1. Open-circuit potential vs. time curves obtained from previously cathodized palladium electrodes in H₂-stirred 2N H₂SO₄ solutions at T = 23° ± 1°C.
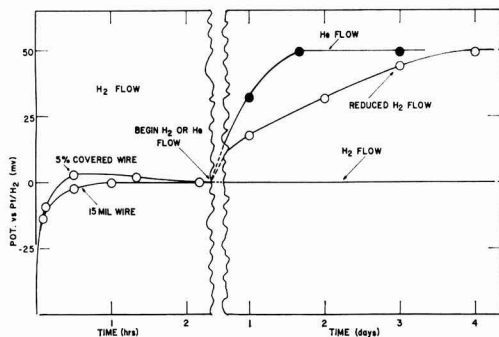
Fig. 3. Open-circuit potential curves obtained on a 15-mil Pd wire toroid after cathodization as a function of time. On the left side a rapid flow of H₂ is maintained at all times. On the right is shown the behavior when the H₂ flow is maintained, reduced to very low flow rates and replaced by He flow.

potential value recorded after the potential had remained steady for about 5 min; then the hydrogen flow was reduced again to the 1 bubble/min rate. The potential-time curve obtained is shown in Fig. 3. It is seen that a value of +50 mv was obtained after about four days.

It seemed possible that, with such a very low hydrogen flow rate, air could have entered the cell through the H₂-outlet tube and could have caused the rise to the positive values. To determine whether this was the case or not, purified helium gas was used to stir the solution rapidly at a steady rate. The potential-time curve obtained by repeating the experiment using He-stirring is shown in Fig. 3. Not only does the potential rise to a steady value of +50 mv, but also it rises faster, reaching the 50 mv value in less than two days. Potential measurements were taken by stopping the He flow and using an H₂ flow until the potential remained steady for about 5 min. The maximum total time for a reading required about 15 min.

The hydrogen content of the palladium wire toroids was determined by placing them in a known quantity of ceric sulfate solution (9), samples of which were titrated for ceric ion (4). These values for the hydrogen content were compared with those determined from Fischer's relationship (6, 10) by using relative resistance measurements which were taken concurrently with the potential measurements.

A palladium wire toroid which had been cathodized and which had come to a steady value of zero volt vs. a Pt/H₂ electrode was found to have an H/Pd atomic ratio of 0.63 using ceric sulfate solution and 0.67 from relative resistance measurements. This is in agreement with that found by other investigators, e.g. (3), and with that reported for a Pd electrode which had been anodized only and then permitted to reach a steady zero volt potential vs. Pt/H₂ (3,5,6). After a previously cathodized Pd wire toroid on open-circuit conditions had come to a steady value of zero volt vs. Pt/H₂ in H₂-stirred 2N H₂SO₄ solution, the H₂-stirring was replaced by He for about 72 hr. Then the toroid electrode was removed from the acid solution and placed in ceric sulfate

solution in order to determine the hydrogen content of the electrode. Duplicate runs showed that the H/Pd atomic ratio was equal to 0.34 even though relative resistance measurements had given a value of 0.63. This agrees with the data reported in Fig. 4 of ref. (4).

These results may explain the conflicting findings reported by Hoare and Schuldiner and by Flanagan and Lewis concerning the open-circuit potential vs. Pt/H₂ of a previously cathodized palladium electrode in acid solution. As pointed out by Fallon (8), Hoare and Schuldiner reduced the flow of hydrogen to extremely low rates overnight (at least 16 hr/day). Under these conditions, as shown by Fig. 3 of this investigation, the potential eventually does return to +50 mv. It was also found in this investigation that the potential of those electrodes which exhibited positive potentials, such as those presented in Fig. 3, would drift slowly to zero if the very low H₂ flow or the He flow was replaced by a rapid stream of hydrogen gas.

In another experiment, a Pd wire was cleaned (7) and wound as a toroid on a polyethylene ring with Pt leads. This electrode was soaked in triply distilled water in a Teflon cell for about 48 hr. The cell was emptied and the Pd wire toroid sealed inside. Purified dry hydrogen was passed through the cell until the relative resistance reached a value of 1.61. This corresponds to the value for β-Pd-H. In another Teflon cell, 2N H₂SO₄ solution was prepared (7) and saturated with purified hydrogen for about 20 min. The gas-charged β-Pd-H toroid was then placed in this H₂-saturated acid solution. A potential of zero volt vs. Pt/H₂ was observed. Next, the hydrogen flow was replaced by helium and these conditions were maintained for about 72 hr. The relative resistance still had a value of 1.61. Finally, the toroid was removed from the acid solution and placed in ceric sulfate solution in order to determine the hydrogen content. In duplicate runs, it was found that the H/Pd atomic ratio was 0.57.

It is interesting to note that gas-phase charged β-Pd-H does not lose hydrogen in He-stirred H₂SO₄ solution while electrolytically charged β-Pd-H does. As reported before (2) these two types of β-Pd-H have very different hydrogen overvoltage characteristics. However, once gas-charged β-Pd-H is anodized in acid solution, the hydrogen overvoltage characteristics become identical to the electrolytically charged β-Pd-H. It was suggested that a film of molecular H₂ gas lies over the layer of adsorbed atomic -H and that, while cathodization does not break up this film, anodization does.

When an anodized palladium electrode in hydrogen-stirred acid solution is put on open-circuit conditions, atoms of hydrogen are transported from the double layer to the electrode surface through an adsorbed water molecule (2). These remove any oxides present thus exposing a pure palladium surface. Adsorbed hydrogen atoms then penetrate the metal skin and are dissolved into the body of the metal as protons. Since the penetration of the metal skin is assumed to be the slow process (6), hydrogen accumulates just inside the metal surface to the

maximum α-Pd concentration (H/Pd $\sim$ 0.03) and a potential of 50 mv more noble than Pt/H$_2$ is observed owing to the atomic hydrogen electrode reaction (11). As more hydrogen is dissolved, more Pd is converted to the α-Pd-H alloy. Only when the entire body of Pd is converted to the α-phase, will the β-phase nucleate and it is the length of the so-called α-plateau (6), observed in the potential-time curves, that represents the time required to charge the Pd to α-Pd.[1] The β-phase then grows from nucleation centers throughout the α-phase until an H/Pd atomic ratio of about 0.6 is reached when the solution process ceases and a potential of zero volt vs. Pt/H$_2$ is observed.

This same charging procedure is assumed to occur on pure dry Pd metal placed in a pure dry hydrogen atmosphere, except that hydrogen molecules do not have to displace adsorbed water molecules and the surface of the final β-Pd-H alloy obtained is covered with an adsorbed film of molecular hydrogen. In both cases, hydrogen ceases to be dissolved at an H/Pd atomic ratio of about 0.6.

If a palladium electrode is cathodized in H$_2$-stirred acid solution, the solvated hydrogen ions are discharged from the double layer to adsorbed atoms on the surface. As described above, the same charging processes from Pd to α-Pd-H to β-Pd-H also occur here. However, the solution process does not stop at H/Pd $\sim$ 0.6, but additional hydrogen may be forced into the Pd electrochemically at high current densities. It has been suggested (13) that this additional hydrogen enters the Pd lattice as atomic hydrogen since it may be possible that there is, at this concentration, enough dissolved hydrogen to form an H1-s impurity band. As a result, the electron is more closely associated with this band than with the Pd 4-d band (14). Hydrogen concentrations approaching H/Pd $\sim$ 1 may be obtained (15). Supersaturated β-Pd-H alloys are quite unstable and the additional hydrogen is lost rapidly after the cathodizing circuit is removed. Then if the H$_2$-flow is replaced by He-flow, more hydrogen will be lost till an H/Pd atomic ratio $\sim$0.35 is reached. However, an anodized Pd wire toroid which had never been cathodized previously and which had come to a steady value of zero volt vs. Pt/H$_2$ was placed in ceric sulfate solution after the H$_2$-flow had been replaced by He for about 72 hr. The hydrogen content so determined was equal to an H/Pd atomic ratio of 0.56. Yet, when an anodized electrode such as this is cathodized, the β-Pd-H obtained has all the characteristics of electrolytically charged β-Pd-H.

It appears from the above work that β-Pd-H alloys obtained by cathodization possess different stability properties than those obtained in other ways. It is suggested here that the β-Pd-H lattice formed electrolytically is much more distorted than

[1] It may be pointed out that Lacher (17) and Moon (18) have shown that α-Pd alloys are homogeneous solid solutions while these data suggest that such alloys are nonhomogeneous solutions. This discrepancy is only apparent since Lacher and Moon considered α-Pd alloys in a hydrogen environment where the partial pressure of the hydrogen was low enough (0-0.026 atm) that α-Pd was the stable phase with respect to the β-phase. In this investigation, the partial pressure of hydrogen was 1 atm and in this region the β-phase is the stable phase but cannot nucleate until the mass of Pd has been converted to the α-phase. Equilibrium is never achieved between the α-phase and the external hydrogen atmosphere and the α-phase exists only during the nonequilibrium charging processes.

Fig. 4. Suggested possible mechanisms for the solution of hydrogen by palladium. Full lines represent stable bonds; dotted, bonds being formed or being broken. Water is adsorbed with H's next to Pd atoms since the potential at zero charge is positive to Pt/H$_2$ (2) and therefore a pure Pd surface has a negative charge. The hydrogen symbol, H, in step 4 of (a) and (b) inside the Pd metal represents a proton; the electron has been donated to the metal d-band. (a) Adsorption of hydrogen by previously anodized Pd from H$_2$-stirred acid solution by complexing with an adsorbed water, an open circuit. (b) Dry gaseous H$_2$ is adsorbed on dry Pd giving a Pd-H alloy whose surface is covered with an adsorbed layer of molecular hydrogen. (c) Discharge of a solvated proton on a gas charged β-Pd-H cathode; the adsorbed H$_2$ in step 3 can be desorbed as a free H$_2$-molecule or adsorbed as two H-atoms shown in step 4.

that formed from gas phase charging due to the formation of the super saturated β-phase. It may be possible that this extra distortion could modify the relative positions and widths of the s- and d-bands in such a way that the free energy is lowered by loss of hydrogen to an H/Pd atomic ratio of about 0.35 only for the case of the electrolytically charge β-Pd-H in acid solution in the absence of hydrogen or oxidizing agents.

Gas-phase charged β-Pd-H alloys cannot be converted to electrolytically charged β-Pd-H by cathodization alone because the adsorbed molecular hydrogen film prevents supersaturation of the alloy as shown by hydrogen overvoltage measurements (2). If, however, this film is destroyed by pre-anodization, then subsequent cathodization will result in a β-Pd-H alloy possessing all the properties of the electrolytically charged alloy (Fig. 4).

After the cathodizing current has been removed from certain palladium cathodes, the potential vs. Pt/H$_2$ swings to positive values before returning to the steady value of zero volt. Conceivably, this might be explained as follows. When the cathodizing circuit is broken, hydrogen above an H/Pd $\sim$ 0.6 is lost rapidly by the supersaturated β-phase. Since the lattice is highly distorted and since there is, without doubt, a readjustment of the partial pressure of hydrogen at points on the surface and within the metal itself, further hydrogen may be lost by inertia which is slowly restored afterward, giving

the observed swing to positive potentials with a subsequent drift to zero. The behavior of such electrodes has been explained by Fallon (8) in terms of the thickness of the diffusion layer at the electrode surface as a function of the stirring rate.

It may be mentioned here that the so-called α-Pd reference electrode, (Pd-H)α/H₃O⁺, used by Schuldiner (14, 16) is a good reference electrode. This is true since such an electrode is prepared from an anodized Pd wire placed in a hydrogen atmosphere and it has been shown (6) that such an electrode will maintain a steady-state potential of 50 mv vs. Pt/H₂ for periods of time up to 48 hr or more. If the wire had been cathodized, this would not have been true. Also, Schuldiner's measurements were made within 8 hr so that this reference electrode system acted as though it were at equilibrium.

Summary

1. β-Pd-H alloys may be obtained by allowing a pure sample of palladium to absorb hydrogen either in a dry state from a gaseous hydrogen atmosphere or in hydrogen-stirred acid solutions after the palladium had been anodized. These alloys are stable (do not lose hydrogen) as long as all oxidizing agents are absent, even if the hydrogen atmosphere is removed.

2. β-Pd-H alloys may also be obtained electrolytically by cathodizing the palladium in H₂-stirred acid solutions. These alloys are stable only in a hydrogen atmosphere provided oxidizing agents are absent. If the hydrogen atmosphere is removed these alloys lose hydrogen until an H/Pd atomic ratio of about 0.35 is reached. If the hydrogen atmosphere is returned, the alloy will regain hydrogen till the H/Pd atomic ratio again reaches about 0.6. It is suggested that this behavior is due to the highly distorted lattice caused by the electrochemically produced supersaturated β-Pd-H alloys during cathodization.

3. β-Pd-H alloys obtained from anodized Pd in H₂-stirred acid solutions can be converted to the electrolytically charged alloy by cathodization since the supersaturated alloy is formed in the process. Unlike β-Pd-H obtained from anodized Pd, that obtained by dry gas phase charging possesses a protective hydrogen film which prevents the formation of the supersaturated lattice during cathodization and thereby prevents the conversion to the electrolytically charged alloy. However if this protective film is destroyed by pre-anodization, then cathodization does convert gas charged β-Pd-H to electrolytically charged β-Pd-H.

REFERENCES

1. D. P. Smith, "Hydrogen in Metals," p. 102, University of Chicago Press, Chicago (1948); L. J. Gillespie and F. P. Hall, J. Am. Chem. Soc., 48, 1207 (1926); H. Bruening and A. Sieverts, Z. physik. Chem., A163, 409 (1932); E. A. Owen and I. J. Jones, Proc. Phys. Soc., 49, 587, 603 (1937).
2. J. P. Hoare, S. Schuldiner, and G. W. Castellan, J. Chem. Phys., 28, 22 (1958).
3. T. B. Flanagan and F. A. Lewis, ibid., 29, 1417 (1958).
4. J. P. Hoare and S. Schuldiner, J. Phys. Chem., 61, 399 (1957).
5. R. J. Ratchford and G. W. Castellan, ibid., 62, 1123 (1958).
6. J. P. Hoare, This Journal, 106, 640 (1959).
7. J. P. Hoare and S. Schuldiner, ibid., 102, 485 (1955).
8. R. J. Fallon, Thesis, Catholic University of America Press, Washington, D.C. (1959).
9. F. A. Lewis and A. R. Ubbelohde, J. Chem. Soc., 1954, 1710.
10. F. Fischer, Ann. phys., 20, 503 (1906).
11. S. Schuldiner, G. W. Castellan, and J. P. Hoare, J. Chem. Phys., 28, 16 (1958).
12. B. Lambert and S. F. Gates, Proc. Roy. Soc., London, 108A, 456 (1925).
13. S. Schuldiner and J. P. Hoare, This Journal, 103, 178 (1956).
14. S. Schuldiner and J. P. Hoare, Can. J. Chem., 37, 228 (1959).
15. F. Krueger and G. Gehm, Ann. Phys., 78, 72 (1925).
16. S. Schuldiner, This Journal, 106, 440 (1959).
17. J. R. Lacher, Proc. Roy. Soc., 161A, 525 (1937).
18. K. A. Moon, J. Phys. Chem., 60, 502 (1956).

Brief Communications

The JOURNAL accepts short technical reports having unusual importance or timely interest, where speed of publication is a consideration. The communication may summarize results of important research justifying announcement before such time as a more detailed manuscript can be published. Consideration also will be given to reports of significant unfinished research which the author cannot pursue further, but the results of which are of potential use to others. Comments on papers already published in the JOURNAL should be reserved for the Discussion Section published biannually.

Submit communications in triplicate, typewritten double-spaced, to the Editor, Journal of The Electrochemical Society, 1860 Broadway, New York 23, N. Y.

Temperature Dependence of Tafel Slope in the Formation of Very Thin Anodic Oxide Films on Niobium

George B. Adams, Jr., and Timothy Kao[1]

Department of Chemistry, University of Oregon, Eugene, Oregon

ABSTRACT

A kinetic study was made of the formation of very thin anodic oxide films on niobium at constant current over the temperature range $-10°$ to $70°C$. Formation voltages were limited to the range below the oxygen evolution potential to eliminate possible interaction of an electronic component of the current with the measured formation field. It was found that the measured temperature dependence of Tafel slope agreed with that predicted by the theory of Mott and Cabrera. Using this theory, a zero field interfacial barrier height of 1.19 ev and barrier half-width of 2.40A were obtained. Values of the differential formation field are reported at current densities of 1000, 100, 10, and 1 $\mu a/cm^2$ at ten degree intervals over the temperature range studied.

Several investigators (1-3), working with tantalum, niobium, and zirconium, respectively, have reported an essentially temperature-independent Tafel slope in the kinetics of formation of anodic oxide films on these metals.

Their results are therefore not in agreement with the simple single-barrier theory of Mott and Cabrera (4, 5), but Dewald's theory (6) which incorporates the assumption of ionic space charge formation in the oxide film is capable of explaining the anomalous temperature dependence.[2]

These investigators worked with oxide films ranging in thickness from several hundreds to several thousands of angstroms. Under these conditions it is probable that a space charge is established in the steady state; some experimental evidence for the presence of space charge has been obtained by Young (7).

The Mott-Cabrera theory for formation of very thin oxide films on metals contains the assumption that no space charge is established in very thin films (<100Å). With the additional assumptions that the rate-determining step in the formation of the oxide is the high-field migration of metal ions from active surface sites on the metal across a metal-oxide interfacial potential energy barrier of height, ϕ, and barrier half-width, b, into interstitial positions in the insulating oxide film, the following equation is derived:

$$F = \frac{\phi}{bq} + \frac{kT}{bq} \ln (I/Ao) \qquad [1]$$

where F is the electrostatic field acting across the oxide film, q is the charge per metal ion, I is the ionic current density, m_s is the surface concentration of metal ions at active surface sites on the metal. V_s is the vibrational frequency of a surface metal ion, and $Ao = qm_s v_s$.

The aim of the present work was to test this theory with an applicable system, namely, for the growth of very thin anodic oxide films in which the metal ion is the mobile species in an otherwise insulating film.[3]

Experimental

The experimental techniques employed in this work have been described previously (8, 9).

Electrodes were made up from ½-in. annealed niobium rod (Fansteel research grade) cut into ½-in. lengths, each fitted with a vertical brass rod for handling and electrical contact. This assembly was then masked with six individual coatings of baked Formvar enamel. The plane circular face of each electrode was exposed by abrasion, to give a nominal area of 1.265 cm^2.

Electrode surfaces were prepared initially on a metallographic polishing wheel with No. 280 and No. 600 grit aluminum oxide abrasive slurries and finished with Linde B polishing alumina, to a highly reflecting surface. Electrodes were repolished after each run with polishing alumina.

The electrolyte was made up of $0.1N$ H_2SO_4 in 35% ethyl alcohol. This electrolyte was also used in the mercury-mercurous sulfate reference electrode. The solution was stirred mechanically during each run and renewed every 8 hr. Temperature was regulated to within $\pm0.1°C$ over the range $-10°$ to $70°C$ with a Wilkens-Anderson refrigerated constant temperature bath.

Current densities from 1 to 100 $\mu a/cm^2$ were regulated to within $\pm0.5\%$ with an electronic current regulator described previously (10). Current density of 1000 $\mu a/cm^2$ was regulated electronically with a regulator described by Teeter (11). Current was measured to within 0.5% with a Weston precision low resistance microammeter, model 627. Voltage was recorded on a L&N AZAR recorder using their

---

[1] Present address: Department of Pediatrics, University of Oregon Medical School, Portland, Oregon.

[2] This theory cannot, however, account for certain characteristics of transients which have been observed with these oxide films.

[3] It is assumed that the niobium ion, because of its small size, is the mobile species in the oxide film (2). The glassy film has an extremely low electronic conductivity (2).

model 7664-N electronic millivoltmeter as a high-input-impedance preamplifier.

Runs made at 1.0 $\mu a/cm^2$ were obtained by first polarizing at 100 $\mu a/cm^2$ and then dropping back to 1.0 $\mu a/cm^2$ on the same electrode surface. It was observed that there was considerably more scatter among the individual formation rates for these runs than for runs made at higher current densities.[4]

All voltage measurements were limited to the range below the potential for reversible evolution of oxygen. By restricting voltage measurements to this range, possible complications involving the action of electronic current on the observed field are avoided, since the ionic current efficiency is then unity.

Results

If Eq. [1] is obeyed, a plot of field vs. absolute temperature should be linear for constant current runs, and the slopes of the regression lines should increase with increasing current density. In addition the lines should extrapolate to a common intercept, ϕ/bq, at the absolute zero of temperature.

Equivalent statements are that the Tafel slope, $[\partial F/\partial \ln I]_T$, should vary in direct proportion to the absolute temperature, or that the barrier half-width, b, should remain constant with temperature.

The results of this investigation are presented in Table I and in Fig. 1.

Each point is the average of at least five individual runs. The lines shown are the least square regression lines. Equations for these lines, with standard deviations of slopes and intercepts are as follows:

$$F_{1000} = (9.88 \pm 0.16 \times 10^6) - (1.65 \pm 0.06 \times 10^4)T$$
$$F_{100} = (9.91 \pm 0.27 \times 10^6) - (1.80 \pm 0.09 \times 10^4)T$$
$$F_{10} = (10.00 \pm 0.26 \times 10^6) - (2.02 \pm 0.09 \times 10^4)T$$
$$F_{1} = (11.15 \pm 0.44 \times 10^6) - (2.59 \pm 0.15 \times 10^4)T$$

The barrier half-width, b, was calculated from Tafel slopes [obtained from the regression lines as $(F_{1000} - F_{10})/4.606$], assuming a pentavalent niobium ion. Values of b so obtained ranged from 2.44 to 2.36Å, with a mean of 2.40Å.

[4] When making a 1.0 $\mu a/cm^2$ run the electrode is immersed continuously for an interval of more than an hour. At the higher temperatures it became necessary to recoat the electrode on one occasion because gross leakage had developed between the enamel mask and the rim of the electrode face. Slight leakage of this sort would give field values that were too low at the higher temperatures. The 1.0 $\mu a/cm^2$ runs would be affected to the greatest extent, because of the protracted immersion times required and the greater percentage effect for a given leakage.

Table I. Variation of field with current and temperature in the formation of very thin anodic oxide films on niobium

T, °K	$F_1 \times 10^{-6}$, v cm^{-1}	$F_{10} \times 10^{-6}$, v cm^{-1}	$F_{100} \times 10^{-6}$, v cm^{-1}	$F_{1000} \times 10^{-6}$, v cm^{-1}
263	4.19±0.05	4.62±0.03	5.09±0.03	5.53±0.03
273	4.06±0.05	4.47±0.01	4.97±0.04	5.41±0.05
283	3.92±0.03	4.32±0.02	4.89±0.01	5.17±0.02
293	3.67±0.02	4.09±0.03	4.73±0.02	4.97±0.01
303	3.23±0.04	3.97±0.02	4.46±0.01	4.88±0.01
313	3.03±0.06	3.78±0.01	4.17±0.01	4.75±0.04
323	2.90±0.07	3.51±0.01	4.07±0.01	4.59±0.01
333	2.51±0.09	3.23±0.01	3.87±0.01	4.38±0.01
343	2.12±0.06	3.01±0.02	3.75±0.02	4.17±0.01

Oxide density, 5 g cm^{-3} (2).
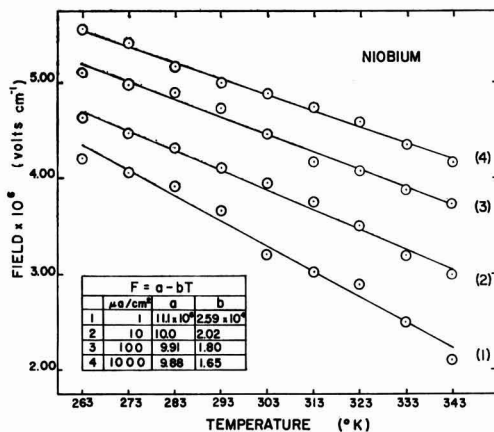
Fig. 1. Temperature dependence of field at 1000, 100, 10, and 1 $\mu a/cm^2$.

Using the mean half-jump distance, 2.40Å, and the mean intercept of the field-temperature regression lines for the three highest currents, 9.91 x 10^6 v cm^{-1}, the interfacial barrier height, ϕ, is 1.19 ev.

From the slopes of the regression lines at each current density, Ao can be determined. The resulting values are 1.0, 0.9, 1.9, and 500 x 10^7 amp cm^{-2}, in order of decreasing current density.

Taking $m_s \leq 8 \times 10^{14}$ atoms cm^{-2} and $V_s = 10^{13}$ sec^{-1} (2), one computes $Ao \leq 6 \times 10^9$ amp cm^{-2}, which is satisfactory, since m_s may be considerably less than the value estimated from the density of the metal.

Discussion

The present investigation indicates that the observed temperature dependence of Tafel slope for growth of *very thin* anodic oxide films on niobium is interpretable on the Mott-Cabrera theory for formation kinetics of such anodic films. Previous studies on niobium, reported by Young (11) were made with thicker, high voltage films. Those results are anomalous on the Mott-Cabrera theory in that the barrier half-width, b, was found to be temperature dependent. The present results are not contradictory, however, since that investigation was made with high-voltage films.

Values of differential formation field given in Table I are in general agreement (except for small differences in temperature coefficients) with those of Young (11) whose work was done with chemically polished electrode surfaces and thick films. A barrier half-width, b, of 2.40Å obtained in the present work is smaller than either of the values $a \geq 4.2Å$, $b \geq 3.1Å$ reported by Young on the Dewald theory but is in good agreement with the 2.42Å reported by Vermilyea (12) for steady-state measurements.

Runs taken at the lowest current density were not used in the evaluation of ϕ and b. Considerably less precision was obtained with these runs, both individually and in the fit to the regression line.

For the remaining data, variation in Tafel slope with current density is of the same magnitude as the

standard deviations of slope. The trend with temperature, however, is unidirectional. Also the three intercepts agree within their respective limits of error.

The precision obtained in this investigation is less than that for similar measurements on high-voltage films (2). Nevertheless it is felt that the results obtained are significant and adequately explained by the Mott-Cabrera theory.

The general agreement between formation fields for both low- and high-voltage anodic oxide films obtained in the present work is contrary to what was observed previously with zirconium (8). This agreement with niobium is probably due to the fact that the ionic current efficiency is essentially 100% for polished niobium over the complete voltage range (2). There is therefore no depression of field due to electronic leakage, as reported for zirconium (8).

The agreement obtained between low- and high-voltage parameters again confirms the assumption (7) that oxide film formation occurs at unit current efficiency over the low-potential range below oxygen evolution.

REFERENCES

1. D. A. Vermilyea, *Acta Met.*, **1**, 282 (1953).
2. L. Young, *Trans. Faraday Soc.*, **50**, 159 (1954).
3. G. C. Willis, Jr., Ph.D. Dissertation, University of Oregon (1958).
4. N. F. Mott, *Trans. Faraday Soc.*, **43**, 429 (1947).
5. N. Cabrera and N. F. Mott, *Repts. Prog. Phys.*, **12**, 163 (1948-49).
6. J. F. Dewald, *This Journal*, **102**, 1 (1955).
7. G. B. Adams, Jr., M. Maraghini, and P. Van Rysselberghe, *ibid.*, **102**, 502 (1955).
8. G. B. Adams, Jr., T. S. Lee, S. M. Dragonov, and P. Van Rysselberghe, *ibid.*, **105**, 660 (1958).
9. G. B. Adams, Jr., M. Maraghini, T. S. Lee, and P. Van Rysselberghe, U. S. Atomic Energy Commission Report AECU-3058 (July 1955).
10. T. Teeter, Ph.D. Dissertation, University of Oregon (1954).
11. L. Young, *Trans. Faraday Soc.*, **52**, 14 (1956).
12. D. A. Vermilyea, *This Journal*, **104**, 427 (1957).

High Current Electronic Interrupter for the Study of Electrode Processes

W. E. Richeson[1] and M. Eisenberg[2]

Stanford Research Institute, Menlo Park, California

ABSTRACT

The design of a fast, high current interrupter capable of handling up to 5 amp is presented. Through small modifications even larger currents can be handled. The electronic interrupter is exceptionally versatile, has a short rise time, a variable output current, and a switching rate from 500 cycles per second to any longer period desired. Interruption periods as short as 1.6 microseconds were found to be quite practical. The high speeds, short rise times, and sizable currents make this interrupter an outstanding device compared to past efforts in this field. The applications of the interrupter in the field of electrochemical kinetics are illustrated through experimental work. Potential-time traces for anodic dissolution of titanium were studied.

Polarization can be measured fundamentally in two different ways. In addition to the direct method involving many forms of liquid junction to a reference electrode and in which the current is maintained constant during the measurement, methods are available to measure the potential of a working electrode against a suitable reference electrode during a short interval following interruption of the electrolyzing current. The chief advantage of a pulse interrupter method is that it allows elimination of the *IR*-drop involved between the working electrode and the reference electrode. This becomes particularly important when the geometry of the cell or changes in the electrolytic conductivity in the boundary layer at the electrode are such that corrections and predictions of *IR* drops are not very

certain. In addition to offering a method for the elimination of the *IR* drop corrections, the interrupter gives several other types of information about the reaction process. For instance, from the decay curve of the polarization potential of the working electrode, deductions about the nature of the process (whether it is under activation control or under mass transfer control) can be made. From the initial slope of such decay curves one can also calculate the pseudo-capacity of the electrode. The latter offers a basic tool for studying the double layer and diffused double layer [according to Stern's theory (1)]. Thus, interrupters are very important research tools yielding important information about electrode processes from both the equilibrium and the kinetic point of view.

The first modern electronic interrupter was described by Hickling (2) in 1937. This device, how-

ever, was still comparatively slow and limited to currents of the order of 10–50 ma. Schuldiner and White (3) obtained current interruptions by applying a disabling pulse to one side of a diode which was in series with the electrolytic cell and a current source. The current capability was in the order of a few milliamperes. More recently, Drossbach (4) used thyratrons to interrupt the current in a circuit containing an electrolytic cell and a current source.

Breiter and Volkl (5) found, however, systematic errors in both thyratron interrupter devices of Hickling and Drossbach. Through the use of calibrated input pulses they found that the error in amplitude of the applied pulse as shown by the measuring thyratron increases as the width of the applied pulse near the peak decreases. The relationship is almost linear. For this reason the thyratron device was found to be more reliable for rectangular input pulses than for sinusoidal or other transient forms. The systematic error is particularly large at low values of potentials. A slight decrease in the systematic error can be achieved by increasing the anode grid potential above 300 v. However, this introduces additional difficulties in fluctuations of the firing point of the thyratron. In addition to these difficulties resulting from the use of thyratrons, the 3 circuits described above were limited by the type of current interruptions which could be obtained, as well as by the level of current that can be handled.

The electronic interrupter described in this paper avoids the use of thyratron tubes and employs an electronic switch consisting essentially of a number of type 6AS7 vacuum tubes operating in parallel. As described here, the interrupter is capable of handling up to 5 amp and performing many different types of interruptions. The "on" and "off" times and switching frequency can be varied practically at will. Furthermore, by addition of more tubes in parallel the current capacity of the interrupter can be increased without involving other major changes.

Design Considerations

The interrupter must act like a near perfect switch which can open and close rapidly without extraneous transients. The device must have a variable conduction level and must be capable of imposing a current function upon some specified steady-state current level. The level of operation must be from a few microamperes to large values, e.g., 5 amp. The period of conduction or no conduction, the ratio between conduction and nonconduction periods, and the frequency of operation of the interrupter should be variable over very wide limits.

The method selected was one in which an electron tube or a group of parallel electron tubes is placed in series with an electrolytic cell and a battery. This electronic switch is controlled by a pulse generator which has a very low output impedance (30 ohms) and a d-c coupling. The pulse generator has a function generator input. This portion of the circuit acts like a power amplifier which controls the electronic switch so that special pulse functions can be used. Provision is made for a potential source and a mercury switch so that the electronic switch will have a step function applied to it which is controlled by a

push button. A third provision is for a time standard to be connected to the pulse generator. This standard drives a pulse generating circuit so as to generate symmetrical or asymmetrical pulses to control the electronic switch over very wide limits (1 μsec to a few tenths of a second intervals). Also on this chassis is the provision to vary the amplitude of the signal and the level of the d.c. to the electronic switch.

The effect of stray pickup would be to introduce noise and extraneous signals into the data. When a current is interrupted the circuit impedance becomes large and it may often become difficult to reduce stray pickup. Due to the fact that the input impedance of the measuring apparatus is large (10 megohms in this case), so as to prevent loading, the noise pickup picture becomes worse. The solution is to make leads short and keep all active portions of the circuit well shielded. Special precautions must be taken in order to prevent capacitively loading high impedance portions of the circuit by shielding these portions too tightly. Special precautions must be taken to prevent grounding loops and to hold stray inductance to a minimum. Large diameter, low resistance, low inductance leads were used when possible. In some cases coaxial and twisted leads to carry currents hence and forth were used in order to reduce the inductance of the system and to reduce radiation or stray pickup. Some portions of the circuit were by-passed with capacitors to reduce their inductive effects. Power line variations and noise were reduced by using voltage-regulated transformers and filters.

Design of Mode of Operation

Power supply.—Figure 1 shows the circuit of the power supply which feeds d-c power to the voltage regulation circuit of Fig. 2. The power supply is designed to supply 400 v d.c. at 1,000 ma. The voltage regulator (Fig. 2) has tubes V_{15}, V_{16}, V_{17}, and V_{18} in parallel which gives a total of 8 triode sections of the 6AS7 variety and can individually pass 125 ma. The maximum output of the regulator is about 1 amp at 100 v drop across these tubes. The tubes V_{19}, V_{20}, T_1, T_2, and T_3 form the error-detecting amplifier which drives the above series of regulator tubes. The voltage regulator tube T_4 produces a 150-v supply whose output current cannot vary by more than ±12 ma about the steady-state current drawn from its 150-v output terminal.
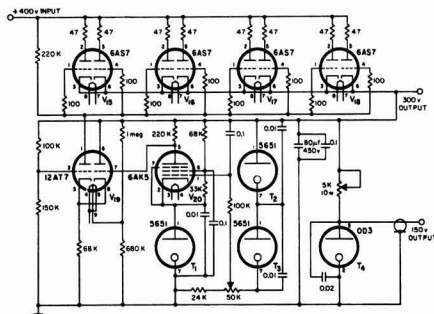

Fig. 1. Power supply

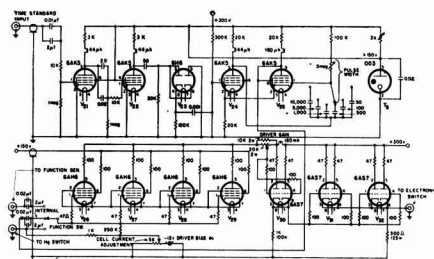Fig. 2. Voltage regulation circuit. Capacity in $\mu\mu$f and resistance in ohms unless specified.

Fig. 3. Pulse generator. Capacity in $\mu\mu$f and resistance in ohms unless specified.

Pulse generator.—The pulse generator (Fig. 3) is the signal source for the electronic switch chassis. The output of the pulse generator is directly coupled to the electronic switch through a coupling box.

Starting with the time standard input jack, signals from the Time Standard (e.g., Hewlett-Packard model 202A) pass through tubes V_{21} and V_{22} which are overdriven amplifiers. When the signal leaves V_{22} it has a squared wave form. This square wave passes to V_{23} which is part of a differentiating and limiting circuit which is responsible for driving V_{24} with sharp positive pips. Tubes V_{24} and V_{25} with associated circuitry form a monostable multivibrator which forms a positive pulse of variable period for each positive pulse coming from V_{23} which is repetitive at the rate prescribed by the time standard. The periods of the positive pulses produced can vary from 2 μsec to 0.15 sec. This positive pulse is fed to point x which is a contact on a selector switch whose other contacts are "To Function Gen" and "Hg Switch." The wiper arms of this switch feed the grids of the parallel combination V_{26}, V_{27}, V_{28}, and V_{29}. This series of tubes forms an amplifier-inverter which feeds a signal to V_{30} which is a cathode follower. V_{30} feeds V_{31} and V_{32} in parallel which is another cathode follower which drives the "electronic switch." Because of the rise time desired and the impedance levels V_{26} to V_{32} were required. The potentiometer, "cell current adjustment," controls the bias on the combination V_{26}, V_{27}, V_{28}, and V_{29}. This controls the d-c level of the output to the electronic switch and therefore its current level. The driver gain control adjusts the magnitude as well as the d-c level of the signal to the electronic switch.
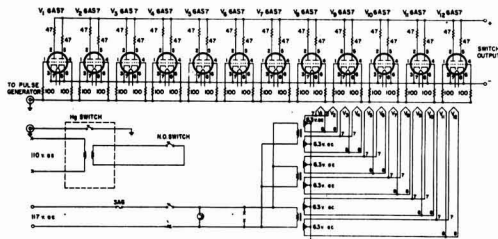

Fig. 4. Electronic switch. Capacity in $\mu\mu$f and resistance in ohms unless specified.

The "function switch" determines the derivation of the "electronic switch" control. The "function generator" position of input at this terminal will be amplified and will control the "electronic switch." Such a function generator might be the Hewlett-Packard low frequency function generator. When the selector switch is on "Hg switch" the pushbutton mercury switch (vide infra) will control the "electronic switch." If the pushbutton is pushed the mercury switch closes and shorts this position to ground. This removes the bias on V_{26} to V_{29} and causes their plate voltage to drop greatly. This step function cuts off the "electronic switch."

Electronic switch.—Tubes V_1 to V_{12} comprise the electronic switch in Fig. 4. With a 50 v drop across the switch, and the grid to cathode voltage equal to zero, the current can be about 5 amp. If the drop across the switch is 60 v, the current can be 6 amp, with a zero grid to cathode voltage. The total dissipation of the present set should not exceed 312 w for any long period of time such as days and weeks. The use of resistors in the plate and grid circuits were for the purpose of avoiding parasitic oscillations. The switch output terminals are in series with the electrolytic cell and the d-c power source.

There is a pushbutton on the panel which actuates a mercury switch. The closure of this switch is grounded. The contact of this switch is brought out to the panel, which allows cabling to one of the inputs to the pulse generator. This input on the pulse generator chassis is labeled "to Hg switch" (left side of Fig. 3).

Coupling box.—Figure 5 shows the coupling circuit between the pulse generator and the electronic switch. The function of this box is to couple the output of the pulse generator to the electronic switch, to set the level of current flowing in the electronic switch, and to assure against grid current being drawn by the electronic switch. The electronic switch current level adjustment should be so adjusted as not to give an indication on the meter M.
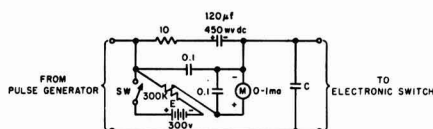

Fig. 5. Coupling box. C, determined the rise time desired; E, 200 v (tapped 300-v miniature battery); M, adjust driver bias control so that this current is always zero; R, electronic switch current level adjust.
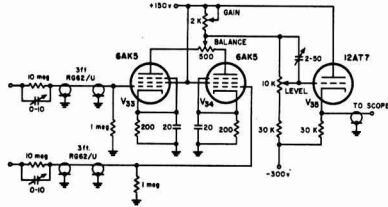
Fig. 6. Difference amplifier. Unless specified, R in ohms, C > 1 in $\mu\mu f$.

The capacitor C (1-50 μf) is included so that the rise time or decay time of the electronic switch may be adjusted.

Difference amplifier.—Tubes V_{33} and V_{34} form the difference amplifier in Fig. 6. The "balance control" is to make adjustments in the event that V_{33} and V_{34} may not have exactly the same characteristics. The gain control adjusts the gain of the difference amplifier. The level control adjusts the d-c level of the output of V_{35} which is a cathode follower. A variable capacitor, C, (2-50 μf) adjusts the shape of the leading edge of fast pulses so as to minimize distortion.

Possible modes of operation.—Figures 7, 8, and 9 present operational block diagrams of Interrupter Circuits No. 1, 2, and 3. The dotted-in capacitors present some of the more important distributed capacitances. Figure 7 shows the circuit which is possible without the use of a difference amplifier and
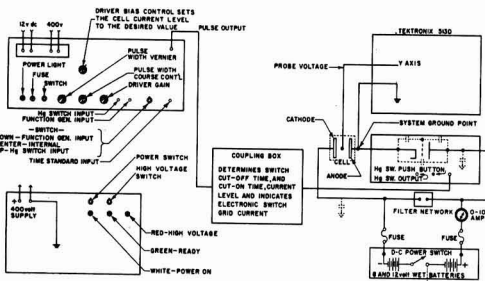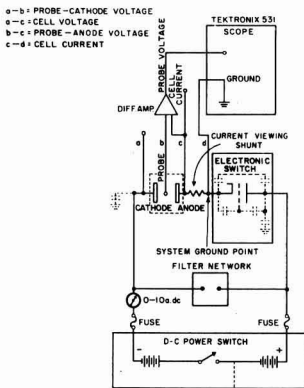

Fig. 7. Interrupter circuit No. 1
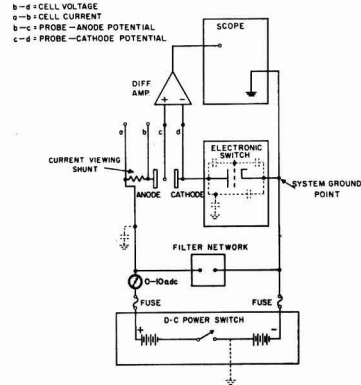

Fig. 8. Interrupter Circuit No. 2

Fig. 9. Interrupter Circuit No. 3

Fig. 8 and 9 show what can be done with the use of difference amplifiers. Due to the existence of distributed inductances in the Interrupter Circuit No. 3 (Fig. 9) is the most desirable circuit since it would have the least ringing.

The method of coupling the electrolytic circuit with the interrupter device is illustrated in Fig. 7. On the right-hand side a bank of lead acid batteries is shown as the source of the electrolytic current. This current passes through an electronic switch (shown directly above the batteries) to the cell and is measured by an ammeter connected in series. The potential developed between the anode in the cell and the reference electrode (probe voltage) is viewed by means of a suitable oscilloscope (in this case Tektronix 513D or 531 was used). After suitable calibration of the oscilloscope in respect to the time as well as voltage axis, visual observations were followed out by photographic records taken with a Polaroid camera. Details of the individual components of the interrupter are shown in Fig. 2, 3, and 4. The voltage regulation circuit as shown in Fig. 2, has an input of +400 v (from the supply unit shown in the lower left-hand corner of Fig. 7) and gives a closely controlled output of either 150 or 300 v. This power is fed into the pulse generator (left upper corner of Fig. 7) whose details are shown in Fig. 3. As a time standard a Hewlett-Packard oscillator is used. Square waves of an adjustable frequency are employed. Whenever a single interruption is desirable a manual switch can be used instead of the time standard. The output of the pulse generator is fed into an electronic switch as shown in Fig. 4. This switch employs a bank of 12 type 6AS7 vacuum tubes. This bank of tubes is necessary to enable the switch to carry and interrupt electrolyzing currents up to 5 amp. The electronic switch is shown in the middle right-hand side of Fig. 7, representing the over-all interrupter circuit arrangement.

Application and Experimental Results

As one method of application of the electronic interrupter a study was made of anodic polarization of titanium. Other possibilities of employing the interrupter were not explored at this time. The main objectives were interruption studies employing elec-

trolyzing currents up to 5 amp for period durations as short as 1 μsec.

The experimental procedure consisted of electrolyzing the cell at a constant current for a sufficient time (usually 5-10 min) to achieve a constant polarization of the anode. Following the calibration of the oscilloscope the electrolytic current was interrupted and a simultaneous photographic recording of the trace on the face of the oscilloscope was taken. This technique was used whenever a full decay of the polarization was wanted. In cases in which the current had to be restored after a desired preset "off" period, this was usually done by employing the time standard as an input to the pulse generator. Usually 1 or 10 cps was used as a frequency for the interruption. In some cases for a given current density interruptions were made for varying (gradually increasing) periods of time. These ranged usually from as little as 1.5 μsec to as long as 4000 μsec. The rise time was found to be about 0.1 μsec.

Results were subsequently evaluated from the photographs of the oscilloscopic traces.

One of the typical experimental situations in studies of electrode kinetics is the inherent involvement of some unknown IR drop in the cell. Even under conditions where efforts have been made to reduce or eliminate such an IR drop, some small IR drops may still exist between the Luggin capillary leading to a reference electrode and the polarized working electrode under study. It is in situations of this type that the use of an interrupter is particularly advantageous.

One of the direct methods for the determination of single electrode polarization which avoids the use of the Luggin capillary with its complicated distortions of the equipotential surfaces and of the hydrodynamic conditions is the so-called "extrapolative method" (6).

This technique is based on the use of two reference electrodes connected to the cell at precisely known distances from the equipotential surface of the electrode itself. The IR drop between the electrode and the nearest reference is then calculated by extrapolating from three measurements, as indicated in Fig. 10. It is obvious that the validity of this method depends primarily on two factors; the first requires a uniform current distribution and the second is based on the assumption that the electrode process does not greatly affect the electrolyte conductivity in its immediate vicinity. The use of an electrolytic trough with well-matched electrodes at the end generally provides a uniform primary current distribution. In most solutions where an excess of supporting electrolyte is employed, the net change in electrolyte conductivity in the vicinity of an electrode at which no new ionic species is created, the conductivity changes are usually sufficiently small to make the extrapolative method useful. However, in the case of an anodic dissolution in an electrolyte which does not contain ionic forms of the metal, sizable changes in the conductivity in the immediate vicinity of the anode occur, and the comparison between the interruption technique and the extrapolation method would then definitely be revealing.

To test this point, as well as to evaluate the overall performance of the interrupter, the anodic polarization of a titanium sheet anode (Ti 75A) was studied in a solution (K-2) of the following composition: 11.5% (wt) HF; 6.2% H_2O; 15.0% tetrahydrofuran; 67.3% ethylene glycol at temperatures from 30° to 55°C. Vigorous stirring was employed in the bulk of the cell Table I shows the analysis of the data obtained from such interruption experiments. In addition, the last column shows IR drop calculations made by the direct extrapolative method. Bright nickel reference electrodes immersed in the same solution in a separate compartment were employed as shown schematically in Fig. 10. At the open circuit the titanium anode potential was negative in respect to the nickel reference electrode by 0.62 v. However, when polarized at a total current of 0.30 amp (i.e., a current density of 6 ma/cm^2) its potential shifted considerably into the positive direction to a value of +105 v. Upon interruption for a period of 2 μsec an instantaneous vertical drop of 0.4 v was recorded. This drop can obviously be assigned to the IR drop component of the potential difference involved between the nearest reference electrode and the polarized titanium anode. Following this rapid IR drop a somewhat slower decay of the actual net polarization of the anode began. Thus, as shown for an interruption period of 48 μsec, the potential decreased from 0.65 to 0.54 v during the period from 2 to 5 μsec (following the current break). This value decayed further to 0.40 v within the subsequent 43 μsec (see line 3, Table I).

In experiments employing a total current of 0.70 amp the IR drop component estimated from the decay curve was 0.7 v. This was lower than the 0.95 to 0.90 value estimated by means of an extrapolative method employed in the direct polarization measurements (last column of Table I). At this current level longer interruption periods were employed and it can be noticed that a decay of about 1.5 v occurred within 1000 to 2000 μsec. This generally is quite rapid compared with the decay one might expect from a pure diffusion mechanism (7). Similarly, it can be observed that at a total current of 2 amp (current density of 40 ma/cm^2) the anode polarization drops from 2.8 v to 0.30 v within 4000 μsec. This, compared with the zero current potential of −0.62 v, amounts to a decay of 72.7% of the total anode polarization within 0.004 sec. On the basis of these observations it may thus be concluded (8) that the anode polarization of titanium consists essentially (if not completely) of chemical polarization associated with
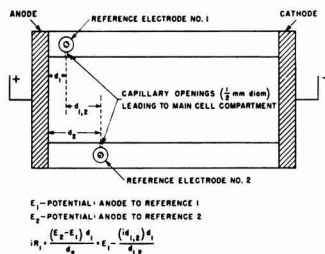

Fig. 10. Schematic top view of polarization cell

Table I. Analysis of potential-time traces for titanium anode (Ti75A)[a]
Solution: K-2 — Anode Area = 50 cm^2

Total current, amp	Temp, °C	Interruption period, μsec	IR drop[b] estim. from decay, v	Just prior to interruption	Anode potential vs. Ni-ref electrode, volts			Final closed circuit value	IR drop[c] estim. in the direct method, v
					5 μsec after interr.	Minimum at end of interr. period	0.5 μsec after closing circuit		
0	30			−0.62					
0.30	30	2	—	+1.05	—	0.65	1.05	1.05 (at once)	0.44
0.30	30	48	0.4	1.05	0.54	0.40	0.90	1.05 (40 μsec later)	0.44
0.30	31	70	0.4	0.95	0.45	0.32	0.83	0.95	0.44
0.70	36	1.6	0.7	1.55	—	0.85	1.50	1.55 (3 μsec later)	0.95
0.70	36	25	0.7	1.55	0.65	0.48	1.10	1.55 (75 μsec later)	0.95
0.70	37	60	—	1.55	0.65	0.40	1.05	1.45 (40 μsec later)	0.93
0.70	37	200	—	1.52	—	0.25	0.90	1.47 (300 μsec later)	0.93
0.70	38	1020	—	1.50	—	0.05	1.00	1.50 (1000 μsec later)	0.90
0.70	38	2000	—	1.48	—	0	—	1.48 (3000 μsec later)	0.90
2.00	40	2.6	1.2	3.30	—	1.90	3.00	3.2 (7 μsec later)	2.48
2.00	40	22	1.4	3.30	1.55	1.30	2.75	3.2 (80 μsec later)	2.48
2.00	55	200	—	2.80	—	0.60	—	2.8 (300 μsec later)	—
2.00	55	4000	—	2.80	—	0.30	—	2.8 (3000 μsec later)	—

[a] All experiments were carried out with a repeat rate of 1 or 10 cps.
[b] The IR drop in the electrolytic cell between the anode and the nickel reference electrode.
[c] These values were estimated by extrapolating the bulk electrolyte conductivity to the solution layer adjacent to the electrode.

the activation energy required for the titanium dissolution reaction.

Another interesting conclusion from this work is that the IR drop values obtained from conductivities in the direct method of polarization measurements (last column Table I) are usually larger than the values obtained from the initial rapid drop in the potential-time trace obtained by the interrupter method. These differences become larger and more significant the larger the current densities employed. This, of course, is to be expected since sizable amounts of titanium ions are going into the solution in the immediate vicinity of the anode. The differences, especially at the higher current densities, are sufficiently large to demonstrate the importance of interruption techniques as a research tool in electrode kinetics.

REFERENCES

1. O. Stern, *Z. Elektrochem.*, **30**, 508 (1924).
2. A. Hickling, *Trans. Faraday Soc.*, **33**, 1540 (1937).
3. S. Schuldiner and R. E. White, *This Journal*, **97**, 433 (1950).
4. P. Drossbach, *Z. Elektrochem.*, **57**, 548 (1953).
5. M. Breiter and W. Volkl, *ibid.*, **58**, 899 (1954).
6. M. Eisenberg, M. S. Thesis, Univ. of California (1951).
7. C. W. Tobias, M. Eisenberg, and C. R. Wilke, *This Journal*, **99**, 359C (1952).
8. A. Hickling and F. W. Salt, *Trans. Faraday Soc.*, **37**, 450 (1941).

The A-C Resistance of a Stainless Steel Electrode and Specific Adsorption

G. M. Schmid and Norman Hackerman

Department of Chemistry, University of Texas, Austin, Texas

ABSTRACT

The a-c resistance of a stainless steel wire electrode was measured in dependence of the type of electrolyte, the polarizing current density, and frequency of the measuring current. It is shown that K^+ is more adsorbed than Na^+ during cathodic polarization, and Cl^- more than F^- during anodic polarization. This method seems to be especially useful in testing the adsorbability of neutral surface active substances during d-c flow.

A wire electrode in contact with an electrolyte represents, with respect to passage of current along the length of the wire, a system similar to two resistors connected in parallel. Thus, when two contacts are made to the same electrode and an a-c or d-c potential is applied, a certain fraction of the total current flow chooses a path through the electrical double layer (edl) and the solution (1). The extent of this leakage can be found by measuring the impedance of the system and comparing it with the impedance of the electrode in air. In doing so, it must be remembered that the impedance of a metal

can vary with the uptake of gas, especially hydrogen (2).

The conduction phenomena of the electrode/electrolyte interface are determined by the structure and composition of the edl. The composition of the edl depends on the kind of electrolyte solution used and on the presence or absence of specifically adsorbed ions and neutral surface active substances. The structure of the edl depends on the potential of the electrode (3). It was found previously that the magnitude of leakage current in the system stainless steel/1.0M Na_2SO_4 depends on the polarizing d-c current density (p.c.d.), or alternatively on the potential of the electrode (4).

The leakage current, besides being governed by the edl, is limited by the conductivity of the solution. It was found to be negligible in the system stainless steel/0.001M Na_2SO_4. Furthermore, when using an electrolytic cell, the current, leaking from the test electrode into solution, may also pass from the solution into the auxiliary electrode, comparable to a circuit with three resistors in parallel.

Measurements of the leakage current, i.e., the impedance of the system, between two contacts on the same electrode should permit conclusions to be drawn regarding specific adsorption. The leakage current will have to be compared with a system, the components of which are not specifically adsorbed.

Experimental

Essentially the same experimental setup was used as in previous work (4). Unless otherwise stated, the impedance of the test electrode was measured with 60 cps a.c. in a Wheatstone Bridge, using a Brown-Honeywell Recorder for continuous measurements, with a precision of 0.005 ohms. In order to obtain data on the frequency dependence of the leakage current, a General Radio Co. (GRC) Type 650-A Impedance Bridge was used between 100 cps and 16 kcps, with a Hewlett-Packard (HP) Wide-range Oscillator Model 200 DC as power supply. The signal drawn from the bridge was preamplified in a HP Model 450-A Amplifier, filtered and amplified in a HP Model 300-A Harmonic Wave Analyser and observed on an oscilloscope, thus giving an accuracy of 0.01 ohms. Measurements between 550 kcps and 2 mcps were made with a GRC Type 821-A Twin-T Impedance Bridge combined with a GRC Type 1001-A Standard Signal Generator. Here the null-detector was a radio receiver.

Reproducible results, especially at the intermediate frequency range, were obtained only after pretreating the electrodes alternatively, anodically, and cathodically for about 1 hr (5).

In all cases, the test electrode was a type 302 stainless steel wire of 0.038 cm diameter and approximately 90 cm long. The auxiliary electrode was made of the same material and length. The two electrodes were arranged in a glass tube and kept apart 2 cm throughout. The polarizing d-c current was supplied by a Lambda Regulated Power Supply Model 32 M operated at 200 v d.c. or by a 180 v battery and controlled by a set of resistors. The power supply was connected to the upper end of the anode and the lower end of the cathode, thus
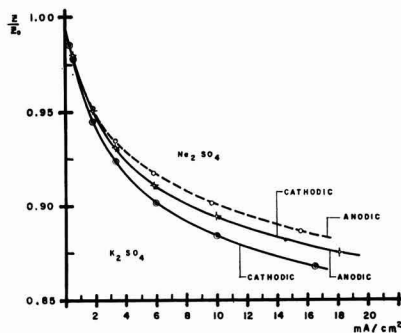

Fig. 1. Relative impedance vs. current density in 0.1M K_2SO_4 and 0.1M Na_2SO_4. (Curves for Na_2SO_4 cathodic and K_2SO_4 anodic coincide. Electrode: Type 302 stainless steel wire, 0.038 cm diameter, surface area 10.6 cm², $Z_0 = 6.556$ ohms.

preventing a d-c potential drop along the wires. All contacts were made outside the electrolyte. Interference of the two circuits was carefully minimized by the use of capacitors and chokes as filters. The potential of the test electrode was measured against a saturated calomel electrode (SCE).

Results

Effect of cations.—The difference between impedance measurements with low-frequency a.c. in air and in solution is very small, either because the coupling capacity of the edl is too small and/or the coupling resistance is too large to allow a significant fraction of the measuring current to leak into solution. When the electrode is sufficiently polarized to make an electrochemical reaction possible, the capacity becomes appreciably higher and/or the resistance drops to low values (6). This causes an a-c leakage as shown in Fig. 1, where the impedance of a stainless steel wire is plotted against the p.c.d. for 0.1M Na_2SO_4 and 0.1M K_2SO_4. Since the anion is the same in both cases, one would expect the curves for anodic polarization to coincide. As stated above however, the leakage current is limited also by the conductivity of the electrolyte (Table I). The better conducting system, K_2SO_4, should in any case show a lower impedance at a given p.c.d., as was found experimentally. The distance between the anodic and cathodic curves is slightly bigger in the case of K_2SO_4, pointing to a more densely packed edl. It was concluded, therefore, that during cathodic polarization K^+ is somewhat more adsorbed than Na^+. This has been reported also on Hg (7) and Pt electrodes (8). In both solutions, the impedance curves for cathodic polarization run lower than those for anodic polarization. This means a larger capacity and/or smaller resistance of the edl on cathodic polarization (6).

Table I. Conductivity in $10^{-4} ohm^{-1} cm^{-1}$ (9)

t°C	Molarity	Na_2SO_4	K_2SO_4	KF	KCl	KBr	KI
25°	0.1	163.08	202.52	107[+]	128.62	131.4	130.5

+ Interpolated.

Effect of anions.—In solutions of the more common cations, the cathodic electrode reaction is H_2 evolution, and it is reasonable to assume that, at a given current density, differences in the behavior of the edl can be attributed to differences in the adsorbability of ions or neutral substances. An electrochemically inert species, like SO_4^{--}, can be taken as common anion. In varying the anion, however, frequently the anodic electrode reaction changes from anion to anion and with it the composition of the edl. Thus, with KF up to 1.0M and 0.1M KCl (at current densities > 3 ma/cm², see next paragraph) O_2 is evolved at the anode, with KBr up to 1.0M the electrode does not become passive in the current density region investigated and iron dissolution occurs, and with KI the anion is oxidized. The above assumption no longer holds and we can reasonably compare only the curves for 0.1M KF and 0.1M KCl with each other. An additional complication derives from the fact that the auxiliary electrode, only 2 cm away, may participate in the over-all conduction phenomena (4). This interference forces the impedance drops on both sides of the polarization curves to be of the same order of magnitude. So, in judging the effect of different ions on the leakage current, both cathodic and anodic impedance curves have to be considered together. With 0.1M KF and 0.1M KCl the impedance curves for cathodic polarization are also lower than the anodic impedance curves (Fig. 2). It seems to be a general rule that the conductivity of the edl at H_2 evolution is higher than at O_2 evolution potentials. The difference between cathodic and anodic curves is more pronounced on comparing F^- and Cl^- than on comparing K^+ and Na^+, showing a larger effect of anion adsorption. The gap is bigger in the case of Cl^-, which apparently can dehydrate more easily than F^- ions (8, 10). The generally smaller impedance changes in KF can be explained by its smaller conductivity.

It is interesting to note that the curve for 0.1M KI and 0.1M KBr differ remarkably, despite the fact that the solutions have about the same conductivity. This could be attributed to stronger adsorption of I^- combined with a higher edl capacity due to adsorbed I_2.

Effect of chloride.—Figure 3 gives recorder graphs of measurements in 0.1M K_2SO_4 and 1.0M KCl. In K_2SO_4 the impedance reaches its steady-state value for the corresponding polarizing current density or open-circuit conditions practically instantaneously. During current flow O_2 evolution takes place. In KCl however a sharp impedance drop occurs, followed by a slow increase to a maximum and a final steady-state value. The electrode exhibits a passive potential shortly after the first sharp drop, and gas evolution was observed. During the following increase a slow potential decay with a sudden breakdown at the impedance maximum was experienced. Gas evolution stops and the bright electrode begins to show dark pits. After the polarizing current is cut off, it takes roughly 1 to 2 min for the impedance to reach its steady-state value for open-circuit conditions. The time during which passivity is maintained is a function of temperature, current density, and KCl concentration. At room temperature stainless steel can be held passive in 0.1M KCl with current densities > 3 ma/cm². Current densities < 20 ma/cm² are not enough to maintain passivity in 1.0M KCl. Increase in temperature shortens the time of passivity. At an anodic current density of 20 ma/cm² in 1.0M KCl, the electrode is passive at 39°C for 38 sec only, whereas at 1°C passivity is maintained "permanently" even at considerably smaller current densities. The time during which passivity is maintained is not reproducible because of the large changes in surface involved (pitting, Fe dissolution). For these phenomena the following explanation is proposed. In the first moments of anodic polarization an adsorbed sheet of water dipoles is converted to chemisorbed oxygen (11). The strongly positive potential facilitates the subsequent adsorption of Cl^- ions. Gradually, adsorbed oxygen is partially replaced by adsorbed Cl^-, passivity breaks down, and the potential falls back to Fe dissolution values.

A passive stainless steel electrode provides for a large amount of leakage current (e.g., KF, Fig. 2, a and b). A fairly rapidly dissolving electrode shows less leakage current (e.g., KBr, Fig. 2, e), despite the fact that the adjacent layer of solution should be crowded with iron ions and have good conductivity. At a dissolving electrode, however, continuous regeneration of the surface prevents a high coverage with chemisorbed species, provided the surface changes fast enough. The importance of the inner edl for the contact between metal and solution is again emphasized. The peak in the impedance/time curve (Fig. 3) represents a maximum coupling impedance, the point, where the coverage with adsorbed oxygen is defective so that the passivity breaks down and iron dissolution begins. Chloride ion adsorption blocks the surface for the leakage current. In order to pass into solution by resistive coupling, the measuring a-c current would have to react with Cl^- or Cl_2 alternatively, which is not pos-
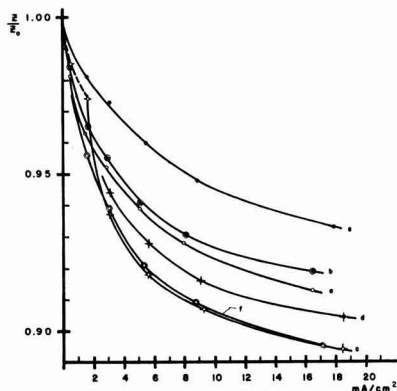

Fig. 2. Relative impedance vs. current density: curve a, 0.1M KF cathodic; curve b, 0.1M KF anodic; curve c, 0.1M KCl cathodic; curve d, 0.1M KCl anodic; curve e, 0.1M KBr anodic; curve f, 0.1M KI anodic. Electrode: Type 302 stainless steel wire, 0.038 cm diameter, surface area 10.5 cm², Z_o = 6.520 ohms.
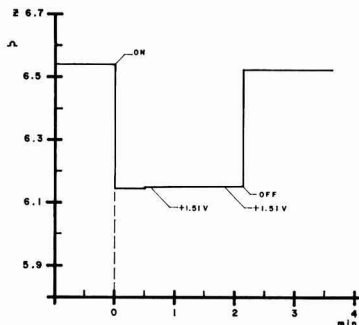
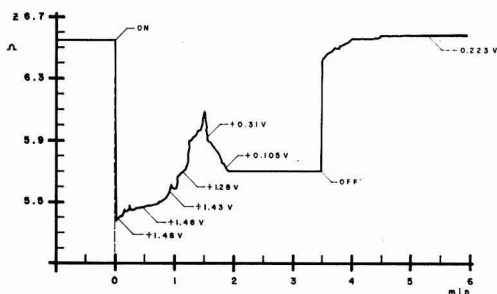Fig. 3a. Impedance vs. time (recorder traces), 0.1M K₂SO₄, 5.8 ma/cm² anodic.

Fig. 3b. Impedance vs. time (recorder traces), 1.0M KCl, 9.3 ma/cm² anodic. Potential values with respect to SCE.

Fig. 4. Relative impedance vs. frequency: 1.0M Na₂SO₄: curve a, open polarizing circuit; curve b, 7 ma/cm² anodic; curve c, 7 ma/cm² cathodic. 1.0M Na₂SO₄ + 0.2M (CH₃)₃N: curve d, open polarizing circuit; curve e, 7 ma/cm² anodic; curve f, 7 ma/cm² cathodic. Electrode: Type 302 stainless steel wire, 0.038 cm diameter, surface area 10.8 cm², Z_o = 6.98 ohms.

sible because of the high overvoltage for this step, thus leaving a capacitive coupling only.

To get further proof for this point of view the potential time pattern of the electrode during cathodic and anodic polarization in 0.5M KCl with a current density of 5 ma/cm² was observed on an oscilloscope. The electrode was made passive and the potential was allowed to decay under current flow. Immediately afterward short cathodic pulses (5-10 sec) were applied, and an attempt was made to passivate the electrode again between each cathodic pulse. The potential however never went beyond +1.0 v, showed a flat maximum, and dropped to about +0.2 v in a total elapsed time of 0.5 sec. Only prolonged cathodic polarization (>1.5 min) restored the ability of the electrode to become passive at once when anodically polarized. The negative potential of the electrode during cathodic polarization probably causes desorption of Cl⁻. This process however requires some time. After short cathodic pulses there is still enough Cl⁻ left adsorbed on the surface to prevent the metal from becoming passive again. Prolonged cathodic polarization provides sufficient time for the Cl⁻ to be desorbed, thus enabling the electrode to achieve passivity when polarized anodically.

Frequency dependence of the leakage current.— The impedance of the electrode in air and in 1.0M Na₂SO₄ without polarizing current is practically the same at low frequencies. Up to about 100 cps the impedance in solution is independent of frequency (Fig. 4,a). The parallel resistance of the edl is high,
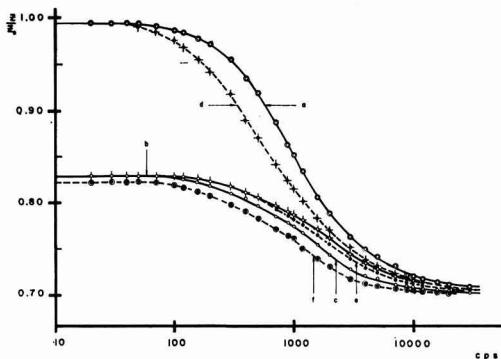
the capacity small under these conditions. This causes the coupling to be negligible. At higher frequencies the impedance of the edl becomes smaller, permitting a larger part of the a.c. to leak into solution. Above 10 kcps this impedance becomes too small to control the leakage current. The coupling becomes "perfect" and the impedance of the system is governed by the constant impedance of the electrolyte. At about 1 mcps the skin effect (12) begins to show, causing the impedance to increase again.

The polarized electrode shows a considerably lower impedance at low frequencies, the parallel resistance of the edl being much smaller. Above 10 kcps the impedance coincides with the values obtained under open-circuit conditions, the coupling being "perfect" again.

Effect of surface active substances.—The frequency dependence of the leakage current was measured in 0.2M (CH₃)₃N with 1.0M Na₂SO₄ as carrier and compared with a pure 1.0M Na₂SO₄ solution (Fig. 4). Under open polarizing circuit conditions, the greater capacity of (CH₃)₃N becomes clearly visible in the intermediate frequency range, the maximum difference being about 0.3 ohms. Here the conductivity of the solutions and the reactions at the electrodes are the same in either case; the difference therefore can be due only to adsorption of the surface active substance on the electrode.

The capacity remains bigger with (CH₃)₃N under polarizing conditions. The effect is larger on the cathodic side. It has been suggested that organic amines are purely cathodic inhibitors (13). One should expect therefore a stronger adsorption during cathodic polarization. Even in the low-frequency range, the impedance of the edl is lower in (CH₃)₃N during cathodic polarization. It has been pointed out however that organic amines are anodic inhibitors as well (14). The curves for anodic polarization with and without (CH₃)₃N coincide for low frequencies, the difference being small in the intermediate frequency range. This shows that the effect of anodic inhibition is probably smaller in this case.

Summary

It has been shown that measurements of the leakage current can be useful to test adsorption of ions and surface active substances, especially under polarizing current flow, where other methods, e.g., measurements of the edl capacity, do not give satisfactory results. The method is at its best where the leakage current in solutions with neutral surface active substances can be compared with a pure carrier solution. This can be done either by separate impedance measurements, as shown above, or by using two identical cells with the solutions to be compared as two arms in a Wheatstone Bridge and observing the error signal. The optimum frequency for the a-c measuring current is around 1000 cps. Difficulties have been met and are explained in cases, where changes in electrode reaction occurred, especially in potassium halide solutions. Nevertheless it has been possible to show that K^+ is more adsorbed than Na^+ and Cl^- more than F^- on stainless steel. An attempt has been made to explain the peculiar effect of Cl^-, which makes it impossible to maintain passivity even under anodic polarization with a current density high enough to passivate the metal initially.

Any discussion of this paper will appear in a Discussion Section to be published in the June 1961 JOURNAL.

REFERENCES

1. C. A. Knorr and E. Schwartz, *Z. Elektrochem.*, **39**, 281 (1933).
2. See for example: F. Fischer, *Ann Physik*, [4] **20**, 503 (1906); A. Coehn and H. Juergens, *Z. Physik*, **71**, 179 (1931); J. P. Hoare and Sigmund Schuldiner, *J. Phys. Chem.*, **61**, 399 (1957).
3. A. Frumkin, *Z. Physik*, **35**, 792 (1926); *Ergebn. Exakt. Naturwiss.*, **7**, 235 (1928); J. A. V. Butler, *Proc. Roy. Soc. [London]*, **A122**, 399 (1929); Electrical Phenomena at Interfaces, London (1951), 63.
4. G. M. Schmid and Norman Hackerman, *This Journal*, **107**, 142 (1960).
5. G. Okamoto, M. Nagayama, and N. Sato, C.I.T.C.E., Proceedings of the Eighth Meeting, Madrid 1956 (London 1958).
6. K. Franke, C. A. Knorr, and M. Breiter, *Z. Elektrochem.*, **63**, 226 (1959).
7. A. N. Frumkin, B. B. Damaskin, and N. V. Nikolaeva-Fedorovich, *Proc. Acad. Sciences, USSR*, **115**, 751 (1957); J. Palacios and A. M. Baptista, *Rev. fac. Cienc, Univ. Lisboa*, 2a, Ser. B, **2**, 137 (1952/53).
8. P. V. Popat and Norman Hackerman, *J. Phys. Chem.*, **62**, 1198 (1958).
9. International Critical Tables, Vol. VI.
10. D. C. Grahame and B. A. Soderberg, *J. Chem. Phys.*, **22**, 449 (1954).
11. Kabanow, Burstein, and Frumkin, *Discussions Faraday Soc.*, **1**, 259 (1947).
12. Radio Engineer's Handbook, New York, (1943) 30.
13. Shih-Jeh Ch'iao and C. A. Mann, *Ind. Eng. Chem.*, **39**, 910 (1947); L. E. Swearingen and A. F. Schram, *J. Phys. Chem.*, **55**, 180 (1951).
14. Norman Hackerman and J. D. Sudbury, *This Journal*, **97**, 109 (1950); Helmut Kaesche and Norman Hackerman, *ibid.*, **105**, 191 (1958).

Technical Notes

Magnesium-Sulfur Dry Cells

C. K. Morehouse and R. Glicksman

Semiconductor and Materials Division, Radio Corporation of America, Somerville, New Jersey

A study of the electrochemical characteristics of the various compounds and elements of the periodic system showed that sulfur has several characteristics which make it worthy of consideration for use as a cathode material in primary batteries. It has a greater ampere-minute capacity per unit of weight (100.3 amp-min/g) and volume (207.6 amp-min/cc) than the cathode materials used in conventional batteries. Although it has a lower reversible potential than the other cathodes, it does have a flat voltage-time discharge curve as measured by the half-cell technique previously described by the authors (1). By the use of this technique, the sulfur cathode has been found to operate at a potential of about —0.4 v

(vs. N.H.E.) when discharged at a rate of 0.030 amp/g in a $MgBr_2$ electrolyte. The efficiency of this electrode, which was computed on the assumption that the reaction involves a two-electron change per sulfur atom, was in excess of 80%. In addition to its favorable electrochemical properties, sulfur has a low solubility in aqueous solutions and is readily available at low cost in this country.

The use of sulfur as a cathode material coupled with a zinc anode in a Leclanché-type cell was first described by Walker (2) in 1887. Other patents have been reported which deal with the addition of small amounts of sulfur to the cupric oxide cathode of the Lalande cell in order to raise the cell voltage
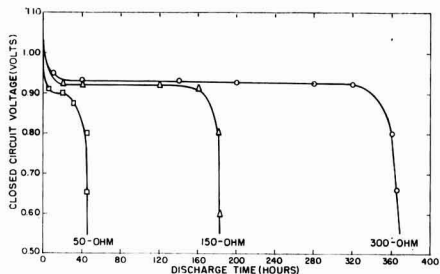
Fig. 1. AA-size Mg/MgBr₂/sulfur dry cells discharged continuously through 50-, 150-, and 300-ohm resistances at 21.1°±1.1°C (50% R.H.).
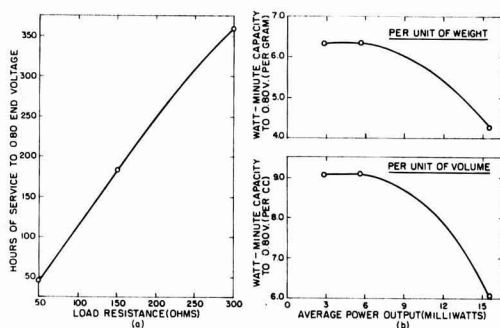

Fig. 2. Capacity data for AA-size Mg/MgBr₂/sulfur cells showing (a) hours of service to 0.80 v end voltage vs. load resistance; (b) watt-minutes per unit of volume and weight vs. average power output (capacity and average power computed to 0.80 end voltages from continuous discharge data).

(3-8). These references refer to coupling sulfur with a zinc anode. Such cells have a low operating voltage and thus have practical limitations.

If a sulfur cathode is coupled with a magnesium anode, the reversible potential of the system calculated from free energy data is 2.2 v, assuming the following reaction occurs when energy is withdrawn from the cell:

$$Mg + 2 OH^- + S = Mg(OH)_2 + S^= \qquad [1]$$

It is well known, however, that magnesium does not operate at its reversible potential in aqueous solutions. For example, in an aqueous $2N$ MgBr₂ solution, saturated with Mg(OH)₂, AZ10A magnesium alloy has a potential (vs. N.H.E.) of 1.42 v under open-circuit conditions and operates at a potential of 1.29-1.32 v over a current density range of 0.5-4.0 ma/cm². Thus the operating potential of a magnesium-sulfur primary cell should be about 0.8-0.9 v.

Experimental

Magnesium-sulfur dry cells were assembled using an impact extruded AZ10A magnesium alloy AA-size can (height 4.62 cm, OD 1.32 cm, ID 1.12 cm). The magnesium cans were lined with a piece of salt-free kraft paper (5.72 x 5.72 x 0.005 cm thick), and an extruded slug of cathode mix was inserted in the lined can and consolidated. A carbon rod (height 4.54 cm, diameter 0.404 cm) containing a brass cap, was then inserted in the center of the cathode mix, and the cells sealed in the conventional manner with a rosin base wax. Each cell weighed approximately 10 g and contained about 5 g of cathode mix. The cathode mix, which consisted of equal parts by weight of Shawinigan acetylene black and sulfur mixed with 3% BaCrO₄, was wet to the proper consistency with an aqueous MgBr₂·6H₂O (500 g/l) solution containing 0.2 g/l Na₂Cr₂O₇.

The performance characteristics of the magnesium-sulfur AA-size dry cells of the above formulation and construction are shown in Fig. 1. These data were obtained by discharging the cells continuously through fixed resistances at 21.1° ± 1.1°C (70° ± 2°F) and 50 ±5% R.H.

The open-circuit voltage of the magnesium-sulfur dry cells ranges between 1.60 and 1.65 v; this high voltage is due to either adsorbed air in the cathode mix, or to the small amount of chromate which is added to inhibit the corrosion of the magnesium

anode. When current is withdrawn from the cells, the voltage falls to between 0.90 and 0.95 v, the operating voltage level of this system. Although these cells operate at a considerably lower voltage than the Leclanché and magnesium-manganese dioxide cells (9), they have a flat discharge curve and give considerably more hours of service to end voltages of 0.9 and 0.8 v than the two manganese dioxide dry cells.

The performance data in terms of continuous service to a 0.80 v end voltage vs. load resistance are presented in Fig. 2. Curves are also given showing the watt-minute capacity per unit of weight and volume as functions of the average continuous power output in milliwatts.

The magnesium-sulfur cell operates at about 0.90 v and offers promise for low drain applications. Its attractive features are high theoretical capacity, constancy of voltage during cell discharge, and the low cost of sulfur. It has problems similar to other magnesium cells. These are: delayed action, high impedance, and loss in capacity on light intermittent tests. The fact that hydrogen sulfide gas is liberated during cell discharge limits its broad applications.

REFERENCES

1. C. K. Morehouse and R. Glicksman, *This Journal*, **103**, 94 (1956).
2. S. F. Walker, U. S. Pat. 361, 794, April 26, 1887.
3. R. C. Benner and H. F. French, U. S. Pat. 1,255,283, Feb. 5, 1918.
4. R. C. Benner and H. F. French, U. S. Pat. 1,316,761, Sept. 23, 1919.
5. R. C. Benner and H. F. French, U. S. Pat. 1,375,647, April 19, 1921.
6. R. C. Benner and H. F. French, Can. Pat. 215,676, Feb. 7, 1922.
7. R. C. Benner and H. F. French, U. S. Pat. 1,415, 860, May 16, 1922.
8. G. W. Armstrong, U. S. Pat. 1,624,460, April 12, 1927.
9. R. C. Kirk, P. F. George, and A. B. Fry, *This Journal*, **99**, 323 (1952).

On the Anodic Oxidation of Columbium

Robert Bakish

The Alloyd Corporation, Cambridge, Massachusetts

Except for the work of Johansen, *et al.* (1), Young (2, 3), and Adams (4), the author knows of no work on the anodic oxidation of columbium. This communication discusses in brief some aspects of the anodic oxidation of this metal.

The work was done on columbium sheet supplied by Murex Ltd., Rainham, Essex, England, which analyzed as follows: Ta 0.58%, C 0.1%, Ni 0.03%, Si 0.013%, Fe 0.015%, Ti 0.081%, Al and Mg 0.01%, B, W, V traces ($\leq 0.01\%$). The specimen were thoroughly degreased and etched in a 5:2:2 solution of H_2SO_4 (95%), HNO_3 (70%), and HF (48%) prior to formation which was carried out at constant current of 5.5 ma/cm^2 in 0.1% H_3PO_4 solution. Constant current and constant voltage power supplies capable of maintaining voltages and currents within 1% of output were utilized, and all measurements were carried out in constant temperature bath controlled to $\pm0.5°$ of the working temperatures and with 1% instruments.

The oxide and its state of crystallinity were identified by standard x-ray diffraction powder techniques supplemented by electron diffraction in transmission. For the electron microscopy triafol replicas shadowed at 30° and 90° incidence with SiO were used.

The voltage current characteristics of columbium and their dependence on temperature as recorded with a two channel recorder are given in Fig. 1, which shows typical data for 1°, 25°, 60°, and 80°C. In these experiments formation at constant current to 300 v was followed by constant voltage once the 300-v value was reached. After the well-known exponential decay of the current to a relatively low value "leakage current plateau," depending on the formation temperature, this value is kept for some time and then rather abruptly increases. The time to current reversal is inversely dependent on temperature with the current hardly reaching a "plateau" value at higher formation temperatures but rapidly getting outside the range of the instrumentation used.

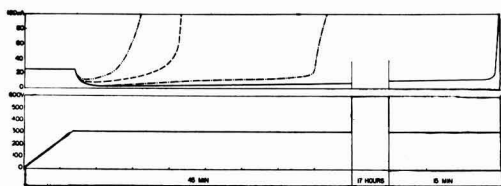This voltage current behavior is the consequence of crystallization of the amorphous oxide film. The leakage current for samples formed to lower voltages and held under these respective voltages remains at the "plateau" value for considerably longer times, and for a 50-v formation at room temperature no reversal was observed for as long as 24 hr under voltage, which was the duration of the measurements.

The oxide itself is identified with the T-Cb_2O_5 oxide form as determined by Brauer (5).

The influence of the potential on the oxide topography is shown by the composite electron micrograph (Fig. 2) showing representative areas identi-
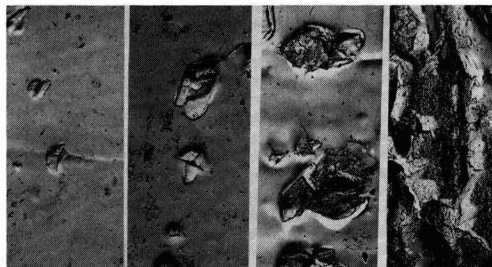
Fig. 2. Dependence of topography on formation voltage. Constant voltage formation to 100, 150, 175, 250. Magnification 5000X before reduction for publication.
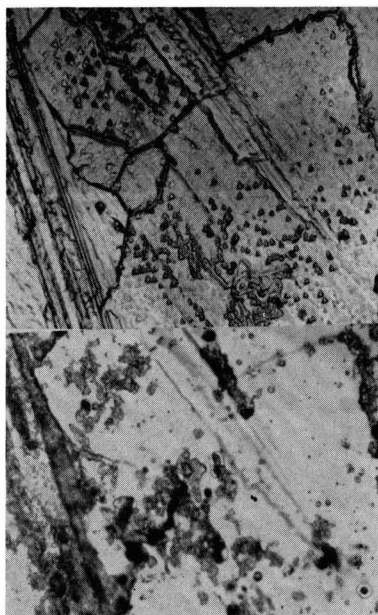

Fig. 3. Topographical changes associated with imperfections. Surface as etched and after formation to 320 v. Magnification 1000X before reduction for publication.

Fig. 1. Voltage-current characteristics of columbium formation. ——— 1°C 1/10% H_3PO_4; —.—. 25°C; — — — 60°C; —..—.. 80°C.

fied with the respective voltages. These observations were made after constant current formations to the voltages indicated. Above 250 v no replicating and, in turn, no electron microscopy are possible due to the disintegration of the oxide. The topographic changes of columbium on crystallization are both different and similar to these changes in tantalum. They are different in that none of the crystalline polygonal areas seen in tantalum (6) are observed here, and similar because here, as well as in tantalum, the crystalline oxide nucleates underneath and grows at the expense of the amorphous oxide, displacing it in the process.

An attempt to evaluate the possible role of cold work and imperfections was also made in this study, with Fig. 3 showing a representative specimen area containing a fine scratch before and after formation to 320 v. Observe the bulk of the crystallization taking place in the area delineated by the scratch and also in the vicinity of the dislocation etch pits (7), indicating, even though not conclusively, the possible catalytic role of imperfections in this crystallization process. It has already been shown that in tantalum crystallization takes place at preferred sites (8).

Results reported here show both similarities and differences between columbium and tantalum. The formation characteristics and the crystallization phenomena are common to both metals, but the greater ease of crystallization of columbium of this purity, as well as some details of the topographic changes brought about with the process, appear different. On the basis of this data, it cannot be asserted whether the observed differences are due to inherent differences between the two metals or to impurities in the columbium acting as crystallization nuclei.

Acknowledgments

REFERENCES

1. H. Johansen, G. B. Adams, Jr., and P. van Rysselberghe, *This Journal*, **104**, 339 (1957).
2. L. Young, *Trans. Faraday Soc.*, **51**, 502 (1955).
3. L. Young, *ibid.*, **51**, 515 (1958).
4. G. B. Adams, Jr. and T. Kao, AECU 3769 (1957).
5. G. Brauer, *Z. anorg. u. allgem. Chem.*, **248**, 1 (1941).
6. D. Vermilyea, *This Journal*, **102**, 207 (1955).
7. R. Bakish, *Trans. Am. Inst. Mining Met. Engrs.*, **212**, 818 (1958).
8. D. Vermilyea, *This Journal*, **104**, 542 (1957).

# The Reaction of Zirconium-Oxygen Alloys with Hydrofluoric Acid

M. E. Straumanis and T. Ejima

Department of Metallurgy, the University of Missouri School of Mines and Metallurgy, Rolla, Missouri

Metallic zirconium dissolves readily in hydrofluoric acid according to the equation (1, 2)

$$Zr + 4HF = ZrF_4 + 2H_2 \qquad [1]$$
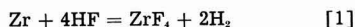
However, the influence of oxygen in the metal on the amount of hydrogen developed is not yet known. There should be a difference in the behavior of such alloys as compared with similar ones of titanium: whereas the oxides of the latter up to Ti_2O_3, inclusively, dissolve in HF (2), no other oxides are known in the Zr-O system (3) except ZrO_2 which practically does not dissolve in the acid, as found by testing. Thus, the α homogeneous solid solutions up to 29 at. % oxygen and those of the two-phase region up to ZrO_2 (with 66.67 at. % oxygen) should differ in their reaction with HF. It is expected that the homogeneous solid solutions similar to Ti-O alloys (4), will react with the acid as follows

$$ZrO_x + 4HF = ZrF_4 + xH_2O + (2-x)H_2 \qquad [2]$$
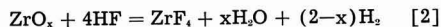
By calculating the volume of H_2, Eq. [2], and comparing it with the experimental one the validity of [2] was checked.

ZrO$_x$ Alloys and Experimental Procedure

Dried Zr powder[1] was used as a starting material. According to the manufacturer the composition of the powder was as follows: Zr-96.6, including about 2% of Hf, Al-0.1, Ca-0.1, Fe-0.5, and Mg-0.13 wt %, or altogether for the metallic part, 97.4%, the remainder being oxygen. However, the present investigation shows that the oxygen is dissolved in the metal not as such but is combined with ZrO_2, which forms a solid solution with the metallic Zr. This is in accordance with the results obtained by de Boer and Fast (5). Therefore, only 87.27% Zr is in the metallic state, and the total of metals present is thus 90.1%, the balance (9.9%) being ZrO_2. The amount of free metals found by this calculation was checked by analyzing the Zr powder by the combustion method (6). Weighed amounts of the dry powder were heated in air up to 1000°C so that complete oxidation occurred (it lasted up to 8 hr). From the composition of the sample given above it was calculated that each gram of the metallic part, which alone is capable of burning to ZrO_2, HfO_2, etc.,

---

[1] Metal Hydrides Incorporated.

Table I. Hydrogen volumes (reduced to normal conditions) developed by Zr powder (sample II) in HF and compared with the volume calculated from combustion analysis

ZrO₂, wt %	Combustion analysis Zr metal and admixt., wt %	Combustion analysis H₂ vol calc, ml/g of alloy	H₂ evolution method; H₂ found, ml/g of alloy
9.51	90.49	440.8	434.9
10.44	89.56	436.2	438.5
8.97	91.03	443.4	436.0
8.34	91.66	446.5	
Avg 9.31	90.68	441.7 ±5.0	436.5 ±2.0

Table II. Hydrogen volumes obtained from ZrOₓ samples dissolved in HF. Comparison with the volumes calculated per gram of the alloy from the combustion data

Sample	Combustion method O₂ (in ZrO₂), wt %	Combustion method Metal (Zr, etc.), wt %**	Combustion method H₂ vol calc, ml/g	H₂ evolution method Vol found, ml/g	H₂ evolution method Δ, %	H₂ evolution method x in ZrOₓ†
I*	0.37	98.58	484.5	488.6	−0.84	0.01
II	2.42	90.69	441.7	436.5	+1.2	0.15
III	3.60	86.13	419.5	419.7	−0.05	0.24
IV	3.99	84.65	412.3	404.6	+1.9	0.27
V	4.30	83.44	406.4	402.4	+1.0	0.29
VI	4.84	81.34	396.2	390.3	+1.5	0.34
VII	4.98	80.86	393.9	386.9	+1.8	0.35
VIII	5.05	80.56	392.4	383.5	+2.3	0.36

* Metallic turnings Hf-free (possibly incomplete combustion).
** Rest—ZrO₂ (source of O₂).
† x—from combustion analyses.

absorbs during the combustion 0.3484 g of oxygen. Hence from the increase in weight and the original weight of the samples the amount of free metal and of ZrO_2 could be calculated. Results are shown in Table I: the Zr powder (sample II) contained 9.31% ZrO_2 or 2.42% oxygen (see Table II) instead of 2.57%, as it follows from the analysis of the manufacturer. This was regarded as a good agreement and, therefore, the Zr powder was used for the preparation of the ZrO_x alloys.

These were prepared by mixing weighed amounts of the dry Zr powder and ZrO_2, and by compressing them in a die under 1500 psi to make a briquette. The latter was heated at 1400°C for 4 hr under a vacuum (2 μ), then quenched in air of room temperature. The color of the samples was silvery gray. They were crushed, pulverized, and parts of the powder were analyzed by burning them in a porcelain crucible to the oxides. From the increase of the sample weight the amount of the metallic part (containing 96.86% Zr) was calculated; the remainder was then the weight of ZrO_2 in the sample before combustion. The volume of hydrogen (STP) which 1 g of samples should develop in HF was computed (487.1 cm³ for the metallic part of them instead of 491.43 ml H_2, Eq. [1] for 100% Zr) and compared with the volume actually obtained in the dissolution experiments. Or, knowing from the combustion analysis the amount of oxygen present in the sample, the volume of hydrogen was also calculated from Eq. [2]. Both methods lead to the same result.

The volume of hydrogen developed by the samples was determined as described previously (4). How-

ever, the procedure is simpler than for Ti, because according to Eq. [1] no lower valency Zr salts are formed and hence no oxidation can occur. Therefore, the air of the apparatus does not have to be replaced by an inert gas or hydrogen. Besides, no side reactions occur and the final volume of hydrogen developed by the sample can be read easily from the gas burette.

Results

Qualitative experiments showed that the homogeneous Zr samples containing up to 29 at. % oxygen dissolve completely in dilute HF (0.3-1N). Sometimes a grayish residue is obtained, but it dissolves slowly and completely in water without gas evolution. It is probably $ZrOF_2$, formed because of hydrolysis ($ZrF_4 + H_2O \rightleftharpoons ZrOF_2 + 2HF$) which is a secondary reaction not affecting Eq. [2]. Samples of the two-phase region always leave a white residue identified as ZrO_2 by x-ray diffraction. However, ZrO_2 always remains behind if the homogeneous ZrO_x samples are heated at about 600°C in a hydrogen atmosphere: they absorb hydrogen which is then released upon dissolution in HF, but a residue of ZrO_2 is obtained. Evidently the dissolving hydrogen forces the ZrO_2 to aggregate to larger particles insoluble in HF.

For checking the validity of reaction [2] only samples from the homogeneous region containing up to 22% ZrO_2 (or 27 at. % oxygen) were used. As samples with a still higher oxygen content were difficult to prepare and to handle, no quantitative studies were made with them. From each sample of the homogeneous region, 3-4 combustion and 2-3 hydrogen evolution analyses were made. How good the separate analyses of one sample are and how the averages obtained by the two methods of analysis agree is shown in Table I on the example of Zr powder, used as starting material.

In the case of sample II the difference between the two methods is about 1.2%. However, the analyses by hydrogen evolution can be reproduced much better than those by the combustion method. The reason may be that ZrO_2 may absorb oxygen similarly as it happens with commercial TiO_2 (7) thus increasing the calculated free Zr amount in the samples; the difference of 1.2% may result in this way. This is evident further when one examines the analyses of 6 more samples of ZrO_x as shown in Table II.

Table II shows that the volumes of hydrogen observed and those calculated from the combustion method agree within 2%, whereby the hydrogen evolution method usually gives smaller volumes. If the x-values of the last column are used to make the calculations according to Eq. [2], an agreement within 0.9% with the volumes observed is obtained. In conclusion, although the results of the combustion and the hydrogen evolution method differ in a systematic fashion, the difference can be attributed to the further absorption of oxygen during the long heating period in the former. Therefore the validity of Eq. [2] is clearly established.

The homogeneous ZrO_x alloys behave as if they would consist of a solid solution of ZrO_2 in metallic Zr. This agrees with the statement of de Boer and

and Fast (5) that oxygen in ZrO_x is in form of O^{2-}. As in case of TiO_x (8) the volumes of H_2 developed by ZrO_x in HF can be used for a rapid determination of oxygen and free metal in those alloys.

Acknowledgment

This investigation was supported by the U. S. Atomic Energy Commission (AT (11-1)-73, Project 5). The authors are grateful to Dr. W. J. James, Professor at the Chemical Engineering Department of the School of Mines, for his interest in this work.

Manuscript received Dec. 28, 1959.

Any discussion of this paper will appear in a Discussion Section to be published in the June 1961 JOURNAL.

REFERENCES

1. M. E. Straumanis and J. I. Ballass, Z. *anorg. u. allgem. Chem.*, **278**, 33 (1955).
2. M. E. Straumanis, W. J. James, and A. S. Neiman, *Corrosion*, **15**, 286t (1959).
3. M. Hansen, D. J. McPherson, and R. F. Domagala, Report COO-123, 1953.
4. M. E. Straumanis, C. H. Cheng, and A. W. Schlechten, *This Journal*, **103**, 439 (1956).
5. J. H. Boer and J. D. Fast, *Rec. trav. chim. P. B.*, **59**, 161 (1940).
6. W. F. Hillerbrand and G. E. F. Lundell, "Applied Inorganic Analysis," p. 449, John Wiley & Sons, Inc., New York (1929).
7. A. W. Czanderna and J. M. Honig, *J. Phys. Chem.*, **63**, 620 (1959).
8. M. E. Straumanis, C. H. Cheng, and A. W. Schlechten, *Analyt. Chem.*, **28**, 1883 (1956).

Gelatin Effects on Polarographic Half-Wave Potentials

A. J. Diefenderfer and L. B. Rogers

Department of Chemistry and Laboratory for Nuclear Science, Massachusetts Institute of Technology, Cambridge, Massachusetts

It is well recognized that the presence of relatively large concentrations of gelatin may lead to cathodic shifts of the half-wave potentials for irreversible reactions. A recent publication from our laboratory (1) reported that the irreversible second reduction of p-dinitrobenzene in weakly acidic solutions was shifted toward *less* cathodic potentials by the addition of small amounts of gelatin. This behavior has since been examined in greater detail because of its theoretical implications with respect to the role of gelatin in the electrical double layer.

Our most recent studies have confirmed the anodic shift using two other samples of gelatin. However, the effect has been shown to be due to an unexpected decrease in pH caused by impurities in the gelatin.[1] It was found that solutions of 0.50% gelatin prepared from warm (60°C) distilled water, which has just been boiled, reached pH values of 4.20 and 4.10 within an hour when stored at 25°C and 2°C, respectively, Several hours later, the pH values were

[1] According to G. Scatchard and O. L. Keller (private communication) pure gelatin would be stable under both the preparative and polarographic conditions employed in our study.

4.07 and 4.00. When approximately a 1-ml portion of such a solution was added to 50 ml of the weakly buffered alcoholic supporting electrolyte, an anodic shift was indeed found. However, when the original pH of the supporting electrolyte was restored by adding potassium hydroxide (which had been dissolved in an alcoholic solvent of the same composition), the half-wave potential returned to the value observed before the addition of gelatin. Thus, the reported anodic shift was not a property of the gelatin *per se*.

The nature of the impurities in our commercial gelatin, which produced the abnormally low pH value, are unknown and are of no further interest to us.

Manuscript received March 28, 1960.

Any discussion of this paper will appear in a Discussion Section to be published in the June 1961 JOURNAL.

REFERENCE

1. L. E. I. Hummelstedt and L. B. Rogers, *This Journal*, **106**, 248 (1959).

December 1960 Discussion Section

A Discussion Section, covering papers published in the January-June 1960 JOURNALS, is scheduled for publication in the December 1960 issue. Any discussion which did not reach the Editor in time for the June 1960 Discussion Section will be included in the December 1960 issue.

Those who plan to contribute remarks for this Discussion Section should submit their comments or questions in triplicate to the Managing Editor of the JOURNAL, 1860 Broadway, New York 23, N. Y., *not later than September 1, 1960*. All discussion will be forwarded to the author(s) for reply before being printed in the JOURNAL.

Brief Communications

Microscopic Observations on Electroluminescent ZnS:Cu Phosphors

Willi Lehmann

Research Department, Westinghouse Electric Corporation, Bloomfield, New Jersey

It is known that the emission of electroluminescence in ZnS:Cu phosphors is concentrated in randomly distributed small spots (1-4). It has also been assumed that electroluminescent ZnS:Cu phosphors contain copper sulfide (probably Cu_2S) as a separate phase segregated in cavities, etc., inside the phosphor particles (Cu_2S on the surface of the particles can be removed by suitable washing procedures) and that these segregations create localized regions of enhanced electric field strength near their edges (5,6). These segregations have now been observed microscopically. The experimental arrangement is shown in Fig. 1. The phosphor particles were stuck on a thin plastic layer between two aluminum electrodes evaporated onto a microscope slide. The space between the particles was filled with a highly refracting liquid [solution of phosphorus and sulfur in methylene iodide (7), $n = 2.06$] in order to obtain a clearer view into the ZnS particles. Even so, some refraction still remained and caused each particle to appear opaque near its edge if illuminated by white light from the rear. The limit of resolution of details inside the particles is estimated to be about 1 μ or somewhat lower.

Because of the smallness of the objects and their three-dimensional extension, the investigation was limited to visual observations. Dark segregations inside of many phosphor particles could be observed. They are frequently, but by far not always, thin and elongated, almost needle-like. They seem to be larger, on the average, in large particles, and *vice*
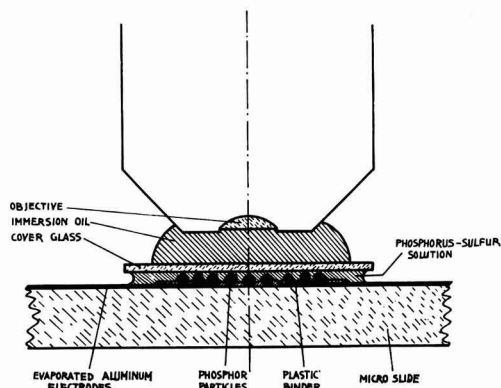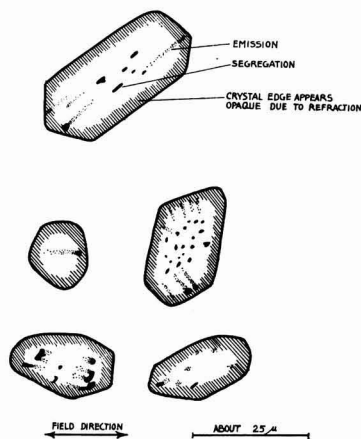

Fig. 2. Phosphor particles containing dark segregations and emitting spots.

versa. The emission spots of electroluminescence are visibly located directly at the ends of the segregations in many, but not in all cases. Some typical examples are shown in Fig. 2. Some emission spots cannot visibly be correlated to dark segregations; perhaps they are actually present but too small to be observed or are hidden by surface irregularities. In other cases, segregations are present without accompanying emission. It may be that these segregations do not have sufficiently sharp edges (submicroscopically) to create localized regions of high field strength. In agreement with old observations (1, 2), the light emission per spot occurs only once per cycle of the exciting voltage. The question whether the emission occurs when the end of the segregation is cathode or anode could not be decided.

The linear dimensions of the segregations approach 5 or 10% of the particle diameter in ordinary phosphor powders. Also the dimensions of the emitting spots range in this order which means that the emission intensity within an average spot is roughly 1000 times higher than the average over the whole phosphor. The brightness of a single spot does not steadily decrease with time (as the integrated emission of an entire electroluminescent cell does) but may undergo all sorts of irregular fluctuations including sudden disappearance after some time of operation or irregular oscillations with time. Even

Fig. 1. Arrangement used in microscopic investigations

a movement of two neighboring spots toward each other and complete union within about one or two minutes could be observed. These observations were made on phosphor particles excited by 20 kcps; the particles did not move under the influence of the electric field.

Manuscript received March 22, 1960.

Any discussion of this paper will appear in a Discussion Section to be published in the June 1961 JOURNAL.

REFERENCES

1. J. F. Waymouth and F. Bitter, *Phys. Rev.*, **95**, 941 (1954).
2. P. Zalm, G. Diemer, and H. A. Klasens, *Philips Res. Rept.*, **10**, 205 (1955).
3. A. Kremheller, *This Journal*, **107**, 8 (1960).
4. W. Lehmann, *ibid.*, **107**, 20 (1960).
5. W. Lehmann, *ibid.*, **104**, 45 (1957).
6. K. Maeda, *J. Phys. Soc. Japan*, **13**, 1352 (1958).
7. "Handbook of Chemistry and Physics," 39th ed., p. 2726, Chemical Rubber Publishing Co., Cleveland, Ohio.

Purification of Tantalum Anodes during Sintering

C. J. B. Fincham and G. L. Martin[1]

Metals Division, National Research Corporation, Cambridge, Massachusetts

It is generally believed that the d-c leakage of a sintered-anode tantalum electrolytic capacitor is affected markedly by the chemical purity of the tantalum metal from which it is made. To substantiate this belief it would be necessary to correlate the d-c leakage of the capacitor with the impurity content of the sintered anode rather than with that of the original tantalum powder, since impurity levels change during sintering to an extent dependent on sintering conditions.

Houtz and Karlik (1) have studied the changes in impurity levels of carbon, oxygen, nitrogen, and general metallic contaminants during the sintering of tantalum anodes and correlated their results with the d-c leakage and life of the finished solid-electrolyte capacitors. However, other than their data on carbon, oxygen, and nitrogen, there is no published information on the quantitative changes in the levels of specific impurities during sintering.

The work reported here is a preliminary study of these quantitative changes during various sintering treatments and of the d-c leakages of the resulting anodes.

Sintered anodes were made from five different tantalum powders (three high-capacitance and two low-capacitance) by pressing pellets of known densities and heating the pellets under vacuum at several different conditions of time and temperature, as shown in Table I. The pelleting and sintering techniques used have been described in detail previously (2). The anodes were all cylindrical, 1.8 g in weight, and had an 'as-pressed' diameter of 0.25 in. Each sinter run was made with anodes of only one powder.

The powders and representative anodes from five batches were analyzed quantitatively for the following elements: O, C, N, Na, Al, Cr, Cu, Fe, Mo, Nb, Ni, Si, and Ti, with the results shown in Table I. The remaining anodes were not analyzed for O, C, N, or Na. Oxygen was determined by vacuum fusion,

Table I. Changes in impurity levels during sintering of anodes and corresponding d-c leakages

Material	Form	Green density, g/cc	Measured temp, °C	Time, hr	L/C* μamp/μfd	O	C	N	Na	Al	Cr	Cu	Fe	Nb	Ni	Si	Ti	Mg
SG-73R (High capacitance)	Powder	—	—	—	—	480	25	30	30	<50	110	<50	87	120	52	81	<10	
	Anode 1	8.5	1750	1.5	0.082	—	—	—	—	<50	<15	<50	20	115	24	29	<10	
	Anode 2	9.5	2050	0.5	0.067	—	—	—	—	<50	<15	<50	18	115	19	25	<10	
	Anode 3	9.0	2050	1.5	0.087	340	8	50	20	<50	<10	<50	<20	110	10	62	<10	
	Anode 4	9.5	2050	3.0	0.062	—	—	—	—	<50	<15	<50	<10	115	<15	26	<10	
L-533 (High capacitance)	Powder	—	—	—	—	930	120	750	—	<50	<10	<50	460	140	25	780	40	
	Anode 1	10.5	1750	1.5	>30.0	—	—	—	—	<50	<15	<50	190	135	<15	64	<10	
	Anode 2	9.0	2050	1.5	0.12	350	10	285	25	<50	<10	<50	47	120	11	78	12	27
ET-76 (High capacitance)	Powder	—	—	—		850	50	25	100	190	130	100-250	190	92	120	160	<10	
	Anode 1	9.0	2050	0.5	24.5	—	—	—	—	<50	<15	<50	20	105	17	<25	<10	
	Anode 2	9.0	2050	1.5	28.0	460	7	40	10	<50	<10	<50	36	110	31	44	<10	
SGL-103R (Low capacitance)	Powder	—	—	—	—	370	25	35	15	<50	170	50	61	150	151	55	<10	
	Anode 1	10.0	2050	0.5	0.07	—	—	—	—	<50	<15	<50	19	145	34	25	<10	
	Anode 2	9.0	2050	1.5	0.074	360	6	60	10	<50	<10	<50	<20	150	16	40	<10	
L-450 (Low capacitance)	Powder	—	—	—	—	770	180	30	<10	200	20	50	250	230	40	450	<10	
	Anode 1	10.5	1750	1.5	27.0	—	—	—	—	70	<15	<50	62	230	<15	98	<10	
	Anode 2	9.0	2050	1.5	27.0	180	58	40	<5	<50	<10	<50	<20	210	<10	40	<10	

Sn, Co, and Mn were <10 in all anodes.
Mg was <10 in all anodes except one (see table).
Pb was <20 in all anodes.
Mo was <25 in all powders and anodes.
< means below limit of detection by method used.
* L/C = d-c leakage at 140 v/unit capacitance for 200-v formation (microamperes per microfarad).

carbon by combustion, nitrogen by micro-Kjeldahl, and sodium by flame-photometry. The remaining elements were determined spectrographically using the carrier technique, calibrated by synthetic standards, and, in the cases of Fe, Ni, and Cr, cross-checked by wet-chemical methods. During the spectrographic analyses of the anodes, the additional elements Co, Mg, Mn, Pb, and Sn were looked for but not detected (except Mg in one anode). The estimated limits of detection are given in Table I.

Anodes from the same batches as those analyzed were tested electrically for d-c leakage and capacitance by the following wet-cell method described in detail previously (2).

The anodes were formed at constant current (35 ma/g), in 0.01% phosphoric acid solution at 92°C, to 200 v, held at voltage for 2 hr, washed and dried. DC leakage was measured at 140 v after 2 min at voltage in 10% phosphoric acid solution at room temperature. Capacitance was measured in the same solution at 120 cycles/sec.

The measured ratios of d-c leakage (L) at 140 v (in microamps), to capacitance (C) (in microfarads), for a 200-v formation are given in Table I. In addition, for those batches of anodes for which complete analyses were obtained, measurements of leakage at 70 v for a 100-v formation and leakage at 35 v for a 50-v formation were made. These results are discussed below.

The analytical and electrical results for each set of powder and anodes are listed in Table I in increasing order of severity of sintering conditions. It can be seen that different impurities behaved differently during sintering. Iron and nickel decreased slowly with increasingly severe sintering conditions. Niobium was unchanged from the level in the powder under any sintering conditions tried, and chromium decreased to below the limit of detection under all sintering conditions tried. Silicon decreased on sintering in every case, but the results were erratic and the final levels did not correlate with severity of sintering conditions. Oxygen, carbon, and sodium decreased on sintering, although the extent of the decrease of oxygen was variable. In the powders where the initial nitrogen content was low, a slight increase in nitrogen level during sintering was observed (presumably due to "pick up" from outgassing or small leaks in the vacuum furnace). However, in the one high nitrogen powder (L-533), there was a marked decrease in nitrogen during sintering. Sodium, aluminum, copper, and titanium, when present in detectable amounts in the powder, all decreased during sintering.

Similar qualitative trends were found by Torti (3) in a study of the purification of tantalum during vacuum arc-melting, which takes place at much higher temperatures (> 3000°C). The main difference was in the relatively large loss of niobium observed during arc melting, compared with essentially no loss during sintering.

The correlation of purity of anode with d-c leakage is not so easily seen. However, one generalization perhaps can be made from these data, namely, that with the exceptions of niobium and oxygen

none of the anodes with low leakage had any specific impurity at a high level relative to the group of data, whereas the high leakage anodes each had one or more impurities at a relatively high level. The anodes made from ET-76 appear to be an exception to this generalization, but the reason for this may be in the high copper level in the original powder which was introduced by accidental contamination in the course of handling. The copper was therefore essentially a surface contaminant, so that bulk analyses have little meaning with regard to the effective concentration of copper at the surface of the powder and anodes. High leakage due to copper contamination has occasionally been observed in other powders.

It is tempting to speculate that the high leakage of anode 1 of L-533 is due either to a high iron content (which was reduced by the more severe sintering conditions used for the low leakage anode 2) or to a high nitrogen level, presumably somewhere between 750 ppm in the powder and 285 ppm in anode 2.

To speculate further, the high leakages of both anodes made from L-450 might be attributed to high carbon contents, 58 ppm in anode 2, and presumably higher in anode 1. This would agree with the conclusions of Houtz and Karlik (1) that to obtain a satisfactory anode the carbon content must be less than 20 ppm.

However, attempts to place an exact limit on an acceptable impurity level must be tempered by the realization that the concentration of impurities at the surface can be either lower or higher than the impurity levels measured on the bulk of the metal.

Surface contamination of the powder (as in ET-76) or of the sintered anode (e.g., during the processing of the anode to make the finished capacitor) can give higher impurity levels on the surface than in the bulk.

Alternatively, the surface can be purer than the bulk if, during sintering, the rate of removal of impurities is limited by diffusion in the metal rather than by vaporization from the surface.
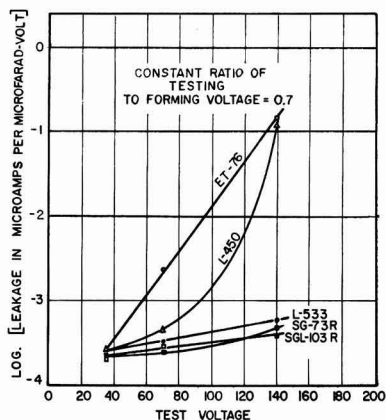

Fig. 1. Variation of d-c leakage per microfarad-volt with test voltage, for a constant ratio of testing to forming voltage and constant sintering conditions.

In discussing the effects of impurities on leakage, results shown in Fig. 1 are of great interest, where the logarithm of the d-c leakage (in microamperes per microfarad-volt) is plotted against test voltage, for a constant ratio of testing to forming voltage. As mentioned above, these measurements were made on anodes from the same batches as anode 4 of SG-73R and anodes 2 of each of the other powders. The results were plotted as leakage per microfarad-volt, since this gives a measure of leakage per unit surface area, irrespective of forming voltage. The points shown at a test voltage of 140 v are those shown as leakage per microfarad (for a 200-v formation) in Table I.

It can be seen from Fig. 1 that the rate of change of leakage with test voltage varies markedly between the different sets of anodes and that whereas at 140 v there is a difference of almost a factor of 400 between the highest and lowest leakage anodes, at 35 v the difference is about 30% and is approach-ing the limits of experimental error Therefore, it would appear that in any study of leakage vs. purity the maximum sensitivity of results can be obtained by working at the highest voltages.

Acknowledgment

REFERENCES

1. C. C. Houtz and S. Karlik, Bell Telephone System Technical Publication, Monograph 3305. (Also published in Proceedings 1959 Electronic Components Conference, p. 116.)
2. G. L. Martin, C. J. B. Fincham, and E. E. Chadsey, Jr., *This Journal*, **107**, 332 (1960).
3. M. L. Torti, *ibid.*, **107**, 33 (1960).

Manuscripts and Abstracts for Spring 1961 Meeting

Papers are now being solicited for the Spring Meeting of the Society, to be held at the Claypool Hotel in Indianapolis, Ind., April 30, May 1, 2, 3, and 4, 1961. Technical sessions probably will be scheduled on Electric Insulation, Electronics (including Luminescence and Semiconductors), Electrothermics and Metallurgy, Industrial Electrolytics, and Theoretical Electrochemistry.

To be considered for this meeting, triplicate copies of abstracts (*not exceeding 75 words in length*) must be received at Society Headquarters, 1860 Broadway, New York 23, N. Y., *not later than January 2, 1961. Please indicate on abstract for which Division's symposium the paper is to be scheduled and underline the name of the author who will present the paper.* Complete manuscripts should be sent in triplicate to the Managing Editor of the JOURNAL at the same address.

Presentation of a paper at a technical meeting of the Society does not guarantee publication in the JOURNAL. However, all papers so presented become the property of The Electrochemical Society, and may not be published elsewhere, either in whole or in part, unless permission for release is requested of and granted by the Editor. Papers already published elsewhere, or submitted for publication elsewhere, are not acceptable for oral presentation except on invitation by a Divisional program Chairman.

Feature Section

Electrochemistry as We Enter the Sixties

Presidential Address*

William C. Gardiner

Since this is the first meeting of The Electrochemical Society in the 1960's, I propose to compare electrochemistry today and our Society as it is today with electrochemistry and the Society at the start of previous decades. This should be of interest to all of you at this time.

I have reviewed the Proceedings of the Society for the annual meetings in the springs of 1910, 1920, 1930, 1940, and 1950. It may be necessary to remind some of you that these dates do not coincide with the tenth, twentieth, and so on, anniversaries of the Society because it was founded in 1902.

It was very interesting for me to read about the activities of our predecessors. The pages are filled with the names of men who contributed greatly to the science and technology of electrochemistry as well as other fields.

In 1910, President Leo H. Baekeland, known to all of you as the inventor of Bakelite, opened the meeting in Pittsburgh with a talk on "Science and Industry." He gave a forceful discourse on the merits of the scientist and engineer and their contributions to progress and industry, giving enlightenment on what a research scientist can do and the way he works. He would still be far from satisfied with the recognition given to scientists and engineers in America.

On Friday, a special train carried the members around to various steel mills and other plants in the Pittsburgh area. It was reported that, at the informal dinner in the evening, "Section 'Q' was strongly in evidence, enjoying itself with its usual ABANDON." On Saturday afternoon, a General Public Meeting was held in Carnegie Music Hall where Professor Joseph W. Richards spoke on "What the Electrochemical Industries are Accomplishing."

In 1920, Professor Wilder D. Bancroft of Cornell was President, and opened the meeting in the Rogers Building at M.I.T. with a paper on "Contact Catalysis" in which he reviewed the theories of catalysis as of that time. He then conducted a "Symposium on Colloid Chemistry." On Friday, joint sessions were held with the A.I.E.E. on "Electrically Produced Alloys" in the morning and then, in the afternoon, *eight electric cars* took the guests to General Electric at Lynn, Mass. It was reported that "A printed itinerary gave all the details of the visit with great accuracy, and it was carried according to plan with military precision." Afterward, the informal dinner was graced by the presence of "our esteemed friend, Professor Elihu Thompson."

On Saturday, they met at Harvard University where Professor T. W. Richards welcomed the Society. He said that there was an historical reason for visiting Harvard occasionally because Benjamin Thompson, later

to become Count Rumford, walked ten or more miles from North Woburn to Harvard Hall to hear John Winthrop's lectures on natural philosophy. About 30 years later, Count Rumford founded The Royal Institution where Davy and Faraday did their great work in electrochemistry. It is to be regretted that we no longer take advantage of meeting on the campuses of some of our leading universities.

By 1930, the Presidential Address had become an evening affair when Dr. Francis C. Frary spoke in St. Louis on "Research as a Vocation." He pointed out that character and temperament are more important than an applicant's technical training, and discussed the value of intellectual integrity, personality, imagination, and curiosity. These are inherent in the character of a good researcher. Training can improve such things as observation, manipulation, attention to detail, accuracy, care in observing and recording data, clarity of thought, and expression; broad training is desirable on fundamentals of science, languages, and mathematics

I noted several other items of interest that occurred at the St. Louis Meeting in 1930. There was final acceptance of the formal resolution for incorporation of the Society. Also, the Joseph W. Richards Memorial Fund was established by a gift of Dr. E. G. Acheson to meet the expenses incurred by inviting and entertaining distinguished guests from foreign countries. We might regret that this fund is so small, because we are inviting more and more foreign scientists to participate in our meetings and can do so only through the benevolence of our National Science Foundation.

In the spring of 1940, we met at Galen Hall, Wernersville, Pa. Professor H. Jermain Creighton of Swarthmore, in his talk on "Forty Years of Electrochemistry," reviewed the development of electrochemical theory. The Society was struggling to recover from the depression, and he challenged 100 fellow members to bring in two new members apiece to bring the number of members back to the pre-depression level. Our membership has increased but we have lost the pleasure of being able to meet in such beautiful surroundings.

When we met in Cleveland in 1950, Professor A. L. Ferguson quoted from letters that he had solicited from former Presidents of the Society and others in speaking on "What the Society Would See if It Looked in a Mirror." He analyzed opinions that had been expressed on the training of electrochemists, on the professional standing of electrochemistry, electrochemists, and our JOURNAL. He noted that there were 337 Charter Members in 1902 and that the membership had risen to 2279 in 1921, then decreased in the depression to 1156 in 1936. It was more or less static from 1936 to 1942 but had increased to 2000 in 1950. He thought that the diverse interests of industrial and academic people had

caused the loss of both to either purely engineering or purely scientific societies. However, the management of The Electrochemical Society had been revised to become more representative of all groups. Professor Ferguson regretted the inadequate facilities for training electrochemists in universities and the general lack of appreciation of the importance of electrochemistry in their departments of chemistry.

The character of our meetings has changed tremendously. In the first four decades, we all met together and there was only one activity at a time. There was much more opportunity for people of different interests to meet and learn about the other fellow's problems. Plant trips were a big feature of the programs. Five Divisions were operating in 1940 but they still could plan their activities without overlapping. By 1950, there were nine Divisions, and simultaneous technical sessions were in operation. We still have nine Divisions but, at this meeting, there are as many as seven simultaneous sessions. Plant trips are becoming rare. Besides the conflict with technical sessions, I think that this is due partly to having to restrict our meetings to the larger cities where traffic problems and distances discourage local committees from planning trips. I wonder whether this is a good trend. I remember that I have gained considerable benefits from such trips, myself.

Publication of our JOURNAL, formerly called the TRANSACTIONS, is one of the most important functions of the Society. As you look at the books on the shelf, there is not a very obvious change through the years except for a change in color and a change in dimensions. However, the content of new scientific knowledge in our JOURNAL has changed considerably. The annual volume of the world's scientific literature is enormous so we must limit manuscripts to original work reported as concisely as possible. Our editors are necessarily very critical and exacting. In 1910, there were 24 papers presented and published. At this meeting in 1960, 214 papers are scheduled. I cannot say how many will be eligible for publication. The papers of special symposia are now being published in book form so that those who wish may obtain the complete collection. This permits publication of reviews by experts without burdening the JOURNAL. During the first four decades, published articles averaged 14 pages and preprints were distributed before the conventions. The necessity for economy has reduced preprints to abstracts and the average length of a published paper in 1950 was 7 pages and, so far this year, it has averaged 5.3. We must reduce every paper to the minimum required for the clear presentation of new material.

The editorial burden is carried by 14 Divisional Editors assisting the Technical Editor. These men are experts in their field but rely further on specialists to review each paper. In addition, there are the News Editor, the Book Review Editor, and over all, the Editor. All of this is done on a voluntary basis by members of our Society. I am sure that most of you, from time to time, have contributed in this way. I have heard criticisms of our JOURNAL to the effect that the quality of papers is not high or that publication takes too long. I know that these matters are also of chief concern to our editors and that they are continually striving to improve the JOURNAL as a service to you. It is also your JOURNAL. It publishes the papers you write and edit. This is a democratic institution, so he who can do better should not hide his light under a bushel but should volunteer his services. Our Managing Editor and her assistant are staff employees. Someday we may be affluent enough to enlarge our staff with people who are qualified to do the technical editing. This might reduce the time required to prepare a paper for publication.

What are electrochemists working on to contribute in the 1960's? In reading the program of this meeting, I see many contributions to the Electronics industry; electrolytic capacitors, luminescence, semiconductors (new materials, theory, preparation, and device technology). In Electrothermics and Metallurgy, I see papers on refractory metals, rhenium, vanadium, and iron. The Industrial Electrolytic and Theoretical Electrochemistry Divisions have a joint symposium to discuss electrochemical engineering as a unit process.

What are the contributions of electrochemistry to the space age? Electrothermics and metallurgy have contributed refractory materials for nose cones and the many special alloys in rockets. Fused salt electrolysis produces titanium, beryllium, and other "rare" metals. Some of the exotic high-energy fuels, fluorine, hydrogen, and hydrazine, depend on electrochemical production or electrochemically produced raw materials. New light batteries power the electronic circuits, printed electrochemically and utilizing electrolytic capacitors, transistors, and other semiconductor devices for their guidance and broadcasting systems.

And can we dream about a few advances that will be made in the sixties! Our fastest growing Division (Electronics) will discover new and better phosphors, new semiconductors to give more efficient rectifiers and transistors. Electrothermics and Metallurgy will contribute cheaper "rare" metals and alloys. Electrolytic cells may reach capacities of half a million amperes. Electrodeposition will be extended to the "rarer" metals. The Battery people will make the fuel cell practical as well as develop many special batteries. Corrosion will be better understood and, I hope, markedly reduced. And, finally, we expect the Theoretical Division to extend our knowledge of electrochemistry in all its branches and lead us into new fields yet to be discovered.

Henry B. Linford Chosen 1960 Acheson Medalist

Henry B. Linford, professor of chemical engineering, Columbia University, New York City, has been selected as the 16th recipient of the Edward Goodrich Acheson Medal and Prize of The Electrochemical Society. Presentation of the award will be made at the banquet to be held during the 118th meeting of the Society in Houston, Texas, at the Shamrock Hotel, October 9-13, 1960.

The award, a gold medal and $1000 prize, is made every two years for conspicuous "contribution to the advancement of the objects, purposes, or activities" of the Society.

Dr. Linford was born in Logan, Utah, on April 23, 1911. He attended Utah State University, receiving the B.S. degree in chemistry in 1931. As a graduate student at Washington State University, he studied with Dr. Wilbur E. Bradt, Dr. Linford was awarded the M.S. degree in 1933 and the Ph.D. in physical chemistry in 1936.

In the same year, he was awarded the Weston Fellowship by The Electrochemical Society and elected to study at Columbia University with Dr. Colin G. Fink. Dr. Linford joined the Society in March 1936. Undoubtedly, his close association with Drs. Bradt and Fink did much to stimulate the interest which resulted in nearly continuous participation in the affairs of the Society over a period of more than 20 years.

From Columbia University in 1937, Dr. Linford went to the research laboratories of the American Smelt-

Henry B. Linford

ing and Refining Co. in New Jersey as research electrochemist. He returned to Columbia as instructor in chemical engineering in 1941, advancing to assistant professor in 1946, associate professor in 1949, and professor in 1952. Working principally in electrochemical engineering, he and his students have published widely in the fields of electroplating and corrosion.

A member of The Electrochemical Society since March 27, 1936, Dr. Linford served as Chairman of the New York Section in 1942 and Chairman of the Electrodeposition Division in 1948. He held the post of national Secretary of the Society

from the spring of 1949 to the spring of 1958, when he took office as Vice-President, for a three-year term. He served concurrently as Vice-President and Interim Secretary from May 1958 to January 1959 when he was succeeded as Secretary by Ivor E. Campbell. At present, he is first Vice-President of the Society.

At the Annual Banquet on May 5, 1959, during the Philadelphia Meeting, President Sherlock Swann, Jr., presented Dr. Linford with a Certificate of Appreciation reading as follows: "In grateful recognition of many years of faithful and distinguished service and unselfish devotion to the interests and welfare of The Electrochemical Society, Incorporated, this scroll is hereby presented to Dr. Henry B. Linford as a token of our genuine appreciation of his outstanding contributions to the progress and building of the Society during his tenure of office as Secretary."

He belongs to the American Electroplaters' Society, of which he has been Director of Research Project No. 12, "Cleaning and Preparation of Metals for Electroplating," since 1949. He also is a member of Alpha Chi Sigma, Phi Lambda Upsilon, Sigma Xi, the American Chemical Society, the American Institute of Chemical Engineers, the National Association of Corrosion Engineers, the Chemists' Club, and is a Fellow of the New York Academy of Sciences.

—L.I.G.

Annual Report of the Board of Directors, April 1, 1959-March 31, 1960

Your Board of Directors has no particular recommendations to make which require action at this meeting (Annual Meeting, Chicago). However, the following matters of special interest which transpired during our fiscal year ending March 31, 1960 are being reported to you.

Young Author's Prize and Francis Mills Turner Memorial Award

Dr. Milton Stern was awarded the Young Author's Prize for 1958 for his paper "The Mechanism of Passivating-Type Inhibitors," and J. Paul Pemsler won the Francis Mills Turner Memorial Award for 1958

for his paper "Diffusion of Oxygen in Zirconium and Its Relation to Oxidation and Corrosion."

Honorable Mention has been made to Frederick F. Morehead, Jr., for his paper "Electron Traps and the Electroluminescence Brightness and Brightness Waveform," and also to

Ralph S. Cooper for his paper "Schlieren Studies of Concentration Gradients at a Cu/HCl Anode."

The winners of these two Awards for 1959 will be announced at our Banquet this evening. [*See* p. 156C of this issue.]

Local Sections

During the past year, we are very pleased to report, the Texas Section was organized and welcomed into the Society. We now have 19 Local Sections functioning in various areas throughout the country and in Canada and India.

Society Meetings

It is quite apparent to your Board of Directors that meetings of our Society are becoming larger each year. Our registered attendance of 1489 in Philadelphia and 1029 in Columbus were the largest of any meeting ever held by the Society. This progress, while most welcome, indicates the necessity for more thorough planning, and a Convention Advisory Committee has been appointed to study this problem. The personnel of the Committee, consisting of some officers of the Society and the three previous General Meeting Chairmen, are particularly qualified to survey this situation and advise us with respect to our future meeting arrangements.

Palladium Medal Award for 1959

On recommendation of our Palladium Medal Award Committee, our Palladium Medal for 1959 was awarded to Professor A. N. Frumkin of the Institute of Electrochemistry of the Academy of Sciences of the U.S.S.R. Unfortunately, due to ill health, Professor Frumkin could not attend our 1959 Fall Meeting, when our presentation would usually have taken place. For this reason, the ceremonies were postponed until this meeting in Chicago.

Second International Conference on Passivity

The Second International Conference on Passivity is scheduled during September 1962. Our Society will be one of the sponsors of this meeting, As soon as details are worked out, an announcement will be made in the JOURNAL.

Assistance Award for 1960

On recommendation of the Honors and Awards Committee, the Board of Directors approved of an Assistance Award (one year only) for the period June–September 1960 to a fellow or teaching assistant pursuing work between the degree of B.S. and Ph.D. on a subject in the field of interest to The Electrochemical Society. The recipient is required to be the possessor of a nine-month grant in this field of interest for the academic year 1960-1961 and shall also have been the holder of a similar grant for the academic year 1959-1960. Our award is intended to cover a period for which the recipient has no financial support. (*See* p. 156C of this issue.)

Society Finances

Special consideration has been given during the past year to the financial affairs of the Society. A detailed report with respect to the action taken will be made in due course.

Hiram S. Lukens

We wish to record with sorrow the passing of Hiram S. Lukens, President of our Society in 1934-1935. It has been reported to us that our Philadelphia Section is sponsoring in his memory the establishment of the Hiram S. Lukens Memorial Undergraduate Chemical Fund at the University of Pennsylvania.

W. C. Gardiner, *Chairman*

Annual Report of the Secretary, April 1, 1959-March 31, 1960

It is a pleasure to review the progress which has been made by your Society for the fiscal year ending March 31, 1960.

Membership

Due to the energetic efforts of Fred W. Koerker and his associates on our Membership Committee, the membership of the Society stands at an all-time high of 3124. This compares with our previous high total of 2972 and shows a net increase of 152.

Sustaining Membership

Corporate support in the form of Patron and Sustaining Memberships in the Society has also shown an increase. During the year, the Committee headed by John T. Owen secured 12 new Sustaining Memberships. However, we lost 5, leaving a net gain of 7. At the end of our fiscal year, we had a total of 5 Patron Memberships and 158 Sustaining Memberships.

Special Symposia

Two international symposia were held at our spring meeting in Philadelphia in 1959 on the subjects of "Electrode Processes" and "Liquid Dielectrics." These were sponsored by our Theoretical and Electric Insulation Divisions, respectively, and were jointly supported by the Society and some agency of the Government.

A special symposium on the subject of "The Chemistry of Metal and Semiconductors" was jointly sponsored by our Corrosion and Electronics Divisions at our Columbus Meeting. This meeting also received Government support and was participated in by speakers from overseas.

The Board of Directors also approved of the special symposium on "The Principles of Electrochemical Engineering" which will be held this week [Chicago Meeting] by our Theoretical and Industrial Electrolytic Divisions. This meeting, too, will receive some measure of Government assistance.

Society Meetings

Our spring meeting in Philadelphia and our fall meeting in Columbus both resulted in record-breaking attendances. A total of 214 papers will be presented at our meeting this week—the largest number ever presented at any previous meeting of the Society.

It is quite apparent that the activities and services of our Society are assuming increasing stature and importance throughout the world.

Journal of the Society

Our JOURNAL, which is our principal medium of communication, aside from our national meetings, is experiencing a continuing period of growth. Last year, 1394 pages were published in the JOURNAL, which included a record number of 235 papers. An additional appropriation of $6000 was made in our budget in order to provide the funds necessary to print the papers which were cleared for publication. We fully expect this growth to continue.

Monographs and Special Publications

During the past year, the publication "Mechanical Properties of Intermetallic Compounds," containing the papers presented at our Phila-

delphia Meeting, came off the press and is now being distributed by John Wiley & Sons, Inc. Others previously approved and now in various stages of production include: "Metal Iodides and Iodide Metals," "Primary Batteries," "Chemistry of Metal and Semiconductor Surfaces," "Electrode Processes," "Modern Electroplating" (revised edition), and "High Temperature Technology" (revised edition).

Guests from Overseas

Once again, it is a pleasure to report that we are favored with a sizeable delegation from overseas at our meeting this week. We are especially pleased to welcome them. We are sure that their participation in our meeting will represent an important contribution to the success of our technical sessions.

Ivor E. Campbell, *Secretary*

Financial Statement of The Electrochemical Society, Inc.

Statement of Income and Expenses

April 1, 1959–March 31, 1960

Income

	Adjusted budget 12 months	General Fund	Society Reserve Fund
Membership Dues	$ 44,000	$ 43,322.85	
Patron and Sustaining Memberships	21,000	20,650.00	
Reprints	3,000	6,296.38	
Nonmember Journal Subscriptions	24,000	27,812.06	
Office Sale Journal and Publications	500	966.64	
Advertising	9,000	13,814.28	
Bound Volumes	3,000	2,654.84	
Conventions	8,000	9,308.58	
Interest Earned on General Funds	750	576.80	
Membership Directory		557.95	
	$113,250	$125,960.38	
Nonmember Journal Subscriptions	4,800		$ 5,158.28
Nonmember Convention Registrations	3,000		3,003.00
Monograph Royalties	1,200		2,719.54
Income from Investments	3,300		4,200.33
	12,300		$15,081.15
	$125,550		

Expenses

Print and Mail Journal	$ 50,000	$ 52,337.16	
Salaries	51,380	47,587.19	
Rent	5,400	5,400.00	
Postage, Supplies, and Miscellaneous	7,000	7,958.20	
Bound Volumes	3,000	2,846.96	
Local Sections and Divisions	1,500	1,040.60	
Membership Directory	800		
Young Author's Prize	100	100.00	
Presidential Office Expense	2,000	354.38	
New York Office Travel	1,400	1,261.88	
Conventions:			
Program Booklets	2,000	1,927.61	
Materials, Supplies, and Postage	1,000	638.75	
	$125,580	$121,452.73	
Contingency— 1% Estimated Income	1,200		
	$126,780		
New Capital Equipment (Cumulative)	600		
	$127,380		
Special Symposium Expenses			2,109.78
			$12,971.37

Excess Expenses Over Income—General Fund	14,130	+4,507.65	
Income Credited to Society Reserve Fund	12,300	12,971.37	
Excess Expenses Over Income	$ 1,830	+$ 17,479.02	

Balance Sheet at March 31, 1960

Statement of Assets

Cash

Chemical Bank New York Trust Company

Electronics Division Monograph Fund	$	137.44
Corrosion Division Monograph Fund		1,899.65
Electrodeposition Division Monograph Fund		1,449.57
Electrothermics & Metallurgy Division Monograph Fund		879.60
Theoretical Division Monograph Fund		1,546.20
New Capital Equipment		37.98
Consolidated Fellowship Fund		250.00
Society Reserve Fund		8,420.76
General Fund		−1,285.56
		$ 13,335.64
Petty Cash—General Fund		150.42
U.S.A. Treasury Bills— General Fund		49,419.45
Excelsior Savings Bank— General Fund		273.01
Greenwich Savings Bank— General Fund		567.27
Chase Manhatten Bank Savings Account— General Fund		683.50 $ 64,429.29

Investments

Edward Goodrich Acheson Fund		
Securities	$33,977.12	
Savings Account	3,564.17	$ 37,541.29
F. M. Becket Memorial Award Fund		
Securities	15,297.37	
Savings Account	1,364.45	16,661.82
Consolidated Fellowship Fund		
Securities		39,118.69
Joseph W. Richards Memorial Fund		
Savings Account		799.49
Edward Weston Fellowship Fund		
Securities		14,428.22

General Portfolio
of Investments

Corrosion Division	20,195.88		
Electrodeposition Division	1,000.00		
Electrothermics & Metallurgy Division	4,000.00		
Society Reserve Fund	92,692.39	117,888.27	226,437.78

Other Assets

Convention Advance		1,000.00	
Accounts Receivable		4,996.26	
Furniture & Fixtures	11,841.71		
Less Reserve for Depreciation	1,048.49	10,793.22	
Inventory		6,757.75	23,547.23
			$314,414.30

Statement of Liabilities and Surpluses

Liabilities

Deferred Income India Section	$	13.96
Overseas Subscriptions Payable (DBG and Faraday)		2,454.40
Life Memberships		2,079.71
Federal and State Taxes Withheld		1,020.74 $ 5,568.81

Surpluses

Special Funds

Edward Goodrich Acheson Fund	$37,541.29	
F. M. Becket Memorial Award Fund	16,661.82	
Consolidated Fellowship Fund	39,368.69	
Joseph W. Richards Memorial Fund	799.49	
Edward Weston Fellowship Fund	14,428.22	108,799.51

Monograph Funds

Corrosion Division	22,095.53	
Electrodeposition Division	2,449.57	
Electrothermics and Metallurgy Division	4,879.60	
Theoretical Division	1,546.20	
Electronics Division	137.44	31,108.34

Society Reserve Fund

Surplus	88,141.78	
Net Income Received	12,971.37	101,113.15
General Fund Surplus Surplus .. $65,333.59		
New Capital Equipment 37.98	65,371.57	

Less Advances:

Electro-Organic Chemistry	500.00	
Technology of Columbium	524.00	
Intermetallic Compounds	160.00	
Vacuum-Metallurgy	186.94	
10-Year Index (1952-1961)	683.79	2,054.73
		63,316.84

Excess Income Over Expenses	4,507.65	67,824.49	308,845.49
			$314,414.30

General Portfolio of Investments

Value of Securities 3/31/59		$ 96,928.64
Additional Investments		
Electrothermics & Metallurgy Division	1,000.00	
Society Reserve Fund:		
Interest and Dividend Shares	1,125.56	
New Purchases	13,195.95	15,321.51
Increased Value of Securities Based on Closing Prices 3/31/60		5,638.12
FUND VALUE 3/31/60		$117,888.27

Society Reserve Fund

Equity Value in General Portfolio 3/31/59		$ 72,732.76
Additional Investments		
*Interest and Dividend Shares	1,125.56	
New Purchases	13,195.95	14,321.51
Increased Value of Securities in General Portfolio as of 3/31/60		5,638.12
Equity Value in General Portfolio 3/31/60		92,692.39
Bank Credit Balance 3/31/59	9,770.90	
*Cash Dividends	3,074.77	
*Monograph Royalties	2,719.54	
*Convention Registration Fees	3,003.00	
*Journal Subscriptions	5,158.28	13,955.59
		23,726.49
Less New Securities Purchased	13,195.95	
Less Special Symposia Expense	2,109.78	15,305.73
Bank Credit Balance 3/31/60		8,420.76
FUND VALUE 3/31/60		$101,113.15

*Total Income From Sources Indicated $15,081.15

Division Monograph Funds

Corrosion Division

Equity in General Portfolio 3/31/59		$20,195.88
Bank Credit Balance 3/31/59	$1,088.92	
Monograph Royalties	1,589.40	2,678.32
Corrosion Research Council	770.62	
Palladium Medal Expense	8.05	778.67
Bank Credit Balance 3/31/60		1,899.65
FUND VALUE 3/31/60		$22,095.53

Electrothermics and Metallurgy Division

Equity in General Portfolio 3/31/59		$ 3,000.00
Additional Investment		1,000.00
		4,000.00
Bank Credit Balance 3/31/59	1,457.20	
Monograph Royalties	422.40	
		1,879.60
Less Additional Investment Purchased	1,000.00	
Bank Credit Balance 3/31/60		879.60
FUND VALUE 3/31/60		$ 4,879.60

Electrodeposition Division

Equity in General Portfolio 3/31/59		1,000.00
Bank Credit Balance 3/31/59	1,161.72	
Monograph Royalties	287.85	
Bank Credit Balance 3/31/60		1,449.57
FUND VALUE 3/31/59		$ 2,449.57

Theoretical Electrochemistry Division

Bank Credit Balance 3/31/59	506.14	
Monograph Royalties	1,040.06	
Bank Credit Balance 3/31/60		$ 1,546.20

Electronics Division

Bank Credit Balance 3/31/59	99.34	
Monograph Royalties	38.10	
Bank Credit Balance 3/31/60		$ 137.44

Special Funds

Edward Goodrich Acheson Fund

Values of Securities 3/31/59	$34,028.00	
New Securities Purchased	328.58	
	34,356.58	
Decreased Value Securities 3/31/60	379.46	
Value Securities 3/31/60		$33,977.12
Savings Account Balance 3/31/59	2,369.71	
Dividends from Investments	$1,437.18	
Interest on Savings Account	85.86	1,523.04
	3,892.75	
Purchase New Securities	328.58	
Savings Account Balance 3/31/60		3,564.17
FUND VALUE 3/31/60		$37,541.29

Consolidated Fellowship Fund

Bank Credit Balance 3/31/60		$ 250.00

Fundamental Investors, Inc.

Value Shares 3/31/59	16,564.04	
Dividend Shares Accumulated	750.29	
	17,314.33	
Less Value Shares 3/31/60	880.21	
Total Value Shares 3/31/60		16,434.12

Wellington Fund Inc.

Value Shares 3/31/59	13,080.11	
Dividend Shares Accumulated	892.74	
	13,972.85	
Decreased Value Shares 3/31/60	328.67	
Total Value Shares 3/31/60		13,644.18

Incorporated Investors

Value Shares 3/31/59	2,971.71	
Dividend Shares Accumulated	323.78	
Shares Puhchased by Lincoln Bequest	474.72	
	3,770.21	
Decreased Values Shares 3/31/60	378.21	
Total Value Shares 3/31/60		3,392.00

Blue Ridge Mutual Fund, Inc.

Value Shares 3/31/59	220.03	
Dividend Shares Accumulated	55.24	
Shares Purchased by Weston Fund	510.98	
	786.25	
Less Value Shares 3/31/60	112.86	
Total Value Shares 3/31/60		673.39

The Anaconda Company

100 Shares Value 3/31/59	6,850.00	
Less Value Shares 3/31/60	1,875.00	
Total Value Shares 3/31/60		4,975.00
FUND VALUE 3/31/60		$39,368.69

F. M. Becket Memorial Award Fund

Value Securities 3/31/59	$14,031.25	
Increased Value Securities 3/31/60	1,266.12	
Value Securities 3/31/60		15,297.37
Savings Account Balance 3/31/59	$ 800.93	
Dividends on Investments	$ 535.29	
Interest Income	28.23	563.52
Savings Account Balance 3/31/60		1,364.45
FUND VALUE 3/31/60		$16,661.82

Edward Weston Fellowship Fund

Value Securities 3/31/59	$14,712.42	
Decreased Value Securities 3/31/60	284.20	
Value Securities 3/31/60		14,428.22
Income From Investments	510.98	
Purchase of Shares Consolidated Fellowship Fund	510.98	
FUND VALUE 3/31/60		$14,428.22

Joseph W. Richards Memorial Fund

Savings Account Balance 3/31/59	$ 772.65	
Interest Income	26.84	
FUND VALUE 3/31/60		$ 799.49

Certificate of Audit

I have examined the balance sheet of The Electrochemical Society, Incorporated, as of March 31, 1960, and the related statement of income and expenses for the period from April 1, 1959 to March 31, 1960. My examination was made in accordance with generally accepted auditing standards and, accordingly, included such tests of the accounting records and such other auditing procedures as I considered necessary in the circumstances.

In my opinion, the balance sheet and statement of income and expenses present fairly the financial position of The Electrochemical Society, Incorporated, at March 31, 1960, and its income and expenses for the 12-month period then ended.

(Signed) H. K. Leicht, *Auditor*

Seen at Chicago—May 1960

Photographs by Len Kohan

Row 1—A. N. Frumkin receiving Palladium Medal from President W. C. Gardiner; Dr. and Mrs. M. Shaw and Dr. and Mrs. Morris Feinleib; Ralph Wehrmann (Chicago Committee—Finance and Registration), A. E. Middleton, Albert Cornish, and M. F. Tomaino. **Row 2**—E. L. Koehler (General Chairman Chicago Meeting) and Mrs. Koehler (Chairman Chicago Ladies' Committee); E. M. Savitski, Valentina Bibikova, and R. K. Shannon; C. V. King and George Dubpernell. **Row 3**—A. W. Smith and L. F. Howard; F. A. Shirland, Ruth G. Sterns, and Sheldon Evans (Chicago Host Committee); R. M. Burns and E. G. Enck. **Row 4**—A. A. Rasch and Eugene Frekko; Mrs. W. C. Gardiner, N. J. Johnson, and A. C. Haskell; Dr. and Mrs. F. C. Mathers; Lottie Fink. **Row 5**—M. C. Udy and R. G. Brown; Al Alexander and Peter Stephens; Donald Tuomi; R. A. Lubker, N. Groell, and J. M. Miller. **Row 6**—Ralph Hovey (Chicago Committee—Hotel Arrangements) and Mrs. Hovey (Chicago Ladies' Committee); E. A. Hollingshead; G. W. Heise; Sherlock Swann, Jr.; Mrs. M. Georgiev.

. . . More of Chicago

Photographs by Len Kohan

Row 1—Mrs. G. W. Heise; W. J. Hamer (Society Vice-President-Elect), Mrs. C. A. Hampel (Advisor and Vice-Chairman Chicago Ladies' Committee), and C. A. Hampel (Chicago Committee—Entertainment); D. A. Vermilyea and P. V. Popat; Oliver Osborn and P. H. Cardwell. Row 2—H. Knight; A. Shtasel; R. A. Schaefer (Society President-Elect) and Mrs. Schaefer; A. Stone, R. Lopez, and T. Ban; R. Sangster and R. Stead. Row 3—L. I. Gilbertson and B. Broch-Smith; M. Brooks, Natalie Michalski, A. N. Frumkin, and H. C. Gatos; Dr. and Mrs. R. B. Mears and J. H. Bartlett. Row 4—Julian Glasser and E. F. Kiefer; C. L. Faust; F. A. Lowenheim, Abner Brenner, J. S. Mackay, and F. P. Peters; R. R. Rogers and A. G. Bureau. Row 5—B. Crawford, C. L. Scheer, and N. Ibl; W. Petrosky, M. Katz, and K. Flodin; H. Crane and D. McDowell. Row 6—G. R. Hoey; A. Black and J. L. Sheldon; C. L. Mantell, E. F. Kiefer, and Steele Malkin; W. C. Gardiner and Bill Veeck (President of American League Champion Chicago White Sox).

Electrochemical Society Awards
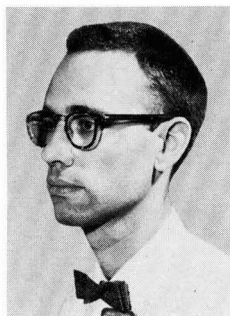
F. A. Posey
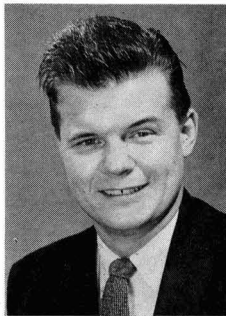
R. G. Carlson

V. E. Hauser, Jr.

Young Author's Prize for 1959

At the Annual Banquet held on Tuesday, May 3, during the Chicago Meeting of The Electrochemical Society, the Young Author's Prize of $100 was presented to Franz A. Posey of the Oak Ridge National Laboratory, Oak Ridge, Tenn. Dr. Posey was selected as the recipient of the award in recognition of his paper "Kinetic Studies on Corrosion Systems, I. Polyelectrodes under Activation Control" which was published in the July 1959 issue of the JOURNAL.

Dr. Posey attended Millsaps College in Jackson, Miss., from 1948 to 1951, receiving his B.S. degree in chemistry in June 1951. He was awarded the M.S. degree in chemistry in 1952 and the Ph.D. degree in inorganic chemistry in 1955 from the University of Chicago, where he held a Graduate Teacher's Scholarship and a General Education Board Scholarship in 1951-1952. His graduate research, conducted under Dr. Henry Taube, was on the chemistry of complex ions in aqueous solution. During the years 1952-1954, he was a research assistant in inorganic chemistry at the University of Chicago.

In September 1954, Dr. Posey joined the staff of the Chemistry Division of the Oak Ridge National Laboratory, operated by Union Carbide Nuclear Co. At the present time, he is engaged in research on the electrochemistry of corrosion systems.

He is a member of the American Chemical Society and the Society of Sigma Xi.

Turner Memorial Award for 1959

Robert G. Carlson of the General Electric Co., Evandale, Ohio, is the winner of The Electrochemical Society's Francis Mills Turner Memorial Award, Sponsored by the Reinhold Publishing Corp., consisting of $100 worth of books, for his paper "Tungsten Zone Melting by Electron Bombardment" which appeared in the January 1959 JOURNAL. Announcement of Mr. Carlson's selection was made at the Annual Banquet of the Society in Chicago on May 3.

Mr. Carlson was awarded a B.S. degree in metallurgical engineering from the Polytechnic Institute of Brooklyn in 1951 and a M.S. degree in metallurgical engineering from Rensselaer Polytechnic Institute in 1955. He has, since graduation, been employed by the General Electric Co., one year as a student engineer on the General Electric Training Program, one year as a metallurgical engineer at the Aeronautics and Ordnance Systems Division in Schenectady, two years engaged in studies on molybdenum-base alloys at the Research Laboratory in Schenectady, and three years as an associate in metallurgy at the Refractory Metals Laboratory of the Lamp Division in Cleveland. He is employed as a research metallurgist while participating full time in the Basic Research Cooperative Program between the General Electric Co. and the University of Cincinnati. At present, he is engaged in the study of the kinetics and phenomenologistics in the densification of columbium and columbium alloy powders.

In addition to The Electrochemical Society, Mr. Carlson is a member of the American Institute of Metallurgical Engineers, American Society of Metals, and the American Vacuum Society.

ECS Assistance Award for 1960

By action of the Board of Directors on May 1, 1960, the first Assistance Award of The Electrochemical Society has been granted to Victor E. Hauser, Jr., a graduate student at the Dept. of Chemical Engineering, Oregon State College, Corvallis, Ore. The award, valued at $800, covers the period June to September 1960.

This award is an experiment suggested by Professor C. W. Tobias, of the University of California at Berkeley, who has been made responsible for the selection and management of it. It is made "without regard to sex, citizenship, race, location, or financial need to a fellow or teaching assistant pursuing work between the degree of B.S. and Ph.D. on a subject in the field of interest to The Electrochemical Society. The recipient must be the possessor of a nine-month grant in this field of interest for the academic year 1960-1961 and must have been the holder of a similar grant for the academic year 1959-1960."

Mr. Hauser is working for a Ph.D. degree in chemical engineering with minors in mathematics and physics. His research project, under the direction of Professor Robert E. Meredith, consists of a study of the problems associated with the development of high-temperature galvanic fuel cells.

Division News

Theoretical Electrochemistry Division

At the Theoretical Electrochemistry Division Business Meeting held during the Chicago Meeting of the Society on May 5, W. J. Hamer of the National Bureau of Standards reported the nomination of the following for officers of the Division for the 1960-1961 term:

Vice-Chairman—L. G. Longsworth, Rockefeller Institute, 66 St. & York Ave., New York 21, N. Y.

Secretary-Treasurer—Paul Rüetschi, Carl F. Norberg Research Center, Electric Storage Battery Co., Yardley, Pa.

Member of Executive Committee—A. J. deBethune, Boston College, Chestnut Hill 67, Mass.

No nominations were received from the floor, and these officers were elected by unanimous vote.

C. W. Tobias, of the University of California, Berkeley, continues as Chairman.

C. W. Tobias, *Chairman*

Section News

Council of Local Sections

The Nominating Committee for the Council of Local Sections of The Electrochemical Society, comprised of W. M. Hetherington, Jr., of the Southern California-Nevada Section, L. B. Rogers of the Boston Section, and M. F. Quaely of the New York Metropolitan Section, the latter serving as Chairman, submits the following slate of nominees for the Council posts to be filled for the 1960-1961 term:

Chairman (1 year)—A. J. Cornish (Pittsburgh)

Vice-Chairman (1 year)—J. C. White (Washington)

Secretary (1 year)—R. F. Bechtold (San Francisco)

Representative on Board of Directors (2 years)—N. C. Cahoon (Cleveland)

Each of the above has indicated that he is ready and willing to serve in the designated post.

M. F. Quaely, *Chairman*
Nominating Committee

Detroit Section

The Detroit Section was pleased to be host to Dr. W. C. Gardiner, Society President, at the meeting held April 21, 1960 at Wayne State University. Dr. Gardiner outlined some of the problems now being faced by the Society and discussed its hopes for the future.

Dr. John J. Lander, director of electrochemical research, Delco-Remy Division, General Motors Corp., presented a technical paper on the topic "Partial Plated Monolayers of Silver on Gold," and discussed the papers of Byrne, Rogers, and Griess. His differing interpretation of their results was most interesting and stimulated a lively discussion.

The next Section meeting, to be held on May 19, will feature a panel discussion by members of the Section on the general theme "The Measurement of Electrochemical Parameters."

A meeting of the planning Committee for the 1961 Fall Meeting of the Society was held on March 28. Considerable progress was made in establishing responsibility for the various tasks which must be carried out.

S. E. Beacom, *Secretary-Treasurer*

New Members

In May 1960, the following were elected to membership in The Electrochemical Society by the Admissions Committee:

Active Members

T. R. Backer, E. I. du Pont de Nemours & Co., Inc., Pigments Dept.; Mail add: 116 Lakeview Dr., Brevard, N. C. (Electronics)

L. M. Conrad, Ion Capacitor Corp.; Mail add: 361 N. Walnut St., Columbia City, Ind. (Electronics)

C. P. Ferguson, E. I. du Pont de Nemours & Co., Inc.; Mail add: 107 Hillcrest Ave., Brevard, N. C. (Electronics)

W. C. Hagel, General Electric Research Labs.; Mail add: 100 St. Stephens Lane W., Scotia 2, N. Y. (Electrothermics & Metallurgy)

T. F. Hanna, E. I. du Pont de Nemours & Co., Inc., Brevard, N. C. (Electronics)

D. N. Hanson, Chemical Engineering Dept., University of California, Berkeley, Calif. (Theoretical Electrochemistry)

W. K. Hooper, Republic Foil Inc., 55

By action of the Board of Directors of the Society, all prospective members must include first year's dues with their applications for membership.

Also, please note that, if sponsors sign the application form itself, processing can be expedited considerably.

Triangle St., Danbury, Conn. (Electric Insulation)

J. G. Kourile, M. W. Kellogg Co.; Mail add: 150 N. Munn Ave., Apt. 3C, East Orange, N. J. (Electrothermics & Metallurgy, Industrial Electrolytic, Theoretical Electrochemistry)

R. J. Lombardo, E. I. du Pont de Nemours & Co., Inc., Brevard, N. C. (Electronics)

F. A. Ludwig, Electro-Optical Systems, Inc.; Mail add: 3584 Monterosa Dr., Altadena, Calif. (Industrial Electrolytic, Theoretical Electrochemistry)

T. W. Manchester, National Carbon Co.; Mail add: 3493 Spring Circle, Decatur, Ga. Industrial Electrolytic)

Harry Meschke, Winkel Machine Co., Inc., Watervliet, Mich. (Battery)

R. L. Recko, Raytheon Co., Semiconductor Div., 150 California St., Newton 58, Mass. (Electronics)

R. C. Ropp, Sylvania Electric Products Inc.; Mail add: R.D. 5, Towanda, Pa. (Electronics)

John Sybalsky, Perfect Electroformed Products, Inc.; Mail add: 33 Cowdrey St., Yonkers 2, N. Y. (Electrodeposition)

G. L. Zucker, Texas Instruments, Inc.; Mail add: 1429 Nantucket Dr., Richardson, Texas (Electronics)

Arthur Cowen, General Motors Corp., Process Dev.; Mail add: 18612 Steel, Detroit 35, Mich. (Theoretical Electrochemistry)

Associate Members

N. W. Kirshenbaum, American Smelting & Refining Co.; Mail add: P. O. Box 646, Plainfield, N. J. (Battery, Electrodeposition, Electrothermics & Metallurgy, Industrial Electrolytic)

B. M. Kolb, Diamond Ordnance Fuze Labs.; Mail add: 3621 Newark St., N.W., Apt. 404, Washington 16, D. C. (Electronics)

Student Members

J. J. Farrell, Cleveland Section Award Winner—Baldwin Wallace College; Mail add: 18502 Holland Rd., Berea, Ohio (Theoretical Electrochemistry)

P. A. Politzer, Cleveland Section Award Winner—Western Reserve University; Mail add: 3728 Warren Rd., Cleveland 11, Ohio (Theoretical Electrochemistry)

Reinstatement to Active Membership

J. S. Dewar, Union Carbide of Canada Ltd., 2221 Yonge St., Toronto 7, Ont., Canada (Electrothermics & Metallurgy)

Transfer to Active Membership

K. J. Martin, Redstone Arsenal Research Div., Rohm & Hass Co., Huntsville, Ala. (Theoretical Electrochemistry)

Deceased Members

H. E. Dunn, Pittsburgh, Pa.
V. F. McDonough, Parma, Ohio
H. R. Van Deventer, New York, N. Y.

Personals

James G. Buck has joined the staff of Battelle Memorial Institute, Columbus, Ohio, where he will be engaged in research in physical electronics and solid-state physics. For eight years, Dr. Buck was head of the thermionics research group at Sylvania Electric Products' Laboratories at Mineola, N. Y.

Samuel M. Fok has been appointed to the technical staff of Fairchild Semiconductor Corp.'s Research and Development Labs., Mountain View, Calif. Dr. Fok, who has been assigned to the Preproduction Section of Fairchild, previously was a senior staff engineer at the Shockley Semiconductor Corp. in Mountain View.

James W. Franklin is now an editor in the publications division, Mohansic research center, International Business Machines Corp., Yorktown Heights, N. Y. Formerly, he was associate editor of *Engineering and Mining Journal*.

John F. Gall has been appointed manager of the Research Products Development Dept., a newly formed part of the Technical Division of Pennsalt Chemicals Corp., Philadelphia, Pa. Previously assistant manager of research and development, Dr. Gall brings to the new post many years of experience in both research direction and product development, the latter being chiefly in the high-energy field.

George W. Healy has been named senior research scientist at the Union Carbide Metals Co., Division of

Union Carbide Corp., Niagara Falls, N. Y. Mr. Healy's promotion is a recognition of his outstanding ability and achievement in the applications of thermodynamics and physical chemistry to the problems of the ferroalloy industry.

W. A. Koehler has been appointed acting dean of the Graduate School at West Virginia University, Morgantown, W. Va. Dr. Koehler gave up his duties as head of the Chemical Engineering Dept. in September 1959 to devote more time to his duties as director of the Engineering Experiment Station, Dr. R. B. Dustman, former dean of the Graduate School, retired in February 1960 and Dr. Koehler is serving as acting dean until a full-time successor is appointed. He is continuing to serve as director of the Engineering Experiment Station.

William M. Raynor has been named general sales Manager of Foote Mineral Co., Philadelphia, Pa. Since 1956, he has been director of purchasing.

Cloyd A. Snavely has joined Sifco Metachemical, Inc., Cleveland, Ohio, as general manager. Formerly, he was assistant manager of the Chemical Engineering Dept. of Battelle Memorial Institute in Columbus.

Semiconductor Analytical Group

During the May 1959 meeting of The Electrochemical Society, an invitation was issued to meet and see if sufficient interest would develop to warrant establishment of an organization for the advancement of analytical methods for trace elements in semiconductor materials. Sufficient interest was shown so that a preliminary organizational meeting was held in New York in June 1959, and a Steering Committee was selected to formulate the purpose, objectives, and method of operation.

In September 1959, the Steering Committee chose a name, Semiconductor Analytical Group, and prepared a questionnaire for prospective members. Also the purpose and scope of SAG were defined as follows: "The purpose and objectives of this organization are to improve, develop, and exchange information on analytical methods for trace elements in semiconductor materials. The scope of this group's activities will be limited to semiconductor materials analyses, through (but not including) final devices. The mate-

rials of primary interest are silicon and germanium, their base starting and intermediate materials, and those things which relate directly to their purity. Consideration of other semiconductor materials is *not* excluded or limited to the aforementioned, and will be included as the requirement develops."

The first formal meeting of SAG was held at Air Force Cambridge Research Center, Bedford, Mass., in January 1960, at which time the Steering Committee plan of operation was adopted and officers elected.

Plans have been made for a SAG Meeting to be held in New York City on September 12, 1960 at the International Division of Merck and Co. The morning session will be limited to three technical papers: "Solid Mass Spectrometry with Reference to Trace Analysis" by L. Herzog, Pennsylvania State University; "Ultra Trace Spectrometric Analysis" by G. Morrison and R. Rupp, Sylvania Division of General Telephone; "The Use of Electrical Measurements for the Determination of Impurity Levels in Single Crystal Semiconductors" by J. Bronson, Raytheon Manufacturing Co. The afternoon sessions will be devoted to informal discussions of analytical problems.

Additional information concerning SAG can be obtained from the Secretary: Mr. James M. Morris, Metal Hydrides Inc., 12-24 Congress St., Beverly, Mass.

Book Reviews

Physical Metallurgy, by Bruce Chalmers. Published by John Wiley & Sons, Inc., New York, 1959. 468 pages; $12.50.

Teachers of undergraduate metallurgy are plagued by the same fears and doubts that beset the entire field of metallurgy—those of not knowing which way metallurgy ought to go. There are conservatives who are convinced that the old way of metallurgical engineering was fitting and proper and should be continued. There are others who believe in a more liberal approach in at least one regard, namely, that an understanding of how structures in alloys form (both from a thermodynamic and kinetic point of view) is at least as important as detailed study of the structures themselves. Professor Chalmers is clearly in the latter

group; a large part of this book is devoted to thermodynamics of alloys and kinetics of proceses in alloys.

The book is divided into eight chapters of widely varying length. An introductory chapter discusses atomic physics and the periodic table. This is a brief and rather uninspired chapter which plays not a much further role in the book. Next, a chapter on aggregation of atoms treats topics all the way from crystal structure through phases and phase diagrams. This chapter is excellently done, generally. It treats equilibrium between phases in contact not solely in terms of bulk thermodynamics, but mainly in terms of equilibrium of atom transfer across the common interface. A relatively short chapter on structure-insensitive properties (which is too encyclopedic to be inspiring) is followed by two better sections on imperfections and structure-sensitive properties. Finally, there are three chapters on change-of-state, deformation, and recovery processes, and solid-state transformation. These are well done.

The reader of this book will note that the entire treatment is topic-oriented, not material-oriented. Martensite, for example, is treated not from the traditional metallurgical-engineering point of view, but simply as the best-studied diffusionless phase transformation. The eutectoid decomposition of steel is treated extensively because the transformations occurring here have received more study than those of any other eutectoid reaction. In the view of this reviewer, this treatment is proper from the point of view of the student, since it puts the materials of specific industries in proper perspective in the whole field of study.

The book has a few annoying flaws. (*A*) The sections on atomic physics and those on electricity and magnetism either should have been done more carefully or omitted. (*B*) The sketches used to illustrate certain topics are not used as effectively as they might be. Oftentimes, figures are inadequately captioned or labeled; others are referred to in the text rather poorly. (*C*) The author does give credit to many original sources of photomicrographs and other data, but he is careless in some cases—it is much better to go back to original sources rather than simply to copy data from other books and review articles.

This is, on the whole, a good book. The basic philosophy of the treatment is excellent. In this reviewer's opinion, metallurgists who learn from texts such as this will be far superior to those who learn under the materials-oriented philosophy. The book fails to be really excellent by not very much—it looks as though a little more care in the actual writing of the manuscript could have made the difference. One hopes that, in another edition, Professor Chalmers might achieve this goal.

Charles Wert

The Principles of Electrophoresis, by R. Audubert and S. de Mende. Published by The Macmillan Co., New York, 1960. 142 pages; $7.00.

This brief work has been translated in excellent style by A. J. Pomerans, who also has increased the value of the book by adding a few pertinent references and comments not included in the French edition.

Beginning with a concise summary of the general properties of electrolytic solutions, the book describes the fundamental electrochemical laws which apply to charged particle displacements in free or supported solutions under the action of an electric field.

Colloidal systems and solutions of macromolecules are treated by extending the concepts of electrolytes to include all states of dispersion as belonging to one category. The authors describe how application of the Debye-Hückel theory of electrolytes to colloidal particles leads to results agreeing with experiments. The concept of mobilities and the phenomenon of electro-osmosis are described in readily understandable terms as manifestations of the electrokinetic potential. The mathematics employed in these descriptions is rather elementary and straightforward.

Following the theoretical section contained primarily in the first four chapters, the moving boundary method of Tiselius is taken up. The diagrams and illustrations have been well selected, giving a clear description of the apparatus and its principles of operation. The translator has expanded the section on interferometric methods to include some recent improvements.

The treatment of electrophoresis in a supporting medium is directed principally toward considerations involving paper electrophoresis, but includes a brief mention of applications of other media for stabilizing the solvent. Continuous paper electrophoresis has been emphasized as a preparative method, even though, for technical reasons, this approach has not proven to be as generally

successful as the use of starch or inert granular horizontal beds.

The book is well supported throughout with experimental data from the authors' own experiences.

Though the discussion of applications, presented in the concluding chapter, is not extensive, a prudent selection of examples has been cited, which succeeds in illustrating the broad range of utility that electrophoresis has begun to assume since the influence of the classical work of Tiselius stimulated progress in these techniques. The book should serve to increase understanding and broaden perspectives among research workers in medicine and biology who at present apply electrophoresis for its practical values without being adequately oriented in principles of electrochemistry.

The book is especially recommended to students, since it seems to represent a judicious blending of essential theoretical considerations, experimental data, descriptions of several forms of equipment, and applications to problems of analysis, identification, separation, and purification.

Kenneth R. Woods

Announcement from Publisher

1959 Supplements to Book of ASTM Standards, heavy paper covers, 10 parts, $4.00 per part, $40.00 per set. Published by American Society for Testing Materials, 1916 Race St., Philadelphia 3, Pa.

The 1959 Supplements give, in their latest form, standard specifications, tests, definitions, and recommended practices which are being issued for the first time or revised since their appearance in the 1958 Book of Standards. Of particular interest to readers of the JOURNAL are the following sections:

Part 2. Non-Ferrous Metals Specifications and Electronic Materials, 280 pages.—Includes 38 standards for

copper and copper-base alloys, ingot, plate, sheet, strip, rolled bar, shapes, wire, die forgings, pipe, and tubes. Also, tin, nickel alloys, titanium, materials for electron tubes and semiconductor devices, metal powders, and electrodeposited metallic coatings. In addition, there are standards for die-cast metals, aluminum and aluminum alloys, magnesium and magnesium alloys, and metallic electrical conductors.

Part 3. Methods of Testing Metals (Except Chemical Analysis), 110 pages.—Includes 14 standards for tests for mechanical properties, effect of temperature, corrosion, electrical and magnetic properties. Also included are nondestructive testing and sampling methods.

Part 9. Plastics, Electrical Insulation, Rubber, Carbon Black, 546 pages.—Includes 74 standards for plastics, molding compounds, and shapes; tests for mechanical, thermal, optical, and permanence properties of plastics, as well as effects of radiation. Also included are electrical insulating materials, such as shellac and varnish, ceramic products, mica products, rubber tapes, etc. There are standards for rubber elastomers, latex, adhesives, sponge, hard rubber and coated fabrics, tape, hose, gaskets, automotive, and aeronautical products.

Literature from Industry

Micro Metallic Bulletin. This newly revised bulletin includes information on porous stainless steel filters which can meet a wide range of flow rates, temperatures, pressures, and slurries. Several new filter types and sizes are described. Full information is given on method of manufacture, particle size removal, flow rates, working, and welding of porous stainless steel.

The bulletin is available free from Micro Metallic Div., Pall Corp., Glen Cove, N. Y.

Baird-Atomic Radioisotope Wall Chart contains information on dosimetry of radioisotopes, decay tables, optimum counts chart, gamma-ray absorption curves, and typical gamma spectra. Diagrams are included.

The chart can be obtained free of charge from Atomic Instrument Sales Manager, Baird-Atomic, Inc., 33 University Rd., Cambridge 38, Mass.

"Olin Aluminum Mill Products," a 24-page illustrated booklet, describes the physical properties, fabrication characteristics, and economic advantages of a wide variety of aluminum sheet, plate, rod, bar, extrusion, and casting alloys. The various tempers, finishes, and patterns available are discussed. Aluminum's yield and tensile strength, thermal conductivity, and electrical conductivity are graphically compared with those of other materials.

Free copies of the booklets can be obtained from Metals Div., Olin Mathieson Chemical Corp., 400 Park Ave., New York 22, N. Y.

Employment Situations

Positions Wanted

Metallurgist—B.S. degree in mathematics, physics, chemistry. Graduate work in mathematics and spectrographic analysis. Three and one half years' experience in spectrographic, metallographic, physical controls of transistor, die cast, and punch press parts. Desires responsible position in production or research. *Reply to Box 368, c/o The Electrochemical Society, 1860 Broadway, New York 23, N. Y.*

Electrochemical Engineer—12 years' R & D experience in almost all phases of electrochemical processes. Extensive theoretical knowledge with ability in practical application. Combine the above with curiosity, resourcefulness, and creativity. Highly adaptable and capable. Supervisory experience. Desires position of considerable responsibility where experience and abilities will be most valuable. Prefers West Coast location, but will go anywhere. Salary, $11-12,000. *Reply to Box 369, c/o The Electrochemical Society, 1860 Broadway, New York 23, N. Y.*

Positions Available

Chemists and Chemical Engineers —We need physical, organic, and inorganic chemists and chemical engineers to carry out Engineering and development work in the rapidly growing power sources field. Research & Development center located in Minneapolis near University of Minnesota. Battery experience preferred but not required.

Send résumés to: J. W. Baxter, Employee & Labor Relations, Gould-National Batteries, Inc., E. 1326 First National Bank Bldg., St. Paul 1, Minnesota.

The Electrochemical Society

(Sustaining Members cont'd)

General Motors Corp.
  Brown-Lipe-Chapin Div., Syracuse, N. Y.
    (2 memberships)
  Guide Lamp Div., Anderson, Ind.
  Research Laboratories Div., Detroit, Mich.
General Transistor Corp., Jamaica, N. Y.
Gillette Safety Razor Co., Boston, Mass.
Globe-Union, Inc., Milwaukee, Wis.
Gould-National Batteries, Inc.,
  Minneapolis, Minn.
Grace Electronic Chemicals, Inc.,
  Baltimore, Md.
Great Lakes Carbon Corp., New York, N. Y.
Hanson-Van Winkle-Munning Co.,
  Matawan, N. J. (2 memberships)
Harshaw Chemical Co., Cleveland, Ohio
  (2 memberships)
Hercules Powder Co., Wilmington, Del.
Hill Cross Co., Inc., New York, N. Y.
Hoffman Electronics Corp., El Monte, Calif.
Hooker Chemical Corp., Niagara
  Falls, N. Y. (3 memberships)
Hughes Aircraft Co., Culver City, Calif.
Industro Transistor Corp.,
  Long Island City, N. Y.
International Business Machines Corp.,
  Poughkeepsie, N. Y.
International Minerals & Chemical
  Corp., Skokie, Ill.
ITT Laboratories, Nutley, N. J.
Jones & Laughlin Steel Corp.,
  Pittsburgh, Pa.
K. W. Battery Co., Skokie, Ill.
Kaiser Aluminum & Chemical Corp.
  Div. of Chemical Research,
    Permanente, Calif.
  Div. of Metallurgical Research,
    Spokane, Wash.
Kennecott Copper Corp., New York, N. Y.
Keokuk Electro-Metals Co., Keokuk, Iowa
Libbey-Owens-Ford Glass Co., Toledo, Ohio
M. & C. Nuclear, Inc., Attleboro, Mass.
Mallinckrodt Chemical Works, St. Louis, Mo.
P. R. Mallory & Co., Indianapolis, Ind.
McGean Chemical Co., Cleveland, Ohio
Merck & Co., Inc., Rahway, N. J.
Metal & Thermit Corp., Detroit, Mich.
Minnesota Mining & Manufacturing Co.,
  St. Paul, Minn.
Monsanto Chemical Co., St. Louis, Mo.
Motorola, Inc., Chicago, Ill.
National Cash Register Co., Dayton, Ohio
National Lead Co., New York, N. Y.
National Research Corp., Cambridge, Mass.
National Steel Corp., Weirton, W. Va.
New York Air Brake Co., Kinney Vacuum
  Div., Boston, Mass.
Northern Electric Co., Montreal, Que.,
  Canada

Norton Co., Worcester, Mass.
Olin Mathieson Chemical Corp.,
  Niagara Falls, N. Y.
    High Energy Fuels Organization
      (2 memberships)
Ovitron Corp., Long Island City, N. Y.
Peerless Roll Leaf Co., Inc., Union City, N. J.
Pennsalt Chemicals Corp.,
  Philadelphia, Pa.
Phelps Dodge Refining Corp., Maspeth, N. Y.
Philco Corp., Philadelphia, Pa.
Philips Laboratories, Inc., Irvington-on-
  Hudson, N. Y.
Pittsburgh Metallurgical Co., Inc.,
  Niagara Falls, N. Y.
Poor & Co., Promat Div., Waukegan, Ill.
Potash Co. of America,
  Carlsbad, N. Mex.
Radio Corp. of America
  Tube Div., Harrison, N. J.
  RCA Victor Record Div., Indianapolis,
    Ind.
Ray-O-Vac Co., Madison, Wis.
Raytheon Manufacturing Co.,
  Waltham, Mass.
Reynolds Metals Co., Richmond, Va.
  (2 memberships)
Rheem Semiconductor Corp.,
  Mountain View, Calif.
Schering Corporation, Bloomfield, N. J.
Shawinigan Chemicals Ltd., Montreal, Que.,
  Canada
Speer Carbon Co.
  International Graphite & Electrode
    Div., St. Marys, Pa. (2 memberships)
Sprague Electric Co., North Adams, Mass.
Stackpole Carbon Co., St. Marys, Pa.
Stauffer Chemical Co., New York, N. Y.
Sumner Chemical Co., Div. of
  Miles Laboratories, Inc., Elkhart, Ind.
Sylvania Electric Products Inc., Bayside,
  N. Y. (2 memberships)
Tennessee Products & Chemical Corp.,
  Nashville, Tenn.
Texas Instruments, Inc., Dallas, Texas
Three Point Four Corp., Yonkers, N. Y.
Titanium Metals Corp. of America,
  Henderson, Nev.
Tung-Sol Electric Inc.,
  Newark, N. J.
Udylite Corp., Detroit, Mich.
  (4 memberships)
Universal-Cyclops Steel Corp.,
  Bridgeville, Pa.
Upjohn Co., Kalamazoo, Mich.
Victor Chemical Works, Chicago, Ill.
Western Electric Co., Inc., Chicago, Ill.
Wyandotte Chemicals Corp.,
  Wyandotte, Mich.
Yardney Electric Corp., New York, N. Y.